Universitat Politècnica de València
Departamento de Máquinas y Motores Térmicos

UNIVERSITAT POLITÈCNICA DE VALÈNCIA

Control and Diagnosis of a SCR-ASC After-Treatment System for NOx and NH3 Emission Reduction Under Real Driving Conditions and Potential System Failures

PhD Dissertation

Presented by

André Nakaema Aronis

Advised by

Dr. Benjamín Pla

Valencia, December 2022

To my parents;
My uncle Raul;
and Christ Jesus.

Not to us, Lord, not to us but to your name be the glory, because of your love and faithfulness.

—Psalm 115.1

Attempt something so impossible that unless God is in it, it's doomed to failure.

—John Haggai

Resumen

Para cumplir los límites de emisiones impuestos por los gobiernos y reducir el impacto negativo en el medio ambiente, el uso de sistemas de postratamiento (ATS) se ha convertido en algo esencial para los motores de combustión interna.

Los ATS en los trenes motrices están planteados para lograr una alta eficiencia de reducción de contaminantes en las condiciones de funcionamiento diseñadas, para lo cual el sistema de control necesita conocer el nivel de desgaste del catalizador, así como confiar en la información de retroalimentación de los subsistemas de los ATS. Además, es posible aumentar la capacidad de reducción de contaminantes de los catalizadores mediante estrategias de control inteligentes.

Ante este escenario, esta tesis pretende aplicar técnicas de monitorización y diagnóstico para garantizar el pleno funcionamiento del ATS, y estrategias de control óptimo para mejorar la reducción de las emisiones de NOx con bajo consumo y deslizamiento de NH3.

Para lograr este objetivo, se han planteado dos caminos:

- Desarrollo de modelos de alta precisión para la predicción de las emisiones de NOx y NH3 acoplados a un algoritmo de fusión de datos, siendo aplicados para diagnosticar el sistema en dos enfoques específicos: detección del nivel de fallo de inyección de amoníaco en el ATS y estimación del estado de envejecimiento del catalizador del ASC.

- Uso de modelos físicos orientados al control para mejorar la estrategia de inyección de amoníaco. Se optimizaron dos escenarios, primero, un enfoque de referencia para la optimización off-line conociendo de antemano el ciclo de conducción, logrando así la máxima capacidad del sistema para reducir los NOx con el mínimo consumo de NH3. En segundo lugar, la optimización on-line mediante la técnica de control predictivo de modelos (MPC) con el objetivo de conseguir la máxima reducción de NOx con un deslizamiento de NH3 aguas abajo del catalizador ASC inferior a un límite preestablecido.

Todos los modelos desarrollados y los enfoques propuestos se implementaron en un banco de pruebas totalmente instrumentado y se validaron experimentalmente, alcanzando resultados satisfactorios en ambos enfoques, diagnóstico y control.

Resum

Per a complir els límits d'emissions imposats pels governs i reduir l'impacte negatiu en el medi ambient, l'ús de sistemes de posttractament (ATS) s'ha convertit en una cosa essencial per als motors de combustió interna.

Els ATS als trens motrius estan plantejats per a aconseguir una alta eficiència de reducció de contaminants en les condicions de funcionament dissenyades, per a això el sistema de control necessita conéixer el nivell de desgast del catalitzador, així com confiar en la informació de retroalimentació dels subsistemes dels ATS. A més, és possible augmentar la capacitat de reducció de contaminants dels catalitzadors mitjançant estratègies de control intel · ligents.

Davant aquest escenari, aquesta tesi pretén aplicar tècniques de monitoratge i diagnòstic per a garantir el ple funcionament de l'ATS, i estratègies de control òptim per a millorar la reducció de les emissions de NOx amb baix consum i lliscament de NH3.

Per a aconseguir aquest objectiu, s'han plantejat dos camins:

- Desenvolupament de models d'alta precisió per a la predicció de les emissions de NOx i NH3 acoblats a un algorisme de fusió de dades, sent aplicats per a diagnosticar el sistema en dos enfocaments específics: detecció del nivell de fallada d'injecció d'amoníac en l'ATS i estimació de l'estat d'envelliment del catalitzador del ASC.

- Ús de models físics orientats al control per a millorar l'estratègia d'injecció d'amoníac. Es van optimitzar dos escenaris, primer, un enfocament de referència per a l'optimització off-line coneixent per endavant el cicle de conducció, aconseguint així la màxima capacitat del sistema per a reduir els NOx amb el mínim consum de NH3. En segon lloc, l'optimització en línia mitjançant la tècnica de control predictiu de models (MPC) amb l'objectiu d'aconseguir la màxima reducció de NOx amb un lliscament de NH3 aigües avall del catalitzador ASC inferior a un límit preestablit.

Tots els models desenvolupats i els enfocaments proposats es van implementar en un banc de proves totalment instrumentat i es van validar experimentalment, aconseguint resultats satisfactoris en tots dos enfocaments, diagnòstic i control.

Abstract

To meet the emission limits imposed by governments and reduce the negative outcome on the environment, the use of after-treatment systems (ATS) has become essential for internal combustion engines.

The ATS in powertrains are devised to achieve high pollutant abatement efficiency under the design operating conditions, for which the control system needs to know the catalyst wear level as well as to rely on feedback information from the ATS subsystems. Furthermore, it is possible to increase the pollutant reduction capacity of catalysts through intelligent control strategies.

Looking at this scenario, this thesis intends to apply techniques of monitoring and diagnosis to guarantee the full operation of the ATS, and optimal control strategies to improve the reduction of NOx emissions with low NH3 consumption and slip.

To this aim, two paths were outlined:

- Development of high accuracy models for the prediction of NOx and NH3 emissions coupled with a data fusion algorithm, being applied to diagnose the system in two specific approaches: detection of the ammonia injection failure level in the ATS and estimation of the ASC catalyst ageing state.

- Use of physical control-oriented models to improve the ammonia injection strategy. Two scenarios were optimised, firstly a benchmark approach for off-line optimisation knowing in advance the driving cycle, thus achieving the maximum capacity of the system to reduce NOx with minimum NH3 consumption. Secondly, on-line optimisation through the model predictive control (MPC) technique aiming the maximum NOx abatement with NH3 slip downstream the ASC catalyst below a pre-established threshold.

All developed models and proposed approaches were implemented in a fully instrumented test bench and experimentally validated, reaching satisfactory results in both approaches, diagnosis and control.

Acknowledgment

I truly believe that this is the most important part of the whole thesis, as the work done here ends, but the small talks, laughs, and friendships made over the last four years remains. I would be a fool if I thought I can thank everyone who in any way helped in the development of this work, but I will take a shot at it and thank a few people who helped me not only in the development of the thesis, but in my life in Valencia.

There is no other way to start this acknowledgement than by thanking my friend and advisor, Benjamín Pla, who without help this thesis would not have been possible. It has always been clear to me that if I ever wanted to become a good researcher, I had to be surrounded by the best, and I have no doubt that Benja is one of the brightest and most supportive people I have had the pleasure to work alongside. There is a Jewish saying "Cover yourselves with the dust of your rabbi's feet", and in those four years that's what I tried my best to do, to be as close as possible to my tutor and absorb all the teachings and advice. Benja, thank you for guiding me through this difficult journey of transforming a student into a researcher, thank you for helping me the (endless) times I was in doubt or lost, and thank you for your kindness the (countless) times I missed deadlines or needed help. It has been an immeasurable pleasure to conduct research with you!

I would also like to thank Carlos Guardiola, who has always been the most smiling person in the office and initially gave me the opportunity to do my PhD studies. Also a special thanks to Pedro Piqueras, who in the last few years has helped me at several moments, either with advice or (adding) work.

I believe I was one of the few students who was lucky enough to have an almost private engine to conduct experimental tests, and extra luck to share such a task with amazing technicians. Tony, who was always there for me the many times I needed help with equipment. Vicenton, who I do not have words to thank for all the help, which I'm sure were countless. Besides saving me several times, made the wait between one test and another less tedious, listening to my complaints or talking about life. Guys, thank you so much for everything, the development of this thesis would be much harder without you.

I would like to extend my gratitude to the CMT direction that gave me the opportunity to conduct my doctoral study. Also to the secretariat, especially Amparo, who was always willing to help in any way necessary.

I could not fail to mention TNO and all the people I had the pleasure to meet there. Frank Kupper, Rob, Thomas, Avedis, Erik, Maarten, Ruud, Robinson, Niels and all the Traffic and Transportation team, especially Prof. Frank Willems, who is one of the brightest and kindest person I have ever had the privilege to work with. Thank you for the many coffees and conversations, without a shadow of a doubt my time in the Netherlands was an immeasurable experience.

Of course, a student's life would be boring and sad without companions to share it with, and in this point, I can't complain, once I had amazing friends to count on. Alexandra, Álvaro, Alvin, Irina, Elena, Rafa, Varun, and now professors Enrique and Pau. Thanks for all the almuerzos, trucos, office chats, laughs and reflections, my days as a student would not be the same without your company.

For a foreign student it is always difficult to be away from home, and in this respect, I was fortunate to have a bit of Brazil here. To my long-time friends Augusto, Cassio, Diego, Douglas, Felipe, Jacson, Rafael, Vitor, and Santiago (the most Brazilian Uruguayan in the world), thank you for being home, I have already said and repeat that these last years would be impossible without your friendship, love you guys.

If home is the place where we find family, I can say that Valencia is home thanks to the countless friends I have gained in my local church, my connection group, and the EnVivo organization, but especially to Josué and Marina, who in these last years have been the family of my family in Valencia, thank you for being here for Dani and me.

To my father's family who have always cared for me, as well as my in-laws, Meri and Sandro, for being a point of refuge and always willing to help, these four years were calmer knowing that you would be there for anything.

To my parents, who unfortunately are no longer here to see the fruit of their work; however, I would like to put on record my gratitude for the teachings, sacrifice, and unconditional love, this achievement is more yours than mine. To my brother and sister. Mauricio, who in the last few years has been my dad, my mom, and my best friend, knowing that you would be there in any situation kept me on track. Jessica, who always had a word of encouragement and was there for me whenever I needed. I love you both and thank you for always believing in me.

No great achievement is possible alone, so I share it with the person who made this thesis as hers, my beloved wife Dani. Who spared no effort to endure the endless complaints, insecurities, and absence, always with a smile and a word of wisdom. Dani, this thesis is the result of your care and love, and no accomplishment would be worth it without you by my side. Thank you for everything, I love you to the moon and back.

And last and most important, Jesus Christ, who helped, cared for, and lifted me up when I didn't even believe it myself. To you is the reason of everything and all my gratitude.

Contents

Glossary

δ_{gas}	Gas Density
$\eta_{\text{NO}_\text{x}}$	SCR NOx Conversion Efficiency
$\overline{\eta_{\text{NO}_\text{x}}}$	Average SCR NOx Conversion Efficiency
Ω_{NH_3}	Maximum Ammonia Storage Capacity
θ_{NH_3}	Surface Coverage Fraction
$\theta^*_{\text{NH}_3}$	Critical Surface Coverage
τ	Prediction Horizon
θ_{NH_3}	Ammonia Stored
ζ_{SCR}	SCR Volume Open Portion
ACR	Ammonia Coverage Ratio
AWS	Accumulation Window Size
C	Centroid
C	Constant
$\text{C}_\text{p}\text{T}_{\text{in}}$	Specific Input Enthalpy
$\text{C}_\text{p}\text{T}_{\text{out}}$	Specific Output Enthalpy
E_{ads}	SCR Adsorption Activation Energy
E_{des}	SCR Desorption Activation Energy
E_{fst}	Fast SCR Activation Energy
E_{slw}	Slow SCR Activation Energy
E_{std}	Standard SCR Activation Energy
$\hat{\text{e}}_\text{k}$	Residual Measurement
F_k	Jacobian of the State
H_k	Jacobian of the Observation
hA	Transfer Between the Cell and Environment
J	Cost Function
$\mathcal{J}$	Cost-To-Go
k_{ads}	SCR Adsorption Frequency Factor
k_{des}	SCR Desorption Frequency Factor
k_{fst}	Fast SCR Frequency Factor
k_{slw}	Slow SCR Frequency Factor
k_{std}	Standard SCR Frequency Factor
K	Constant
K	Near-Optimal Gain
$\underline{\text{K}_{\text{CS}}}$	NOx Sensor Cross-Sensitivity
$\overline{\text{K}_{\text{CS}}}$	Average Sensor Cross-Sensitivity
K_k	Kalman Gain

k_{stch}	Stoichiometric Constant
M	Mass of the Gas in the Sensor Cell
$\dot{m}_{exh}$	Exhaust Mass Flow
$\dot{m}_{in}$	Flow Entering the Sensor Cell
$\dot{m}_{out}$	Flow Leaving the Sensor Cell
n	Number of Elements Allocated in Memory
n_t	Discretization of the Prediction Horizon
n_x	Discretization of the States
N_u	Number of Control Variables
N_x	Number of System States
NH_3	Ammonia Concentration
$\overline{NH_3}$	Average Ammonia Slip
$NH_{3,adsorbed}$	Amount of Ammonia Adsorbed
$NH_{3,ANN}$	NH3 slip Artificial Neural Network
$NH_{3,desorbed}$	Amount of Ammonia Desorbed
$NH_{3,ds}$	Ammonia Slip
$NH_{3,injected}$	Ammonia Injected Into the SCR Catalyst
$NH_{3,oxidised}$	Amount of Ammonia Oxidised
NO_{ds}	Nitrogen Oxide Downstream Catalyst
NO_{us}	Nitrogen Oxide Upstream Catalyst
$NO_{2,ds}$	Nitrogen Dioxide Downstream Catalyst
$NO_{2,us}$	Nitrogen Dioxide Upstream Catalyst
NO_x	NOx Concentration
$\underline{NO_x}$	NOx slip
$\overline{NO_x}$	Average NOx Slip
$NO_{x,ANN}$	NOx slip Artificial Neural Network
$\underline{NO_{x,sensor}}$	NOx Sensor Signal
$\overline{NO_{x,sensor}}$	Average NOx Sensor Signal
$\underline{NO_{x,ds,sensor}}$	NOx Sensor Signal Downstream Catalyst
$\overline{NO_{x,ds,sensor}}$	Average NOx Sensor Signal Downstream Catalyst
$NO_{x,us}$	NOx Upstream of the SCR
$\underline{NO_{x,us,sensor}}$	NOx Sensor Signal Upstream Catalyst
$\overline{NO_{x,us,sensor}}$	Average NOx Sensor Signal Upstream Catalyst
$NO_{x,us}^{thr}$	NOx SCR Upstream Threshold
P_k	Observer Covariance
Q_k	Process Covariance
r_{ads}	NH3 SCR Adsorption Reaction Rate
r_{des}	NH3 SCR Desorption Reaction Rate
r_{fst}	Fast SCR Reaction Rate
r_{slw}	Slow SCR Reaction Rate
r_{std}	Standard SCR Reaction Rate
R	Universal Gas Constant
R_k	Measurement Covariance
S_k	Residual Covariance
SV	Spatial Velocity
t	Time
T_{cell}	Temperature Inside the Sensor Cell
T_{ref}	Reference Temperature
T_{SCR}	SCR Catalyst Temperature

u	Control Variables
V	SCR Volume
w	Noise
x	System State
$\hat{x}$	State Observer
y	Sensor Reading
$\hat{y}$	Observer Estimation of the Sensor Reading

Acronyms

0D	zero-dimensional
2RTS	Twice Standardised Random Test
ACR	Ammonia Coverage Ratio
ANN	Artificial Neural Network
ASC	Ammonia Slip Catalyst
ATS	After-Treatment Systems
AWS	Accumulation Window Size
Ce	Cerium
CI	Compression-Ignition engine
CO	Carbon Monoxide
CO2	Carbon Dioxide
CSTR	Continuously Stirred Tank Reactor
DEF	Diesel Exhaust Fluid
deNOx	Denitrification
DM	Direct Method
DOC	Diesel Oxidation Catalyst
DoE	Design of Experiments
DP	Dynamic Programming
DPF	Diesel Particulate Filter
ECU	Electronic Control Unit
EKF	extended Kalman Filter
EMF	Electromagnetic Field
ESC	European Steady-State Cycle
ETC	European Transient Cycle
FMEA	Failure Mode and Effects Analysis
FTA	Fault Tree Analysis
FTIR	Fourier Transform Infrared
GHG	Greenhouse Gases
HC	Hydrocarbon
HC-SCR	Hydrocarbon-Selective Catalytic Reduction
HIL	Hardware-In-the-Loop
HP-EGR	High Pressure Exhaust Gas Recirculation
I.F.	Injection Factor
ICE	Internal Combustion Engines
IEA	International Energy Agency
IPCC	Intergovernmental Panel on Climate Change

K_{CS}	Sensor cross-sensitivity
KF	Kalman Filter
LNT	Lean NOx Trap
MIL	Malfunction Indicator Light
MPC	Model Predictive Control
MRAC	Model Reference Adaptive Controller
NASA	National Aeronautics and Space Administration
NDC	New Driving Cycle
Ni	Nickel
NLP	Non-Linear Programming
NO	Nitric Oxide
NO2	Nitrogen Dioxide
NOx	Nitrogen Oxide
OBD	On-Board Diagnostics
OCP	Optimal Control Problem
ODE	Ordinary Differential Equations
PEMS	Portable Emissions Measurement System
PID	Proportional, Integral and Derivative
PM	Particulate Matter
RDE	Real Driving Emissions
RNN	Recurrent Neural Network
RTI	Real-Time Interface
SCR	Selective Catalytic Reduction
SCRF	Selective Catalytic Reduction Filter
SI	Spark-Ignition engine
SSA	Sensor signal analysis
VGT	Variable Geometry Turbine
WLTC	Worldwide harmonized Light vehicles Test Cycles
WLTP	Worldwide harmonized Light vehicles Test Procedures
WVTA	Whole Vehicle Type Approval

Part I

Thesis overview

Chapter 1

Introduction

The mystery of human existence lies not in just staying alive, but in finding something to live for.

— Fyodor Dostoyevsky

Contents

1.1 Background

It is impossible to imagine a society without engines, today there are around two billion internal combustion engines (ICE) in use around the world [1]. For most daily activities ICE are used, from powering our many vehicles, to industrial production and electricity generation. Since its invention in 1876, when Nicolaus Otto invented the spark-ignition (SI) engine, and 1892 Rudolf Diesel developed the compression-ignition (CI) engine [2], ICE has been demanded in the most diverse areas and applications. Over time new technologies have appeared and our understanding of how engines work has

increased, leading to an improvement in engine performance and reliability [3]. However, with growing demand, market and regulatory requirements have become more stringent as well.

One of the main concerns of the use of ICE powered by fossil fuels is the emissions of greenhouse gases (GHG), which in turn are the main drivers of greenhouse effect [4, 5]. The advent of global warming, has led countries and their governments to adopt drastic measures to mitigate its devastating impacts, paralleled by a social common sense demanding lower levels of pollution, a tightening of emission limits and a desire of the governments to transition to zero emissions vehicles, thus forcing a rapid development of better engines, fuels, and efficient alternative approaches to deal with these pollutant emissions.

It is widely known that the increase in global temperature is a consequence of GHG emissions in the atmosphere [6,7], whereby carbon dioxide (CO2) is the main GHG emitted by human activities, approximately 79% [8]. According to National Aeronautics and Space Administration (NASA) data (Figure 1.1), global surface temperature and the CO2 concentration in the Earth's atmosphere have increased substantially over the past few years [**?**, 9].

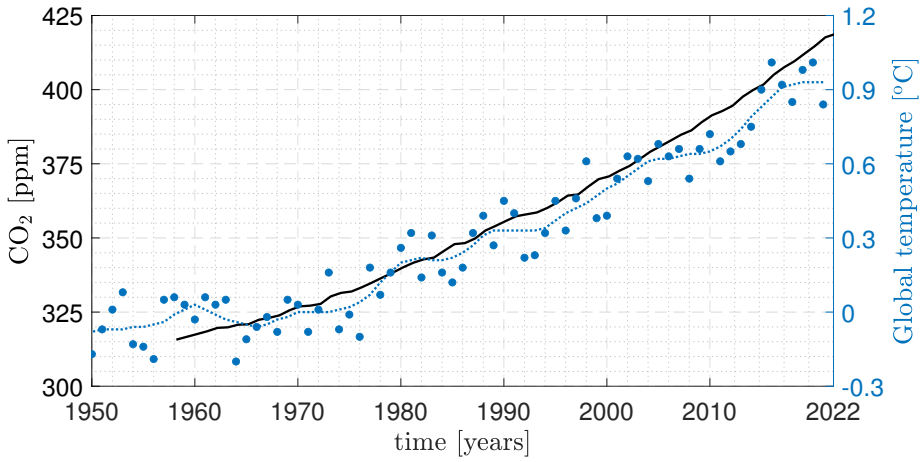

Figure 1.1: CO2 concentration in the Earth's atmosphere between 1958 and 2022 (dark line) and global surface temperature between 1950 and 2021 (dots: annual mean; dotted line: trend line). Data extracted from [**?**].

As can be seen, the increase in global temperature and CO2 are highly correlated. Between the years 1960 and 2020, CO2 concentration in the atmosphere increased by 23.9% while the earth's surface warmed by 1.01 °C. This temperature change has already impacted various aspects of the climate

system, however, at progressively higher levels of global warming, there are greater consequences, as shown in Figure 1.2.

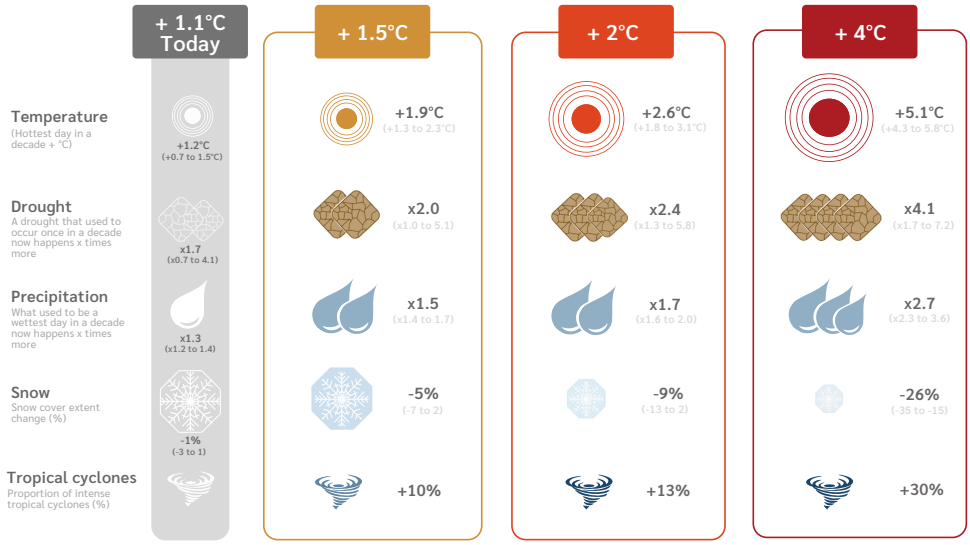

Figure 1.2: Impact of increasing global surface temperature on weather patterns. Data extracted from [10].

According to the 2021 climate change report by the Intergovernmental Panel on Climate Change (IPCC) [10], the increase in global temperature has several consequences such as, a greater frequency of drought and rainy seasons, more intense tropical cyclones, and a reduction in snow cover extent. Thus, collaborative global strategies must be designed and implemented to reduce the current very high levels of GHG emissions and avoid such shifts [11].

Several sectors and processes are responsible for the escalating levels of global emissions. However, the energy sector has the largest share, accounting for about 73% of GHG emissions released into the atmosphere in 2021 [12], this percentage can be justified due to the significant increase in world energy consumption. Figure 1.3 presents the evolution of world energy consumption by sector over the last 70 years and the significant participation of the transport one [13], as well as the forecast of energy demand by fuel on "Net-Zero Emissions by 2050 Scenario", which outlines the changes that must be made in mix and energy demand for the world to achieve net zero CO2 emissions by 2050 [14], thus limiting the global temperature rise to 1.5 °C.

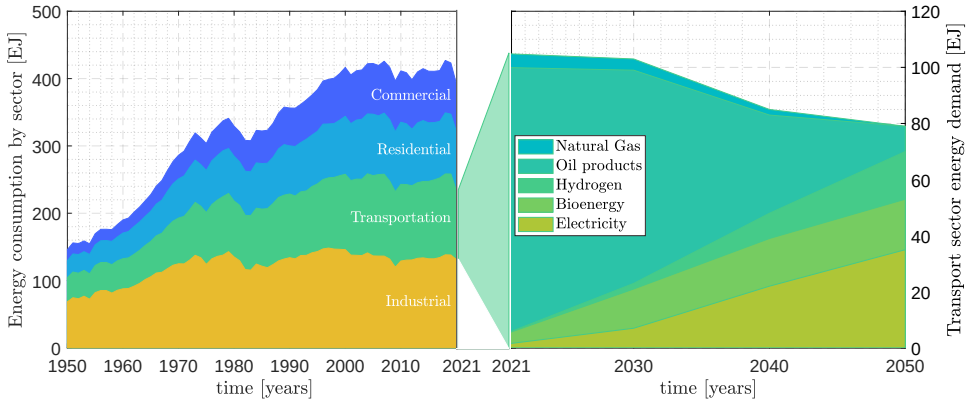

Figure 1.3: World energy consumption by source and transport sector energy demand by fuel in the NZE. Source: adapted from BP Statistical Review of World Energy and IEA Net zero by 2050. Data extracted from [13, 14].

Analysing Figure 1.3, it is possible to see that the evolution of energy consumption by the transport sector followed the same increasing trend of other essential sectors, being supplied mainly by fossil fuels (almost 90%) [15]. Looking to the future scenario, the International Energy Agency (IEA) has devised a plan to achieve zero net CO2 emissions by 2050, where the structure of the world's energy matrix must be drastically changed, however, even in this scenario not favourable to fossil fuels they have a relevant role, with a 47.2% share in 2040 and 11.4% in 2050 [14].

With the same thought of mitigating the impact of pollutant gas emissions in the atmosphere, initiatives have been implemented since the 1960s [16], with the first automobile emissions standards enacted in 1963 in the United States, primarily as a reaction to the smog problems in Los Angeles [17]. Emission standards define the allowed quantitative limits of specific pollutants that can be released within specific timeframes. Usually they are designed to meet air quality standards and protect human life, with different standards depending on regions and countries, some examples are presented in Figure 1.4.

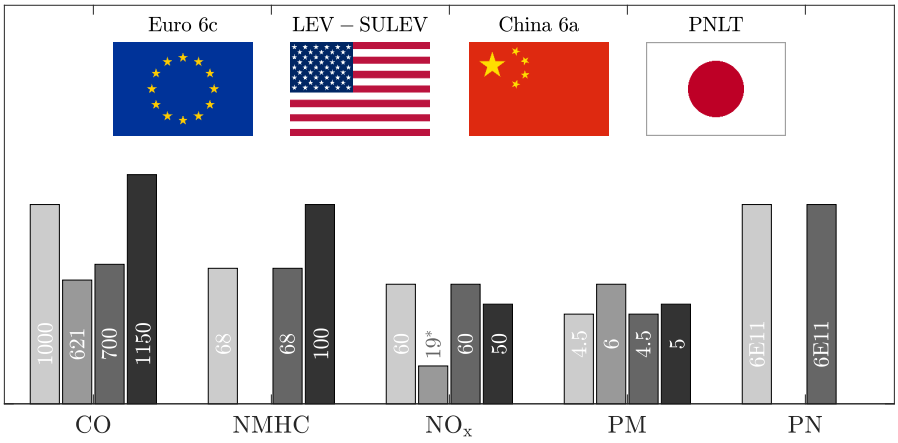

Figure 1.4: Emission limit standards for the European Union, United States, China, and Japan (mg/km; PN/km). $* = \text{NMOG} + \text{NO}_\text{x}$

Similar emission standards are applied in other countries of the world, in India the legislation in force BS VI is equivalent to Euro 6, as well as in the case of Brazil, the Proconve L8 that is in the implementation phase.

Currently, the verification of vehicle emission rates is done through the Whole Vehicle Type Approval (WVTA), where emissions are measured in a laboratory test cycle Worldwide harmonized Light vehicles Test Procedures (WLTP) [18]. To ensure that there is no cheating and a minimal difference between laboratory testing and real driving conditions, the vehicles are additionally submitted to Real Driving Emissions (RDE) cycles where the car is driven outdoors in random patterns of acceleration and deceleration and their emissions measured using Portable Emissions Measurement System (PEMS) [19].

1.2 Engine emissions and control

As discussed, when it comes to ICE, pollutant emissions are an important topic, for diesel engines even more after the dieselgate scandal [20, 21]. Due to intrinsic combustion process, CI engines emitted high levels of nitrogen oxide (NOx) and particulate matter (PM). However, owing to several reasons, as fuel power density, low operation costs and high thermal efficiency, they are still the most suitable as a power source in the transportation field, marine carriers, and heavy-duty vehicles [22, 23]. The main pollutants produced by the diesel combustion are next described:

- Nitrogen Oxide (NOx) – NOx is mainly composed by nitric oxide (NO) and nitrogen dioxide (NO2), and its formation is due to the high temperature and lean conditions inside the combustion chamber. NOx emissions are responsible for acid rain and smog, also the human exposure to the NO2 gases can leads to respiratory diseases [24].

- Particulate Matter (PM) – is formed by the agglutination of several small particles, whose are mainly composed by carbon, unburned fuel, unburned lubrification oil, ash, sulphates, and water, with a common diameter range of 14-55 nm. PM is responsible for air, water, and soil health contamination, as well as human health problems [25].

- Carbon Monoxide (CO) – it is a result of incomplete combustion in operation with rich mixture, thus being a problem more related with spark ignition engines, that may run on fuel-rich at high loads and accelerations. It is a colourless, odourless, and flammable gas, being dangerous as it is an asphyxiating gas that can lead to intoxication or death [26].

- Carbon Dioxide (CO2) – is the result of complete combustion. CO2 is considered minimally toxic by inhalation, in high concentrations it can cause mental confusion, increased heart pressure, and in extreme cases death by suffocation [2].

- Hydrocarbon (HC) – is related to incomplete combustion of hydrocarbon fuel, typically used to measure combustion efficiency. The level of unburned hydrocarbons for SI engines are typically 1 to 2% of the fuel, while for CI are much lower. The toxic effect depends on the molecular structure, and its simultaneous presence with NOx and ultraviolet rays are responsible for the photochemical smog [27].

Since the emissions control become an important issue to be addressed, over the years new technologies were developed to achieve the imposed standards [28]. Figure 1.5 presents the evolution of the EURO limits and the respective common solution adopted by the industry [29].

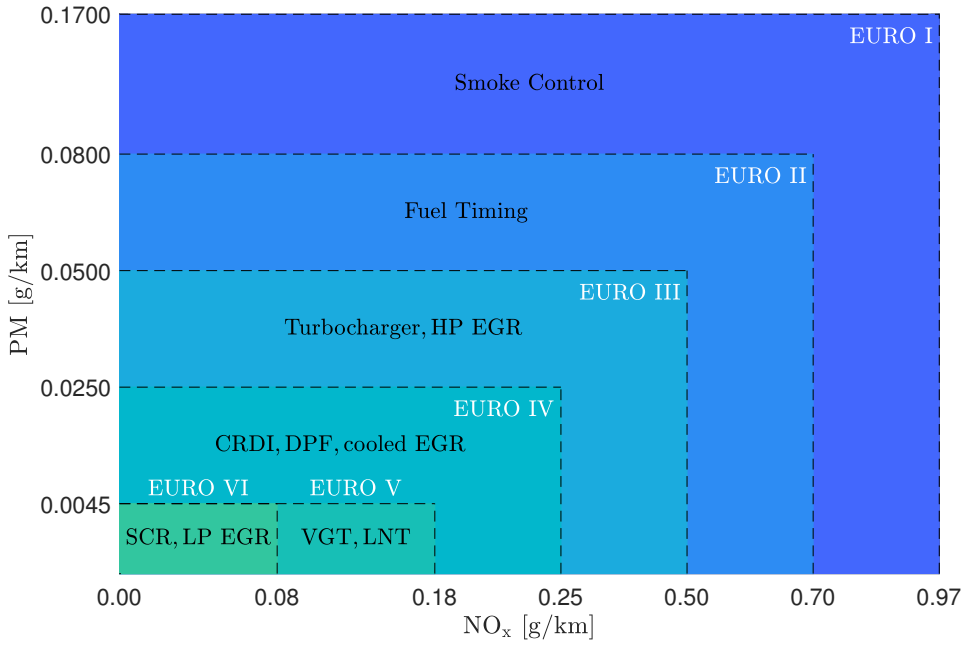

Figure 1.5: Incremental emission standards with corresponding diesel technology adopted popularly to fulfil. Adapted from [29].

Even with the huge effort to reduce the emissions by improving the engine design, thermal efficiency, new combustion process, etc. engine raw emissions are still too high to achieve the emissions targets without the use of after-treatment systems (ATS), leading them to play a main role in abatement of engine pollutants [30].

1.2.1 After-treatment systems

Achieving the required emission limit levels is a challenging task, and it is unfeasible to do so without the use of ATS on an industrial scale [31, 32]. In a diesel engine the ATS layout is mainly composed by the following treatment systems:

- Diesel Oxidation Catalyst (DOC) – Their functionality is to oxidise the HC and CO species in the exhaust gas. After light-off, at around 100 °C, the efficiency of the catalyst is almost 90%. DOCs are simple, inexpensive, and maintenance-free, having as a point of concern the possible increase in the NO2 fraction of the total NOx emissions, with the amount produced depending on the catalyst formulation [33].

- Diesel Particulate Filter (DPF) – Captures and retains soot particles from the exhaust gases. The trapped particles are burned either by passive regeneration through soot oxidation with NO2 (to this aim, the NO2 production is usually promoted in a DOC upstream the DPF), or by active regeneration increasing the exhaust temperature through post injections or injecting fuel into the exhaust pipe [34].

- Selective Catalytic Reduction (SCR) – It is one of the most widespread devices for emission after-treatment in diesel engines. In the SCR system, the injected urea is converted into ammonia by hydrolysis and thermolysis, and then the NOx reacts with the ammonia activated by the catalyst. In theory, higher concentrations of ammonia in the catalyst lead to better NOx conversion. However, not all ammonia is adsorbed by the catalyst surface, and the excess is released into the atmosphere as an additional contaminant [35].

- Ammonia Slip Catalyst (ASC) – The catalyst has basically the same reactions and functionalities as the SCR catalyst. The ASC adsorbs the ammonia released by the SCR catalyst, using it to oxidise NOx emissions and avoiding excessive ammonia slip [36, 37].

1.2.2 After-treatment monitoring

The ATS system in normal operation is extremely capable of converting pollutants into non-harmful gases. However, over time, the converters age and peripheral systems can malfunction, leading to inefficient operation. Currently, the use of ATS is mandatory, as well as its monitoring. The control is performed from on-board diagnostics (OBD) systems that provide self-diagnostic functionality built into the engine control system, which includes detecting malfunction, storing a trouble code, and activating the malfunction indicator light (MIL) [38].

1.3 Scope of the work

To achieve future emission standards, it is necessary, at the same time, improve the performance of the ATS and ensure its correct operation. Therefore, this work aims to present a methodology to improve the NOx conversion efficiency of the SCR and ASC catalyst minimising ammonia slip, as well as propose a methodology to diagnose the ammonia injection failure and catalyst ageing.

The work was divided into four main steps:

- Use of an off-line zero-dimensional model to assess the maximum enhancement capability of ATS.
- Development of control-oriented models combined with the extended Kalman filter data-fusion technique to accurate estimate NOx and NH3 emissions in real driving conditions.
- Through the models developed previously and with the use of statistical models evaluate the level of failure in the ammonia injection system and the ageing state of the catalyst.
- Application of the zero-dimensional model with reduced states in an on-line model predictive control aiming to optimise ammonia injection into the SCR catalyst reducing NOx and NH3 emissions downstream of the ASC catalyst.

1.4 Objectives

This dissertation aims at proposing a new approach to improve the abatement of NOx and NH3 emissions, particularly on the control and diagnosis side. The approaches are proposed in three main branches: development of accurate computational models for NOx and NH3 emission prediction, improvement of ammonia injection control strategy and ATS monitoring and diagnostics. On the control side, pursue the maximum reduction of NOx emissions with the lowest NH3 slip, including situations of abnormal ATS operation, in the case of monitoring and diagnostics, detect possible failures in the ammonia injection system and the ageing state of the catalyst. The overall objective can be identified through the following partial objectives.

- Development of control-oriented models (physical and data-driven models) of SCR and ASC catalyst to estimate NOx and NH3 emissions. Aiming to understand the catalyst behaviour and reactions, as well as the complexity level of the system for further optimisation (Chapter 5).
- Use of observers, such as extended Kalman filter, combined with different control-oriented models aiming to increase the accuracy of NOx and NH3 emission prediction even under conditions of ammonia injection system failure and catalyst ageing (Chapter 6).
- Optimal control using a zero-dimensional model in a previously known cycle, thus presenting a benchmarking of the maximum performance that the system is capable to achieve (Chapter 7).

- Real-time optimal control aiming at the highest NOx emission reduction without exceeding a NH3 slip threshold. The strategy controls the amount of ammonia injected and uses the zero-dimensional model with reduced states embedded in a model predictive control (MPC) approach. (Chapter 7).

1.5 Thesis organization

The thesis is structured in four parts. The first (Part I) presents an overview of the current scenario in terms of pollutants, regulations and approaches to control and monitor ICE emissions. The second part (Part II) is related to the experimental set-up and the tests performed, followed by Part III which deals with the developed methodology and the proposed approaches applied during the development of the thesis. Finally, in the last part (Part IV) the conclusion and the results of the work are discussed. A further breakdown of the sections is outline below.

To achieve the presented objectives, the thesis is composed of eight chapters. The Chapter 1 has presented an overview of the current global scenario of energy demand an future prospection for the transportation one, as well as its contribution to GHG production. Engine emissions, government regulations and ATS for their control were briefly introduced as well.

Chapter 2 outlines the state-of-the-art of zeolite-based SCR and ASC catalysts, as well as the diagnostic and monitoring system.

Chapter 3 describes the experimental set-up used for the development of the thesis. In all set-ups the same engine and hardware-in-the-loop structure were used, with the difference only in the ATS. (I) SCR; (II-a) SCR+ASC aged; (II-b) SCR+ASC partially aged; (II-c) SCR+ASC new. Specification and position of the pollutant measurement systems are also provided.

Chapter 4 presents in detail the procedures and the test campaign carried out for the development of the thesis. Each test consists of the pre-conditioning of the engine and the ATS, definition of the ammonia injection strategy and the cycle to be performed.

Chapter 5 introduces the physical and data-driven control-oriented models for the estimation of NOx and NH3 emissions:

- Zero-dimensional model - development of a zero-dimensional physical model of the SCR catalyst, as well as a version with reduced states and extended to the SCR+ASC catalyst.

- Artificial neural network - data analytics-based model which seeks to reconstruct the underlying catalyst relationships through the interpretation

of a dataset.

- Sensor signal analysis - data analytics-based model that uses the information stored in a time-window to estimate the NOx conversion efficiency of the ATS.

- Extended Kalman filter - implementation of the data fusion technique aiming to increase the emission estimation accuracy of the data analytics-based models.

Chapters 6 and 7 present the tools developed for diagnostics, and optimisation of the ATS, as well as their use embedded in the previously proposed models. Chapter 6 deals with control and diagnosis of the ammonia injection system in failure situations, and detection of the ageing state of the ASC catalyst. While chapter 7 presents two approaches to improve the ammonia injection strategy, an optimal control problem (OCP) design and model predictive control.

Finally, conclusions and future work are introduced in the last chapter (Chapter 8).

References

[1] Leach Felix, Kalghatgi Gautam, Stone Richard and Miles Paul. "The scope for improving the efficiency and environmental impact of internal combustion engines". *Transportation Engineering*, Vol. 1 n^o April, jun 2020. (cited in p. 3)

[2] Heywood John B. *Internal Combustion Engine Fundamentals*. McGraw-Hill Education, Cambridge, Massachusetts, second edition, 2018. (cited in pp. 3, 8, and 20)

[3] Sinigaglia Tiago, Eduardo Santos Martins Mario and Cezar Mairesse Siluk Julio. "Technological evolution of internal combustion engine vehicle: A patent data analysis". *Applied Energy*, Vol. 306, jan 2022. (cited in p. 3)

[4] Rosa William. *A New Era in Global Health*. Springer Publishing Company, New York, NY, jun 2017. (cited in p. 4)

[5] Ajanovic Amela and Haas Reinhard. "The impact of energy policies in scenarios on GHG emission reduction in passenger car mobility in the EU-15". *Renewable and Sustainable Energy Reviews*, Vol. 68, pp. 1088–1096, feb 2017. (cited in p. 4)

[6] Andress David, Nguyen T. Dean and Das Sujit. "Reducing GHG emissions in the United States' transportation sector". *Energy for Sustainable Development*, Vol. 15 n^o 2, pp. 117–136, jun 2011. (cited in p. 4)

[7] Arioli Magdala Satt, D'Agosto Márcio de Almeida, Amaral Fernando Gonçalves and Cybis Helena Beatriz Bettella. "The evolution of city-scale GHG emissions inventory methods: A systematic review". *Environmental Impact Assessment Review*, Vol. 80 n^o November 2019, jan 2020. (cited in p. 4)

[8] Charabi Y., Al Nasiri N., Al Awadhi T., Choudri B.S. and Al Bimani A. "GHG emissions from the transport sector in Oman: Trends and potential decarbonization pathways". *Energy Strategy Reviews*, Vol. 32, nov 2020. (cited in p. 4)

[9] Yuan Xueliang, Zhang Mofan, Wang Qingsong, Wang Yutao and Zuo Jian. "Evolution analysis of environmental standards: Effectiveness on air pollutant emissions reduction". *Journal of Cleaner Production*, Vol. 149, pp. 511–520, apr 2017. (cited in p. 4)

[10] Masson-Delmotte V., Zhai P., Pirani A., Connors S.L., Péan C., Berger S., Caud N., Chen Y., Goldfarb L., Gomis M.I., Huang M., Leitzell K., Lonnoy E., Matthews J.B.R., Maycock T.K., Waterfield T., Yelekçi O., Yu R. and Zhou B. "Climate Change 2021: The Physical Science Basis". Technical report, Cambridge University Press, Cambridge, England, 2022. (cited in p. 5)

[11] Sreekanth K.J. "Review on integrated strategies for energy policy planning and evaluation of GHG mitigation alternatives". *Renewable and Sustainable Energy Reviews*, Vol. 64, pp. 837–850, oct 2016. (cited in p. 5)

[12] Ritchie Hannah, Roser Max and Rosado Pablo. "CO2 and GHG emissions", 2020. (cited in p. 5)

[13] International Energy Agency (IEA). "Energy Statistics Data Browser", 2022. (cited in pp. 5 and 6)

[14] International Energy Agency (IEA). *Net Zero by 2050: A Roadmap for the Global Energy Sector*. OECD, 2021. (cited in pp. 5 and 6)

[15] Environmental Protection Agency. "Inventory of U.S. Greenhouse Gas Emissions and Sinks: 1990-2020". Technical report, 2022. (cited in p. 6)

[16] Vestreng V., Ntziachristos L., Semb A., Reis S., Isaksen I. S. A. and Tarrasón L. "Evolution of NOx emissions in Europe with focus on road transport control measures". *Atmospheric Chemistry and Physics*, Vol. 9 n^o 4, pp. 1503–1520, feb 2009. (cited in p. 6)

[17] Haagen-Smit A J. "The Control of Air Pollution". *Scientific American*, Vol. 210 n^o 1, pp. 24–31, 1964. (cited in p. 6)

[18] Hjelkrem Odd André, Arnesen Petter, Aarseth Bø Torstein and Sondell Rebecka Snefuglli. "Estimation of tank-to-wheel efficiency functions based on type approval data". *Applied Energy*, Vol. 276 n^o February, oct 2020. (cited in p. 7)

[19] Hooftman Nils, Messagie Maarten, Van Mierlo Joeri and Coosemans Thierry. "A review of the European passenger car regulations – Real driving emissions vs local air quality". *Renewable and Sustainable Energy Reviews*, Vol. 86 n^o January, pp. 1–21, apr 2018. (cited in p. 7)

[20] Bowen Melanie, Freidank Jan, Wannow Stefanie and Cavallone Mauro. "Effect of Perceived Crisis Response on Consumers' Behavioral Intentions During a Company Scandal – An Intercultural Perspective". *Journal of International Management*, Vol. 24 n^o 3, pp. 222–237, sep 2018. (cited in p. 7)

[21] Brand Christian. "Beyond 'Dieselgate': Implications of unaccounted and future air pollutant emissions and energy use for cars in the United Kingdom". *Energy Policy*, Vol. 97, pp. 1–12, oct 2016. (cited in p. 7)

[22] Xin Qianfan. "The analytical design process and diesel engine system design". In *Diesel Engine System Design*, pp. 3–112. Elsevier, 2013. (cited in p. 7)

[23] Ni Peiyong, Wang Xiangli and Li Hu. "A review on regulations, current status, effects and reduction strategies of emissions for marine diesel engines". *Fuel*, Vol. 279 n^o May, nov 2020. (cited in p. 7)

[24] Palash S.M., Masjuki H.H., Kalam M.A., Masum B.M., Sanjid A. and Abedin M.J. "State of the art of NOx mitigation technologies and their effect on the performance and emission characteristics of biodiesel-fueled Compression Ignition engines". *Energy Conversion and Management*, Vol. 76, pp. 400–420, dec 2013. (cited in p. 8)

[25] Wang Ying, Liu Hong and Lee Chia-Fon F. "Particulate matter emission characteristics of diesel engines with biodiesel or biodiesel blending: A review". *Renewable and Sustainable Energy Reviews*, Vol. 64, pp. 569–581, oct 2016. (cited in p. 8)

[26] Chenoweth James A., Albertson Timothy E. and Greer Matthew R. "Carbon Monoxide Poisoning". *Critical Care Clinics*, Vol. 37 n^o 3, pp. 657–672, jul 2021. (cited in p. 8)

[27] Matula R A. *Mechanism of Hydrocarbon Formation in Combustion Processes*, pp. 77–151. Springer US, Boston, MA, 1973. (cited in p. 8)

[28] Asghar Usama, Rafiq Sikander, Anwar Adeel, Iqbal Tanveer, Ahmed Ashfaq, Jamil Farrukh, Khurram M. Shahzad, Akbar Majid Majeed, Farooq Abid, Shah Noor S. and Park Young-Kwon. "Review on the progress in emission control technologies for the abatement of CO2, SOx and NOx from fuel combustion". *Journal of Environmental Chemical Engineering*, Vol. 9 n^o 5, oct 2021. (cited in p. 8)

[29] Velmurugan Dhinesh Vilwanathan. *Supervisory control of complex propulsion subsystems*. PhD Thesis, Chalmers University of Technology, 2022. (cited in pp. 8 and 9)

[30] Ayodhya Archit Srinivasacharya and Narayanappa Kumar Gottekere. "An overview of after-treatment systems for diesel engines". *Environmental Science and Pollution Research*, Vol. 25 n^o 35, pp. 35034–35047, dec 2018. (cited in p. 9)

[31] Reşitoğlu İbrahim Aslan, Altinişik Kemal and Keskin Ali. "The pollutant emissions from diesel-engine vehicles and exhaust aftertreatment systems". *Clean Technologies and Environmental Policy*, Vol. 17 n^o 1, pp. 15–27, jan 2015. (cited in p. 9)

[32] Beatrice Carlo, Rispoli Natale, Di Blasio Gabriele, Konstandopoulos Athanasios G., Papaioannou Eleni and Imren Abdurrahman. "Impact of Emerging Engine and After-Treatment Technologies for Improved Fuel Efficiency and Emission Reduction for the Future Rail Diesel Engines". *Emission Control Science and Technology*, Vol. 2 n^o 2, pp. 99–112, apr 2016. (cited in p. 9)

[33] Russell April and Epling William S. "Diesel Oxidation Catalysts". *Catalysis Reviews*, Vol. 53 n^o 4, pp. 337–423, oct 2011. (cited in p. 9)

[34] Khair Magdi K. "A Review of Diesel Particulate Filter Technologies". In *SAE Technical Papers*, number 724, jun 2003. (cited in p. 10)

[35] Han Lupeng, Cai Sixiang, Gao Min, Hasegawa Jun-ya, Wang Penglu, Zhang Jianping, Shi Liyi and Zhang Dengsong. "Selective Catalytic Reduction of NO x with NH 3 by Using Novel Catalysts: State of the Art and Future Prospects". *Chemical Reviews*, Vol. 119 n^o 19, pp. 10916–10976, oct 2019. (cited in p. 10)

[36] Guan Bin, Zhan Reggie, Lin He and Huang Zhen. "Review of state of the art technologies of selective catalytic reduction of NOx from diesel engine exhaust". *Applied Thermal Engineering*, Vol. 66 n^o 1-2, pp. 395–414, may 2014. (cited in pp. 10, 70, 95, and 135)

[37] Zhang Yunhua, Lou Diming, Tan Piqiang, Hu Zhiyuan and Fang Liang. “Effect of SCR downsizing and ammonia slip catalyst coating on the emissions from a heavy-duty diesel engine”. *Energy Reports*, Vol. 8, pp. 749–757, nov 2022. (cited in pp. 10 and 135)

[38] Posada Francisco and German John. “Review of Ldv Obd Requirements Under the European , Korean and Californian Emission Programs”. Technical Report March, 2016. (cited in p. 10)

Chapter 2

State of the art: Emissions control and monitoring

The future will be green or not at all.

— Jonathon Porritt

Contents

2.1 Introduction

The control and monitoring systems are designed to ensure the proper operation of the engine, also guaranteeing that the emissions level does not exceed the established thresholds. To this end, airpath, after-treatment

and fuel systems, among other subsystems must be carefully controlled and monitored [1]. Regarding the ATS it is composed by the catalysts, sensors, and peripheral systems as reductant agent unit, while its architecture may have several arrangements, either in terms of catalysts or sensors. In the current work, four different combinations were used, which are described in detail in the following chapter.

Many works have been developed in the past few years related to diesel engines. Figure 2.1 presents the bibliometric network analysis of twelve thousand most relevant articles on diesel engines according to the Web of Science database [2], where it is possible to verify three main areas of research: combustion process (red cluster), pollutant emissions (blue cluster) and ATS (green cluster). Furthermore, elucidates the importance of treating NOx and NH3 emissions.

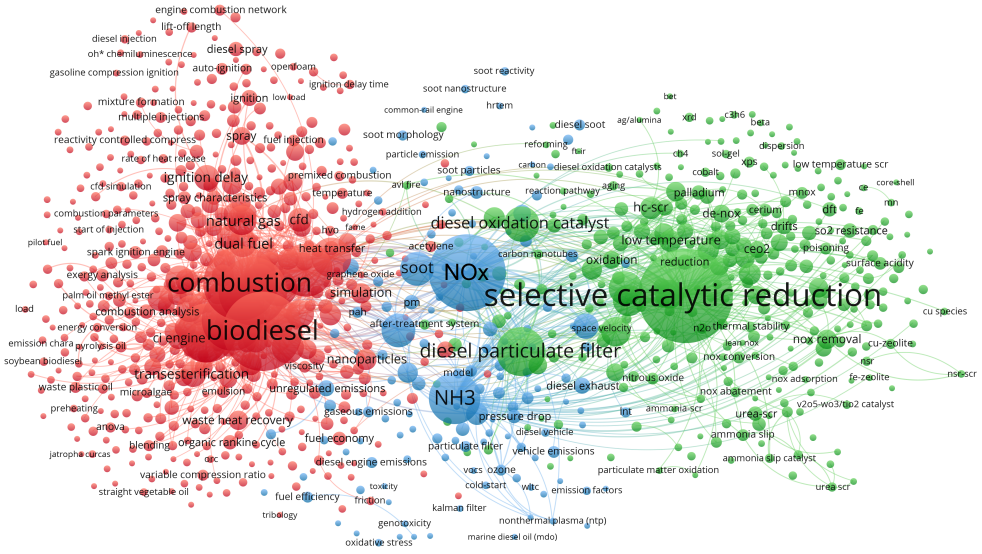

Figure 2.1: Bibliometric network analysis of the author's keywords of the fourteen thousand most relevant articles on diesel engines according to the Web of Science database. Each colour represents a cluster, and the lines are connected to co-related words.

For the analysis, authors' keywords were used. Thus, the size of the spheres is related to the number of occurrences and the lines connect co-related terms, in this way it is possible to visualize the main issues addressed by the academia when it comes to diesel engines.

According to the same database, research works related to ATS developed in the last decade were, approximately, 650 about DOC, 800 about DPF, 4700

about SCR and 100 about ASC. Figure 2.2 presents the bibliometric analysis of 6307 articles with the authors' most recurrent keywords for each ATS type.

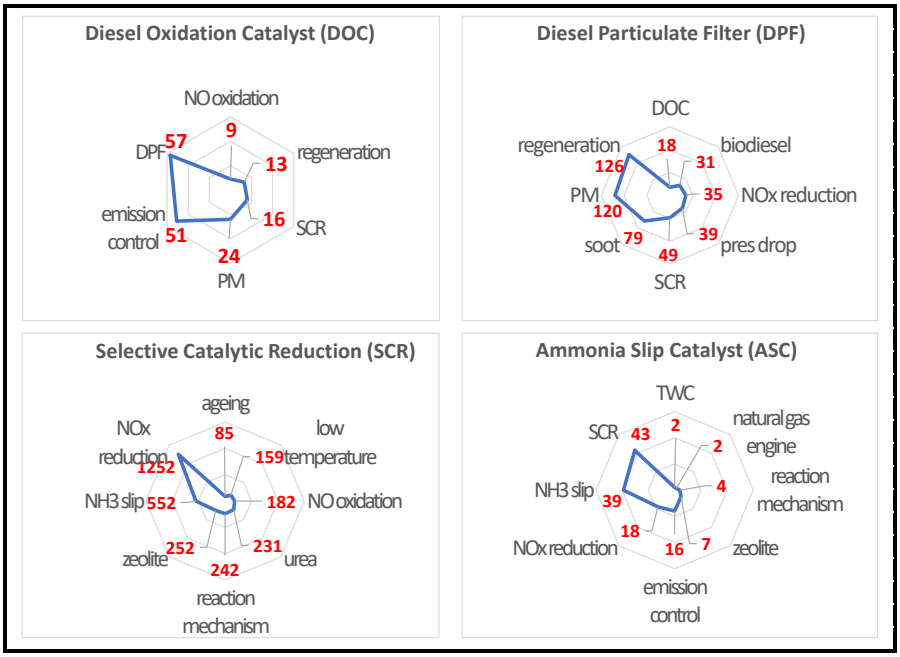

Figure 2.2: Bibliometric analysis of the top four diesel engine ATS, evaluating the author's most relevant keywords from 6307 articles on diesel ATS.

These analyses highlight efforts made to improve SCR catalysts, and more specifically, addressed to NOx and NH3 emission reduction. On the other hand, they show a broad field of research available aimed to develop and improve the ASC catalyst, and that there is still great interest in improving the SCR catalyst performance.

2.2 Selective catalytic reduction

The SCR catalyst is the main after-treatment in diesel engines to abate emissions [3], as it is able to reduce NOx by up to 95% [4], and can also be coupled with a DPF (usually called SCRF) to achieve even higher PM reductions [5]. SCR works through an aqueous urea injection (67.5% water and 32.5% ammonia) inside the catalyst. After injected, the NH3 is decomposed due to the high temperature of the exhaust gases and is then adsorbed and

stored by the catalyst [6]. Once the NH3 is adsorbed on the catalyst surface, it is ready to react with the NOx present. Note that the catalyst does not have the capacity to retain NOx, so if there is not enough NH3 storage these NOx will be released as slip [7]. Conversely, if the amount of NH3 stored in the catalyst exceeds its maximum capacity, the NH3 will not be retained, thereby the NH3 slip is the ammonia injected into the SCR but not consumed by the reduction reaction [8].

Since the NOx exhaust emissions are mainly composed as a mixture of NO and NO2 [9], the stored ammonia reacts with these gases through three main reactions to convert it into harmless nitrogen and water [10].

$$4NH_3 + 4NO + O_2 \rightarrow 4N_2 + 6H_2O \text{ (standard SCR reaction)} \quad (2.1)$$

$$2NH_3 + NO + NO_2 \rightarrow 2N_2 + 3H_2O \text{ (fast SCR reaction)} \quad (2.2)$$

$$8NH_3 + 6NO_2 \rightarrow 7N_2 + 12H_2O \text{ (slow SCR reaction)} \quad (2.3)$$

Eq.2.1 being the dominant reaction of the SCR, since most of the NOx produced during the combustion phase is in the form of NO (90-95%) [11].

One of the characteristic issues of the SCR is its slow dynamics. In particular, it is not possible to reduce the NOx concentration by injecting an equivalent amount of NH3 at a given time, as well as the characteristic times of adsorption, desorption and chemical reactions in the catalyst require a certain amount of NH3 previously stored to effectively reduce NOx [12]. As the EURO VI for heavy duty limits NH3 emissions by 10 ppm, ammonia injection must be accurately controlled, excess leads to unwanted NH3 slip and shortage decreases NOx conversion efficiency [13]. This situation is doubly undesirable since wasting NH3 has an economic cost and its emission to the environment is harmful. Thus, a proper ammonia injection strategy translates into both cost and emissions reduction.

As the SCR is a complex dynamic system that interacts with other systems and phenomena in the ICE, different problems may appear, Figure 2.3 reports several possible SCR system malfunctions, enabling proactive management of risks that may be associated with the operation, as well as addressing them for system improvement.

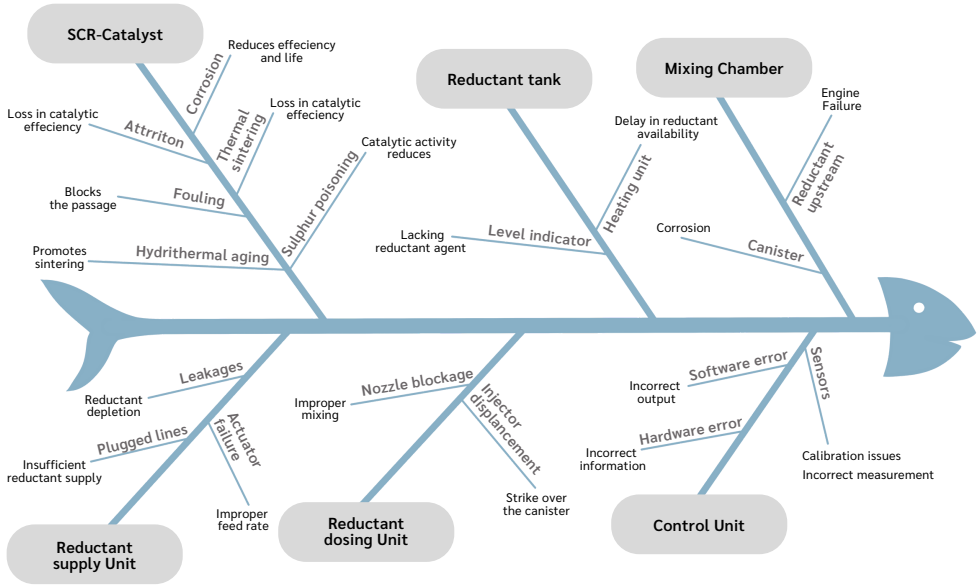

Figure 2.3: Fish-bone diagram for the SCR system possible failures and their effects. Adapted from [1].

As main sources of failure one can highlight, exhaust gas temperature, since temperatures below 250 °C generate soot and ammonium sulphate deposition on the catalyst surface [14], and temperatures above 500 °C may lead to hydrothermal ageing of the catalyst [15, 16]. Other reasons for failure can be: corrosion and poisoning of the monolith, reducing the adsorption capacity of the catalyst, and consequently the NOx conversion efficiency [17,18], reductant agent supply failure, affecting NOx conversion rates [19], and failure in the control unit of the after-treatment system, leading to inefficient catalyst operation [1, 20].

Due to the mentioned reasons, the improvement of the SCR catalyst performance is a challenging task, some possible approaches are:

- Catalyst: Since the catalyst is the main part of the ATS, the catalytic activity performance has a direct influence on emission abatement. Several researchers have investigated this topic, such as: Xu et al. [21], evaluated the performance of a vanadium-based SCR catalyst with different impregnations of cerium (Ce) and nickel (Ni). The results showed that Ce and/or Ni doping can improve the catalytic activity and depending on the composition extend the temperature window to a range of 200-400 °C with NO conversion efficiency above 90%. Bian et al [22], proposed a new catalyst assembly strategy to improve NOx conversion efficiency and

N2 selectivity at low-temperature operation (100-300 °C). The assembly of the manganese-based nano catalyst showed improvement on both points, besides being extendable to other types of catalysts. Yan et al. [23], investigated the effect of lead poisoning of an SCR catalyst, and a possible regeneration approach with nitric acid. As a result the catalyst activity was almost completely recovered and improved at very low temperatures (80-150 °C) when compared to the fresh catalyst. Miao et al. [24], analysed the cold start of a prototype SCR catalyst using a simplified energy balance aiming to understand the impact of the ATS design on SCR catalyst performance. Seven layouts were evaluated, demonstrating that depending on the ATS design (pipe length, DOC, and SCR placement) it is possible to achieve similar light-off times as with an external heater (170 s to reach 473 K at the SCR catalyst inlet).

- Reductant: In the deNOx system the composition of the injected reductant and its mixture with the exhaust gases has a substantial influence on the NOx reduction capacity as well as on the slip of the reductant itself. Some work in this field are: Payri et al [25], researched the liquid atomization process of a urea-water solution under normal engine operating conditions. As a result it proved that increasing the injection pressure produces smaller and faster particles in tangential and axial directions, thus promoting wider spray angles, which in turn combined with higher temperatures can improve catalyst performance. The work also presented an innovative technique for the determination of droplet size and velocity. Maass et al. [26], investigated through experimental trials in an optical test bench and 3D simulations the best arrangement of the dosing and mixing devices aiming to improve the distribution of the reductant agent. The work highlighted some important points of the optimisation, such as doser position, spray shape and mixer size and design. Gu et al. [27], investigated the response of a Hydrocarbon-selective catalytic reduction (HC-SCR) at low temperatures using several reductant agents plus hydrogen. As a result an improvement in NOx reduction efficiency of 36% at 315 °C and 58% at 245 °C was obtained when hydrogen was added. Investigations of other types of reductant agents have also been addressed by Brookshear et al. [28] (isobutanol), Nakatsuji et al. [29] (CO and hydrogen), and Yadav et al. [30] (liquefied petroleum gas).

- Control system: The control system in the ATS is where the emission abatement policy is assembled. The control framework defines from the reductant injection strategy up to the necessary corrections to reach

the desired emission levels. The deNOx systems have substantial control challenges in terms of prediction and controller design, due to the non-linearity of the system, high number of parameters, and complex chemical processes. Thus, researchers have presented several approaches addressing the ATS control system, such as: Dooren et al. [31], designed a supervisory control system based on Pontryagin's minimal principle, aiming to reduce fuel consumption and NOx emissions. The approach was tested in three different cycles, with and without sensor feedback, and in all cases, there were fuel savings and NOx emission reductions when compared to the standard ECU strategy. D'Aniello et al. [32], developed a control strategy for an SCR system based on the effective EGR rate, aiming to simultaneously limit NOx emissions to a predetermined level and minimise the overall engine operating cost. As a result, when compared to the baseline strategy there was a reduction in NOx emissions and overall operating cost of 48% and 42%, respectively. Willems and Cloudt [33], proposed a model-based SCR control strategy, experimentally validated on European type-approval cycles and subjected to a 30% underdose disturbance. The approach uses a one-dimensional physical model with two control strategies, using either the NH3 sensor signal or the NOx sensor signal as feedback information. As a result, the strategy based on NH3 feedback was able to keep the NOx conversion rate above 92% with NH3 slip below 10 ppm, while the strategy using the NOx sensor obtained in the same conditions 77% of NOx conversion efficiency with NH3 slip of 16 ppm. Similar approaches aimed at controlling the urea injection rate have been addressed by several researchers: Zhang et al. [34], used a control strategy based on artificial neural network (ANN) and proportional, integral and derivative (PID) fuzzy controller that estimates the optimal amount of urea to be injected to minimise the NOx emissions estimated by ANN. McKinley et al. [35], proposed an adaptive MPC aiming to manage the ammonia injection rate that reduces the NOx and NH3 slip. And Ofoli [36] developed a urea injection controller based on the ammonia loading of the SCR catalyst, thereby maximising NOx conversion efficiency with low urea consumption.

- Diagnostic: The addition of several components and more sophisticated strategies to ATS in order to ensure an acceptable level of pollutant emissions has made it a highly complex system to be controlled; thus, to guarantee its correct operation, monitoring and diagnostic systems are mandatory. Some approaches proposed by researchers are: Canova et al. [37] created a model-based fault detection to monitor a lean NOx trap (LNT) after-treatment system and detect and isolate possible faults

in the sensors and LNT parameters. The approach was capable of robustly and reliably detect critical faults such as sulphur poisoning, deactivation of catalyst storage due to thermal ageing, and sensor failures. Finally, it showed that the methodology can be extended to SCR and DPF systems. Pezzini et al. [38] applied the Failure Mode and Effects Analysis (FMEA) and Fault Tree Analysis (FTA) methodology to detect and isolate problems in each ATS component. This information was used to develop a control-oriented model applied to monitoring and diagnostics, which was able to detect faults in temperature and NOx emissions measurement. Soleimani et al. [39] proposed a methodology for fault detection and isolation of complex systems using training model history. The approach considers seven critical parameters of possible failure: average SCR temperature, NH3 load, upstream NOx level, NO2/NOx, exhaust gas mass flow, SCR degradation and downstream NOx level. As a result, the authors submitted the system to one of the failures and the proposed methodology was able to identify with a probability of 92% of occurrence.

Overall, SCR technology has great potential to meet the increasingly stringent NOx emissions legislation in automotive applications, and its development can be enhanced by addressing the pathways presented.

2.3 Ammonia slip catalyst

During engine operation with a urea-based system, NH3 slip is inevitable. To solve this problem it is possible to place an additional catalyst after the SCR to deal with the NH3 leaving the SCR brick. This type of application allows the avoidance of NH3 slip as well as a more aggressive NOx abatement strategy. In this way, it is possible to summarise that the main functionality of the ASC catalyst is to deal with the unreacted NH3 that would be released into the atmosphere while increasing the overall NOx conversion efficiency [40].

The physicochemical processes in SCR catalyst are well understood and modelled, whilst the same is not true for ASC, for which there are only a few reports in the literature [40–42]. However, the functionality of the ASC catalyst is the same as that of SCR, to oxidise the NH3 into harmless nitrogen and water (eq.2.4).

$$2NH_3 + 1.5O_2 \rightarrow N_2 + 3H_2O \tag{2.4}$$

The newest generations of ASC catalysts have two layers, a platinum-based oxidation catalyst in the bottom and an active SCR in the upper layer.

At high temperatures the poor selectivity of platinum to N2 leads to the N2O and NOx formation, this design allows the NOx formed to react with NH3 in the upper layer, so that the global amount of NO produced is minimised and the selectivity for N2 is increased (Figure 2.4).

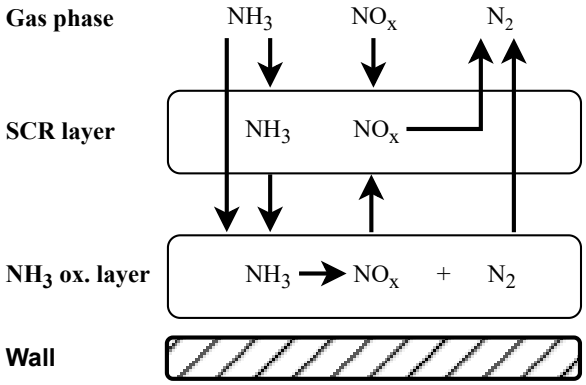

Figure 2.4: Schematic of the dual-layer ASC catalyst. Adapted from [40].

As it can be seen the SCR+ASC architecture can assist in meeting the high requirements of pollutant reduction leading this design as an option to be increasingly explored for NOx and NH3 emission reduction.

2.4 After-treatment control and diagnosis

Newer ATSs have high emission abatement capabilities; however, these systems are also more complex and need to be adequately controlled. As commented by Vignesh et al. [1] challenges faced by deNOx systems are narrow activity temperature range, cold start problems, catalyst ageing and control unit failure (incorrect feedback information for fault diagnosis and control). Challenges that must be addressed and solved for ATS installation in automobiles.

Among the disadvantages presented, catalyst ageing, and incorrect feedback information directly affect the control strategy to reduce pollutant emissions. Regarding catalyst ageing, this phenomenon develops after the catalyst is subjected to a long period of high temperature operation [43]. The modern ATS uses Selective Catalytic Reduction Filter (SCRF) catalyst technology, which integrates SCR technology coated on a DPF, to be able to control both NOx and PM [44]. However, the DPF needs for its regeneration to operate at temperatures above 500 C [45] (i.e., regeneration of the DPF system is

necessary, as the system is gradually blocked by carbon deposits, increasing back pressure and, consequently, reducing engine power [46], hence, the ATS will accelerate the ageing of the system.

To access the effects of catalyst ageing, Dhillon et al. [47] carried out a parametric study of the impact on the ASC catalyst performance, through moderate and intense hydrothermal ageing. The results show that ageing reduced the monolith coverage area by 15.92% for moderate and 19.75% for intense, which in turn reduced the ammonia oxidizing capacity by approximately 7.22% and 17.53%, respectively. The results being extended to other types of Pt/Al2O3 washcoated monolith, such as SCR catalyst. Bartley et al. [48] created a model to determine the maximum NH3 storage capacity of three SCR catalysts with different compositions (Fe-Zeolite, Cu-Zeolite and V/W/TiO2) at continuous ageing levels, through the use of a database that correlates the operating history, and catalyst temperature. As a result, an average error of 6.3% was obtained in the emissions prediction, thus allowing adjustments in the ammonia injection strategy to improve NOx conversion efficiency and reduce NH3 slip. Xue et al. [16] compared the performance between a new and an aged SCR catalyst in terms of the physical adsorption capacity of gas molecules on a solid surface, and by the interactions of the gases reactions with the catalyst surface. The results showed that when compared to the aged catalyst, the new one has an adsorption capacity and reaction area 2.46 and 3.11 times higher, respectively. Hu et al. [49], created a model to estimate the ageing level of the SCR catalyst through an extended Kalman filter (EKF) observer, and using this information to improve the ATS performance by means of a model reference adaptive controller (MRAC), when compared, the proposed approach improved NOx conversion efficiency by 4.16% and 9.93% in European transient cycle (ETC) and 2.77% and 6.78% in European steady-state cycle (ESC), for an ageing of 80% and 60%, respectively.

Regarding the feedback information, a recurring failure is to report the wrong amount of ammonia injected to ECU. This failure can be generated by the blockage of the urea injection nozzles due to the progressive deposition of urea over time, leading to a reduction in the amount of injected ammonia demanded and, consequently, to low levels of NOx conversion.

To address the problem, Tan et al. [50], evaluated the impact of insufficient urea injection at three levels of NH3-NOx ratio, 0.6, 0.8 and 1.0 in a temperature range of 200 to 450 ºC, as a result the highest NOx conversion efficiencies were 65.3% at 454.3 ºC, 85.8% at 376.2 ºC and 98.1% at 295.5 ºC, respectively. Mora et al. [51], proposed an OBD strategy to monitor the urea injector operation, as well as to estimate the catalyst ageing. The fault monitoring was carried out through a 400-second temporal analysis of NOx

and NH3 emissions, comparing the measured and estimated values. As a result, the proposed approach was submitted to four different levels of failure in the injector and five of ageing, being the strategy capable to detect all failures. Wang et al. [52] created a fault detection and fault tolerant control of the urea injection system, the proposed strategy uses the line pressure sensor feedback combined with a Kalman filter to estimate the actual effective area of the urea injector orifice, thus the ratio of current and expected effective area is used to compensate the line pressure. As a result, the proposed methodology was able to detect and correct an injection failure when the dosage falls below 80%.

As can be seen, catalyst ageing and failure to correctly inject ammonia are anomalies presented by the ATS that compromise the expected behaviour of the catalyst, leading to a low NOx conversion rate and, consequently, to unwanted levels of pollutant emission. These undesired behaviours make it difficult for ICEs to operate within the limits imposed by legislation, therefore, they must be monitored and controlled.

2.5 On-board monitoring

Increasing tightening of emission limits has led to more complex after-treatment systems. To ensure the correct operation of these systems, on-board diagnostics and monitoring systems have been introduced. In addition, the use of OBD protocol has been mandatory since 1996 [53] and regulations require monitoring of the after-treatment system for malfunction and performance degradation [54].

There are significant benefits of adopting OBD systems for the environment as well as for vehicle owners. OBD is designed to assist in the correct operation of the emission control unit and ensure that vehicles comply with emission limits during daily use [55]. OBD systems are a useful tool for users and technicians, as they provide important feedback information on the need for component maintenance and potential urgent repairs, are also a key component of monitoring and maintenance programmes to reduce on-site emissions and control high emitters [56].

The OBD system covers several components and operating conditions, such as: boost pressure control system; fuel system; engine cooling system; misfire; among others [57]. Specifically the aspects to be monitored in catalysts are: the correct injection of the reductant, as well as its quality, availability and consumption rate, the NOx conversion efficiency, and the correct functioning of the NOx sensors, air-fuel sensor, and other monitors with emission thresholds [58].

2.5.1 Reductant agent monitoring

The proper operation of the SCR catalyst depends on the availability and quality of the reducing agent, also called diesel exhaust fluid (DEF). Its operation without or with low quality DEF inevitably results in high NOx concentrations downstream of the catalyst. Therefore, control monitoring of some DEF related parameters is incorporated in the OBD system [59].

DEF monitoring has three main warnings: Low fluid level in the reservoir; Incorrect fluid; Failure or incorrect dosing, These alarms have different penalty levels, ranging from a light on the vehicle's dashboard to the inability to start the engine [60].

The aim of this monitoring is to avoid deviations in catalyst performance due to inconsistencies in the DEF, thus ensuring that the catalyst operates as it was designed to.

2.5.2 NOx sensors

The development of NOx sensors made significant progress in the late 1990s [61, 62], from the know-how acquired in the development of the λ sensor [63] a NOx sensor based on a dual-cavity with a mixed potential sensor was proposed [64]. However, as a disadvantage this concept has difficulty in distinguishing the different components of the gas composition [65]. At the same time, NGK developed amperometric sensors with a three-layer multi-electrode system, which is currently the most widely used architecture [66, 67].

The working principle of amperometric sensors is based on the measurement of an electric current proportional to the NOx gas dissociated into N2 and O2 in the sensor [68], as shown in Figure 2.5.

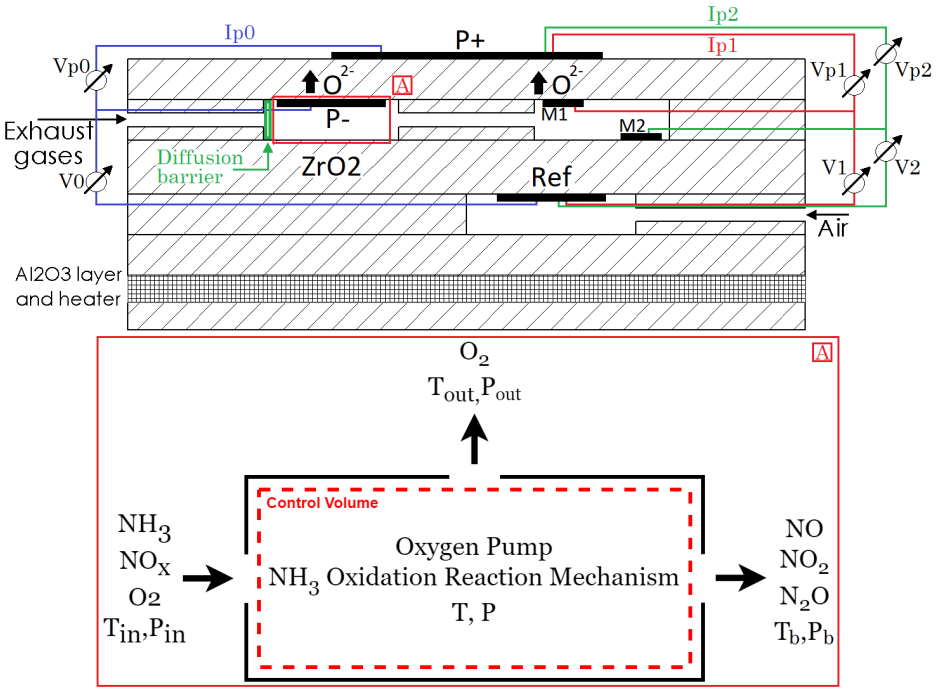

Figure 2.5: NOx sensor internal structure scheme.

The exhaust gases are introduced into a first cavity containing a zirconia-based electrochemical oxygen pump, in which the NO2 is reduced to NO through the porous wall. The reductants such as HC and CO are converted into the diffusive barrier allocated between the exhaust gases and the first cavity. In the second cavity, another electrochemical oxygen pump depletes oxygen, leaving an almost oxygen-free atmosphere. Then, NO breaks down into N2 and O2. The NOx concentration is calculated based on the measurement of the oxygen concentration in the second cavity. However, NO, NO2, and N2O are produced with the presence of ammonia. The products of ammonia oxidation affect the measurement of oxygen concentration and, consequently, the measurement of NOx concentration in the sensor [65, 69].

According to the measuring principle, the NOx sensor is sensitive to both NO and NO2 [70]. The sensor has different sensitivity to those species due to their different oxygen content. NO2 is a larger molecule, so there is higher resistance to its transport through the diffusion barrier between the exhaust gas and first cavity. In addition, NO2 accounts for two oxygen atoms instead of one (NO), and since the final species measured is O2, the gain should be double for NO2. As both effects are opposite, depending on the sensor and operating conditions the sensitivity to NO2 can be between 70% and 130% of

that to NO [62].

2.5.2.1 NOx sensor cross-sensitivity

NOx sensors have the drawback of cross-sensitivity to ammonia (K_{CS}), which means that actual NOx emissions may not correspond to the sensor reading (Figure 2.6). If the incorrect reading of the NOx sensor is used in the feedback dosing control, the performance of the designed control would be unsatisfactory, leading, amongst other consequences, to high NOx emissions or, conversely, to high ammonia consumption and NH3 slip [7, 12].

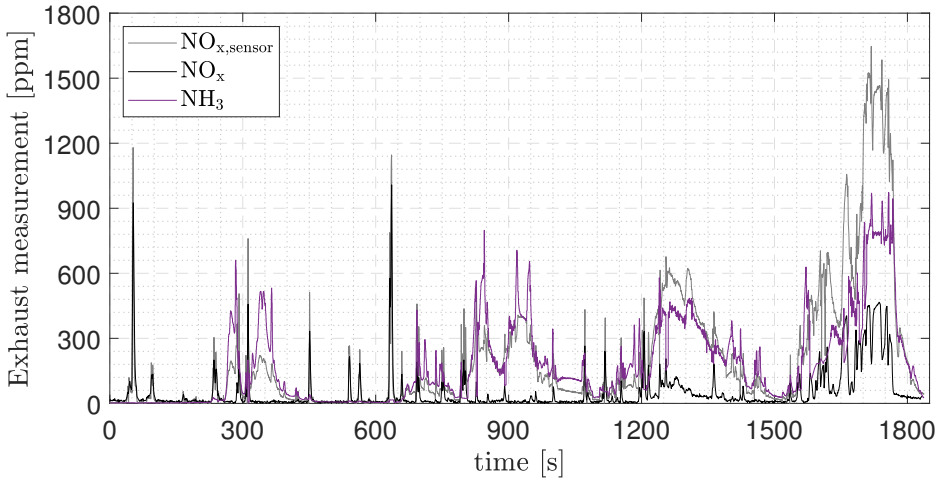

Figure 2.6: Influence of NH3 slip on NOx sensor measurement.

Regarding the reason for such sensitivity to NH3, Frobert et al. [65] describes that reductant as NH3, are converted inside the first cavity. Three main reactions can be expected:

$$2NH_3 + 2O_2 \rightarrow N_2O + 3H_2O \tag{2.5a}$$
$$2NH_3 + 2.5O_2 \rightarrow 2NO + 3H_2O \tag{2.5b}$$
$$2NH_3 + 3.5O_2 \rightarrow 2NO_2 + 3H_2O \tag{2.5c}$$

The different stoichiometry of the three different reactions leads to different cross sensitivities:

- In reaction eq. 2.5a 2 molecules of NH3 lead to 1 molecule of N2O so to $1O^{2-}$. Then, the cross sensitivity, which can be estimated as the ratio between O2 in the NOx produced and NH3, becomes $K_{CS} = \frac{O^{2-}}{NH_3} = 0.5$.

- In reaction eq. 2.5b 2 molecules of NH3 lead to 2 molecules of NO so to $2O^{2-}$. Then, $K_{CS} = \frac{O^{2-}}{NH_3} = 1$.
- In reaction eq. 2.5c 2 molecules of NH3 lead to 2 molecules of NO2 so to $4O^{2-}$. Then, $K_{CS} = \frac{O^{2-}}{NH_3} = 2$.

Like most chemical reactions, the three oxidation processes presented previously (eq.2.5) require different activation energies, such that the reaction rates can change with temperature. Since the fractions of N2O, NO, and NO2 generated by the ammonia oxidation processes change mainly according to the predominant oxidation reaction, the cross-sensitivity factor will depend mainly on the temperature of the exhaust gases [71, 72] and should range between 0.5 and 2 [65, 71]. Since the predominance of reactions eq.2.5 can be based on temperature, Hsieh and Wang [71] suggests that eq.2.5a dominates at low temperatures and eq.2.5c dominates at high temperatures.

Note that the cell temperature, is the temperature inside the first cavity, and increases due to oxidation reactions. Therefore, the sensor cell temperature will be a function of the exhaust gases temperature plus the temperature released by the oxidation reactions.

Figure 2.7 shows the correlation of the K_{CS} and NOx with NH3 (left), SCR outlet temperature (centre) and NO2/NOx ratio (right) for two different NOx sensors, in 60 test cycles, including transient and steady state conditions.

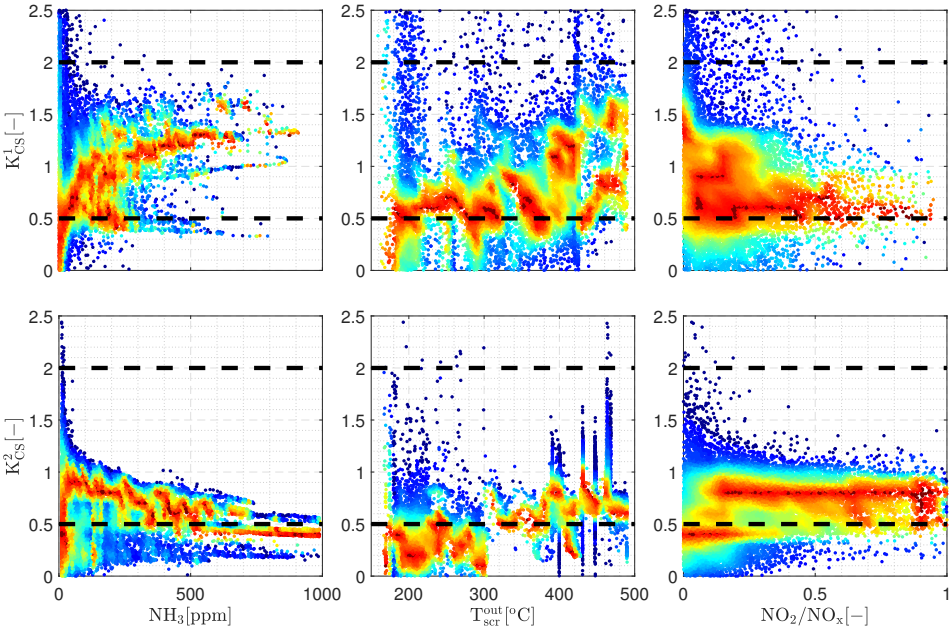

Figure 2.7: K_{CS} depending on NH3 (left column), SCR outlet temperature (medium column) and NO2 to NOx ratio (right column) for a set of 60 tests including Worldwide harmonized Light vehicles Test (WLTC) and other driving cycles, engine mapping and steady state conditions. Colour-scale ranges from blue (low frequency) to red (high frequency).

The following conclusions can be extracted:

- There is a correlation of cross sensitivity with NH3 emissions. Results show that for sensor 1 K_{CS} increases asymptotically from 0 to 1.5 approximately, and for sensor 2 there is an inverse trend from 1 to 0.5 approximately.
- No clear correlation is observed with SCR outlet temperature, despite higher cross-sensitivities appear at higher temperatures. When cell temperature may be related with exhaust gas temperature, cell heating and the slow dynamics of the temperature sensors may prevent observing a clear relation.
- No correlation between NO2/NOx ratio and K_{CS} is observed in the experimental results.

- According to the results, sensor 1 is more sensitive to NH3 and temperature, as its operating range is greater compared to sensor 2.

2.5.3 NH3 sensor

The NH3 sensor based on the electrochemical non-equilibrium principle is the most suitable for vehicular application [73], in which the sensor emits an electromagnetic field (EMF) signal linearly proportional to the logarithms of the NH3 concentration in the exhaust gas [74]. The sensor has a simple architecture as presented in Figure 2.8.

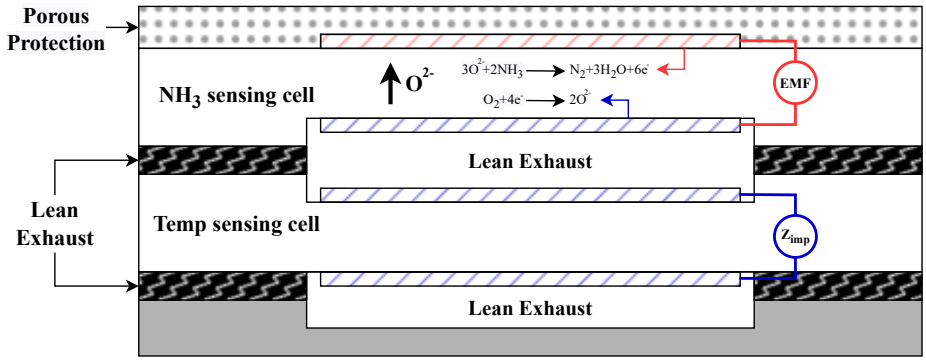

Figure 2.8: NH3 sensor structure. Adapted from [73].

The sensor has a NH3 sensing electrode and a reference electrode, both exposed to the same exhaust gas. The potential difference between the two electrodes produces an EMF according to the following equation.

$$\mathrm{EMF} \approx \frac{\mathrm{kT}}{3\mathrm{e}}\mathrm{Ln}(\mathrm{P}_{\mathrm{NH_3}}) - \frac{\mathrm{kT}}{4\mathrm{e}}\mathrm{Ln}(\mathrm{P}_{\mathrm{O_2}}) - \frac{\mathrm{kT}}{2\mathrm{e}}\mathrm{Ln}(\mathrm{P}_{\mathrm{H_2O}}), \tag{2.6}$$

where, k is a calibration constant, T is the temperature, e is the electron charge unit, and P is the partial pressure of the species.

The main advantage of using sensors is linked to the improvement of the control strategy, as shown in the Figure 2.9.

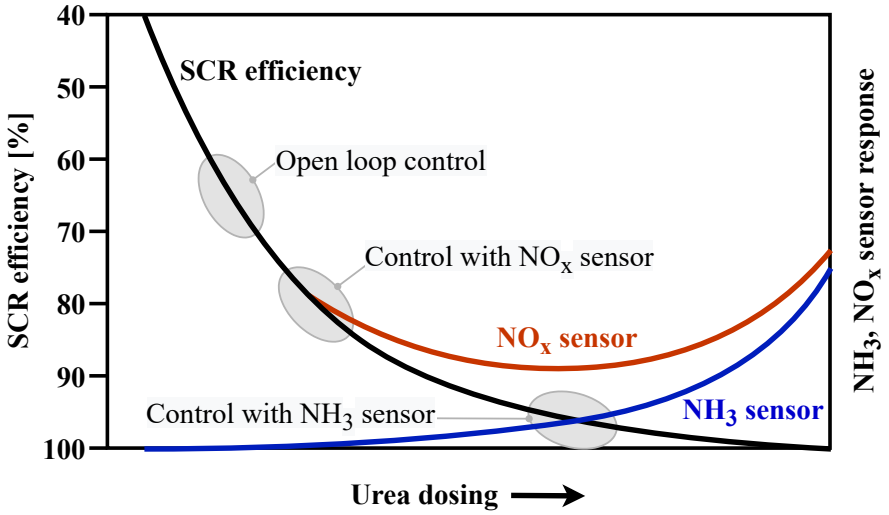

Figure 2.9: Effect of urea dosage on SCR efficiency, and NH3 and NOx sensor response. Adapted from [75].

As it can be seen, the more technology embedded in the ATS, the greater its effectiveness. The use of NOx sensors makes possible to improve the ammonia injection strategy through a closed-loop control, which in turn has limitation due to the sensor's cross-sensitivity to ammonia. This drawback can be circumvented by adding a NH3 sensor to the control system, thus driving the efficiency of the ATS to higher rates.

It is clear that the integration of the diverse technologies available to the control system increases the ATS capability to abate harmful pollutants, but also an increase in the overall cost of the system and a greater complexity to control it, so it is still needed a strong effort by researchers and companies to develop more robust systems and strategies and reduce the cost of new technologies.

2.6 Conclusion

After-treatment systems have big room for improvement, driving their contaminant reduction capacity beyond current levels, therefore, placing them as still one of the best options for meeting restrictive pollutant emission limits.

Possible scenarios for such improvement contemplate, intelligent and robust ammonia injection strategies, improved architectural composition of the after-treatment system with respect to catalysts and sensors, as well as

novel approaches to monitor and control the entire system.

References

[1] Vignesh R. and Ashok B. "Critical interpretative review on current outlook and prospects of selective catalytic reduction system for De-NOx strategy in compression ignition engine". *Fuel*, Vol. 276 n^o March, sep 2020. (cited in pp. 17, 21, 25, 83, and 181)

[2] of science Web. "Web of Science Core Collection". (cited in p. 18)

[3] Selleri Tommaso, Nova Isabella and Tronconi Enrico. "An efficient reduced model of NH3-SCR converters for mobile aftertreatment systems". *Chemical Engineering Journal*, Vol. 377, dec 2019. (cited in p. 19)

[4] Praveena V and Martin M Leenus Jesu. "A review on various after treatment techniques to reduce NOx emissions in a CI engine". *Journal of the Energy Institute*, Vol. 91 n^o 5, pp. 704–720, oct 2018. (cited in p. 19)

[5] Hu Jie, Liao Jianxiong, Hu Youyao, Lei Jun, Zhang Ming, Zhong Jing, Yan Fuwu and Cai Zhizhou. "Experimental investigation on emission characteristics of non-road diesel engine equipped with integrated DOC + CDPF + SCR aftertreatment". *Fuel*, Vol. 305 n^o August 2021, dec 2021. (cited in p. 19)

[6] Shibata Gen, Shibayama Naoki, Araki Keita, Kobashi Yoshimitsu, Ogawa Hideyuki, Nakasaka Yuta and Shimizu Ken-ichi. "Steady-state kinetic modeling of NH3-SCR by monolithic Cu-CHA catalysts". *Catalysis Today*, n^o June, jun 2022. (cited in p. 19)

[7] Wang Guoyang, Qi Jinzhu, Liu Shiyu, Li Yanfei, Shuai Shijin and Wang Zhiming. "Zonal control for selective catalytic reduction system using a model-based multi-objective genetic algorithm". *International Journal of Engine Research*, Vol. 22 n^o 3, pp. 911–920, mar 2021. (cited in pp. 20 and 30)

[8] Heywood John B. *Internal Combustion Engine Fundamentals*. McGraw-Hill Education, Cambridge, Massachusetts, second edition, 2018. (cited in pp. 3, 8, and 20)

[9] Zeng Yiqing, Wu Zihua, Guo Lina, Wang Yanan, Zhang Shule and Zhong Qin. "Insight into the effect of carrier on N2O formation over MnO2/MOx (M = Al, Si and Ti) catalysts for selective catalytic reduction (SCR) of NOx with NH3". *Molecular Catalysis*, Vol. 488 n^o March, jun 2020. (cited in p. 20)

[10] Raza Hassan, Woo Sanghee and Kim Hongsuk. "Investigation of an ammonium carbamate–based SCR system for NOx reduction in diesel engines under transient conditions". *Energy*, Vol. 251, jul 2022. (cited in p. 20)

[11] Zhu Minghui, Lai Jun-Kun and Wachs Israel E. "Formation of N2O greenhouse gas during SCR of NO with NH3 by supported vanadium oxide catalysts". *Applied Catalysis B: Environmental*, Vol. 224 n^o November 2017, pp. 836–840, may 2018. (cited in p. 20)

[12] Pla Benjamin, Bares Pau, Sanchis Enrique and Aronis André. "Ammonia injection optimization for selective catalytic reduction aftertreatment systems". *International Journal of Engine Research*, Vol. 22 n^o 7, pp. 2169–2179, jul 2021. (cited in pp. 20, 30, and 133)

[13] Yuan Xinmei, Gao Ying and Wang Xiulei. "A novel NH 3 slip control for diesel engine selective catalytic reduction aftertreatment system". *International Journal of Engine Research*, Vol. 17 n^o 2, pp. 169–178, feb 2016. (cited in p. 20)

[14] Majewski W Addy. "Selective catalytic reduction". *Ecopoint Inc. Revision*, 2005. (cited in p. 21)

[15] Xi Yuanzhou, Su Changsheng, Ottinger Nathan A. and Liu Z. Gerald. "Effects of hydrothermal aging on the sulfur poisoning of a Cu-SSZ-13 SCR catalyst". *Applied Catalysis B: Environmental*, Vol. 284 n^o November 2020, may 2021. (cited in p. 21)

[16] Xue Lina, Xiong Ka, Chen Haijun, Cho Kyeongjae and Wang Weichao. "Investigation of the hydrothermal aging of an Mn-based mullite SmMn 2 O 5 catalyst of NO oxidation". *RSC Adv.*, Vol. 7 n^o 77, pp. 49091–49096, 2017. (cited in pp. 21 and 26)

[17] Seo Choong-kil, Kim Hwanam, Choi Byungchul, Lim Myung Taeck, Lee Chun-Hwan and Lee Chun-beom. "De-NOx characteristics of a combined system of LNT and SCR catalysts according to hydrothermal aging and sulfur poisoning". *Catalysis Today*, Vol. 164 n^o 1, pp. 507–514, apr 2011. (cited in p. 21)

[18] Xi Yuanzhou, Ottinger Nathan A. and Liu Z. Gerald. "New insights into sulfur poisoning on a vanadia SCR catalyst under simulated diesel engine operating conditions". *Applied Catalysis B: Environmental*, Vol. 160-161 n^o 1, pp. 1–9, nov 2014. (cited in p. 21)

[19] Pla Benjamin, Piqueras Pedro, Bares Pau and Aronis André. "Simultaneous NOx and NH3 slip prediction in a SCR catalyst under real driving conditions including potential urea injection failures". *International Journal of Engine Research*, Vol. 23 n^o 7, pp. 1213–1225, jul 2022. (cited in p. 21)

[20] Pla Benjamín, Bares Pau, Sanchis Enrique José and Nakaema Aronis André. "Ammonia injection failure diagnostic and correction in engine after-treatment system by NOx and NH3 emissions observation". *Fuel*, Vol. 322 n^o March, aug 2022. (cited in pp. 21 and 62)

[21] Xu Junqiang, Zou Xianlin, Chen Guorong, Zhang Yanrong, Zhang Qiang and Guo Fang. "Tailored activity of Ce–Ni bimetallic modified V2O5/TiO2 catalyst for NH3-SCR with promising wide temperature window". *Vacuum*, Vol. 191 n^o 66, sep 2021. (cited in p. 21)

[22] Bian Mengyao, Liu Kaijie, Han Xinyu, Fang Yangfei, Liu Qiuwen, Zhang Yibo and Yang Xiangguang. "Novel manganese-based assembled nanocatalyst with "nitrous oxide filter" for efficient NH3-SCR in wide low-temperature window: Optimization, design and mechanism". *Fuel*, Vol. 331, jan 2023. (cited in p. 21)

[23] YAN Dong-jie, GUO Tong, YU Ya and CHEN Zhao-hui. "Lead poisoning and regeneration of Mn-Ce/TiO2 catalysts for NH3-SCR of NO at low temperature". *Journal of Fuel Chemistry and Technology*, Vol. 49 n^o 1, pp. 113–120, jan 2021. (cited in p. 22)

[24] Miao Yong, Chen Lea-Der, He Yongsheng and Kuo Tang-wei. "Study of SCR cold-start by energy method". *Chemical Engineering Journal*, Vol. 155 n^o 1-2, pp. 260–265, dec 2009. (cited in p. 22)

[25] Payri Raul, Bracho Gabriela, Gimeno Jaime and Moreno Armando. "Investigation of the urea-water solution atomization process in engine exhaust-like conditions". *Experimental Thermal and Fluid Science*, Vol. 108 n^o March, pp. 75–84, nov 2019. (cited in p. 22)

[26] Maass J., Eppler A., Scholz J., Gentgen H., Grumbrecht F. and Marohn R. "Influences of AdBlue® spray targeting and mixing devices on the UWS distribution upstream of the SCR catalyst". In *Fuel Systems for IC Engines*, number 1, pp. 21–41. Elsevier, 2012. (cited in p. 22)

[27] Gu Hyerim, Chun Kwang Min and Song Soonho. "The effects of hydrogen on the efficiency of NO x reduction via hydrocarbon-selective catalytic reduction (HC-SCR) at

low temperature using various reductants". *International Journal of Hydrogen Energy*, Vol. 40 n^o 30, pp. 9602–9610, aug 2015. (cited in p. 22)

[28] Brookshear D. William, Pihl Josh A., Toops Todd J., West Brian and Prikhodko Vitaly. "The selective catalytic reduction of NO over Ag/Al2O3 with isobutanol as the reductant". *Catalysis Today*, Vol. 267, pp. 65–75, jun 2016. (cited in p. 22)

[29] NAKATSUJI T, YAMAGUCHI T, SATO N and OHNO H. "A selective NOx reduction on Rh-based catalysts in lean conditions using CO as a main reductant". *Applied Catalysis B: Environmental*, Vol. 85 n^o 1-2, pp. 61–70, dec 2008. (cited in p. 22)

[30] Yadav Deepak, Singh Pratichi and Prasad Ram. "MnCo2O4 spinel catalysts synthesized by nanocasting method followed by different calcination routes for low-temperature reduction of NOx using various reductants". *International Journal of Hydrogen Energy*, Vol. 43 n^o 10, pp. 5346–5357, mar 2018. (cited in p. 22)

[31] van Dooren Stijn, Amstutz Alois and Onder Christopher H. "A causal supervisory control strategy for optimal control of a heavy-duty Diesel engine with SCR aftertreatment". *Control Engineering Practice*, Vol. 119 n^o November 2021, feb 2022. (cited in p. 23)

[32] D'Aniello Federica, Arsie Ivan, Pianese Cesare and Stola Federico. "Development of an Integrated Control Strategy for engine and SCR system basedon effective EGR rate". *IFAC-PapersOnLine*, Vol. 53 n^o 2, pp. 14034–14039, 2020. (cited in p. 23)

[33] Willems Frank and Cloudt Robert. "Experimental Demonstration of a New Model-Based SCR Control Strategy for Cleaner Heavy-Duty Diesel Engines". *IEEE Transactions on Control Systems Technology*, Vol. 19 n^o 5, pp. 1305–1313, sep 2011. (cited in p. 23)

[34] Zhang S. M., Tian F., Ren G. F. and Yang L. "SCR control strategy based on ANNs and Fuzzy PID in a heavy-duty diesel engine". *International Journal of Automotive Technology*, Vol. 13 n^o 5, pp. 693–699, aug 2012. (cited in p. 23)

[35] McKinley Thomas L. and Alleyne Andrew G. "Adaptive Model Predictive Control of an SCR Catalytic Converter System for Automotive Applications". *IEEE Transactions on Control Systems Technology*, Vol. 20 n^o 6, pp. 1533–1547, nov 2012. (cited in p. 23)

[36] Ofoli Abdul R. "Experimental Demonstration of Ammonia Storage and Slip Modeling With Control for an SCR Aftertreatment System". *IEEE Transactions on Industry Applications*, Vol. 50 n^o 4, pp. 2342–2348, jul 2014. (cited in p. 23)

[37] Canova Marcello, Midlam-Mohler Shawn, Pisu Pierluigi and Soliman Ahmed. "Model-based fault detection and isolation for a diesel lean trap aftertreatment system". *Control Engineering Practice*, Vol. 18 n^o 11, pp. 1307–1317, nov 2010. (cited in p. 23)

[38] Pezzini A., Canova M., Onori S., Rizzoni G. and Soliman A. "A Methodology for Fault Diagnosis of Diesel NOx Aftertreatment Systems". *IFAC Proceedings Volumes*, Vol. 42 n^o 8, pp. 911–916, 2009. (cited in p. 24)

[39] Soleimani Morteza, Campean Felician and Neagu Daniel. "Integration of Hidden Markov Modelling and Bayesian Network for fault detection and prediction of complex engineered systems". *Reliability Engineering & System Safety*, Vol. 215 n^o May, nov 2021. (cited in p. 24)

[40] Scheuer A., Hauptmann W., Drochner A., Gieshoff J., Vogel H. and Votsmeier M. "Dual layer automotive ammonia oxidation catalysts: Experiments and computer simulation". *Applied Catalysis B: Environmental*, Vol. 111-112, pp. 445–455, 2012. (cited in pp. 24 and 25)

[41] Scheuer A., Votsmeier M., Schuler A., Gieshoff J., Drochner A. and Vogel H. "NH3-slip catalysts: Experiments versus mechanistic modelling". *Topics in Catalysis*, Vol. 52 n^o 13-20, pp. 1847–1851, 2009. (cited in p. 24)

[42] Colombo Massimo, Nova Isabella, Tronconi Enrico, Schmeißer Volker, Bandl-Konrad Brigitte and Zimmermann Lisa. "Experimental and modeling study of a dual-layer (SCR+PGM) NH3 slip monolith catalyst (ASC) for automotive SCR aftertreatment systems. Part 1. Kinetics for the PGM component and analysis of SCR/PGM interactions". *Applied Catalysis B: Environmental*, Vol. 142-143, pp. 861–876, oct 2013. (cited in p. 24)

[43] Tan Pi-qiang, Zhang Shu-chen, Wang Shi-yan, Hu Zhi-yuan and Lou Di-Ming. "Simulation on catalytic performance of fresh and aged SCR catalysts for diesel engines". *Journal of the Energy Institute*, Vol. 93 n^o 6, pp. 2280–2292, dec 2020. (cited in pp. 25 and 83)

[44] Chundru Venkata Rajesh, Parker Gordon G. and Johnson John H. "The Effect of NO 2 /NO x Ratio on the Performance of a SCR Downstream of a SCR Catalyst on a DPF". *SAE International Journal of Fuels and Lubricants*, Vol. 12 n^o 2, jun 2019. (cited in pp. 25 and 83)

[45] Wang De-yuan, Cao Jian-hong, Tan Pi-qiang, Wang Zhi-xin, Li Wen-long, Liu Zuo-wei and Wang Jun. "Full course evolution characteristics of DPF active regeneration under different inlet HC concentrations". *Fuel*, Vol. 310, feb 2022. (cited in pp. 25 and 83)

[46] Feng Renhua, Hu Xiulin, Li Guanghua, Sun Zhengwei and Deng Banglin. "A comparative investigation between particle oxidation catalyst (POC) and diesel particulate filter (DPF) coupling aftertreatment system on emission reduction of a non-road diesel engine". *Ecotoxicology and Environmental Safety*, Vol. 238 n^o April, jun 2022. (cited in pp. 26 and 83)

[47] Dhillon Pritpal S., Harold Michael P., Wang Di, Kumar Ashok and Joshi Saurabh Y. "Enhanced transport in washcoated monoliths: Application to selective lean NOx reduction and ammonia oxidation". *Chemical Engineering Journal*, Vol. 377 n^o August, dec 2019. (cited in pp. 26, 84, and 111)

[48] Bartley Gordon J., Chadwell Christopher J., Kostek Theodore M. and Zhan Reggie. "SCR Deactivation Kinetics for Model-Based Control and Accelerated Aging Applications". In *SAE Technical Papers*, apr 2012. (cited in p. 26)

[49] Hu Jie, Zeng Jiawei and Wei Li. "Failure diagnosis and tolerant control method for hydrothermally aged SCR system by utilizing EKF observer and MRAC controller". *Energy*, Vol. 156, pp. 103–121, aug 2018. (cited in pp. 26 and 111)

[50] Tan Piqiang, Li Xiaoyu, Wang Shiyan, Hu Zhiyuan and Lou Diming. "Selective catalytic reduction failure of low NH3-NO ratio". *Chinese Journal of Chemical Engineering*, Vol. 32, pp. 231–240, apr 2021. (cited in p. 26)

[51] Mora J., Willems F., Seykens X. and Guardiola C. "An OBD strategy to estimate SCR ageing and detect urea injection faults". *IFAC-PapersOnLine*, Vol. 51 n^o 31, pp. 369–376, 2018. (cited in pp. 26, 119, and 125)

[52] Wang Yue-Yun, Sun Yu, Chang Chen-Fang and Hu Yiran. "Model-Based Fault Detection and Fault-Tolerant Control of SCR Urea Injection Systems". *IEEE Transactions on Vehicular Technology*, Vol. 65 n^o 6, pp. 4645–4654, jun 2016. (cited in pp. 27 and 125)

[53] Rizzoni Giorgio, Kim Yong-wha and Soliman Ahmed. "Estimation Problems in Engine Control and Diagnosis". *IFAC Proceedings Volumes*, Vol. 33 n^o 11, pp. 125–131, jun 2000. (cited in p. 27)

[54] Mohammadpour Javad, Franchek Matthew and Grigoriadis Karolos. "A survey on diagnostics methods for automotive engines". In *Proceedings of the 2011 American Control Conference*, pp. 985–990. IEEE, jun 2011. (cited in p. 27)

[55] Zhang Shaojun, Zhao Pei, He Liqiang, Yang Yanyan, Liu Baoxian, He Weinan, Cheng Ying, Liu Ying, Liu Shijie, Hu Qingyao, Huang Cheng and Wu Ye. "On-board monitoring (OBM) for heavy-duty vehicle emissions in China: Regulations, early-stage evaluation and policy recommendations". *Science of The Total Environment*, Vol. 731, aug 2020. (cited in p. 27)

[56] Jiang Yu, Yang Jiacheng, Tan Yi, Yoon Seungju, Chang Hung-Li, Collins John, Maldonado Hector, Carlock Mark, Clark Nigel, McKain David, Cocker David, Karavalakis Georgios, Johnson Kent C. and Durbin Thomas D. "Evaluation of emissions benefits of OBD-based repairs for potential application in a heavy-duty vehicle Inspection and Maintenance program". *Atmospheric Environment*, Vol. 247 n^o December 2020, feb 2021. (cited in p. 27)

[57] Müller Volker, Pieta Holger, Schaub Joschka, Ehrly Markus and Körfer Thomas. "On-Board Monitoring to meet upcoming EU-7 emission standards – Squaring the circle between effectiveness and robust realization". *Transportation Engineering*, Vol. 10 n^o March, dec 2022. (cited in p. 27)

[58] Kim Hyung Jun, Jo Seongin, Kwon Sangil, Lee Jong-Tae and Park Suhan. "NOX emission analysis according to after-treatment devices (SCR, LNT + SCR, SDPF), and control strategies in Euro-6 light-duty diesel vehicles". *Fuel*, Vol. 310, feb 2022. (cited in p. 27)

[59] Posada Francisco and Bandivadekar Anup. "Global overview of on-board diagnostic (OBD) systems for heavy-duty vehicles". *The International Council on Clean Transportation*, n^o January, 2015. (cited in p. 28)

[60] Posada Francisco. "On-board diagnostics for heavy-duty vehicles : Considerations for Mexico". *International Council on Clean Transportation*, n^o February, 2014. (cited in p. 28)

[61] Kunimoto Akira, Hasei Masaharu, Yan Yongtie, Gao Yunzhi, Ono Takashi and Nakanouchi Yukio. "New Total-NOx Sensor Based on Mixed Potential for Automobiles". In *SAE Technical Papers*, number 724, mar 1999. (cited in p. 28)

[62] Inagaki Hiroshi, Oshima Takafumi, Miyata Shigeru and Kondo Noriaki. "NOx Meter Utilizing ZrO2 Pumping Cell". volume 1998, feb 1998. (cited in pp. 28 and 30)

[63] Riegel Johann. "Exhaust gas sensors for automotive emission control". *Solid State Ionics*, Vol. 152-153, pp. 783–800, dec 2002. (cited in p. 28)

[64] Ono Takashi, Yan Yongtie, Hasei Masaharu, Sato Masayuki, Kunimoto Akira, Tanaka Akio and Saito Toshitaka. "Total-NOx Sensor Based on Mixed-Potential for Detecting of Low NOx Concentrations". In *SAE Technical Papers*, number 724, apr 2005. (cited in p. 28)

[65] Frobert Arnaud, Raux Stephane, Creff Yann and Jeudy Eric. "About Cross-Sensitivities of NOx Sensors in SCR Operation". In *SAE Technical Papers*, volume 2, apr 2013. (cited in pp. 28, 29, 30, 31, 77, 78, 79, and 179)

[66] Kato Nobuhide, Kokune Nobuyuki, Lemire Bertrand and Walde Tim. "Long Term Stable NOx Sensor with Integrated In-Connector Control Electronics". In *SAE Technical Papers*, number 724, mar 1999. (cited in p. 28)

[67] Sasaki Hisashi, Scholl David, Parsons Mike, Inagaki Hiroshi, Shiotani Koji, Visser Jaco, Zawacki Garry, Kawai TakeshiI, Teramoto Satoshi and Kubinski David. "Development of an Al2O3/ZrO2-Composite High-Accuracy NOx Sensor". apr 2010. (cited in p. 28)

[68] Aliramezani Masoud, Koch Charles Robert, Secanell Marc, Hayes Robert E. and Patrick Ron. "An electrochemical model of an amperometric NOx sensor". *Sensors and Actuators B: Chemical*, Vol. 290, pp. 302–311, jul 2019. (cited in p. 28)

[69] Bonfils Anthony. *Experimental closed-loop control of SCR aftertreatment systems using NOx sensors cross-sensitive to NH3*. Theses, Ecole Nationale Supérieure des Mines de Paris, 2013. (cited in p. 29)

[70] Peyton Jones James C. and Geveci Mert. "Smart Sensing and Decomposition of NO x and NH 3 Components from Production NO x Sensor Signals". *SAE International Journal of Engines*, Vol. 4 n^o 1, apr 2011. (cited in p. 29)

[71] Hsieh Ming-Feng and Wang Junmin. "Development and experimental studies of a control-oriented SCR model for a two-catalyst urea-SCR system". *Control Engineering Practice*, Vol. 19 n^o 4, pp. 409–422, apr 2011. (cited in p. 31)

[72] Tang Wei, Cai Yixi and Wang Jun. "Experimental studies on the diesel engine urea-SCR system using a double NOx sensor system". *Environmental Engineering Research*, Vol. 20 n^o 4, pp. 397–402, dec 2015. (cited in p. 31)

[73] Wang Da Yu, Yao Sheng, Shost Mark, Yoo Joon Ho, Cabush David, Racine David, Cloudt Robert and Willems Frank. "Ammonia sensor for closed-loop SCR control". *SAE Technical Papers*, Vol. 1 n^o 1, 2008. (cited in p. 33)

[74] Lee Ingun, Jung Byounghyo, Park Jinsu, Lee Chunbum, Hwang Jeongsug and Park C.O. "Mixed potential NH3 sensor with LaCoO3 reference electrode". *Sensors and Actuators B: Chemical*, Vol. 176, pp. 966–970, jan 2013. (cited in p. 33)

[75] Willems Frank, Cloudt Robert, van den Eijnden Edwin, van Genderen Marcel, Verbeek Ruud, de Jager Bram, Boomsma Wiebe and van den Heuvel Ignace. "Is Closed-Loop SCR Control Required to Meet Future Emission Targets?". In *SAE Technical Papers*, volume 2007, apr 2007. (cited in pp. 34 and 95)

Part II

Experimental set-up and performed tests

Chapter 3

Experimental set-up

The more thoroughly I conduct scientific research, the more I believe that science excludes atheism.

— Lord Kelvin

Contents

3.1 Engine

During the development of this work all tests were carried out on a Euro 6c compliant 1.5 l light duty diesel engine installed in a chassis dynamometer test cell. The engine has common rail direct injection, variable geometry turbine (VGT) and intercooled high pressure exhaust gas recirculation (HP-EGR). The complementary engine information is presented in Table 3.1. The test bench is also equipped with an HORIBA FQ-2100DP fuel consumption measurement system and other conventional sensors (boost pressure, mass air flow, etc).

Table 3.1: Additional engine information.

Cylinder arrangement	four, in line
Displaced volume	1499 cm3
Bore	75 mm2
Stroke	84.8 mm2
Compression ratio	16.4:1
Maximum torque	300Nm@1750 rpm
Maximum power	96 kW@3750 rpm
Emission standard	Euro 6c

Figure 3.1 presents the complete engine schematic.

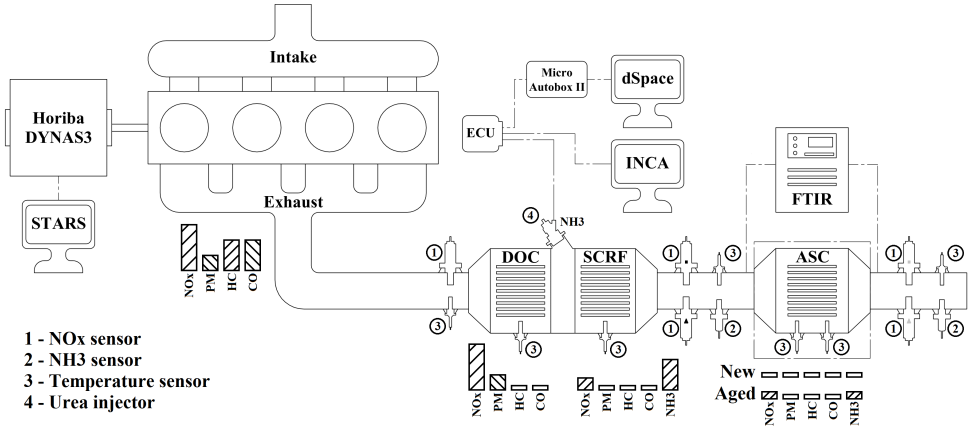

Figure 3.1: Schematic diagram of engine, after-treatment system, measurement system and the emission levels after each catalyst.

The engine and ATS assembly has been designed to enable a highly flexible control and design environment. As far as engine control is concerned, it is possible to implement the most diverse engine driving cycles and steadstate conditions. Regarding the ATS it can be easily interchangeable, both the catalysts and the placement of the monitoring system (sensors and gas analyser). With respect to the control unit, it is capable to act on the most diverse engine variables, such as: amount and timing of fuel injection, EGR valve opening, ammonia injection rate, among others. Therefore, during the course of the thesis, it was possible to carry out a broad variety of tests.

3.2 After-treatment structure and monitoring

Regarding the ATS, it is composed of a DOC, an SCRF and an ASC catalyst. In the case of ASC, three catalysts with different ageing levels were used: new, partially aged, and completely aged. Table 3.2 shows the catalysts characteristics and Figure 3.2 the complete after-treatment experimental set-up. Note that the ASC catalyst is the only element changed during the tests, since three catalysts with different levels of ageing were used.

Table 3.2: Complementary characteristics of SCRF and ASC catalysts.

Parameters	SCRF	ASC
Diameter x length	0.070x0.30 m2	0.014x0.10 m2
Cell density	600 cpsi	600 cpsi
Wall thickness	0.80 mm	0.08 mm
Catalyst composition	Cu/ZSM 5	Pt/Al2O3@Cu/ZSM 5

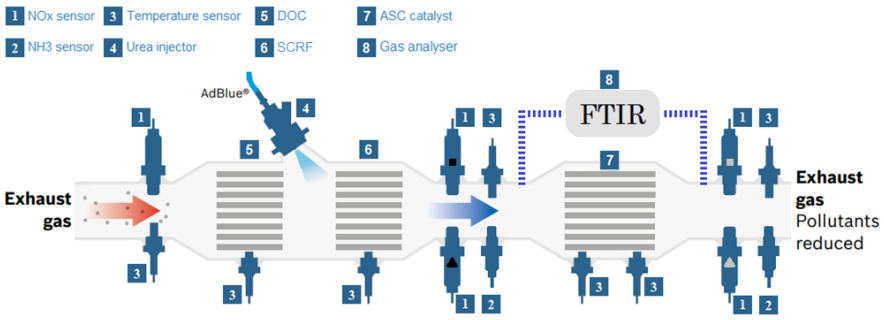

Figure 3.2: Complete after-treatment system with SCR and ASC catalyst fully instrumented.

The architecture concept of the ATS aims to achieve the highest NOx conversion efficiency with minimum NH3 slip, analysing such behaviour in four different scenarios: SCR catalyst only, or SCR catalyst plus ASC catalyst at three different ageing levels. For this reason, the ATS monitoring system has two NOx sensors and one NH3 placed before and after the ASC catalyst and a NOx sensor before the SCR, as well as thermocouples before and after the catalysts and in the monoliths.

The sensors arrangement layout (NOx, NH3 and temperature) was designed for two main reasons:

- To allow the acquisition of as much information as possible from the ATS, as this thesis uses such information to develop models and strategies, this concept broadens the horizon of possibilities.

- The NOx sensor placement before the SCR catalyst enables to take advantage of the non-influence of ammonia cross-sensitivity on the sensor. As well as the use of two NOx sensors located at the same place, but with different sensibility to ammonia allows to understand such behaviour.

Note that in the approaches where only one NOx sensor was used at each position (before the SCR catalyst and before or after the ASC catalyst), the signals from the sensors with square markers were considered (dark markers upstream of the ASC catalyst and light grey downstream). In the case where the two NOx sensors were taken into account, squares refer to sensors 1 and triangles refer to sensors 2.

To compare the signals provided by the sensors described above, a HORIBA MEXA-ONE-FT gas analyser based on Fourier Transform Infrared (FTIR) was placed before and after the ASC catalyst. Table 3.3 shows the measurement equipment information.

Table 3.3: Measurement equipment information.

Equipment	Measurement
FTIR	NOx 0–2000 ppm$\leqslant$ 1.0% of full scale NH3 0–1100 ppm$\leqslant$ 1.0% of full scale
NOx sensor	0–1860 ppm$\pm$15 ppm@0–1000 ppm $\pm$1.5%@<1000 ppm
NH3 sensor	0–6550 ppm$\pm$1.5% of full scale
Thermocouple	-270-1260 °C $\pm$2.2% °C - Type K
Fuel mass flow meter	0.2–108 kg/h – uncertainty$\leqslant$ 0.12%

3.3 Control environment

Engine control is separated into three main systems: INCA, dSpace and STARS.

- INCA is responsible for acquiring the information from the open electronic control unit (ECU) through an Ethernet based ETK port connected to the ETAS910 rapid prototyping system.

- For the variables that is desired to control independently of the ECU, such as the ammonia injection, a bypass signal is created in the INTECRIO and compiled in the dSpace system, which is also responsible for recording the information from the NOx and NH3 sensors through a CAN connection. The communication between the dSpace system and the ECU is done through the MicroAutobox II microcontroller.
- The engine is coupled to a HORIBA DYNAS3 asynchronous dynamometer, and its control and monitoring is carried out through the HORIBA SPARC platform and the HORIBA STARS automation interface. This system allows the performance of stationary tests, engine maps and transitory homologation cycles, as well as responsible for recording the temperature and pressure information of the test cell environment, the ATS and the entire powertrain.

Table 3.4 shows how each device in the Hardware-in-the-loop (HIL) system is used in the experimental set-up, and

Table 3.4: Hardware-in-the-loop systems description.

Programming software	User software	Hardware	Use
	Horiba STARS	Horiba SPARC	Engine control Engine monitoring Record system temperatures Record system pressures
		ECU	Standard engine calibration
INTECRIO	INCA	ETAS 910	ECU management Record ECU signals Enable ECU bypass
MATLAB Simulink	dSpace	MicroAutobox II	Generate test signals Record sensor signals ECU bypass signal Access to model structure

Chapter 4

Engine test procedure

Without data, you're just another person with an opinion.

— William Edwards Deming

Contents

4.1 Test procedure

During the development of the thesis, nearly 700 hours of tests were carried out. The procedure for performing each test has the following steps.

- Preconditioning - procedure performed before each test to ensure equal initial conditions, thus enabling comparison between tests. During the thesis, two different types of preconditioning were performed: methods 1 and 2.
- Ammonia injection strategy - several ammonia injection strategies were used in the SCR catalyst, such as: standard injection, off-line optimisation, real-time control, and ammonia injection failure simulation.
- Engine test - different types of tests were performed, such as engine maps, tests for sensor characterization and driving cycles. Engine tests can be classified as modelling, which are the tests used for the development of computational models and control strategies, and validation, tests used to prove the level of accuracy of the models and the effectiveness of the proposed control strategies.

Since the thesis focused on the study of different combinations of ATS as: SCR, SCR + new/partially aged/aged ASC, depending on the ATS design different preconditions, ammonia injection strategies, and tests were performed.

4.2 Preconditioning

The reactivity of SCR and ASC catalysts depends on the amount of ammonia stored within the catalyst; therefore, characterisation tasks require knowledge of the initial conditions of the cycles. The following procedures are proposed to guarantee that the catalyst is ammonia-free by selecting an operating point that secures a high temperature and an oxidizing atmosphere to remove the accumulated ammonia, or ensuring that the catalyst is fully charged. Only these two initial operating conditions (empty and saturated) are defined, since estimating an intermediate state of charge is a rather difficult task as there are no sensors for this purpose.

The preconditioning procedure starts with an operating point at 2000 rpm and 140 Nm without urea injection for approximately 3600 seconds. In these conditions, SCR inlet temperature is above 500 °C and ASC above 300 °C, with NOx concentration close to 1000 ppm; therefore, the accumulated ammonia is reacting with NOx, provoking a progressively ammonia consumption and coverage convergence to zero, followed by a stabilization of the engine parameters (mass flow, pressures, temperature, etc.). In Figure 4.1, is presented a set of preconditioning tests performed before starting the test and the test itself, with the respective engine conditions and ammonia injection strategy.

4.2.1 Method 1 – Performed to aged and new catalyst

Method 1 is performed to ensure that the catalyst is completely empty at the beginning of the test, and is carried out for the new and aged catalyst (upper plot Figure 4.1). The catalyst depleting is followed by the stabilization of the engine parameters with an operating point of 1800 rpm and 30 Nm for approximately 3600 seconds. In this approach, during the preconditioning non ammonia is injected.

4.2.2 Method 2 – New catalyst

Method 2 is used to ensure a saturated state of the catalyst at the beginning of the test, and is performed only for the new ASC catalyst (bottom plot Figure 4.1). The catalyst depleting is followed by the stabilization of the engine parameters; however, during this phase a constant amount of ammonia is injected (32mg/s - 52Nm@1250rpm) until the saturation of the ASC catalyst (<3600 seconds). This approach was applied for the new catalyst, as with Method 1 the observable ammonia downstream of the new ASC is very low.

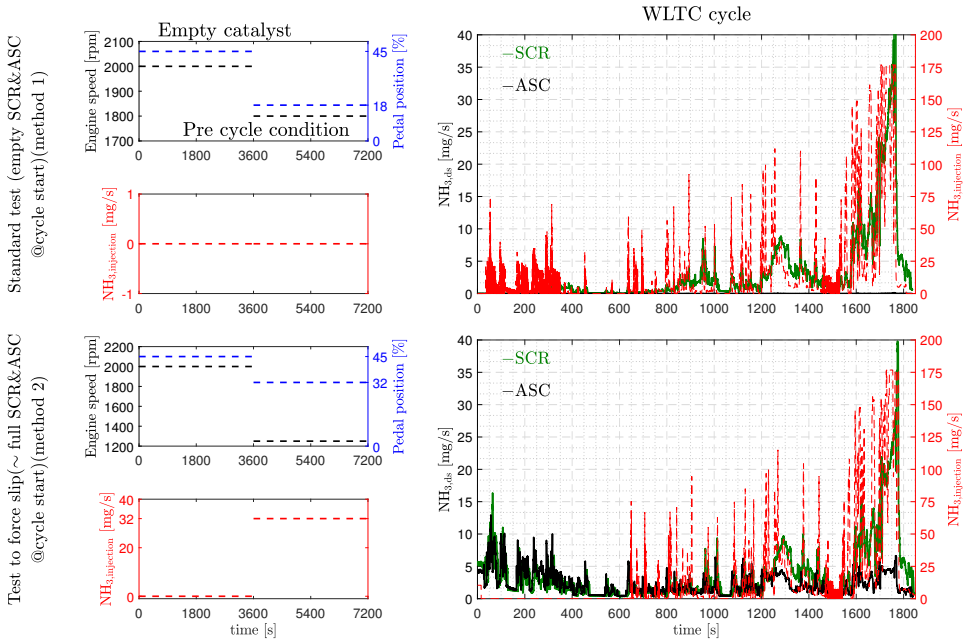

Figure 4.1: Complete conditioning to perform a cycle for 2 different methods. In the exemplified case followed by a WLTC cycle. For each method. Left side plots are related to preconditioning. The upper left plot: the engine operation condition. Bottom left plot: NH3 injection. Right side plot: NH3 slip evolution and the NH3 injection strategy.

4.3 Ammonia injection strategy

The ammonia injection strategy can be divided into four main approaches:

4.3.1 Standard injection

The standard strategy is the one assembled within the ECU. This strategy is intended to maintain the ammonia load within the catalyst between a predetermined interval. Figure 4.2 shows an example of the evolution of ammonia load inside the catalyst, ammonia injection and NOx concentration at engine outlet during a WLTC cycle starting with empty catalyst.

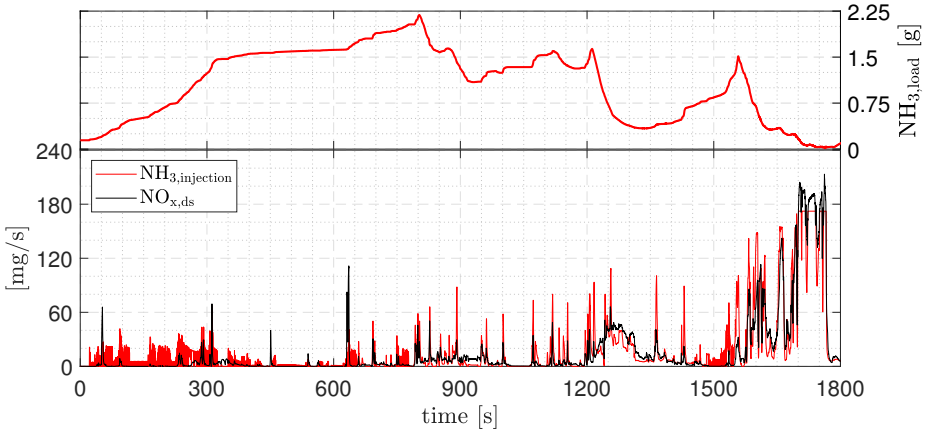

Figure 4.2: Evolution of NOx slip, ammonia injection (Bottom plot) and ammonia loading inside the SCR (Upper plot) during a WLTC cycle starting with the catalyst empty.

As can be seen, in a first step (∼800 s) the control strategy aims to increase the catalyst load through injection pulses, then the control system tries to maintain the load by injecting the same amount of NH3 as the exhaust NOx. As expected, the control system is not able to maintain constant ammonia loading and at a high value, since the ATS is very dynamic and at high mass flow rates (∼1650 to 1750 s) it is difficult to control the adsorption and desorption capacity of the catalyst.

4.3.2 Off-line optimisation

In the case of ammonia injection of the off-line optimisation the whole injection profile is bypassed. In this strategy the ECU signal to the urea injector is blocked, and a new value is provided, this same value is sent as a feedback signal to the ECU.

Note that the ammonia injection is optimised off-line and the entire injection profile resulting from the optimisation is compiled in advance, thus any change in the cycle behaviour will not affect the injection signal. As can be seen in Figure 4.3, the engine and cycle variables do not affect the injection profile as it is only time dependent.

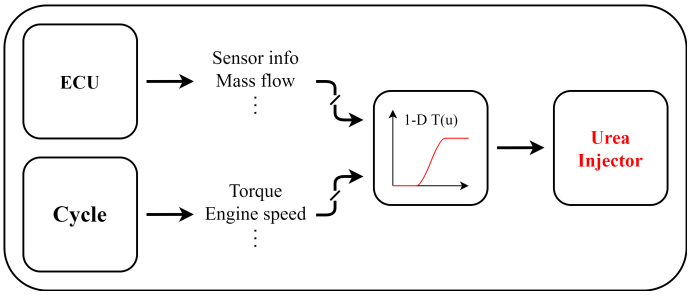

Figure 4.3: Ammonia injection layout with off-line optimisation.

4.3.3 Real-time optimisation

In real-time optimisation, just as in off-line, the injection signal coming from the ECU is blocked. However, other information from the ECU and the cycle are used to feed the model, which in turn decides on the amount of ammonia that should be injected, as can be seen in Figure Figure 4.4.

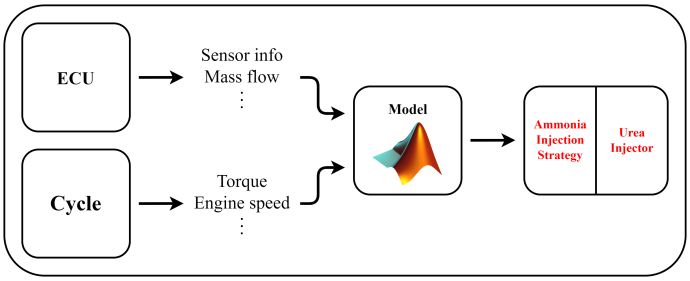

Figure 4.4: Ammonia injection layout with real-time optimisation.

4.3.4 Injection failure simulation

The injection failures are produced artificially, multiplying the nominal value of ammonia injection by an Injection Factor (I.F.), thus changing the injector opening time. During the work the I.F. is represented by values that vary between 0 and 1, and depending on the desired approach, a constant value or a time-varying can be used.

As an example (Figure 4.5), the application of an I.F. = 0.80, represents that the amount of injected ammonia is approximately 80% of the demanded by the ECU. However, the feedback of the signal to the ECU is the integral value of the injection. In this way, the I.F. refers to the ammonia failure level invisible to the control strategy.

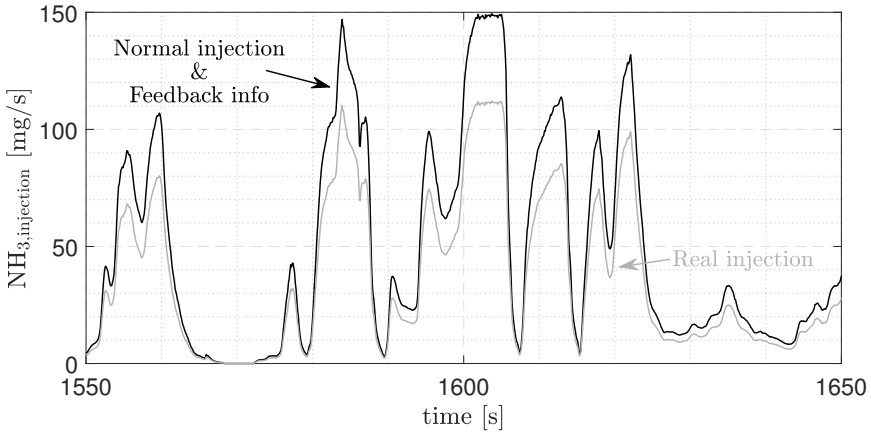

Figure 4.5: Example of the I.F. approach regarding the signal sent and received by the control unit.

4.4 Engine test

During the development of the thesis several cycles were performed. They are aimed to support the model development, as well as evaluate the proposed emissions control strategies and access the accuracy of the models.

4.4.1 Steady-state cycles

Steady-state cycles include engine map and characterization of catalysts and sensors. The engine map was used in the initial phases of model development since controlled conditions make it easier to identify the system behaviour. The same applies for the characterization tests of the catalysts and sensors, however in these cases the influence of different amounts of NH3 injection in different operational conditions was sought.

Figure 4.6 shows all the stationary conditions which were tested, where the filled circles refer to the constant injection test, and the squares to the NH3 injection varying during the test.

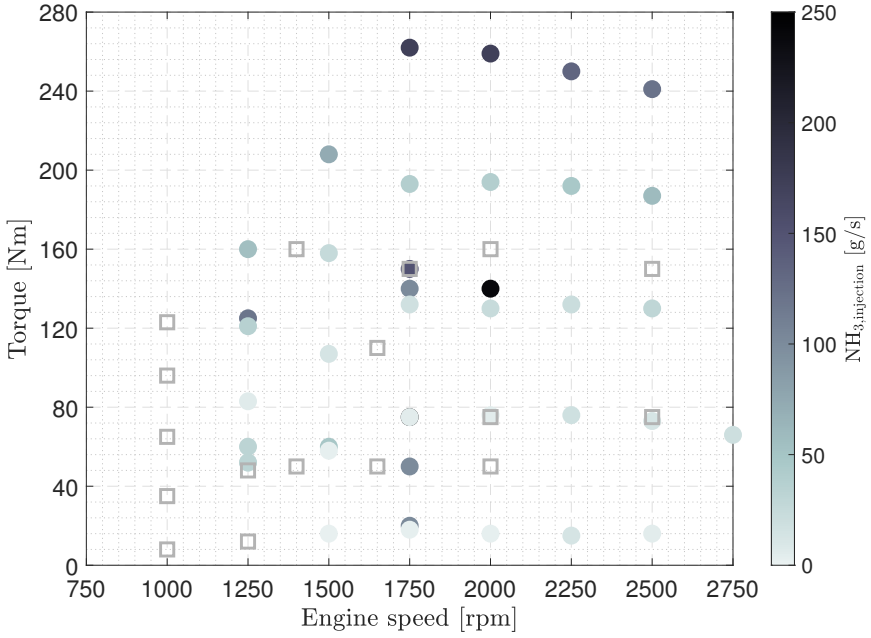

Figure 4.6: Operating conditions of steady-state cycles. Filled circles: constant NH3 injection test, where the injection rate is represented in the scale colour bar. Squares: NH3 injection varying during the test.

4.4.2 Driving cycles

Regarding transient tests, standard driving cycles were used, such as WLTC, RDE and Twice Standardised Random Test (2RTS), but also some alternative cycles, called, New Driving Cycle (NDC) 1, NDC 2 and merged.

Standard driving cycles The standard cycles were used for both the development and validation of the models. The comparison of the operating zone in terms of engine speed and torque, and complementary cycle information can be seen in Figure 4.7 and Table 4.1, respectively.

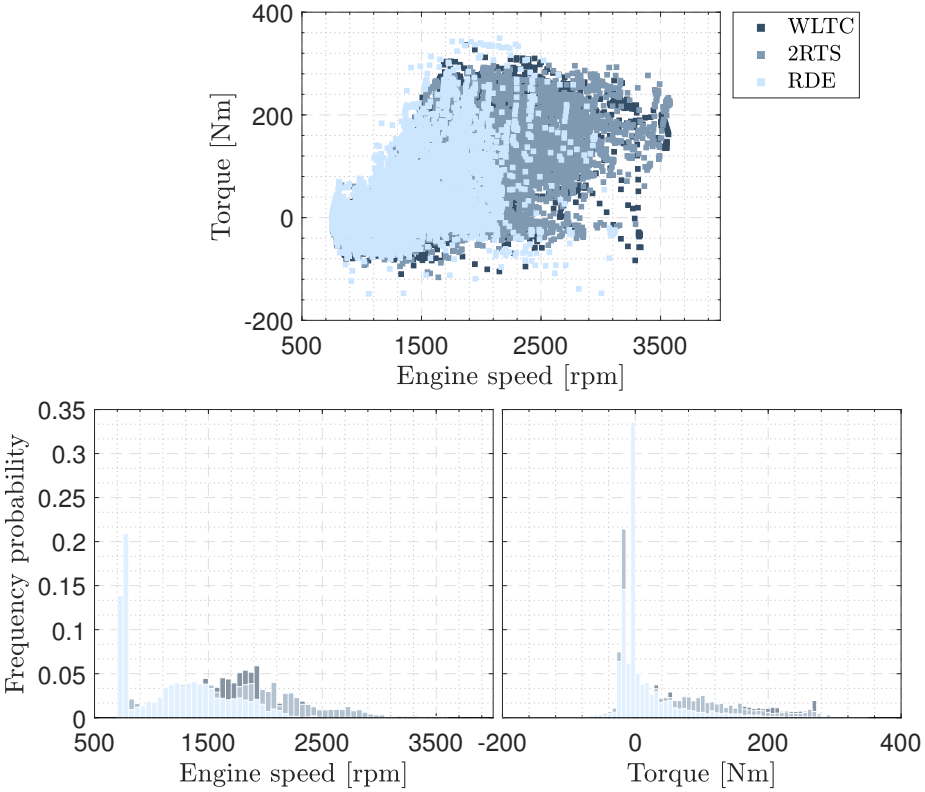

Figure 4.7: Comparison of the standard cycles' operating zone. Upper plot: operating points of the cycles in terms of engine speed (x-axis) and torque (y-axis). Bottom plots: distribution of the operating zones of each cycle.

Table 4.1: Additional cycle information.

	Distance (km)	Duration (s)
WLTC	23.79	1830
2RTS	26.00	1762
RDE	16.65	1816

Alternative cycles In the case of alternative cycles, they were used only for validation, thus demonstrating that the models have a good performance not only in the specific cycles used in their calibration. Its operating zone is shown in Figure 4.8 and complementary cycle information in Table 4.2.

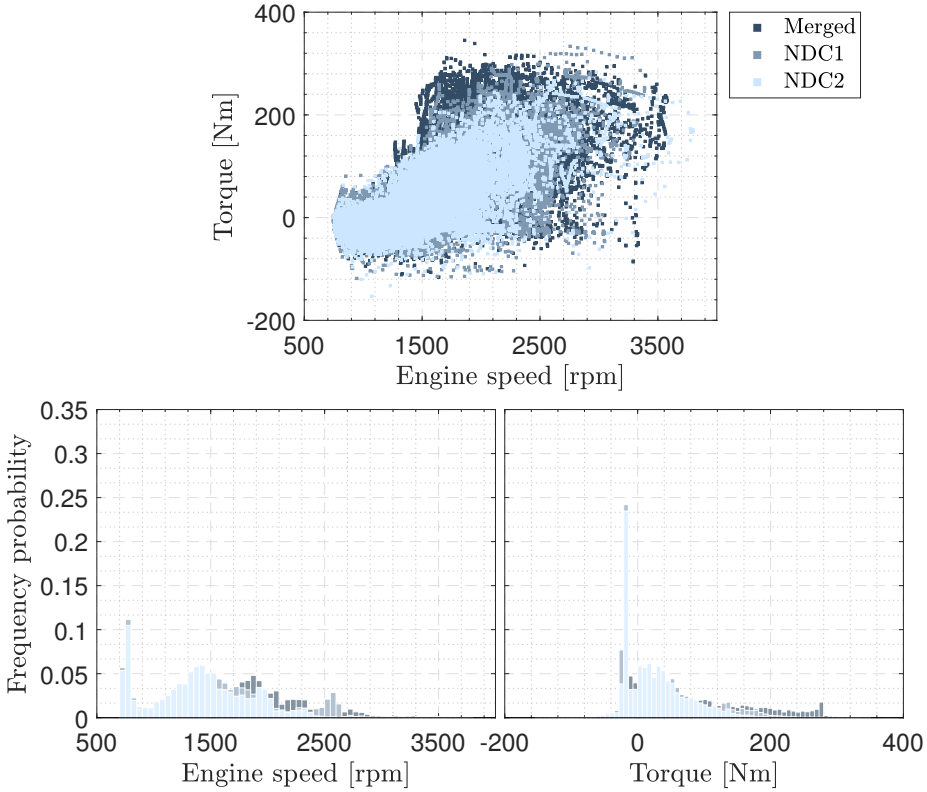

Figure 4.8: Comparison of the alternative cycles' operating zone. Upper plot: operating points of the cycles in terms of engine speed (x-axis) and torque (y-axis). Bottom plots: distribution of the operating zones of each cycle.

Table 4.2: Additional cycle information.

	Distance (km)	Duration (s)
Merged	73.60	5400
NDC1	70.70	5926
NDC2	73.31	6151

Part III

Control-oriented modelling

Chapter 5

NOx and NH3 slip prediction models

Programming isn't about what you know; it's about what you can figure out.

— Chris Pine

Contents

5.1 Introduction

Computational modelling is a technique used for the development of new technologies and/or improvement of current ones [1], having a wide range of applications, from the reconstruction of a previous event, to estimating the behaviour of complex systems [2]. The use of computational models has several advantages, such as: the possibility of joint use with monitoring and diagnostic strategies, feasibility check before real-world application, implementation of new strategies and their potential advantages and disadvantages, etc [3]. However, depending on the system to be represented, the computational cost may be too high, or due to its complexity, the estimation error may be higher than expected [4]. In this sense, the modelling process is a compromise between using as much mathematical complexity as necessary to correctly describe the phenomena, while keeping the model as simple as possible [5].

5.2 Zero-dimensional model

To analyse the impact of a strategy and assess its effect on emission abatements it is necessary that the model developed be capable to represent the phenomena occurring in the ATS. However, there are usually several intermediate processes taking place inside the catalyst, which in turn affect the final result. As a regular approach, these intermediate processes are simplified and/or ignored, thus turning the engine into a computational model with outputs that are totally dependent on some input signals [6]. Meantime, in the implementation of control strategies, the analysis of the intermediate processes affected when a certain strategy is followed, is interesting because it helps to identify the control factors that improve the emissions abatement [7].

In the case of zeolite-based catalysts, the main control parameter is the ammonia coverage ratio (i.e., the ratio of the amount of ammonia adsorbed by

the catalyst to the maximum adsorption capacity [8]), which is affected by the intermediate processes of ammonia adsorption, desorption, and consumption through different reactions. Moreover, these intermediate factors may have competing effects on ammonia coverage ratio, and it is not always easy to quantify and isolate them [9].

Building computational models capable to assess the behaviour of such reactions can be quite a challenging task. However, unlike high-dimensional, zero-dimensional (0D) models do not require high computational effort and are able to provide accurate results in a short time given a proper preliminary calibration [10]. Thus, 0D catalyst models are suitable candidates for emissions prediction and use in conjunction with control strategies.

5.2.1 SCR Zero-dimensional model

The proposed SCR zero-dimensional model follows the standard control-oriented modelling approach reported in the literature [11–13], which considers the NH3 storage and the NOx main reactions. The model is based on the continuously stirred tank reactor (CSTR) approach (i.e. the concentration of one gas species is homogeneous in all the directions) [14] to compute the NO, NO2, and NH3 balances. A general outline of the model states, inputs and outputs is shown in Figure 5.1.

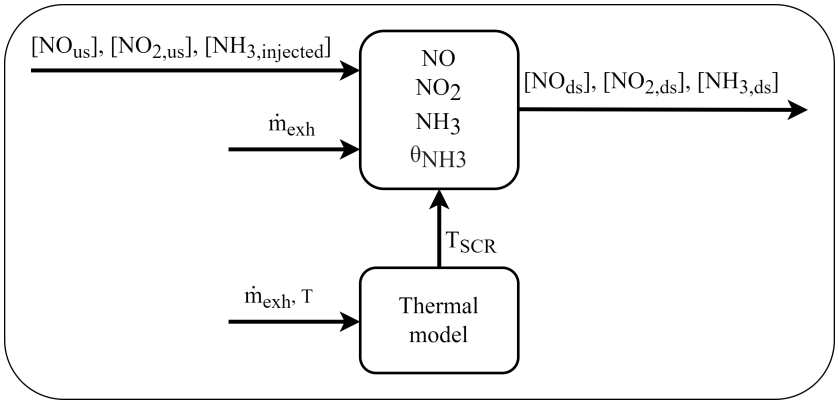

Figure 5.1: SCR 0D model scheme.

The model uses as input signals, nitrogen oxide (NO_{us}) and nitrogen dioxide ($NO_{2,us}$) of the engine exhaust gas, ammonia injected into the SCR catalyst ($NH_{3,injected}$), exhaust mass flow ($\dot{m}_{exh}$) and catalyst temperature (T_{SCR}), which, in turn, uses a filter on the temperature coming from the thermocouple placed in the middle of the catalyst. The output signals of the

model are nitric oxide (NO_{ds}), nitrogen dioxide ($NO_{2,ds}$), and ammonia slip ($NH_{3,ds}$), which in this case is the ammonia concentration after the reactions inside the SCR catalyst.

The reducing agent for NOx abatement into the SCR catalyst is an aqueous urea solution (AdBlue) which is decomposed into NH3. The model used does not include urea decomposition and assumes that the available ammonia is a constant proportion of the urea injection (32.5%). The model considers the main SCR reactions; standard (eq.2.1), fast (eq.2.2), and slow (eq.2.3) to calculate the balances of NO, NO2 and NH3 species, as well as the adsorption (eq.5.1), desorption (eq.5.1), and NH3 storage on the catalyst surface (eq.5.2).

$$NH_3 + {}^* \Leftrightarrow NH_3^*, \tag{5.1}$$

where, towards the right represents the adsorption equation and the opposite desorption.

$$\Delta\theta_{NH_3} = NH_{3,\text{adsorbed}} - NH_{3,\text{desorbed}} - NH_{3,\text{oxidised}}, \tag{5.2}$$

Note that the equation defining the variation in the amount of ammonia stored in the catalyst depends on how the model is designed, in the case at hand, it is considered that the $\Delta\theta_{NH_3}$ depends on the amount of ammonia adsorbed ($NH_{3,\text{adsorbed}}$) minus the amount of ammonia desorbed ($NH_{3,\text{desorbed}}$) and oxidised in the presence of NOx ($NH_{3,\text{oxidised}}$).

Due to the 0D approach, the equations presented above are discretised in time, thus the reactions are calculated with the following Arrhenius equations.

NH3 reacts with NO, which is responsible for most of the raw NOx emissions in diesel engine exhaust. This reaction is called the SCR standard reaction rate (r_{std}) [15].

$$r_{std} = k_{std} e^{\left[\frac{-E_{std}}{R}\left(\frac{1}{T_{SCR}} - \frac{1}{T_{ref}}\right)\right]} [NO]\theta_{NH_3}^* \left(1 - e^{\left(\frac{-\theta_{NH_3}}{\theta_{NH_3}^*}\right)}\right), \tag{5.3}$$

where k_{std} [m^3/mol·s] is the standard SCR frequency factor, E_{std} [J/mol] is the standard SCR activation energy, R [J/mol · K] is the universal gas constant, T_{SCR} [K] is the SCR temperature, T_{ref} [K] is the reference temperature, NO [mol/m^3] is the nitrogen oxide concentration, and θ_{NH_3} [−] is the surface coverage fraction. The parameter critical surface coverage ($\theta_{NH_3}^*$ [−]) has been included since the standard reaction rate of SCR is essentially independent of ammonia surface coverage above a critical surface concentration of NH3 [8].

As usually a DOC is installed prior to the SCR, NO in the exhaust gas is oxidized to NO2. With the production of NO2, NH3 reacts in the presence of

NO and NO2. This is called the SCR rapid reaction rate (r_{fst}) because it is the fastest of the major SCR reactions [16].

$$r_{fst} = k_{fst} e^{[\frac{-E_{fst}}{R}(\frac{1}{T_{SCR}} - \frac{1}{T_{ref}})]} [NO][NO_2]\theta_{NH_3}, \tag{5.4}$$

where k_{fst} [$m^6/mol^2 \cdot s$] is the fast SCR frequency factor, E_{fst} [J/mol] is the fast SCR activation energy, and NO_2 [mol/m^3] is the nitrogen dioxide concentration.

Meanwhile, NH3 may react with NO2 alone. This is the slow reaction rate of SCR (r_{slw}) since the reaction occurs more slowly than the main SCR reactions [17].

$$r_{slw} = k_{slw} e^{[\frac{-E_{slw}}{R}(\frac{1}{T_{SCR}} - \frac{1}{T_{ref}})]} [NO_2]\theta_{NH_3}, \tag{5.5}$$

where k_{slw} [$m^3/mol \cdot s$] is the slow SCR frequency factor and E_{slw} [J/mol] is the slow SCR activation energy. The NH3 adsorption (r_{ads}) and desorption (r_{des}) reaction rate equations are presented below.

$$r_{ads} = k_a e^{[\frac{-E_a}{R}(\frac{1}{T_{SCR}} - \frac{1}{T_{ref}})]} [NH_3](1 - \theta_{NH_3}) \tag{5.6}$$

$$r_{des} = k_d e^{[\frac{-E_d(1-\alpha\theta_{NH_3})}{R}(\frac{1}{T_{SCR}} - \frac{1}{T_{ref}})]} \theta_{NH_3}, \tag{5.7}$$

where k_{ads} [$m^3/mol \cdot s$] is the adsorption frequency factor, E_{ads} [J/mol] is the adsorption activation energy, k_{des} [1/s] is the desorption frequency factor, E_{des} [J/mol] is the desorption activation energy, and NH_3 [mol/m^3] is the ammonia concentration.

For the NH3 storage, a standard mass balance is applied, so the accumulated NH3 in a given instant depends on its previous state, adsorption, desorption, and the consumption through different reactions with their corresponding stoichiometry.

$$\frac{\partial \theta_{NH_3}}{\partial t} = r_{ads} - r_{des} - r_{std} - 2r_{fst} - \frac{4}{3} r_{slw} \tag{5.8}$$

Intended to include the effect of spatial velocity (SV) of the exhaust gas flow of the NO, NO2, and NH3 and have the effect of the residence time of the species inside the catalyst, the CSTR approach are used.

$$SV = \frac{\dot{m}_{exh}}{\delta_{gas}} \times \frac{\zeta_{SCR}}{V_{SCR}}, \tag{5.9}$$

where $\dot{m}_{exh}$ [kg/s] is the exhaust mass flow, δ_{gas} [kg/m^3] is the gas density, ζ_{SCR} [−] is the factor that represents the open portion of the SCR volume, and V_{SCR} [m^3] is the SCR volume. The species concentration states are presented in the following equations:

$$\frac{\partial NO}{\partial t} = -\Omega(r_{std} + r_{fst}) + SV([NO_{us}] - [NO]) \tag{5.10}$$

$$\frac{\partial NO_2}{\partial t} = -\Omega(r_{fst} + r_{slw}) + SV([NO_{2,us}] - [NO_2]) \tag{5.11}$$

$$\frac{\partial NH_3}{\partial t} = -\Omega(r_{ads} - r_{des}) + SV([NH_{3,us}] - [NH_3]), \tag{5.12}$$

where Ω [mol/m^3] is the maximum ammonia storage capacity of the SCR catalyst.

To fully characterize the catalyst behaviour, it is necessary to estimate some parameters based on the measured input–output data from an operational SCR catalyst. If the temperature of the catalyst was too low or the initial value for the surface coverage was wrong, the estimated results may be affected. To minimise these errors and improve the 0D model, a design of experiments (DoE) was used to identify the SCR model tunable parameters (i.e. for each parameter, the maximum and minimum values were defined; after applying the DoE, the combinations of parameters that showed the smallest error between experimental and simulated values were selected). Table 5.1 shows the estimated values for all parameters, including the tunable parameters (frequency factors k_i and activation energy factors E_i) after the calibration.

Table 5.1: SCR 0D model tunable parameters.

Tunable Parameter	Symbol	Value	
`Ads frequency factor`	k_{ads}	175	$[m^3/mol \cdot s]$
`Des frequency factor`	k_{des}	0.02	$[1/s]$
`Fst SCR frequency factor`	k_{fst}	3.39e4	$[m^6/mol^2 \cdot s]$
`Slw SCR frequency factor`	k_{slw}	1.85	$[m^3/mol \cdot s]$
`Std SCR frequency factor`	k_{std}	36	$[m^3/mol \cdot s]$
`Ads activation energy`	E_{ads}	11.47	[J/mol]
`Des activation energy`	E_{des}	1.11e5	[J/mol]
`Fst SCR activation energy`	E_{fst}	3.58e4	[J/mol]
`Slw SCR activation energy`	E_{slw}	4.75e4	[J/mol]
`Std SCR activation energy`	E_{std}	3.14e4	[J/mol]

Parameter	Symbol	Value	
`Critical Surface Coverage`	$\theta^*_{NH_3}$	0.1995	$[-]$
`Gas Density`	δ_{gas}	0.7327	[kg/m3]
`Reference Temperature`	T_{ref}	600	[K]
`SCR Storage Capacity`	Ω	80	$[mol/m^3]$
`SCR Volume`	V	0.0012	$[m^3]$
`SCR Volume Open Portion`	ζ_{SCR}	0.83	$[-]$
`Surface Coverage Fraction`	θ_{NH_3}	0.35	$[-]$
`Universal Gas Constant`	R	8.3145	$[J/mol \cdot K]$

5.2.2 Model results

The model was tested under different engine conditions and ammonia injections, the results obtained with the model were compared with those provided by the FTIR gas analyser to determine the accuracy of the model. In a first step the model was calibrated in a steady-state of 124 Nm@1500 rpm, with the SCR catalyst temperature of 478 °C±8. The main variation was in the ammonia injection profile, which is presented in Figure 5.2.

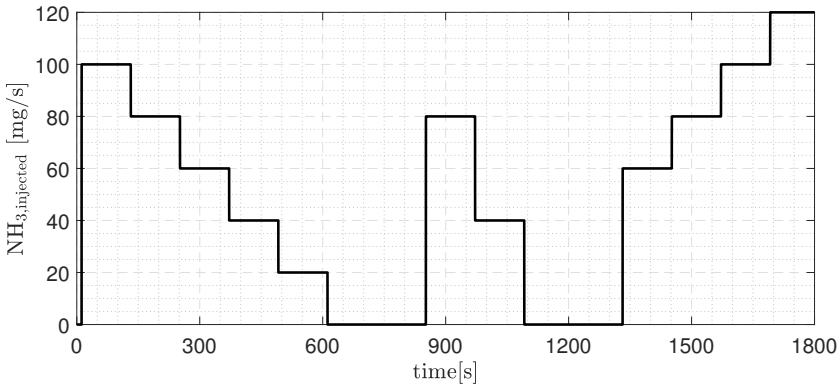

Figure 5.2: Evolution of the ammonia injection profile used in the calibration of the 0D model.

Figure 5.3 shows the comparison between the experimental data and the 0D model in terms of NOx and NH3 emissions.

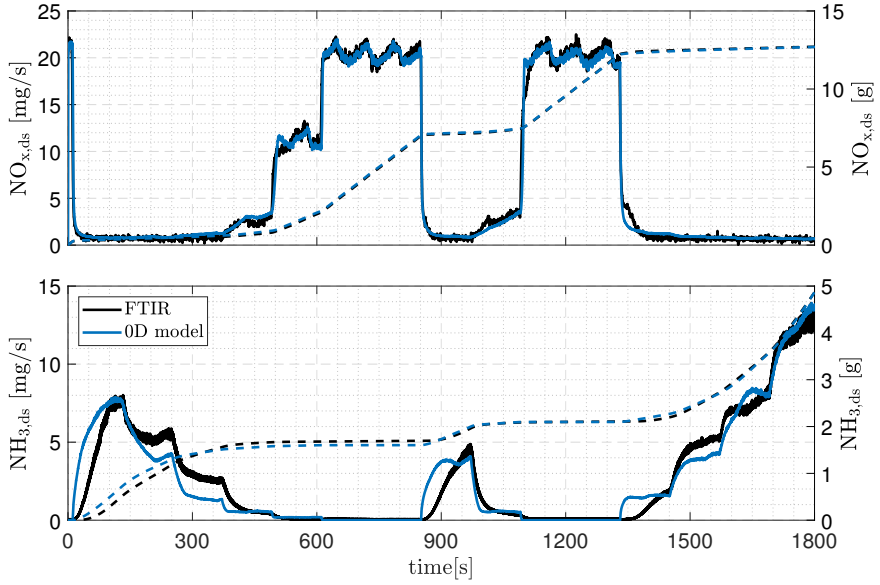

Figure 5.3: Comparison between FTIR and 0D model for NOx (upper plot) and NH3 (bottom plot) slip. Continuous lines represent the instantaneous value (left axis), and dashed lines represent the cumulative value (right axis).

As can be seen, the measured and modelled signals (both instantaneous and accumulated) present a high similarity, especially in terms of NOx (upper

plot). Regarding NH3, the model can follow the same slip trend, however, at the slip onset points the model shows an abrupt increase in slip, whereas the evolution should be smoother. The higher model error in terms of NH3 than NOx can be justified by the fact that NH3 slip is more sensitive to the ammonia coverage ratio, therefore potential errors in estimating the amount of ammonia stored in the SCR catalyst are transmitted to the NH3 slip. Another point is that NH3 slip is highly dependent on catalyst temperature, so a more complex temperature model may be required, also the emission behaviour is highly related to the ammonia injection profile, thus any deviation or delay in the feedback signal will affect the result.

For validation, the model was tested on driving cycles such as WLTC and 2RTS. To analyse the results, the σ_2 error was applied in the estimation of NOx and NH3. σ_2 is an empirical rule stating that, for many reasonably symmetrical unimodal distributions, different proportions of the population are within two standard deviations of the mean (95.45% of instantaneous errors) [18].

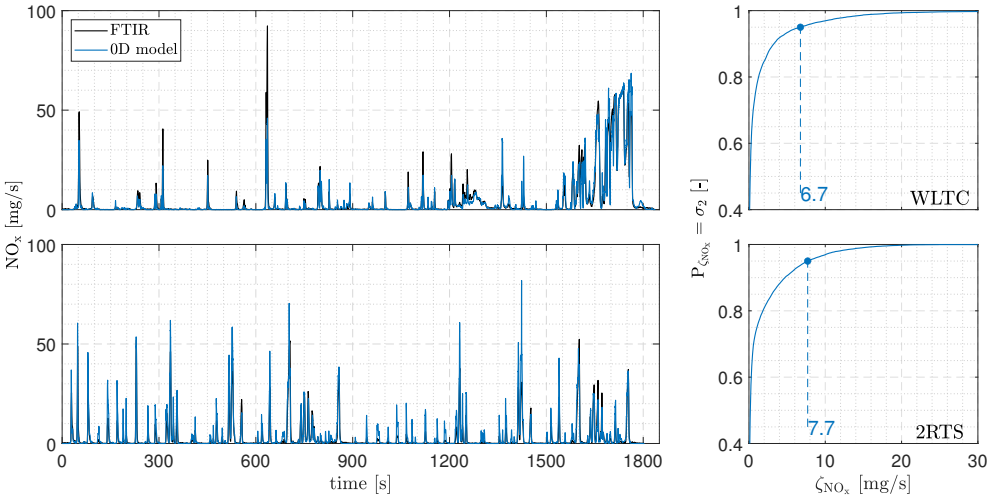

Figure 5.4: Comparison between FTIR and 0D model for NOx downstream in a WLTC (upper plots) and 2RTS (bottom plots) cycle. The left plots represent the emissions evolution, while the right ones the σ_2 error.

For the NOx signal, differences can be appreciated at very high concentrations, when the evolution of NOx changes quickly. The use of 0D models without spatial discretization usually leads to this kind of limitations, as the transport of species between two sections is not properly captured.

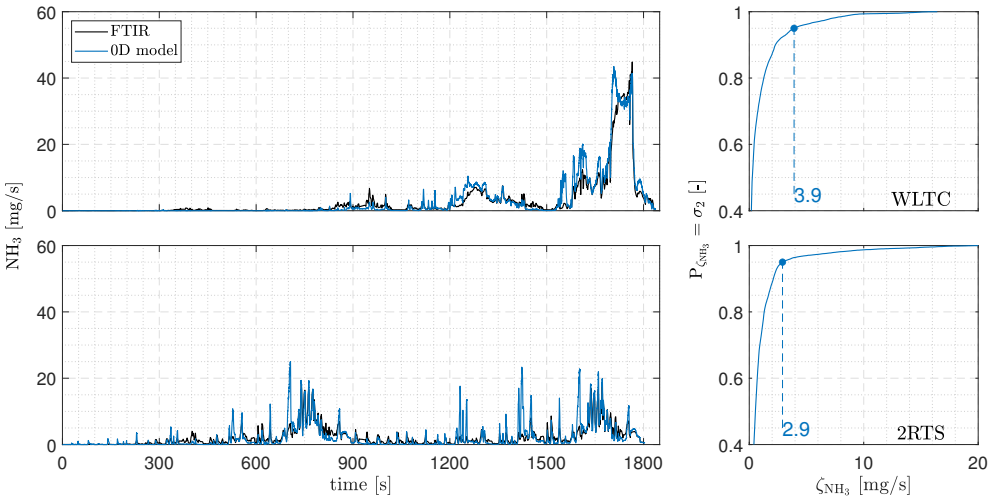

Figure 5.5: Comparison between FTIR and 0D model for NH3 downstream in a WLTC (upper plots) and 2RTS (bottom plots) cycle. The left plots represent the emissions evolution, while the right ones the σ_2 error.

As expected, higher differences can be appreciated in the NH3 signal. The detachment between the two signals can be attributed to the boundary conditions of the model, since the adsorption and desorption of ammonia depend on the exact amount stored in the SCR, and these variables are difficult to control in an experimental dynamic test. Even so, the error between estimated and measured is considerably low. Note that higher error values are observed in the NOx slip since the emission level is also higher.

Thus, the results show that the proposed SCR zero-dimensional model is able to represent with a substantial degree of accuracy the behaviour of the catalyst with low computational burden so it can be integrated in optimisation tools and control strategies.

5.2.3 SCR+ASC Zero-dimensional model with reduced states

As described previously, ASC catalyst is usually coupled after the SCR. This design allows for a more aggressive ammonia dosing strategy, achieving greater NOx abatement without increasing ammonia emissions [19]. However, to represent such an ATS architecture through a zero-dimensional physical model for real-time control strategy applications, the number of model states plays an important role, since for each additional state the computational cost increases exponentially [20].

Considering that the main states of SCR and ASC catalyst are the same

(eqs.5.8, 5.10-5.12), creating an eight-state model aiming real-time optimal control becomes unfeasible. Thus, it was sought to create a SCR+ASC model with reduced states capable to operate in real-time but maintaining a high level of accuracy in the emission prediction. For such implementation, three main hypotheses were assumed:

(i) The functionalities of both catalysts are the same: reduction of NOx emissions in the presence of ammonia, capacity to store ammonia and subject to the same reactions (eqs.5.8, 5.10-5.12).

(ii) Since the functionalities of the catalysts are considered the same, and the proposed approach ignores the mass transfer inside the model itself, both systems are considered as one. Thus, the ATS becomes a four-state system instead of an eight.

(iii) After the SCR catalyst, the NOx emissions are mainly composed of NO. As can be seen in Figure 5.6, in a WLTC cycle during 99% of the time, NO2 emissions are below 7 ppm; therefore, the zero-dimensional model starts to consider NOx only as NO and transforming the model into a three-state system.

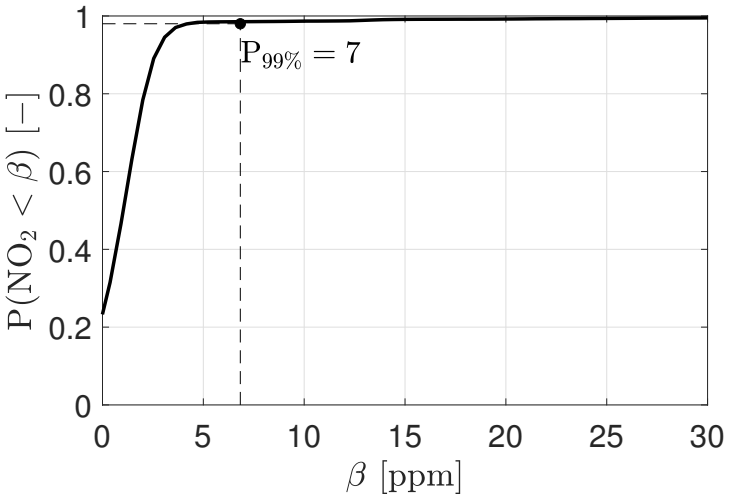

Figure 5.6: Cumulative distribution of the NO2 emissions at the SCR outlet during the WLTC cycle.

Based on the previous assumptions the species concentrations of the zero-dimensional SCR+ASC model are calculated from the following equations:

$$\frac{\partial \theta_{\mathrm{NH_3}}}{\partial \mathrm{t}} = \mathrm{r_{ads}} - \mathrm{r_{des}} - \mathrm{r_{std}}, \tag{5.13}$$

$$\frac{\partial \mathrm{NO_x}}{\partial \mathrm{t}} = -\Omega \cdot \mathrm{r_{std}} + \mathrm{SV}([\mathrm{NO_{x,us}}] - [\mathrm{NO_x}]), \tag{5.14}$$

$$\frac{\partial \mathrm{NH_3}}{\partial \mathrm{t}} = -\Omega(\mathrm{r_{ads}} - \mathrm{r_{des}}) + \mathrm{SV}([\mathrm{NH_{3,us}}] - [\mathrm{NH_3}]), \tag{5.15}$$

Note that in this approach Ω represents the sum of the maximum storage capacity of both catalysts.

Regarding the level of accuracy, as can be seen in Figure 5.7, the reduction from eight to three states represents a worsening of 3.6% and 19.4% in the prediction of NOx and NH3 emissions, respectively. However, although NH3 emissions show a significant worsening, in absolute values the impact is lower.

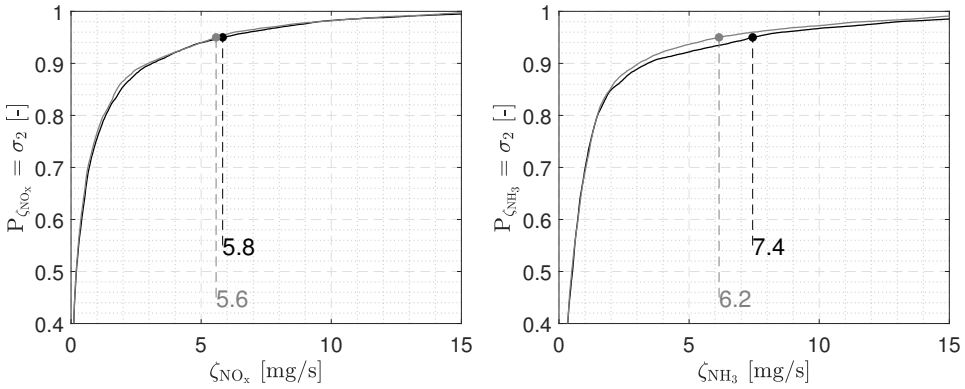

Figure 5.7: Comparison of σ_2 error for NOx (left plot) and NH3 (right plot) emission estimation between models with three-states (grey) and eight-states (dark).

The great advantage is that the model with three-states reduces in 75% the amount of allocated memory demanded in relation to the eight-states model; thus, enabling its implementation in a real-time control system.

5.3 Cross-sensitivity models

As described in Section 2.5.2, the cross-sensitivity to ammonia is one of the main problems faced by NOx sensors, since its incorrect identification provides wrong information to the control system, which in turn may lead

to wrong decisions for emission control. In this section two approaches for estimating cross-sensitivity are proposed, as well as their applications to two NOx sensors with different sensitivities to ammonia, thus ensuring that the methodology is extended to sensors with distinct sensitivities.

5.3.1 Cross-sensitivity cell temperature model

According to the analysis of the physical principle of the NOx sensor presented in Chapter 2.5.2, the sensor cell temperature plays an important role in the cross-sensitivity. As this information is not available, it may be interesting to explore modelling as an alternative to obtain an estimate of this temperature and, therefore, K_{CS}.

Assuming that the energy balance in the sensor cell can be approximated as:

$$Mc\frac{dT_{cell}}{dt} = \dot{m}_{in}c_pT_{in} - \dot{m}_{out}c_pT_{out} - hA(T_{cell} - T_{env}) + HR + EH, \quad (5.16)$$

where the term on the left side represents the energy variation in the gas inside the cell; M is the mass of the gas in the cell, c its heating capacity and T_{cell} its temperature inside the sensor cell. In the right side the different contributions are represented. The energy associated to the gas entering the cell is accounted by its flow ($\dot{m}_{in}$), and specific enthalpy (c_pT_{in}). The same for the energy associated to the gas leaving the cell ($\dot{m}_{out}$), and specific enthalpy (c_pT_{out}). The heat transfer between the cell and environment is represented by $hA(T_{cell} - T_{env})$. HR is the exothermics due to reductant species ($NH3, HC, ...$) oxidation and EH is the electrical heating of the sensor cell.

The energy balance in the sensor is not trivial due to the complexity associated with the number of parameters to be identified and the unknown nature of some of the variables. (i.e., the exhotermics is not known since the amount and composition of reductant species is unknown, or little is known about the term EH). For this reason, the following simplification hypotheses are proposed:

- Negligible heat transfer so $hA(T_{cell} - T_{env}) \sim 0$
- Negligible cell volume, which implies:
  - Steady mass: M=ct & $\dot{m}_{in} = \dot{m}_{out}$
  - $T_{in} = T_{gas}$ at the SCR outlet where the sensor is placed
  - $T_{out} = T_{cell}$

- Constant heating: EH = ct
- Exothermics proportional to NH_3, so the impact of other species (HCs, CO) is neglected since they are oxidized with high efficiency in the DOC: HR$\propto NH_3$ [21]

Applying these conditions to eq.5.16 and rearranging leads to:

$$\frac{dT_{cell}}{dt} = C_1(T_{catalyst} - T_{cell}) + C_2NH_3 + C_3, \tag{5.17}$$

where C_1, C_2, and C_3 are constants related to physical parameters in eq.5.16, that can be experimentally determined. Transforming eq.5.17 to a discrete time yields.

$$T_{cell,z+1} = k_1T_{ATS,z} + (1 - k_1)T_{cell,z} + k_2NH_3 + k_3, \tag{5.18}$$

where k_1, k_2, and k_3 are constants related with C_1, C_2, and C_3 and the time step can be identified with experimental data.

Once the cell temperature is estimated, the reaction rates (eq.2.5a-2.5c) can be theoretically calculated based on the use of Arrhenius functions to estimate the K_{CS}. However, this approach is too complex due to the lack of experimental data concerning the specific surface or the difficulties to account for internal pore diffusion processes, competitivity between species or selectivity dependence on operating conditions. Due to the requisites of on-board diagnostics concerning computational and calibration effort, for this reason, an empirical correlation is proposed. The main idea of the proposed approach is to vary the value of K_{CS} with the variation of the temperature, thus, as introduced in Section 2.5.2.1, at low temperatures eq.2.5a is predominant (K_{CS}=0.5), while at high temperatures eq.2.5c dominates (K_{CS}=1.5). The error function (erf) was introduced since it can be modulated, thus allowing a smooth transition between K_{CS} values. In this sense, the following expression is proposed to model the relation between cell temperature and K_{CS}:

$$K_{CS,z} = 1 + k_4\text{erf}\left(\frac{T_{cell,z} - k_5}{k_6}\right) \tag{5.19}$$

Figure 5.8 shows the shape of expression eq.5.19 modelling the relation between cell temperature and K_{CS}. In eq.5.19, the constant k_4 represents a symmetric range variation of K_{CS} around 1.25, k_5 represents the temperature at which K_{CS}=1.25 and k_6 is a measure of the range of temperatures that lead K_{CS} to vary from minimum to maximum values.

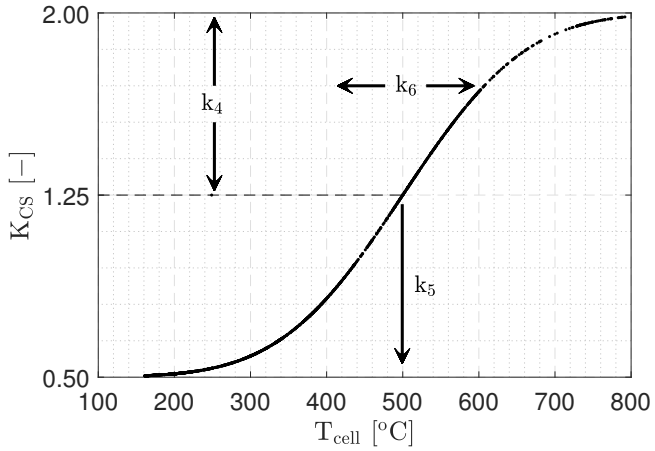

Figure 5.8: Correlation between K_{CS} and cell temperature according to expression eq.5.19 and effect of parameters k_4, k_5, and k_6.

The optimisation of k_i variables are solved through eq.5.20, where the minimum of the constrained non-linear multivariable function is sought, the values found for the two analysed NOx sensors are presented in Table 5.2.

$$\text{argmin}_{k_j} \left(\sum_{\text{cycle}} \left\| \frac{NO_{x,\text{sensor}} - NO_x}{NH_3} - k_{CS} \right\| \right), \tag{5.20}$$

subject to:

$$\min(k_j) \leqslant k_j \leqslant \max(k_j),$$

where $\min(k_j)$ and $\max(k_j)$ represent sensible boundaries for parameters k_j.

Table 5.2: Experimental constants of equation 5.18 and 5.19.

Parameter	k_1	k_2	k_3	k_4	k_5	k_6
`Sensor 1`	0.248	0.658	1.245	0.686	296.9	112.4
`Sensor 2`	0.797	0.017	4.746	0.643	579.7	299.9

As conclusion obtained through the results of Table 5.2, it is possible to verify that:

- The cell temperature in sensor 2 is less sensitive to the oxidation of NH3 (k_2).

- The maximum range of the cross sensitivity is similar for both sensors (k_4).
- The transition of K_{CS} in relation to temperature is much more abrupt for sensor 1 (k_6).

5.3.2 Model results

The comparison between K_{CS} evolution obtained from exhaust gas analyser (dark line) during a WLTC and K_{CS} model based on cell temperature for sensor 1 (blue dotted line) and sensor 2 (blue solid line) are shown in Figure 5.9. Only the results when NH3 > 10 ppm are shown since the analyser uncertainties may lead to inconsistent K_{CS} for lower NH3 levels.

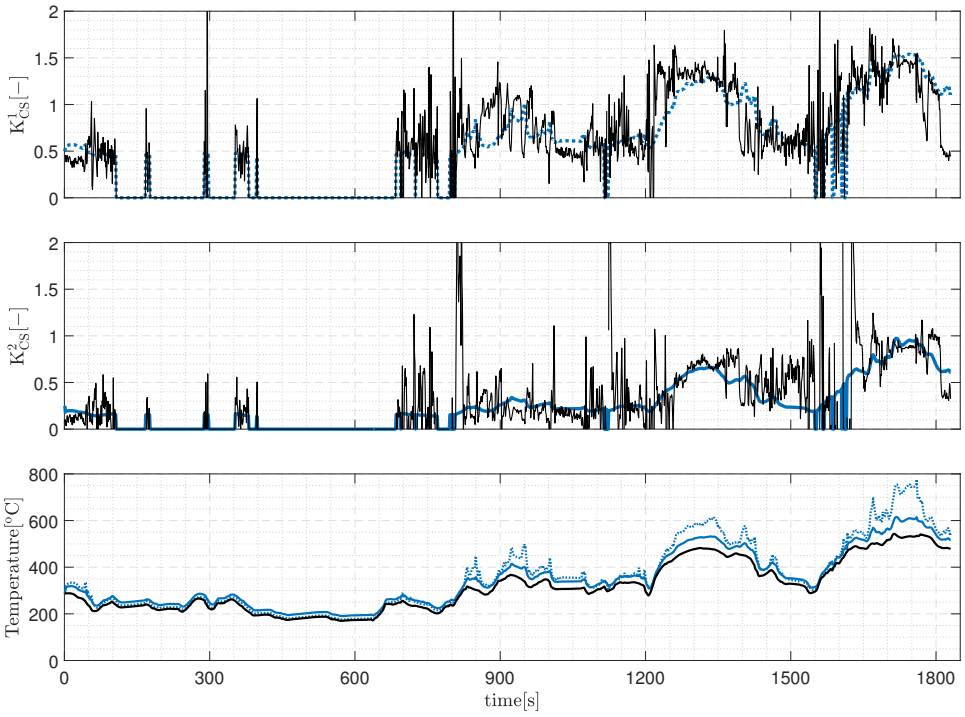

Figure 5.9: Evolution of K_{CS} during the WLTC cycle obtained experimentally (dark line), and with cell temperature model for sensor 1 (blue dotted line - upper plot) and for sensor 2 (blue solid line - middle plot). Bottom plot: Evolution of exhaust gas temperature (black) and model cell temperature for sensor 1 (blue dotted line) and sensor 2 (blue solid line).

As can be seen, the method is capable to capture the K_{CS} behaviour for different NOx sensors. The low cross sensitivity of sensor 2, indicates the possibility that part of the ammonia is completely oxidized to nitrogen, as proposed in eq.5.21 [22]:

$$4NH_3 + 3O_2 \rightarrow N_2 + 6H_2O \tag{5.21}$$

In this case, it is inferred that a substantial part of ammonia is directly reduced to N2.

The bottom plot of Figure 5.9 shows the temperature calculated for the sensor cell. As can be seen, in the high load part of the cycle, the temperature difference between the model and the exhaust gas temperature reaches 250 °C for sensor 1 and 80 °C for sensor 2. This difference in temperature is since the sensor cell temperature (blue line) considers not only the exhaust gases temperature (black line), but also the heating of the sensor and the oxidation reactions. This observation is important, since the estimation of the cross-sensitivity depends mainly on the temperature, underestimating it, directly affects the impact of the cross-sensitivity on the final measurement of the sensor, which occurs when only the exhaust gases temperature is considered.

5.3.3 NH3-dependent and constant cross-sensitivity

A simpler approach is to consider only the influence of NH3 slip in the cross-sensitivity estimation. Through analysis of the data presented in Figure 2.7, it was possible to observe a strong asymptotical relationship between K_{CS} and NH3 slip. In this case, it is possible to create a curve from the experimental data to capture the evolution of K_{CS} based on eq.5.22.

$$K_{CS} = K_{CS_0} - k_1 \exp(-k_2 NH_3), \tag{5.22}$$

The values that best fit the curve to the experimental data are presented in Table 5.3 and the result can be seen in Figure 5.10.

Table 5.3: Experimental constants of eq. 5.22.

Parameter	k_{CS_0}	k_1	k_2
`Values`	1.5686	1.0992	5.3475
`Values`	0.9432	0.7990	4.4997

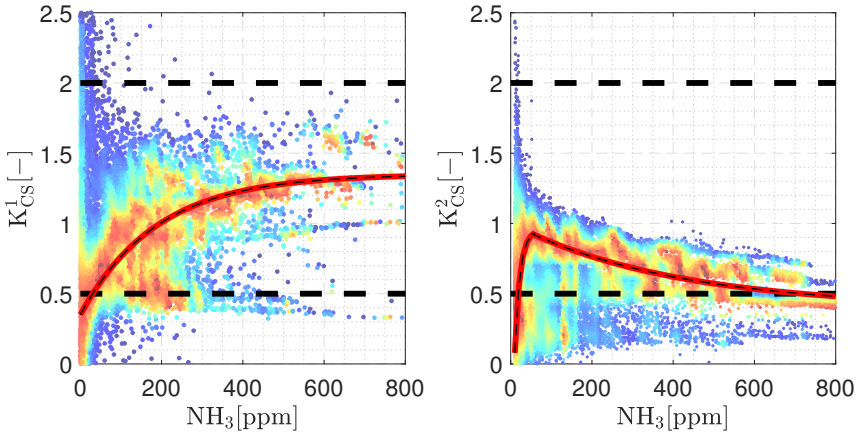

Figure 5.10: K_{CS} depending on NH3 for a set of tests including WLTC and other driving cycles, engine mapping and steady state conditions. Colour-scale ranges from blue (low frequency) to red (high frequency). The dashed red/black line represents eq.5.22 with the corresponding constants from Table 5.3.

A second simplified approach is the use of a constant based on the correlation between the real value, and the one measured by the sensor. This approach is commonly used by automakers [23], as no modelling is required.

Frobert et al. [22] suggest a constant value of 0.67 for the cross-sensitivity. However, as previously presented, NOx sensors have different cross-sensitivity behaviours. Figure 5.11 shows the instantaneous cross-sensitivity of NOx sensors for 60 test cycles, including transient and steady state conditions.

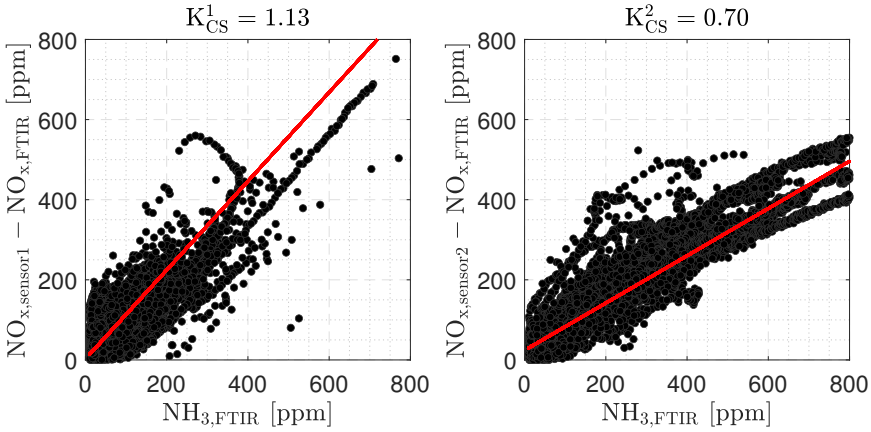

Figure 5.11: Instantaneous cross-sensitivity of NOx sensors for a set of 60 tests including WLTC and other driving cycles, engine mapping and steady state conditions.

As can be seen, the constant K_{CS} for sensor 2 is consistent with that presented by Frobert et al. [22] However, the K_{CS} for sensor 1 is higher, which was already expected since sensor 1 is more sensitive to ammonia. Therefore, the K_{CS} values used for sensor 1 and sensor 2 were 1.13 and 0.70, respectively, that is, the constant K_{CS} values that according to the data contained in Figure 5.11 minimise the error in the K_{CS} estimation.

5.3.4 Model results

Figure 5.12 shows the comparison of the cross-sensitivity evolution between experimental (dark line), NH3-dependent (red line) and constant value (green line) for both sensors (upper plot sensor 1, bottom plot sensor 2) in a WLTC cycle. Again, only the results when NH3 > 10 ppm are shown since the analyser uncertainties may lead to inconsistent K_{CS} for lower NH3 levels.

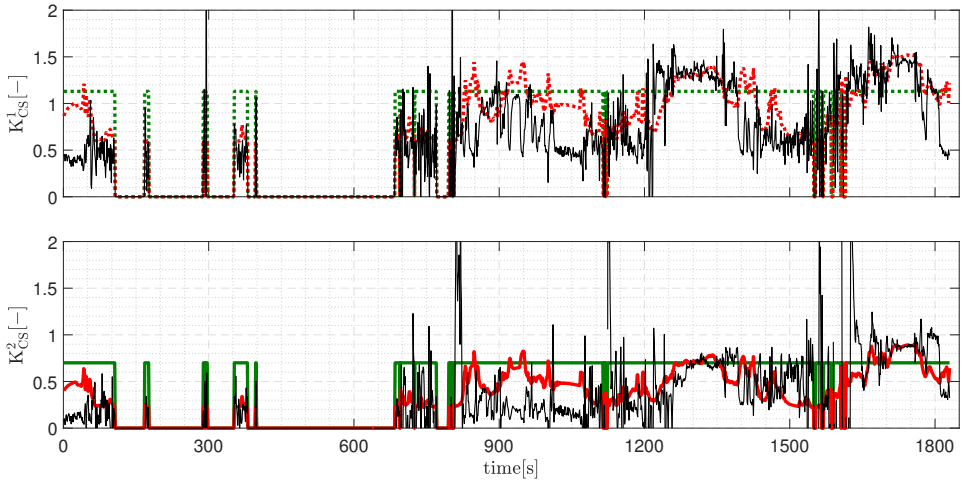

Figure 5.12: Evolution of K_{CS} in a WLTC cycle obtained experimentally (dark line), with NH3 dependent (red line), and constant (green line) value. Upper plot refers to sensor 1 and lower plot to sensor 2.

As can be seen, the simplified approach using only the correlation between cross-sensitivity and NH3 concentration is able to follow the K_{CS} trend for most of the cycle, and as expected, the constant cross-sensitivity switches only when there is or is not ammonia in the exhaust gases.

5.3.5 Comparison between cross-sensitivity estimation methods

The approach that best matches the experimental results can be seen in Figure 5.13. The left part shows how the estimation of K_{CS} based on the cell temperature model is able to capture the duality of cross-sensitivity at NH3 concentration greater than 100 ppm, where K_{CS} can be at two different levels for the same NH3 slip. On the right side of Figure 5.13, it is possible to observe the distribution of errors in the cross-sensitivity estimates. The distribution is shifted to lower errors in the case of the cell temperature model (blue line), and to higher values when using the constant value (green line).

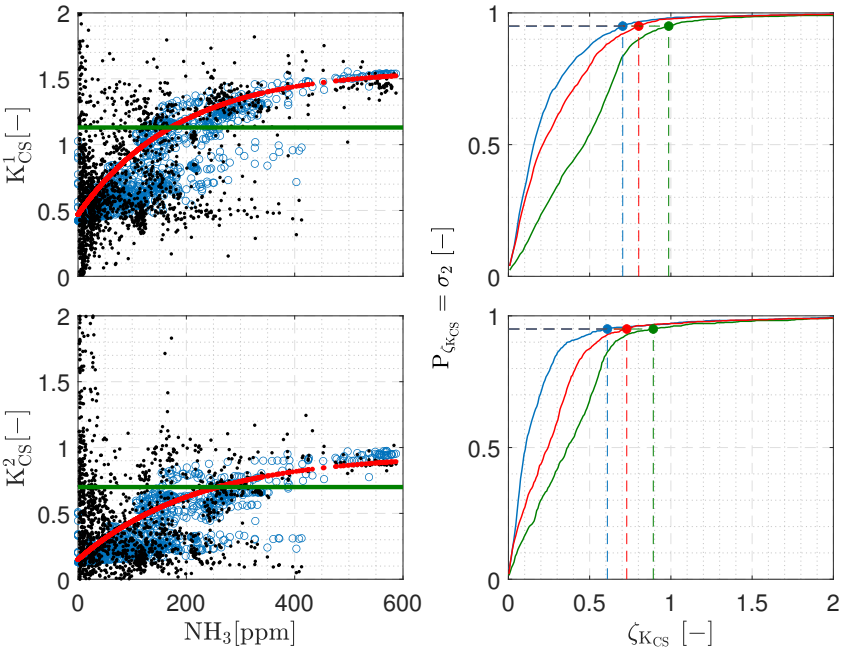

Figure 5.13: Left plot: K_{CS} versus NH3 (experimental in black, cell temperature model in blue, NH3-dependent in red, and constant K_{CS} in green). Right plot: σ_2 error distribution of the K_{CS} estimation.

The absolute error and the level of improvement of cell temperature model over the other approaches can be checked in Table 5.4. For both sensors, the cell temperature model is the most accurate to estimate the cross-sensitivity of the NOx sensor, when compared to the NH3-dependent approach, the improvement is 14.0% and 14.1% for sensor 1 and 2, respectively. In the case of constant value, the improvement of the cell temperature model is even greater, 44.8% for sensor 1 and 61.8% for sensor 2.

Cycle	Cell temperature		NH3-dependent		Constant	
	Sens 1	Sens 2	Sens 1	Sens 2	Sens 1	Sens 2
WLTC 1	0.70	0.61	0.80 [14.0%]	0.73 [19.6%]	0.99 [40.2%]	0.89 [46.4%]
WLTC 2	0.65	0.63	0.73 [11.4%]	0.84 [23.7%]	0.89 [36.5%]	0.90 [42.9%]
fullmap 1	0.45	0.28	0.51 [13.7%]	0.30 [8.9%]	0.83 [55.2%]	0.61 [88.7%]
fullmap 2	0.39	0.42	0.53 [16.8%]	0.43 [4.2%]	0.57 [47.4%]	0.70 [69.1%]
Overall average improvement			[14.0%]	[14.1%]	[44.8%]	[61.8%]

Table 5.4: σ_2 error for cross-sensitivity estimation.

Thus, the proposed methods proved that it is possible to estimate the cross-sensitivity from the temperature or from the correlation with the NH3 concentration in the exhaust gases. In the first case, the temperature inside the sensor cell should be used as a basis, instead of the exhaust gas temperature, as it underestimates the real value and, consequently, the cross-sensitivity. In the second case, a large sampling is required to determine the correlation

between NH3 slip and K_{CS}.

5.4 Control-oriented models

For a wide use of physical models, it is necessary to simplify their complexity at the expense of calibration effort, however for real-time application depending on the model that is desired to represent the required simplification leads to a high level of uncertainty. A possible approach to circumvent this drawback is the use of computational models without physical interpretation, which are models developed from the information acquired in experimental tests. In relation to the modelling of after-treatment systems there are some main points of concern, such as:

- ATS are complex systems with important non-linearities and although high accuracy physical models are reported in the literature [24], the associated computational cost makes them useless for control purposes. The strong simplifications in physical based models (e.g. zero-dimensional, limited set of reactions, ...) needed to reach real-time requirements lead to the introduction of calibration parameters which reduce the physical interpretation and prediction capabilities.

- In the case of zeolite-based catalysts the model provides an estimate of the state and outputs (usually NO, NO2 and NH3) based on system inputs such as exhaust mass flow, catalyst temperature, concentration of contaminants at the inlet of ATS, and urea injection. Considering that the urea injection cannot be measured on-line, the standard solution is to map the amount of urea injected with the injector actuation. While this approach may be accurate enough at the beginning of injector's life, it is well documented in literature [25] that urea deposits often appear in the injectors and the relation between injector actuation and urea flow may evolve with time as the engine ages.

- Another point is the ageing of the catalyst monolith. Ageing develops after the catalyst has been subjected to long periods of high temperature operation [26]. Modern ATS uses SCRF catalyst technology, which integrates SCR technology coated on a DPF, to be able to control both NOx and PM [27]. However, the DPF needs for its regeneration to operate at temperatures above 500 °C [28] (i.e., regeneration of the DPF system is necessary, as the system is gradually blocked by carbon deposits, increasing back pressure and, consequently, reducing engine power [29]), hence, the ATS will accelerate the ageing of the system. The

ageing process affects the ammonia storage capacity within the catalyst, thus reducing the NOx conversion efficiency [30].

Therefore, control-oriented models are an attractive option, as they have good accuracy and low computational effort. Throughout this work, three control-oriented models were developed based on the following assumptions:

(i) The ammonia coverage ratio is controlled at a relatively high level to achieve high NOx conversion efficiency [31], thus allowing the dynamics of the NOx after the SCR catalyst to be mainly dependent on the NOx dynamics before the catalyst [32]. This hypothesis rests on the fact that the need for high NOx conversion efficiencies requires the SCR catalyst to work with high ammonia load. Current urea injection strategies are designed to operate the SCR at maximum ammonia covering ratios to maximise NOx efficiency but keeping NH3 slip below certain constraints [13, 33].

(ii) The NH3 emissions dynamics are considerably slower than NOx. Since the ammonia coverage varies slowly, the NH3 slip that depends on it will also vary slowly [32, 34].

(iii) NOx sensors working properly, being the only deviation between the actual and measured NOx value due to the impact of cross-sensitivity to ammonia on the sensor reading.

$$NO_x = NO_{x,sensor} - K_{CS} \times NH_3, \tag{5.23}$$

where, the real NOx concentration (NO_x) is the signal read by the sensor ($NO_{x,sensor}$), minus the cross-sensitivity of the sensor to ammonia (K_{CS}) times the current concentration of ammonia (NH_3).

5.4.1 Artificial neural networks

A possible approach to the use of computational models without physical interpretation is the artificial neural networks (ANN), which are parallel processing algorithms whose inherent property is the ability to learn non-linear relationships, such as engine emissions.

The hypotheses (i) and (ii) make it possible to model the NOx concentration downstream of the SCR as an input-output model problem, that is, when the identification and control of a system can be observed only through the input and output data [35].

Figure 5.14 shows the exhaust gas measurement in the frequency domain on a WLTC cycle. Note that both NOx signals have similarity, as the difference

between the two remains relatively constant. While the dynamic response of the NH3 signal at the catalyst output is not high enough, clearly showing a filtered signal. In this sense, NOx seems to be a better candidate for ANN modelling, where the dynamics of the system can be neglected.

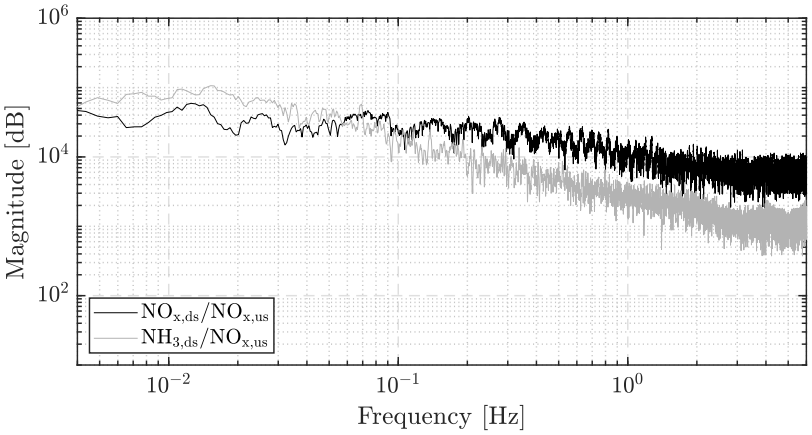

Figure 5.14: Exhaust gas measurements in the frequency domain for the WLTC cycle. Dark line: Ratio between NOx signal downstream and upstream of the SCR catalyst. Grey line: Ratio between downstream NH3 signal and upstream NOx signal of the SCR catalyst.

Considering the previous observations, an ANN was created using a fitting model with a two-layer feed-forward. The ANN has four input and one output signal, with one hidden and one output layer. The model uses information acquired experimentally from several driving cycles, such as WLTC and 2RTS, and from stationary operating, as engine map and steady-state conditions. The ANN assembly has three main points:

- **Network structure**: The hidden layer of ANN has ten hidden neurons and uses a sigmoid transfer function, while the output layer has one neuron and linear transfer function.
- **Training set**: NOx upstream of the SCR ($NO_{x,us}$ [ppm]), ammonia injected ($NH_{3,inj}$ [mg/s]), exhaust gas mass flow ($\dot{m}_{exh}$ [kg/h]) and SCR catalyst temperature (T_{SCR} [°C]) were set as inputs, whilst NOx slip ($NO_{x,ANN}$ [mg/s]) as output. The ANN structure can be seen in Figure 5.15.

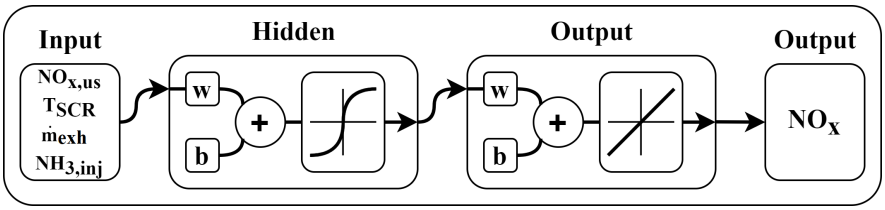

Figure 5.15: Structure of the developed artificial neural network.

- **Network training and validation**: The ANN algorithm training uses the Levenberg-Marquardt back-propagation approach (least squares analysis widely used to train and solve feed-forward ANN) [36]. The training process recursively adjusts the bias and weight of the ANN to minimise a given function to its local minimum. For all training input and output variables, the error was calculated as:

$$\zeta(\mathrm{w},\mathrm{b}) = \frac{1}{2}\sum_{\mathrm{n}=1}^{\mathrm{N}}(\mathrm{y_n} - \hat{\mathrm{y}}_\mathrm{n})^2, \tag{5.24}$$

  where w is the weight and b the bias vector; N the inputs; $\mathrm{y_n}$ the target vector and $\hat{\mathrm{y}}_\mathrm{n}$ the output vector.

The dataset distribution used in each stage of the ANN development are: 70% for model training, and 15% for each of the other processes, validation and testing. Regarding the feeding signals, different cycles were used at each stage, thereby ensuring that the ANN was not over-fitted for a specific set of cycles. The evolution of the signals and the cycles that feed each stage of the model development are presented in Figure 5.16.

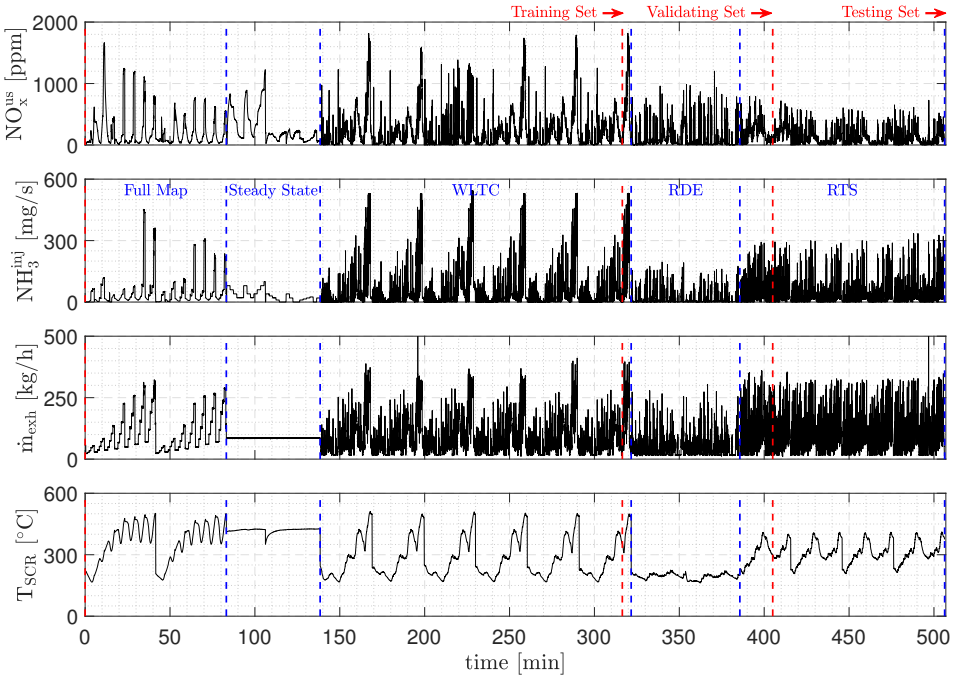

Figure 5.16: Evolution of the signals that feed the development of the neural network in its different stages.

With the NOx estimated by the ANN and the cross-sensitivity estimated by the models proposed in the previous subsection 5.3, it is possible to calculate the NH3 slip through eq.5.23.

The same approach was used for the development of the SCR+ASC artificial neural network, since the response dynamics of the NOx sensor downstream of the ASC remains similar to the sensor placed before the SCR catalyst, as can be seen in Figure 5.17. Where the shift to lower levels of the $NO_{x,dsASC}/NO_{x,usSCR}$ ratio is due to lower NOx concentrations downstream of the ASC catalyst than the SCR.

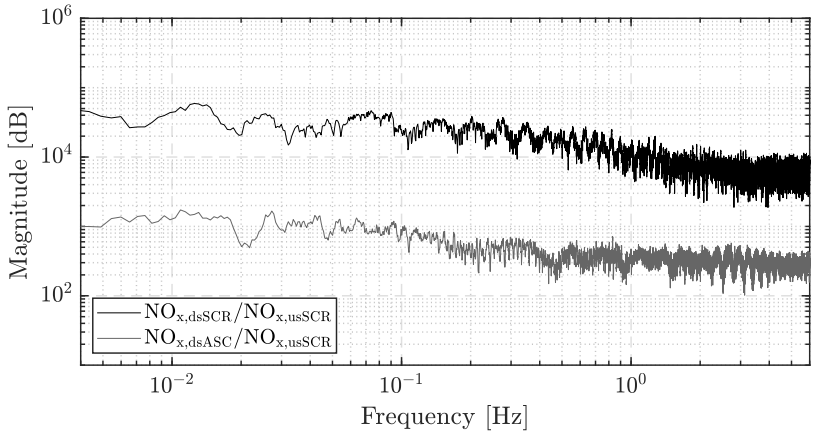

Figure 5.17: Exhaust gas measurements in the frequency domain for the WLTC cycle. Dark line: Ratio between NOx signal downstream and upstream of the SCR catalyst. Grey line: Ratio between NOx signal downstream of ASC catalyst and NOx signal upstream of SCR catalyst.

The main difference was the set of tests used. For the development of the ANN with the SCR+aged ASC catalyst, the tests carried out with method 1 (4.2.1) were used, while for the SCR+new ASC the cycles were performed with method 2 (4.2.2).

5.4.1.1 Model results

After implementation the model was evaluated over WLTC and 2RTS driving cycles, and the results were compared with those obtained by FTIR gas analyser to assess the accuracy of the model. The evolution of NOx and NH3 emissions, as well as the σ_2 error are presented in Figure 5.18.

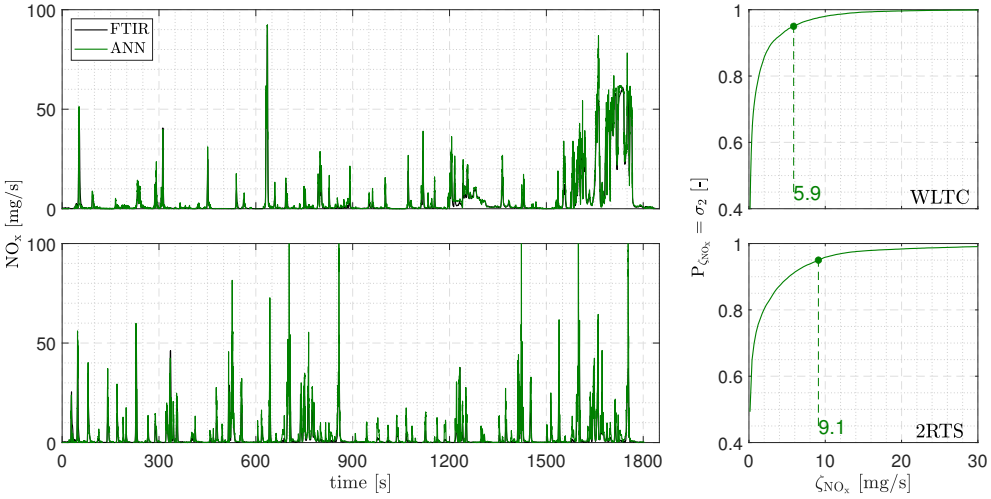

Figure 5.18: Comparison between FTIR and ANN model for NOx downstream in a WLTC (upper plots) and 2RTS (bottom plots) cycle. The left plots represent the emissions evolution, while the right ones the σ_2 error.

As can be observed, the ANN is able to estimate NOx emissions with high accuracy, having a σ_2 error level similar to the zero-dimensional physical model. The largest differences can be appreciated in the 2RTS cycle at the highest peak points, where ANN overestimates the level of NOx emissions. This is possibly due to the fact that the ANN model is not able to capture the emissions behaviour at very high mass flow rates. In Figure 5.19 it is possible to verify that the highest error levels are linked to the highest mass flow rates of the cycle.

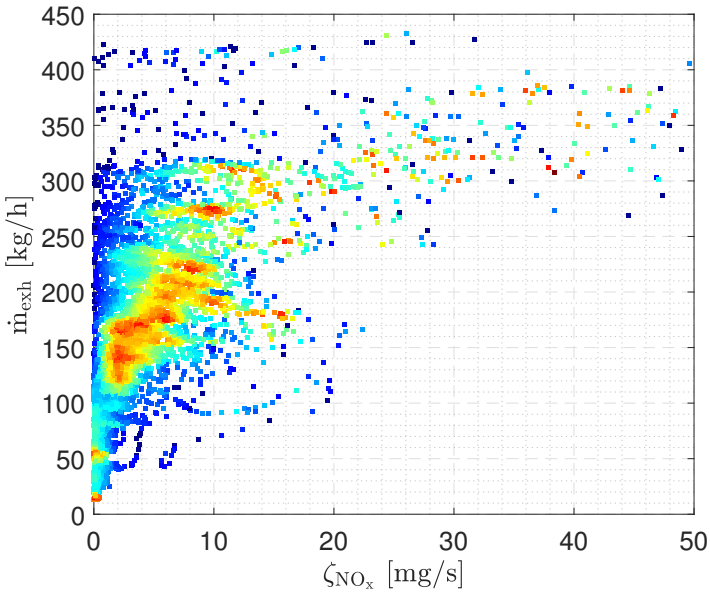

Figure 5.19: Error level in NOx emissions estimation by ANN model (x-axis) in relation to exhaust gas mass flow rate (y-axis) in the 2RTS cycle. Colour-scale ranges from blue (low frequency) to red (high frequency).

Regarding NH3 slip it can be calculated through the NOx predicted by ANN and the general equation of the NOx sensor (eq.5.23).

$$NH_{3,ANN} = \frac{NO_{x,ANN} - NO_x}{K_{CS}}, \tag{5.25}$$

The result can be seen in Figure 5.20.

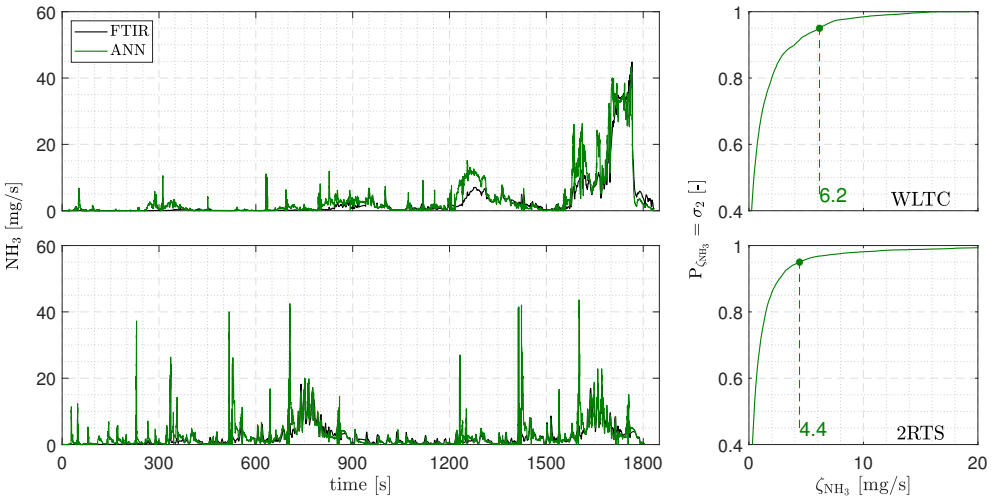

Figure 5.20: Error level in NOx emissions estimation by ANN model (x-axis) in relation to exhaust gas mass flow rate (y-axis) in the 2RTS cycle. Colour-scale ranges from blue (low frequency) to red (high frequency).

As can be seen, the model is able to provide a good estimate of the NH3 slip, however, with some overestimation peaks, mainly in the points of increasing slip. This deviation was expected due to two main factors: the NH3 slip behaviour depends on factors, such as adsorption, desorption, ammonia load on the catalyst, among others that show slow dynamics. Thus, modelling the NH3 slip as an input-output system has limitations (this drawback may be overcome through the use of recurrent neural network (RNN), which allows modelling the dynamics of systems, as suggested by Arsie et al. [37]). A second point is that the NH3 slip estimate takes cross-sensitivity into account, hence the uncertainty in the cross-sensitivity estimate is an additional source of error.

As an overall conclusion, the model has high accuracy to estimate NOx emissions, with similar levels to the physical 0D model, while the level of the NH3 slip error are slightly higher. Thus, the model has proven to be a viable option of low computational cost and high accuracy for the prediction of NOx emissions.

5.4.2 Sensor signal analysis model

The previous model relies in the information from the NOx sensor upstream the SCR, exhaust mass flow, temperature, and urea injection. However it does not use information from the NOx sensor downstream the catalyst

that can be helpful to better estimate emissions. In the same way, since the model relies on the urea injection estimation, any error in such signal will lead to high degrees of uncertainty. To complement the previous model, an additional estimator that exclusively relies on the sensor signals (upstream and downstream) was developed.

Considering the hypothesis (i) and (ii), the model was developed as follows. A buffer with calibrate duration is applied to NOx signals upstream ($NO_{x,us,sensor}$) and downstream ($NO_{x,ds,sensor}$) of the SCR catalyst. Then, the average value is extracted from both buffers. According to eq.5.23, the average SCR NOx conversion efficiency ($\overline{\eta_{NO_x}}$) in the considered time-window can be estimated as:

$$\overline{\eta_{NO_x}} = 1 - \frac{\overline{NO_{x,ds,sensor}} - \overline{K_{CS}} \times \overline{NH_3}}{\overline{NO_{x,us,sensor}}}, \tag{5.26}$$

where $\overline{K_{CS}}$ is the average cross sensitivity and ($\overline{NH_3}$) is the average NH3 slip during the time window. Considering hypothesis (i), it is possible to assume that during the time-window the instantaneous SCR NOx conversion efficiency is equal to the average SCR NOx conversion efficiency $\eta_{NO_x} = \overline{\eta_{NO_x}}$.

An estimation of the NOx slip during the considered window can be done by applying the conversion efficiency calculated by eq.5.26 to the NOx upstream as:

$$NO_x = NO_{x,us,sensor}(1 - \eta_{NO_x}), \tag{5.27}$$

Then, the NH3 slip can be computed assuming the standard sensor model (eq.5.23) considering an average cross sensitivity during the window and the average NOx slip from eq.5.27.

$$\overline{NH_3} = \frac{\overline{NO_{x,ds,sensor}} - \overline{NO_x}}{\overline{K_{CS}}}, \tag{5.28}$$

$\overline{NH_3}$ and $\overline{NO_x}$ are the average emissions during the time-window. Since the dynamics of the NH3 slip varies slowly, a proper calibration of the buffer size (in the present case of 200 samples at 10 Hz) may allow a suitable estimation of the NH3, as can be seen in Figure 5.21. In this sense and according to hypothesis (ii), it is assumed that: $NH_3 = \overline{NH_3}$.

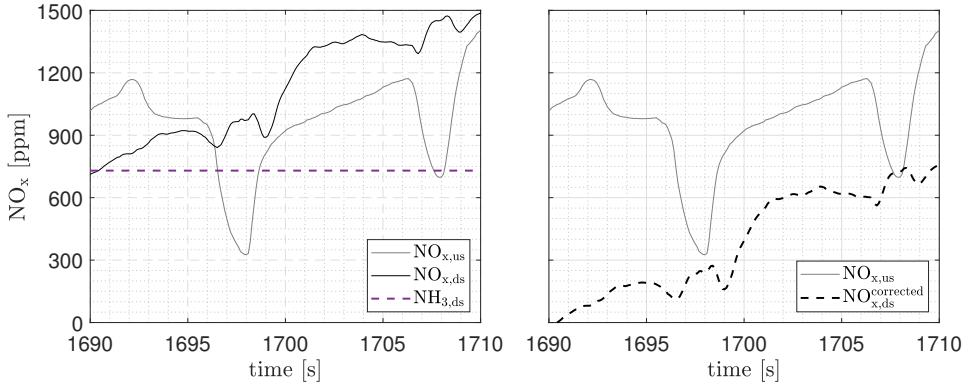

Figure 5.21: Time Interval of 20 s in a WLTC cycle. Left plot: NOx sensor signals before (grey line) and after (dark line) the SCR catalyst and constant NH3 (purple dashed line). Right plot: NOx sensor signals before (grey line) and corrected NOx after (dark dashed line) the SCR catalyst.

Figure 5.22 shows the flowchart of the implemented method.

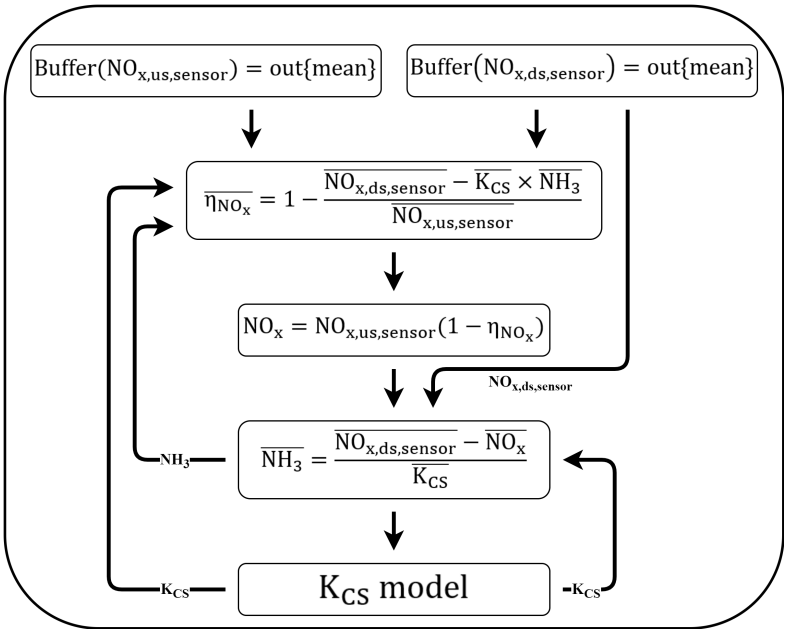

Figure 5.22: Sensor signal analysis (SSA) model flowchart.

5.4.2.1 Model results

Once the proposed methodology has been implemented, the model can be evaluated. Thereby the model and FTIR results were compared in terms of NOx and NH3 emissions, as well as σ_2 error. The comparison of the results are presented in Figure 5.23 and Figure 5.24 for NOx and NH3 slip, respectively.

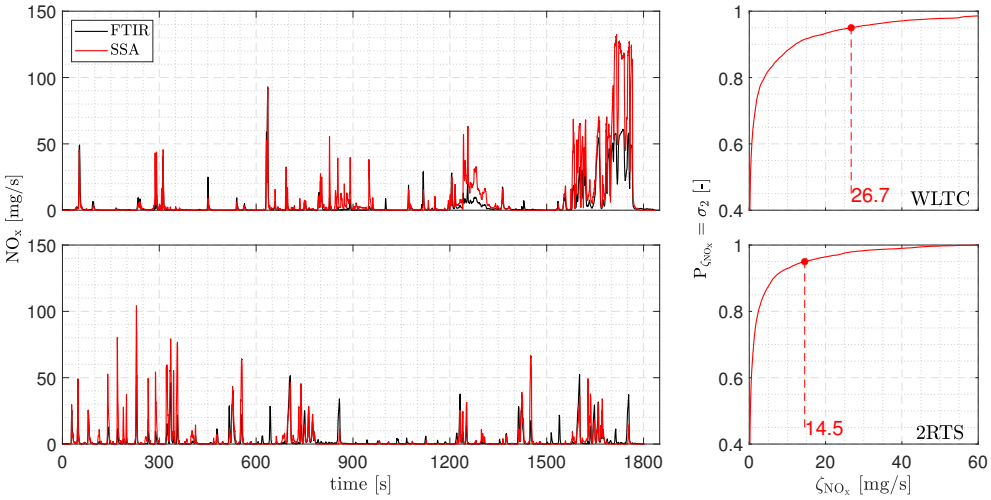

Figure 5.23: Comparison between FTIR and SSA model for NOx downstream in a WLTC (upper plots) and 2RTS (bottom plots) cycle. The left plots represent the emissions evolution, while the right ones the σ_2 error.

As can be seen, the proposed SSA model shows very low accuracy to estimate NOx emissions, especially in the high dynamic intervals of the cycles, where the model overestimates the slip level.

As previously commented, the NH3 signal has a considerably lower dynamics when compared to the NOx signal. Once the proposed approach is based on average values in a time-window (buffer), the signal is filtered and consequently its dynamics is reduced. Although this behaviour is a drawback for NOx, it is an advantage for NH3 slip estimation. As can be seen in Figure 5.24, the prediction of NH3 slip by the SSA model is more accurate than the other models presented, with only an underestimation in the zone of highest slip in the WLTC cycle (upper plot).

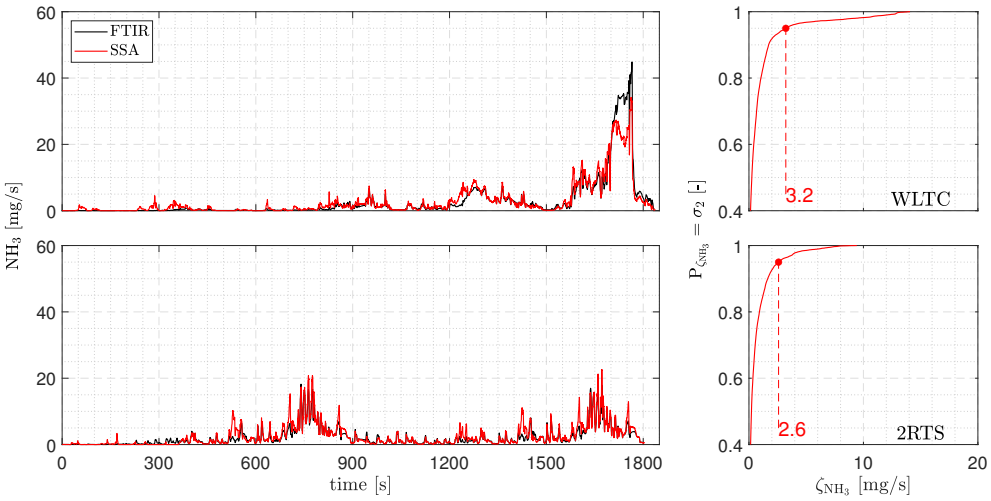

Figure 5.24: Comparison between FTIR and SSA model for NH3 downstream in a WLTC (upper plots) and 2RTS (bottom plots) cycle. The left plots represent the emissions evolution, while the right ones the σ_2 error.

As it can be seen, the SSA model, unlike the ANN model, has high accuracy in estimating NH3 slip (even higher than the physical model), but with low accuracy to predict NOx emissions. Therefore, the proposed methodology can be used as an option of low computational cost and high accuracy. Note that this approach only uses information from the NOx sensors at the inlet and outlet of the catalyst to accurately estimate the NH3 slip.

5.4.3 Data fusion – Kalman filter

In control engineering it is possible to model a system through state space models [19]. In general terms, state space models are a set of states (even if hidden) that evolve over time and are the physical representation of the system that is intended to be known and/or controlled. These states can be observed, however, due to the intrinsic noise of the system, their estimation may differ from the real value [38].

In control theory, a state observer is an element that provides an estimate of the state of a system ($\hat{x}_k$) from the measurement of its inputs (u_k) and outputs (y_k) and a model of the system dynamics. Note that the difference with a model, is that the observer requires a measurement of the output, while the model does not. As a counterpart, a higher accuracy can be expected from the observer since more information is considered for the estimation. Figure 5.25 shows a schematic representation with inputs and outputs for the model

and the observer, where the differences can be clearly identified.

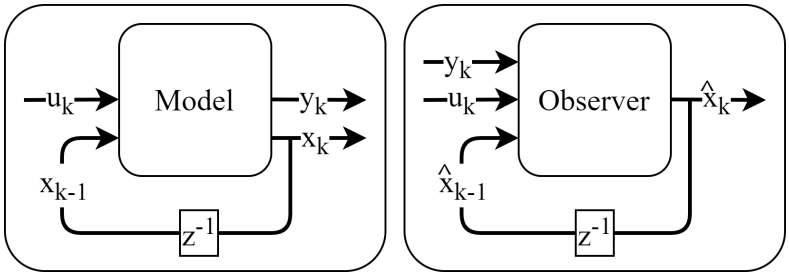

Figure 5.25: Schematic representation of a dynamic model (left) and observer (right).

How to integrate the model with the measurement of the system output can become a concern. It makes sense that if the model perfectly predicts how the system will behave, the sensor data is useless and can be ignored. Conversely, if significant discrepancies are found between the measured and simulated systems modifications to the model should be made. The simplest function that satisfies the preconditions is a linear correction of the model using the difference between measured and modelled outputs, which results in the structure of the observer being as follows:

$$\hat{x}_k = f(\hat{x}_{k-1}, u_k) + K(y_k - \hat{y}_k), \tag{5.29a}$$

$$\hat{y}_k = h(\hat{x}_k), \tag{5.29b}$$

$\hat{y}_k$ is the output of the observed state estimation $\hat{x}_k$, u_k is the measurement of the inputs and K is the Near-optimal gain. Where the state of the system is continuously updated by the observer through new measurements $(K(y_k - \hat{y}_k))$.

There is a lot of literature addressing what is the proper value of K to make the observer estimation $\hat{x}_k$ converge to the actual value of x_k. Kalman Filter (KF) is one of the methods to obtain the observer gain K in a linear system such that represented by equations (eq.5.29). Unfortunately, like many real systems, catalysts such as SCR and ASC exhibit many non-linearities. The extended Kalman filter (EKF) is the non-linear version of the Kalman filter that consists of applying the KF to a linearised system.

The EKF algorithm is based on two main steps: Predict and Update. In the first step, a prediction of the next state and covariance is made by applying the model and the model gradient (Jacobian) to the last observation. In the update step, the prediction is combined with the current observation to

refine the state and covariance estimate [39]. The EKF algorithm consists of applying the next steps to each iteration.

- Predict state and covariance:
  - Predict state observer: $\hat{x}_{k|k-1} = f(\hat{x}_{k-1}, u_k)$ the model is applied to the previous state observation ($\hat{x}_{k-1}$) with current inputs (u_k) leading to a first estimation of the state.
  - Predict observer covariance: $P_{k|k-1} = F_k P_{k-1} F_k^T + Q_k$ an initial estimation of the observer covariance (uncertainty in the state observer) is calculated from the previous value of the covariance (P_{k-1}), the Jacobian of the state F_k defined as: $F_k = \left|\frac{\partial f}{\partial x}\right|_{\hat{x}_{k-1}, u_k}$, and the process covariance (Q_k) in which it was used a constant value that minimises the error between estimated and measured NOx and NH3 emissions in one calibration cycle and extended to all other cycles.
- Update state and covariance:
  - Estimate measurement residual: $\hat{e}_k = y_k - \hat{y}_k = y_k - h(\hat{x}_{k|k-1})$ the difference between the sensor reading (y_k) and the observer estimation of the sensor reading ($h(\hat{x}_{k|k-1})$) is computed.
  - Estimate residual covariance: $S_k = H_k P_{k|k-1} H_k^T + R_k$ the covariance in the residual estimation is computed from the state covariance prediction ($P_{k|k-1}$), the Jacobian of the model output function (H_k) defined as: $H_k = \left|\frac{\partial h}{\partial x}\right|_{\hat{x}_{k|k-1}}$, and the measurement covariance (R_k) which was set as 1. Note that F_k and H_k are the linearisation of the model functions f and h around the last estimations of the state.
  - Compute Kalman gain: The Kalman gain is directly proportional to the observer covariance and inversely proportional to the residual covariance $K_k = \frac{P_{k|k-1} H_k^T}{S_k}$.
  - Update state observer: $\hat{x}_k = \hat{x}_{k|k-1} + K_k \hat{e}_k$ the observer is calculated applying to the state prediction, the estimated residual weighted with the Kalman gain.
  - Update the covariance of the observer: $P_k = (I - K_k H_k) P_{k|k-1}$.

5.4.4 Extended Kalman filter applied to the models

Considering the signal provided by the ANN as a reasonably good estimate of the actual NOx slip ($NO_{x,ANN}$), it is possible to define a dynamic system composed of two states:

$$\begin{cases} x_1 = \zeta_{NO_x}, \\ x_2 = NH_3, \end{cases} \tag{5.30}$$

where ζ_{NO_x} is the NOx bias and NH_3 the NH3 concentration, which dynamics are governed by the following expression:

$$x_k = f(x_{k-1}, u_{k-1}) = \begin{cases} x_{1,k} = x_{1,k-1} + w_{1,k}, \\ x_{2,k} = \frac{X_{NO_{x,sensor,k-1}} - (X_{NO_{x,NN,k-1}} + x_{1,k-1})}{K_{CS}(x_{2,k-1})} + w_{2,k}, \end{cases} \tag{5.31}$$

where subindex k represents the current instant and w_1 and w_2 are the noises associated to the states. Note that, in the first state (x_1), the bias in the NOx estimate is assumed not to change abruptly and the changes are only associated with noise, the second state (x_2) is calculated according to eq.5.23. Regarding the dynamic equation for the second state, $NO_{x,sensor}$ and $NO_{x,ANN}$ are known since can be obtained from sensor and ANN, respectively, and can be considered as system inputs:

$$\begin{cases} u_1 = NO_{x,sensor} \\ u_2 = NO_{x,ANN} \end{cases} \tag{5.32}$$

Regarding the measurement information, it is possible to identify the NH3 slip of the SSA model as a measurement, then:

$$y = NH_3 \tag{5.33}$$

Eq.5.31 and the previous identifications lead to a dynamic system with two inputs, two states and one output measurement as follows:

$$x_k = f(x_{k-1}, u_{k-1}) = \begin{cases} x_{1,k} = x_{1,k-1} + w_{1,k}, \\ x_{2,k} = \frac{u_{1,k-1} - (u_{2,k-1} + x_{1,k-1})}{K_{CS}(x_{2,k-1})} + w_{2,k}, \end{cases} \tag{5.34}$$

$$y_k = h(x_k) = x_{2,k} + v_k, \tag{5.35}$$

For the system to be considered observable, the observability matrix and the number of states of the system must be equal [40]. Once the system provides two states, it is possible to analyse the observability matrix defined by:

$$\Omega = \begin{bmatrix} \frac{\partial h}{\partial x} \\ \left[\frac{\partial h}{\partial x}\right]\left[\frac{\partial f}{\partial x}\right] \end{bmatrix} \tag{5.36}$$

From the dynamic system eqs.5.34 and 5.35

$$\frac{\partial h}{\partial x} = [0\ 1] \tag{5.37a}$$

$$\frac{\partial f}{\partial x} = \begin{bmatrix} 1 & 0 \\ -\frac{1}{K_{CS}(x_{2,k-1})} & -\frac{\frac{\partial K_{cs}}{\partial x_2}(u_{1,k}-(u_{2,k}+x_{1,k-1}))}{K_{CS}(x_{2,k-1})^2} \end{bmatrix} \tag{5.37b}$$

Therefore, the observability matrix becomes:

$$\Omega = \begin{bmatrix} 0 & 1 \\ -\frac{1}{K_{CS}(x_{2,k-1})} & -\frac{\frac{\partial K_{cs}}{\partial x_2}(u_{1,k}-(u_{2,k}+x_{1,k-1}))}{K_{CS}(x_{2,k-1})^2} \end{bmatrix} \tag{5.38}$$

Note that, according to the system definition, the rank of Ω is clearly 2 since $K_{CS}(x_{2,k-1})$ is bounded. Therefore, it can be concluded that the system defined by eqs.5.34 and 5.35 is observable. Once the observability of the system has been demonstrated, the EKF can be directly applied to the models.

5.4.4.1 Model results

Once the feasibility of the model has been identified and its implementation carried out, the result of the EKF approach can be compared with the values obtained with the FTIR gas analyser. Figure 5.26 shows the evolution of NOx measured and estimated by the EKF for the WLTC (upper plot) and 2RTS (lower plot) cycles, while Figure 5.27 presents the evolution in terms of NH3 slip. As expected, the EKF approach was able to take advantage of both models (ANN and SSA).

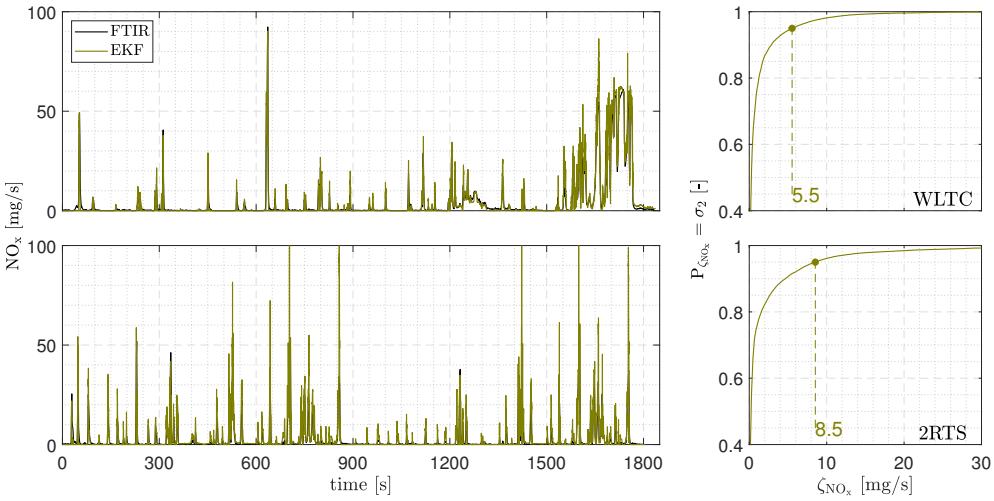

Figure 5.26: Comparison between FTIR and EKF model for NOx downstream in a WLTC (upper plots) and 2RTS (bottom plots) cycle. The left plots represent the emissions evolution, while the right ones the σ_2 error.

As can be seen, the EKF approach obtained high accuracy in the prediction of the NOx slip, thus it was able to track the dynamics of NOx emissions estimated by ANN. While it took advantage of the high accuracy of the SSA model in estimating NH3 slip.

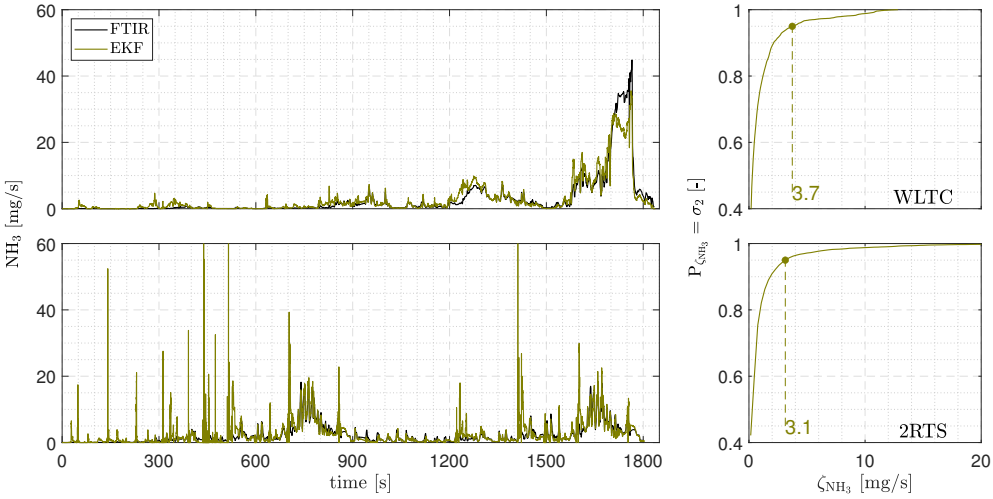

Figure 5.27: Comparison between FTIR and EKF model for NH3 downstream in a WLTC (upper plots) and 2RTS (bottom plots) cycle. The left plots represent the emissions evolution, while the right ones the σ_2 error.

The estimation of NOx and NH3 emissions from the proposed models is compared in Figure 5.28 in terms of σ_2 error. As can be seen, the EKF approach was able to take advantage of the best of each model, achieving similar levels of NOx and NH3 slip prediction as the 0D physical model.

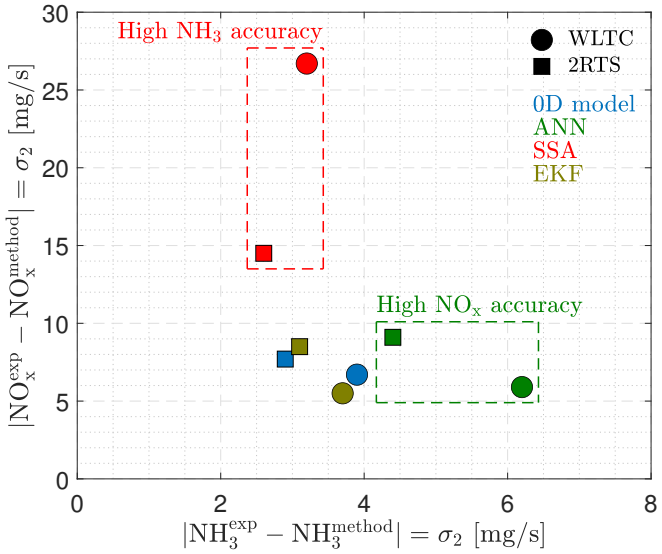

Figure 5.28: Comparison of NOx (y-axis) and NH3 (x-axis) emissions prediction of the proposed models in terms of σ_2 error.

Table 5.5 summarizes the results found for the different models and cycles. Each value refers to the σ_2 error and the percentage is the comparison with the corresponding value of the 0D model. EKF and SSA are the best overall approaches to estimate NOx and NH3 slip, respectively.

Table 5.5: σ_2 error for NOx and NH3 slip prediction, and comparison between the proposed models and 0D model.

Cycle	NOx [mg/s]						
	0D	ANN	[%]	SSA	[%]	EKF	[%]
WLTC	6.7	5.9	[11.9%]	26.7	[-298.5%]	5.5	[17.9%]
2RTS	7.7	9.1	[-18.2%]	14.5	[-88.3%]	8.5	[-10.4%]
Average error	7.2	7.5	[-4.2%]	20.6	[-186.1%]	7.0	[2.8%]

Cycle	NH3 [mg/s]						
	0D	ANN	[%]	SSA	[%]	EKF	[%]
WLTC	3.9	6.2	[-59.0%]	3.2	[17.9%]	3.7	[5.1%]
2RTS	2.9	4.4	[-51.7%]	2.6	[10.3%]	3.1	[-6.9%]
Average error	3.4	5.3	[-55.9%]	2.9	[14.7%]	3.4	[0.0%]

5.5 Slip prediction based on different sensitivities of NOx sensors to ammonia

An additional approach to estimate the emissions slip is to use the different sensitivities of NOx sensors to ammonia. The fundamental idea behind the proposed methodology is to use data from two NOx sensors with very different cross-sensitivity placed downstream of the catalyst to build a given linear system and estimate the NOx and NH3 slip. Rearranging eq.5.23 as a system leads to:

$$NH_3 = \frac{NO_{x,sensor^2} - NO_{x,sensor^1}}{K_{CS^2} - K_{CS^1}}, \tag{5.39}$$

Note that K_{CS} is an unknown variable. However, according to the previous analysis (subsection 5.3) can be written as a function of the cell temperature.

$$NH_3 = \frac{NO_{x,sensor^2} - NO_{x,sensor^1}}{f_2(T_{cell^2}) - f_1(T_{cell^1})}, \tag{5.40}$$

Replacing eq.5.40 in eq.5.23 leads to:

$$NO_x = NO_{x,sensor^1} - f_1 T_{cell^1} \frac{NO_{x,sensor^2} - NO_{x,sensor^1}}{f_2(T_{cell^2}) - f_1(T_{cell^1})}, \tag{5.41}$$

Note that, the difference in the cross-sensitivity is in the denominator of eq.5.39, what means that small differences lead to high values of NH3. Consequently, an important condition is that NOx sensors must have a very distinct sensitivity to ammonia, as small differences can amplify measurement errors.

5.5.1 Model results

The proposed methodology was tested in a dynamic cycle (WLTC) and a steady-state cycle (fullmap). The results related to NOx and NH3 slip can be seen in Figure 5.29 and Figure 5.30, respectively.

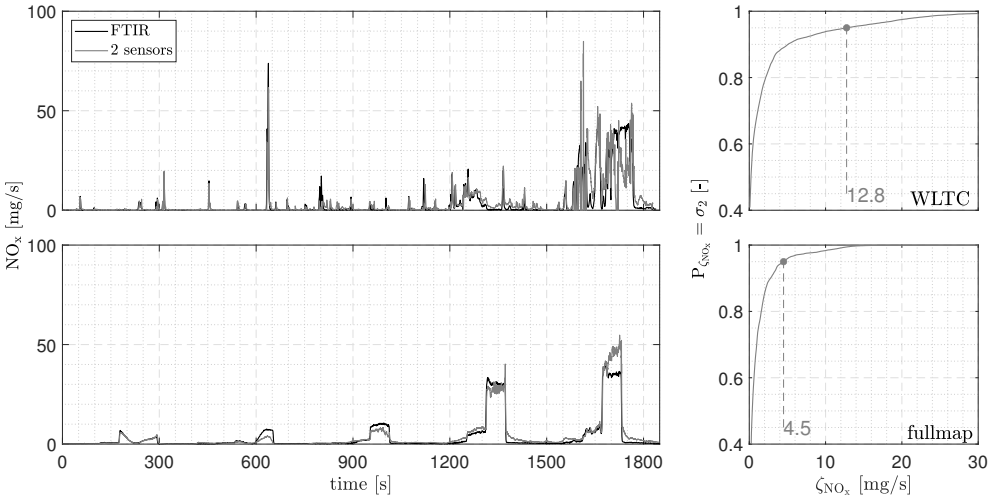

Figure 5.29: Comparison between FTIR and proposed approach for NOx downstream in a WLTC (upper plots) and fullmap (bottom plots) cycle. The left plots represent the emissions evolution, while the right ones the σ_2 error.

As can be seen in Figure 5.29, the proposed approach is able to estimate with good accuracy the NOx slip in situations of low dynamics of the exhaust gases, otherwise the emissions present a high oscillation. This behaviour can be associated to the fact that at high dynamics the cross-sensitivity of the sensors also have high dynamics, thus strongly affecting eq.5.41.

Regarding NH3 slip (Figure 5.30), although high dynamics affect the prediction, as mentioned before, NH3 emissions have a smoother evolution, so the impact of these dynamics are smaller.

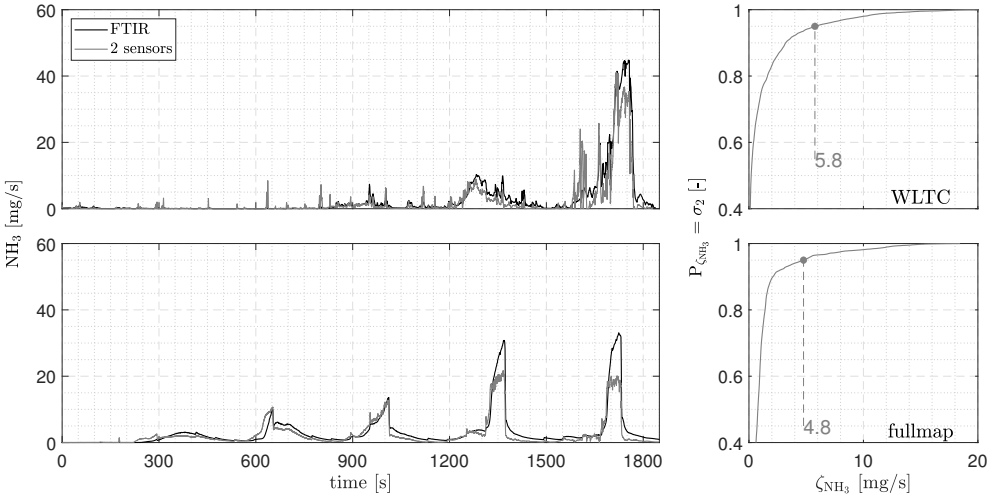

Figure 5.30: Comparison between FTIR and proposed approach for NH3 downstream in a WLTC (upper plots) and fullmap (bottom plots) cycle. The left plots represent the emissions evolution, while the right ones the σ_2 error.

As can be seen the approach is able to achieve a relatively good accuracy in estimating both NOx and NH3 emissions, however this model was not considered for the combined use with the Kalman filter due to two main factors. Firstly, although the model is able to estimate NOx and NH3 with a good accuracy, this approach is not the best neither in estimating the NH3 slip nor the NOx emissions, this way there is no advantage in using it combined with Kalman filter. A second point is that for this approach it is necessary to use two NOx sensors placed in the same position, being this type of arrangement not commonly used in emission control applications.

References

[1] Salam Satishchandra, Choudhary Tushar, Pugazhendhi Arivalagan, Verma Tikendra Nath and Sharma Abhishek. "A review on recent progress in computational and empirical studies of compression ignition internal combustion engine". *Fuel*, Vol. 279 n^o May, nov 2020. (cited in p. 62)

[2] Sinha A.K. and Loparo K.A. "A computational model for complex systems analysis: Causality estimation". *Physica D: Nonlinear Phenomena*, Vol. 423, sep 2021. (cited in p. 62)

[3] Pla Benjamín, Bares Pau, Sanchis Enrique José and Nakaema Aronis André. "Ammonia injection failure diagnostic and correction in engine after-treatment system by NOx and NH3 emissions observation". *Fuel*, Vol. 322 n^o March, aug 2022. (cited in pp. 21 and 62)

[4] Filip Florin-Gheorghe and Leiviskä Kauko. *Large-Scale Complex Systems*, pp. 619–638. Springer Berlin Heidelberg, Berlin, Heidelberg, 2009. (cited in p. 62)

[5] Bernad A Reig. *Optimal Control for Automotive Powertrain Applications*. PhD Thesis, Universitat Politècnica de València, 2017. (cited in pp. 62 and 158)

[6] Romiti Filippo, del Pozo Juan, Paioti Paulo H S, Gonsales Stella A, Li Xinghan, Hartrampf Felix W W and Hoveyda Amir H. "Different Strategies for Designing Dual-Catalytic Enantioselective Processes: From Fully Cooperative to Non-cooperative Systems". *Journal of the American Chemical Society*, Vol. 141 n^o 45, pp. 17952–17961, nov 2019. (cited in p. 62)

[7] Chen Guisheng, Di Lei, Shen Yinggang, Zhang Wei and Mao Bin. "Strategies for emissions control in heavy-duty diesel engines to achieve low-emissions combustion with a high efficiency". *Proceedings of the Institution of Mechanical Engineers, Part D: Journal of Automobile Engineering*, Vol. 230 n^o 5, pp. 593–608, apr 2016. (cited in p. 62)

[8] Nova Isabella, Lietti Luca, Tronconi Enrico and Forzatti Pio. "Transient response method applied to the kinetic analysis of the DeNOx–SCR reaction". *Chemical Engineering Science*, Vol. 56 n^o 4, pp. 1229–1237, feb 2001. (cited in pp. 62 and 64)

[9] Nahavandi M. "Selective Catalytic Reduction (SCR) Of No By Ammonia Over V2o5/Tio2 Catalyst In A Catalytic Filter Medium And Honeycomb Reactor: A Kinetic Modeling Study". *Brazilian Journal of Chemical Engineering*, Vol. 32 n^o 4, pp. 875–893, dec 2015. (cited in p. 63)

[10] Henle Jeremy J., Zahrt Andrew F., Rose Brennan T., Darrow William T., Wang Yang and Denmark Scott E. "Development of a Computer-Guided Workflow for Catalyst Optimization. Descriptor Validation, Subset Selection, and Training Set Analysis". *Journal of the American Chemical Society*, Vol. 142 n^o 26, pp. 11578–11592, jul 2020. (cited in p. 63)

[11] Shost Mark, Noetzel John, Wu Ming-cheng, Sugiarto Tanto, Bordewyk Todd, Fulks Gary and Fisher Galen B. "Monitoring, Feedback and Control of Urea SCR Dosing Systems for NOx Reduction: Utilizing an Embedded Model and Ammonia Sensing". In *SAE International*, number 724, apr 2008. (cited in p. 63)

[12] Upadhyay Devesh and Van Nieuwstadt Michiel. "Modeling of a Urea SCR Catalyst With Automotive Applications". In *Dynamic Systems and Control*, pp. 707–713. ASMEDC, jan 2002. (cited in p. 63)

[13] Wu Binyang, Deng Longfei, Liu Yize, Sun Dezeng and Su Wanhua. "Urea injection control strategy in urea-selective catalytic reduction for heavy-duty diesel engine under transient process". *International Journal of Engine Research*, Vol. 22 n^o 2, pp. 516–527, feb 2021. (cited in pp. 63 and 84)

[14] Zhang Hui and Wang Junmin. "Improved NO and NO2 Concentration Estimation for a Diesel-Engine-Aftertreatment System". *IEEE/ASME Transactions on Mechatronics*, Vol. 23 n^o 1, pp. 190–199, feb 2018. (cited in p. 63)

[15] Colombo Massimo, Nova Isabella, Tronconi Enrico, Schmeißer Volker, Bandl-Konrad Brigitte and Zimmermann Lisa. "NO/NO2/N2O–NH3 SCR reactions over a commercial Fe-zeolite catalyst for diesel exhaust aftertreatment: Intrinsic kinetics and monolith converter modelling". *Applied Catalysis B: Environmental*, Vol. 111-112 n^o 2, pp. 106–118, jan 2012. (cited in p. 64)

[16] Colombo Massimo, Nova Isabella and Tronconi Enrico. "A comparative study of the NH3-SCR reactions over a Cu-zeolite and a Fe-zeolite catalyst". *Catalysis Today*, Vol. 151 n^o 3-4, pp. 223–230, jun 2010. (cited in p. 65)

[17] Shin Youngjin, Jung Yongjin, Cho Chong Pyo, Pyo Young Dug, Jang Jinyoung, Kim Gangchul and Kim Tae Min. "NOx abatement and N2O formation over urea-SCR systems with zeolite supported Fe and Cu catalysts in a nonroad diesel engine". *Chemical Engineering Journal*, Vol. 381, feb 2020. (cited in p. 65)

[18] Pukelsheim Friedrich. "The Three Sigma Rule". *The American Statistician*, Vol. 48 n^o 2, pp. 88–91, may 1994. (cited in p. 69)

[19] Guan Bin, Zhan Reggie, Lin He and Huang Zhen. "Review of state of the art technologies of selective catalytic reduction of NOx from diesel engine exhaust". *Applied Thermal Engineering*, Vol. 66 n^o 1-2, pp. 395–414, may 2014. (cited in pp. 10, 70, 95, and 135)

[20] Keogh Eamonn and Mueen Abdullah. *Curse of Dimensionality*, pp. 314–315. Springer US, Boston, MA, 2017. (cited in pp. 70 and 152)

[21] Rheaume Jonathan Michael. *Solid State Electrochemical Sensors for Nitrogen Oxide (NOx) Detection in Lean Exhaust Gases*. PhD Thesis, University of California, Berkeley, 2010. (cited in p. 74)

[22] Frobert Arnaud, Raux Stephane, Creff Yann and Jeudy Eric. "About Cross-Sensitivities of NOx Sensors in SCR Operation". In *SAE Technical Papers*, volume 2, apr 2013. (cited in pp. 28, 29, 30, 31, 77, 78, 79, and 179)

[23] Afzal Adeel, Cioffi Nicola, Sabbatini Luigia and Torsi Luisa. "NOx sensors based on semiconducting metal oxide nanostructures: Progress and perspectives". *Sensors and Actuators B: Chemical*, Vol. 171-172 n^o 2012, pp. 25–42, aug 2012. (cited in p. 78)

[24] Olabi A.G., Maizak David and Wilberforce Tabbi. "Review of the regulations and techniques to eliminate toxic emissions from diesel engine cars". *Science of The Total Environment*, Vol. 748, dec 2020. (cited in p. 83)

[25] Vignesh R. and Ashok B. "Critical interpretative review on current outlook and prospects of selective catalytic reduction system for De-NOx strategy in compression ignition engine". *Fuel*, Vol. 276 n^o March, sep 2020. (cited in pp. 17, 21, 25, 83, and 181)

[26] Tan Pi-qiang, Zhang Shu-chen, Wang Shi-yan, Hu Zhi-yuan and Lou Di-Ming. "Simulation on catalytic performance of fresh and aged SCR catalysts for diesel engines". *Journal of the Energy Institute*, Vol. 93 n^o 6, pp. 2280–2292, dec 2020. (cited in pp. 25 and 83)

[27] Chundru Venkata Rajesh, Parker Gordon G. and Johnson John H. "The Effect of NO 2 /NO x Ratio on the Performance of a SCR Downstream of a SCR Catalyst on a DPF". *SAE International Journal of Fuels and Lubricants*, Vol. 12 n^o 2, jun 2019. (cited in pp. 25 and 83)

[28] Wang De-yuan, Cao Jian-hong, Tan Pi-qiang, Wang Zhi-xin, Li Wen-long, Liu Zuo-wei and Wang Jun. "Full course evolution characteristics of DPF active regeneration under different inlet HC concentrations". *Fuel*, Vol. 310, feb 2022. (cited in pp. 25 and 83)

[29] Feng Renhua, Hu Xiulin, Li Guanghua, Sun Zhengwei and Deng Banglin. "A comparative investigation between particle oxidation catalyst (POC) and diesel particulate filter (DPF) coupling aftertreatment system on emission reduction of a non-road diesel engine". *Ecotoxicology and Environmental Safety*, Vol. 238 n^o April, jun 2022. (cited in pp. 26 and 83)

[30] Dhillon Pritpal S., Harold Michael P., Wang Di, Kumar Ashok and Joshi Saurabh Y. "Enhanced transport in washcoated monoliths: Application to selective lean NOx reduction and ammonia oxidation". *Chemical Engineering Journal*, Vol. 377 n^o August, dec 2019. (cited in pp. 26, 84, and 111)

[31] Jiang Kai, Zhang Hui and Lin Jing. "NH3 Coverage Ratio Estimation of Diesel-Engine SCR Systems by a Dual Time-Scale Extended Kalman Filter". *IEEE Transactions on Vehicular Technology*, Vol. 67 n^o 4, pp. 3625–3629, apr 2018. (cited in p. 84)

[32] Skaf Zakwan, Aliyev Timur, Shead Leo and Steffen Thomas. "The State of the Art in Selective Catalytic Reduction Control". In *SAE Technical Papers*. SAE International, apr 2014. (cited in p. 84)

[33] Yang Shichun, Feng Song, Sun Kangfeng, Wang Shuai and Cao Yaoguang. "Square-root unscented Kalman filter for ammonia coverage ratio and input ammonia estimations in diesel-engine urea-SCR system". *ISA Transactions*, Vol. 96, pp. 299–308, jan 2020. (cited in pp. 84 and 135)

[34] Mora Pérez Javier. *Control-oriented modelling and diagnostics of diesel after-treatment catalysts*. PhD Thesis, Universitat Politècnica de València, Valencia (Spain), dec 2018. (cited in p. 84)

[35] Ebrahimi Mojtaba, Najafi Mohammad and Jazayeri Seyed Ali. "Multi-input–multi-output optimization of reactivity-controlled compression-ignition combustion in a heavy-duty diesel engine running on natural gas/diesel fuel". *International Journal of Engine Research*, Vol. 21 n^o 3, pp. 470–483, mar 2020. (cited in p. 84)

[36] Wang Guoyang, Awad Omar I., Liu Shiyu, Shuai Shijin and Wang Zhiming. "NOx emissions prediction based on mutual information and back propagation neural network using correlation quantitative analysis". *Energy*, Vol. 198, may 2020. (cited in p. 86)

[37] Arsie Ivan, Cricchio Andrea, De Cesare Matteo, Lazzarini Francesco, Pianese Cesare and Sorrentino Marco. "Neural network models for virtual sensing of NO x emissions in automotive diesel engines with least square-based adaptation". *Control Engineering Practice*, Vol. 61, pp. 11–20, apr 2017. (cited in p. 91)

[38] Willems Frank, Cloudt Robert, van den Eijnden Edwin, van Genderen Marcel, Verbeek Ruud, de Jager Bram, Boomsma Wiebe and van den Heuvel Ignace. "Is Closed-Loop SCR Control Required to Meet Future Emission Targets?". In *SAE Technical Papers*, volume 2007, apr 2007. (cited in pp. 34 and 95)

[39] Rajesh Chundru Venkata, Parker Gordon G. and Johnson John H. "Development of a Kalman filter estimator for simulation and controlof NO x and PM in a SCR catalyston a DPF". *International Journal of Engine Research*, Vol. 22 n^o 8, pp. 2407–2421, aug 2021. (cited in pp. 97 and 119)

[40] Rocha Cachim Pedro, Gomes João and Ventura Rodrigo. "Autonomous orbit determination for satellite formations using relative sensing: Observability analysis and optimization". *Acta Astronautica*, Vol. 200 n^o August, pp. 301–315, nov 2022. (cited in p. 98)

Chapter 6

After-treatment control and diagnosis

Control, control, you must learn control!

— Yoda

Contents

6.1 Introduction

As mentioned, the SCR and ASC catalysts are complex dynamic systems, this characteristic makes the ammonia injection strategy the biggest challenge of the deNOx systems, since insufficient injection reduces the NOx conversion efficiency and the opposite leads to an undesired NH3 slip [1]. This behaviour can be seen in Figure 6.1, which shows the total slip of NOx and NH3 downstream the SCR catalyst for different ammonia injection strategies during a WLTC cycle.

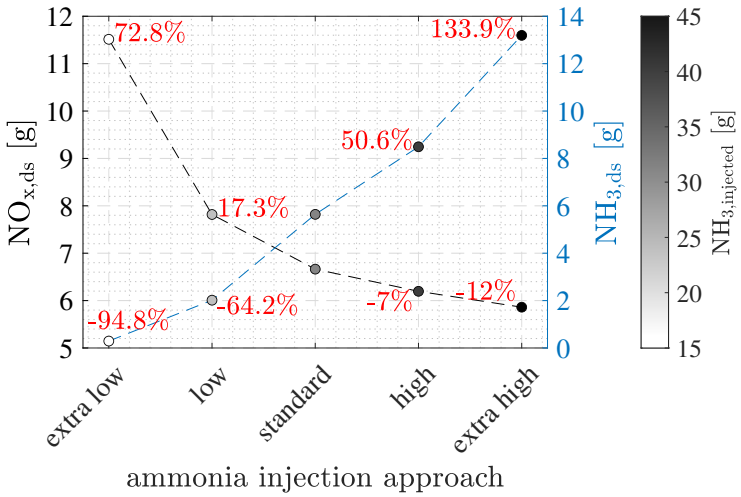

Figure 6.1: Evolution of the total amount of NOx (left axis) and NH3 (right axis) emissions downstream of the SCR catalyst for different amounts of ammonia injected (colourbar) during the complete WLTC cycle. The values highlighted in red are the percentage increase or decrease in emissions over the values using the standard injection strategy.

As can be seen, increasing ammonia injection leads to higher NOx reduction rates, however to higher ammonia slip rates as well. The x-axis refers to the amount of ammonia that is injected in relation to the amount demanded by the system, and the highlighted numbers represent the emissions percentage increase or decrease in emissions compared to the standard strategy. Note

that the standard strategy may vary, as it depends on the emission levels of NOx and NH3 expected to be achieved and the ATS technology itself [2]. In any case, as the impact of ammonia injection on NOx and NH3 emissions is an important matter, the European OBD regulation has a pre-requirement for under/overdose detection [3].

6.2 Impact of the ammonia injection strategy and the catalyst ageing on the NOx and NH3 slip

The proposed methodology is based on the observation that if there is any anomaly in the ATS, it should impact the emissions behaviour [4]. With an over ammonia injection, there is a reduction in NOx although an increase in NH3 emissions, while the opposite happens with under ammonia injection. In the case of catalyst ageing, it shifts both pollutants to a higher emissions zone, as ageing reduces NOx conversion efficiency rates and the catalyst capacity to store ammonia [5]. This behaviour can be analysed over the following simplified model of the ATS:

$$\dot{\theta}_{\mathrm{NH_3}} = \mathrm{NH_{3,injected}} - \mathrm{NH_{3,ds}} - \mathrm{NH_{3,oxidized}} \tag{6.1}$$

The stored ammonia ($\theta_{\mathrm{NH_3}}$), evolves according to the amount of NH3 entering ($\mathrm{NH_{3,injected}}$) minus the amount leaving the catalyst ($\mathrm{NH_{3,ds}}$) and the NH3 used to reduce the NOx engine out ($\mathrm{NH_{3,oxidized}}$). $\theta_{\mathrm{NH_3}}$ refers to the ammonia adsorbed by the catalyst; therefore, it is directly linked to the NOx conversion efficiency [6]. Thus, as the ageing of the catalyst affects the adsorption capacity of ammonia, the reduction of $\mathrm{NH_{3,oxidized}}$ leads to higher concentrations of NOx and NH3 slip. Adapting eq.6.1 leads to:

$$\mathrm{NH_{3,injected}} = \dot{\theta}_{\mathrm{NH_3}} + \mathrm{NH_{3,ds}} + \mathrm{k_{stch}}(\mathrm{NO_{x,us}} - \mathrm{NO_{x,ds}}) \tag{6.2}$$

where $\mathrm{k_{stch}}(\mathrm{NO_{x,us}} - \mathrm{NO_{x,ds}})$ ammonia needed to reduce the $\mathrm{NO_{x,up}}$ to $\mathrm{NO_{x,ds}}$ levels. As can be seen, changing the amount of ammonia injected will directly affect the ammonia slip. The same analysis can be done for NOx slip, since $\mathrm{NH_{3_{ds}}}$ and $\mathrm{NH_{3,injected}}$ are inversely proportional, the increase in ammonia injection reduces the NOx slip, as the opposite is true. Note that these behaviours are regardless of whether the catalyst is aged or not.

In summary, as shown in Figure 6.2, under injection (green line) limits catalyst loading, consequently leading to lower levels of NOx conversion efficiency, as well as lower ammonia slip. In the case of the catalyst ageing (red lines), it affects the ammonia adsorption capacity, thus leading to lower NOx conversion rates and higher ammonia slip levels.

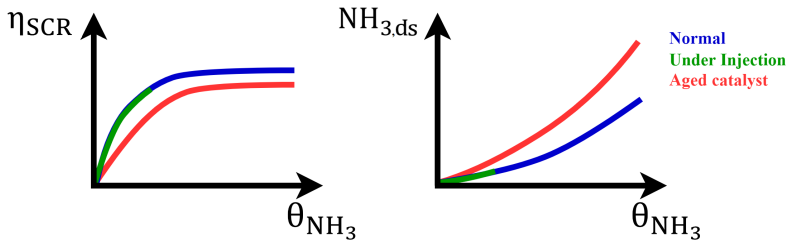

Figure 6.2: Effect of under ammonia injection (green lines) and catalyst ageing (red lines), in terms of NOx conversion efficiency (left plot) and ammonia slip (right plot).

6.3 Ammonia injection fault observation

Aiming to detect the failure of the ammonia injection into the SCR catalyst, the first step was to evaluate the behaviour of the proposed models (0D, ANN, SSA, and EKF) when subjected to such failure. To this end the models were subjected to the tests with different levels of ammonia injection failure.

In this part of the work, several WLTC and 2RTS cycles were carried out with constant failure in the ammonia injection. The tests were performed with two levels of injection factor (I.F.), 25% and 120% of the standard injection, which are, respectively, I.F. = 0.25 and 1.20, and with the standard injection (I.F. = 1.00). As described in the "Engine tests" subsection these injection failures are artificially produced, bypassing the nominal value of the ammonia injection multiplied by the I.F., thus changing the injector opening time. Note that, for I.F. = 0.25, the amount of ammonia injected is approximately 25% of what is required. However, the signal feedback to the ECU is the original value of the injection, so the engine control strategy is not aware of the injection bias and there are not correction measures applied. The same strategy has been used to simulate other failure levels. Thus, the I.F. refers to the level of the ammonia failure invisible to the control strategy.

Figure 6.3 shows the evolution of the experimental NOx slip and models in two different driving cycles (WLTC and 2RTS) and three different ammonia injection factors (I.F.=0.25; 1.00; 1.20).

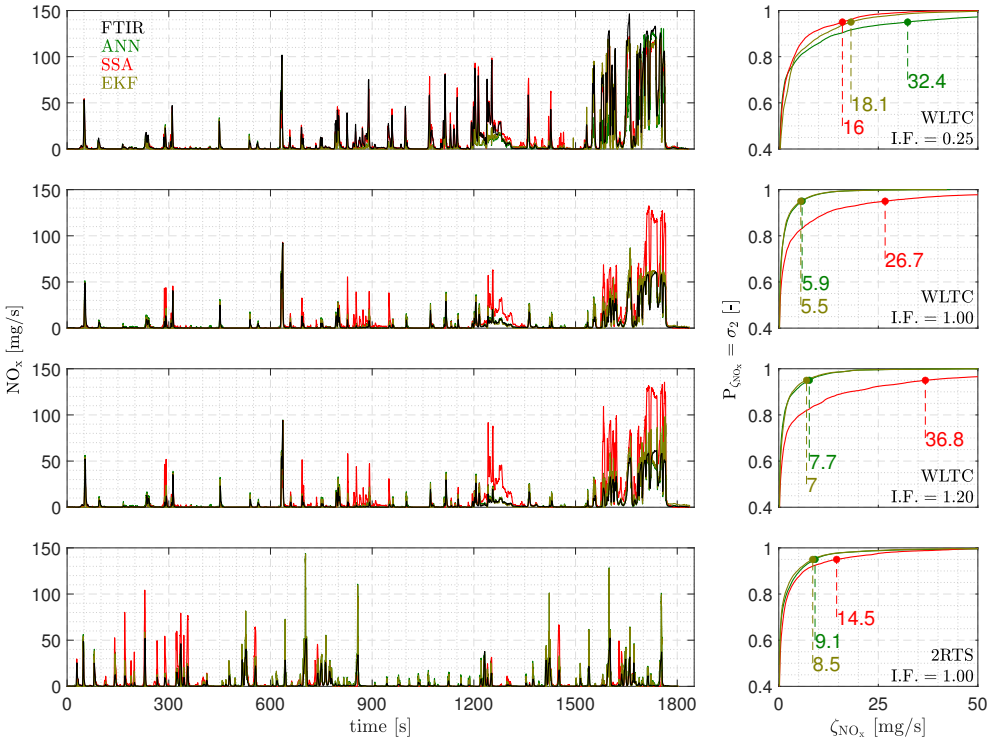

Figure 6.3: Evolution of the experimental NOx slip (black), ANN (green), SSA (red) and EKF (yellow) models with different ammonia injection factors during different driving cycles. Three upper plots: WTLC cycle with I.F.= 0.25, 1.00 and 1.20, respectively. Bottom plots: 2RTS with I.F.= 1.00. The left plots represent the emissions evolution, while the right ones the σ_2 error.

As shown in Figure 6.3, EKF has higher accuracy in all tests, following the ANN model trend, except in tests with I.F. =0.25, since a strongly biased ammonia injection is used by ANN. Consequently, the bias in the injection is transferred to the NOx result. Conversely, the SSA provides poor NOx estimation results since, although the dynamics of the NOx slip is conserved, the level depends on the calculated conversion efficiency, which according to the SSA method is an average value during the time-window. As expected, EKF was able to track the best strategy that predicts NOx slip.

The corresponding results in terms of NH3 slip are shown in Figure 6.4. The SSA has high accuracy in all tests (except for WLTC I.F.=1.20 which is EKF), while the ANN has good accuracy only in tests without ammonia injection failures, since the ammonia injection is used as an input signal for the ANN training procedure. Again, as expected, EKF tracks the best strategy

that predicts NH3 slip.

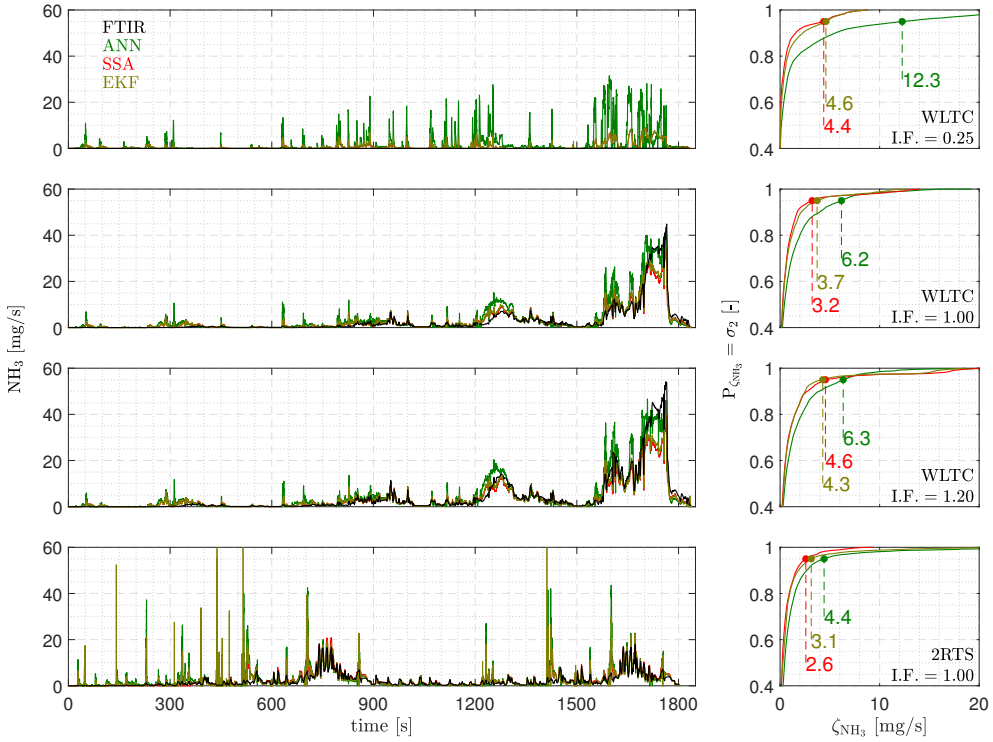

Figure 6.4: Evolution of the experimental NH3 slip (black), ANN (green), SSA (red) and EKF (yellow) models with different ammonia injection factors during different driving cycles. Three upper plots: WTLC cycle with I.F.= 0.25, 1.00 and 1.20, respectively. Bottom plots: 2RTS with I.F.= 1.00. The left plots represent the emissions evolution, while the right ones the σ_2 error.

Aiming to assess the level of improvement of the proposed methodology, the EKF was compared with the zero-dimensional model when subjected to ammonia injection failure situations. For this, both models were tested in WLTC and 2RTS cycles with two different levels of ammonia injection failure.

Figure 6.5 compares the evolution of NOx slip for the experimental (black), 0D (blue), and EKF (yellow) models for two levels of ammonia injection failure (I.F.=0.25 and I.F.=1.20) and two driving cycles (WLTC and 2RTS). Both models are equally accurate when there is an over-ammonia injection; this may be because the catalyst always performs with a high conversion efficiency. Therefore, excessive ammonia injection might not have an impact on NOx prediction. The 0D model considers the ammonia injection while calculating

the ammonia coverage ratio, hence the EKF has a significantly higher accuracy in the situation of under ammonia injection. As a result, the predicted NOx from an under-ammonia injection is substantially lower than the actual NOx slip.

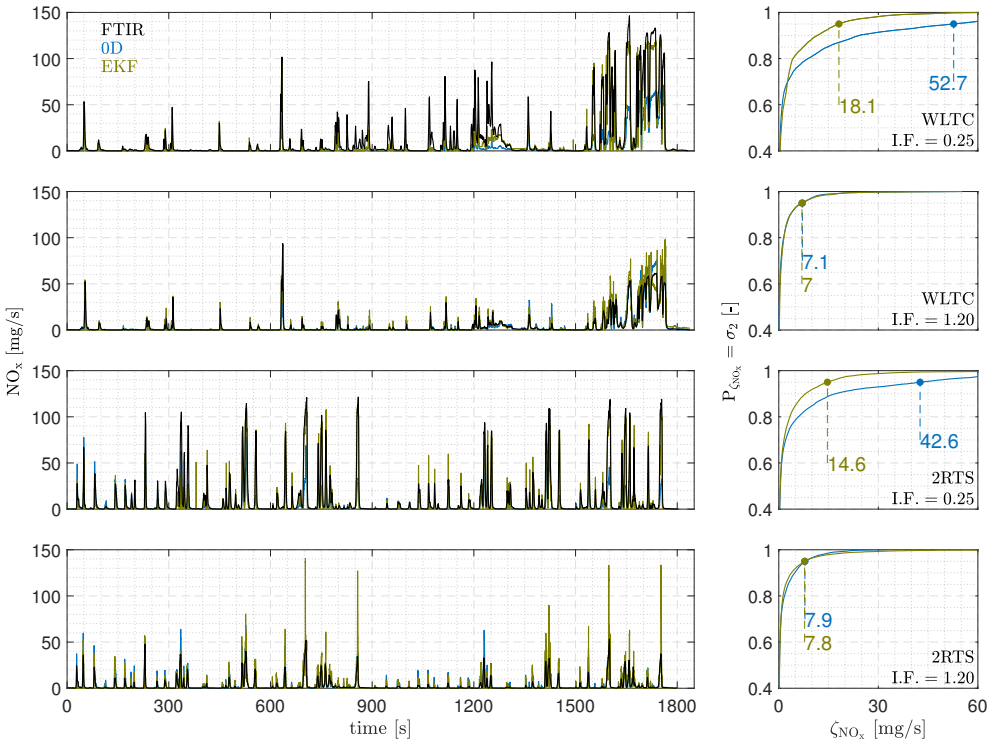

Figure 6.5: Evolution of the experimental NOx slip (black), 0D (blue) and EKF (yellow) models with different ammonia injection factors during different driving cycles. Two upper plots: WTLC cycle with I.F.= 0.25 and 1.20, respectively. Two bottom plots: 2RTS with I.F.= 0.25 and 1.20, respectively. The left plots represent the emissions evolution, while the right ones the σ_2 error.

The comparison of NH3 slip development is shown in Figure 6.6. The EKF model is more accurate in every situation. The maximum catalyst load is attained more quickly when there is an over-ammonia injection. As a result, the ammonia that the catalyst is unable to store goes straight to exhaust. When there is an under-ammonia injection, the catalyst adsorbs all injected ammonia, which is then used to react with NOx. Therefore, in this instance, there is no ammonia slip.

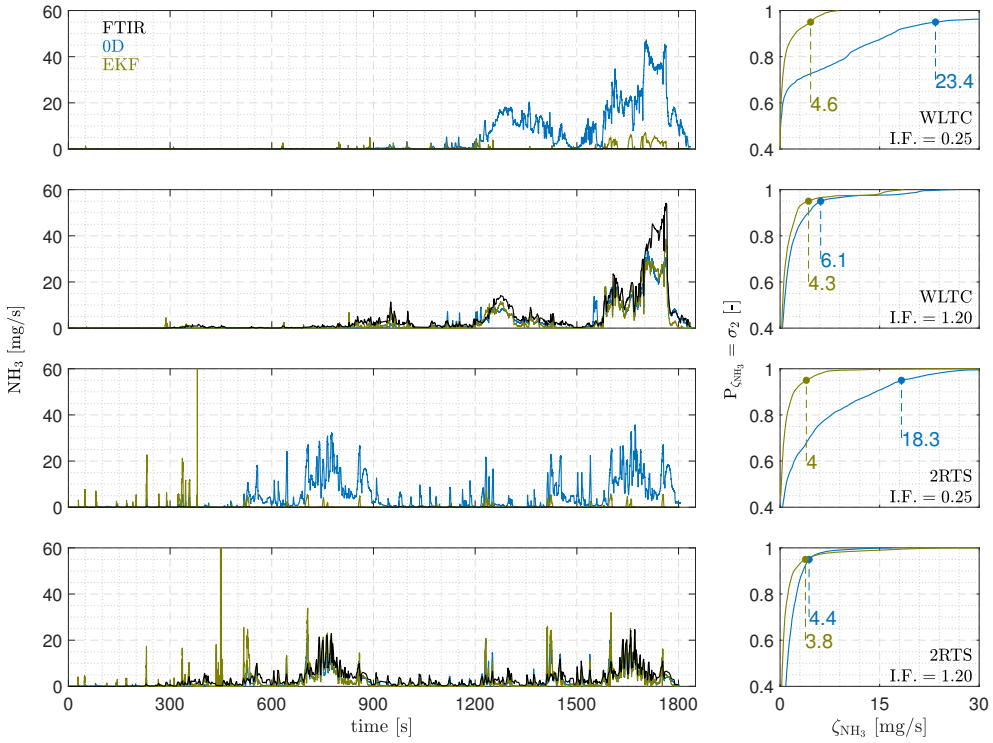

Figure 6.6: Evolution of the experimental NH3 slip (black), 0D (blue) and EKF (yellow) models with different ammonia injection factors during different driving cycles. Two upper plots: WTLC cycle with I.F.= 0.25 and 1.20, respectively. Two bottom plots: 2RTS with I.F.= 0.25 and 1.20, respectively. The left plots represent the emissions evolution, while the right ones the σ_2 error.

It should be noted that EKF and 0D models have comparable levels of accuracy when there is no ammonia injection problem. The 0D model is heavily reliant on the urea injector signal feedback, so it makes sense that in situations where there is an injection failure, the EKF model has a higher accuracy.

Table 6.1 summarises the results found for different injection failures and approaches. Each value refers to the σ_2 error and the percentage is the comparison with the corresponding value of the 0D model. Being EKF the best approach, since it has similar levels to SSA in the prediction of NH3 slip, but with a higher accuracy on NOx emissions estimation.

Table 6.1: σ_2 error for NOx and NH3 slip prediction, and comparison between the proposed models and 0D model.

Cycle	I.F.	NOx [mg/s]						
		0D	ANN	[%]	SSA	[%]	EKF	[%]
WLTC	0.25	52.7	32.4	[38.5%]	16.0	[69.6%]	18.1	[65.7%]
	1.00	6.7	5.9	[11.9%]	26.7	[-298.5%]	5.5	[17.9%]
	1.20	7.1	7.7	[-8.5%]	36.8	[-418.3%]	7.0	[1.4%]
2RTS	0.25	42.6	42.1	[1.2%]	17.9	[58.0%]	14.6	[65.7%]
	1.00	7.7	9.1	[-18.2%]	14.5	[-88.3%]	8.5	[-10.4%]
	1.20	7.9	9.1	[-15.2%]	17.2	[-117.7%]	7.8	[1.3%]
Average error		20.8	17.7	[14.8%]	21.5	[-3.5%]	10.3	[50.7%]

Cycle	I.F.	NH3 [mg/s]						
		0D	ANN	[%]	SSA	[%]	EKF	[%]
WLTC	0.25	23.4	12.3	[47.4%]	4.4	[81.2%]	4.6	[80.3%]
	1.00	3.9	6.2	[-59.0%]	3.2	[17.9%]	3.7	[5.1%]
	1.20	6.1	6.3	[-3.3%]	4.6	[24.6%]	4.3	[29.5%]
2RTS	0.25	18.3	16.4	[10.4%]	3.4	[81.4%]	4.0	[78.7%]
	1.00	2.9	4.4	[-51.7%]	2.6	[10.3%]	3.1	[-6.9%]
	1.20	4.4	5.7	[-29.5%]	2.6	[40.9%]	3.8	[13.6%]
Average error		9.8	8.6	[13.1%]	3.5	[64.7%]	3.9	[60.2%]

As conclusion, The EKF proposed method to estimate the NOx and NH3 slip proved to predict exhaust emissions with high accuracy, even under conditions of urea injection failure. When compared to the 0D model, under conditions without ammonia injection failure, the EKF approach has a similar performance to estimate NOx and NH3 emissions, while improving considerably in failure conditions. Therefore, the use of the EKF approach is justified by the lower computational cost, enabling its use in real-time applications and higher accuracy in ammonia injection failure conditions.

6.4 Ammonia injection fault diagnosis

As previously described, a failure in the feedback signal from the sensors and/or actuators affects the ammonia dosage, generating a supply rate different

from that required, leading to an inefficient NOx conversion rate. The impact on ammonia supply is highly damaging as it reduces the performance of harmful gases converted before they are released into the environment.

Aiming to evaluate the impact of the ammonia injection failure and the ability of the proposed methodology to diagnose and correct possible failures, three sets of tests were performed. First, tests were carried out with constant failure in the ammonia injection. Followed by several WLTC cycles performed in sequence with different I.F. to validate the proposed methodology. Finally, in the merged cycle, tests were performed without failure in the ammonia injection system, and with failure with and without correction. In cases where injection failure is considered, a constant degradation rate was applied to check the capability of the proposed strategy of tracking the injection fault and applying the proper correction. Figure 6.7 shows the impact of ammonia injection failure on NOx and NH3 slip.

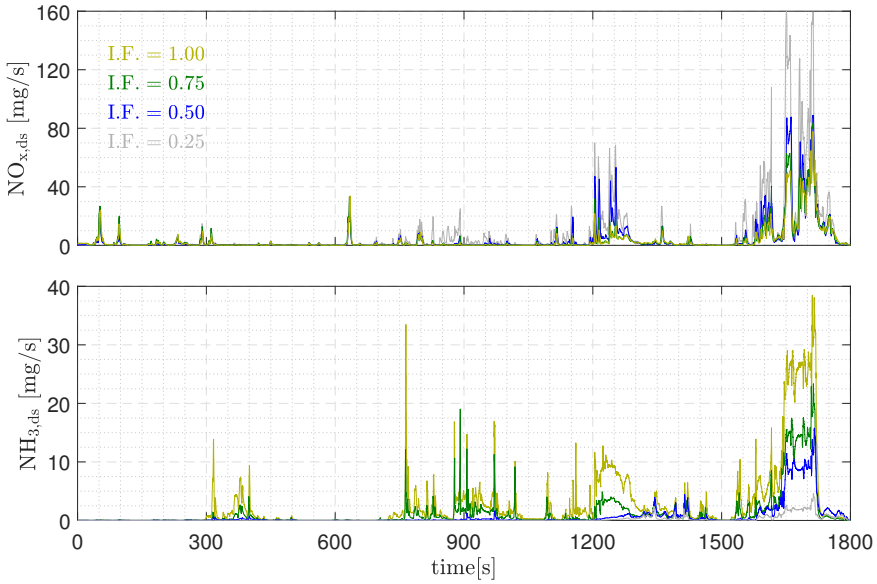

Figure 6.7: Slip of NOx (upper plot) and NH3 (bottom plot) for different levels of ammonia injection failure in a WLTC cycle.

As can be seen in Figure 6.7, with the increase of the error in the ammonia injection, the NH3 slip is reduced since all the ammonia injected is adsorbed and used in the reduction reaction with NOx entering the catalyst. Otherwise, NOx slip remains similar for errors below 50% (I.F. = [0.5; 0.75; 1.00]) of the nominal injection. This is related to two main facts: first, due to the strong NOx restrictions, the SCR catalyst is forced to work with high NOx

conversion rates, which usually leads to some level of NH3 slip [7]. Second, to reduce NOx, the ammonia injected must be previously adsorbed and stored by the catalyst, so the SCR is a dynamic system with complex relations between ammonia injection and emissions that makes difficult its control without any slip in changing conditions such as the WLTC [8].

These concepts are important, since the proposed method to determine the degree of ammonia injection failure is based on the comparison of NOx and NH3 accumulated over a predetermined period, between cycles with and without ammonia injection failure. Thus, allowing access and quantifying errors between these situations.

Once it has been proven that injection failures can be observed through the analysis of emissions, the following steps were taken to verify the viability of the proposed strategy.

During the engine operation, the NOx emissions before the SCR are accumulated until reaching a calibrated value. The time needed to reach these NOx emissions will define a window where the analysis will be done. Contrary to the strategy adopted by Mora et al. [9], instead of accumulating in a fixed time-window, NOx emissions before the catalyst are used as a reference, then the considered window is adapted to the operating conditions. The NOx threshold should be calibrated to allow injection fault detection, considering aspects such as the impact of injection fault on NOx reduction efficiency, modelling, and sensor errors. Furthermore, the window length was linked to a physical-chemical parameter and not to a temporal one.

The size of the accumulation window i in a given test (AWS_i) will be determined by the time needed by the NOx emissions upstream the SCR to reach a given mass according to the following expression eq.6.3

$$\sum_{n=1}^{AWS_i} NO_{x,us,n}\delta t = NO_{x,us}^{thr}, \tag{6.3}$$

where, the SCR NOx upstream ($NO_{x,us}$ [mg/s]) is integrated until reaching the threshold value ($NO_{x,us}^{thr}$ [g]). To minimise the impact of measurement noise, constraints were included in the accumulation process of eq.6.3.

$$\underline{x} \leqslant x \leqslant \overline{x}, \tag{6.4}$$

where, x is a vector containing the NOx downstream of the SCR ($NO_{x,ds}$), ammonia injected into the ATS ($NH_{3,injected}$) and the SCR catalyst temperature (T_{SCR}). In the case of $NO_{x,ds}$ only a lower limit of 20 ppm was applied, as the relative measurement uncertainty is very high at small values. The same is true for $NH_{3,injected}$, where a lower limit of 10 kg/h was defined. Regarding

T_{SCR} it was defined boundaries of 200-500 °C, since this is the ideal operating temperature range of the catalyst.

The AWS values found from eq.6.3 are applied to compute the NOx (eq.6.5) and NH3 (eq.6.6) slip during the accumulation window.

$$\text{Accumulated } NO_{x,ds,i} = \sum_{n=1}^{AWS_i} NO_{x,ds,n}\delta t, \tag{6.5}$$

$$\text{Accumulated } NH_{3,ds,i} = \sum_{n=1}^{AWS_i} NH_{3,ds,n}\delta t, \tag{6.6}$$

Figure 6.8, shows the FTIR-measured cumulative evolution of NOx (second plot) and NH3 (third plot) emissions downstream of the SCR catalyst, until the NOx sensor emissions upstream of the SCR (first plot) reach the threshold value. Note that when the value is reached ($NO_{x,us}^{thr}$), the window is restarted.

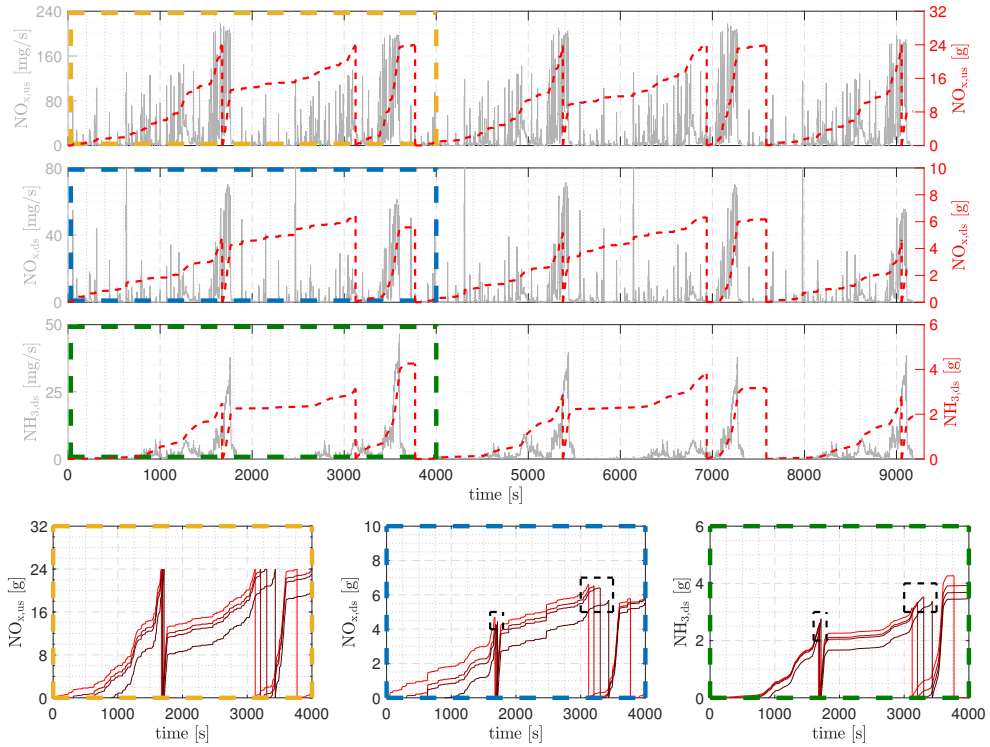

Figure 6.8: Evolution of NOx emissions upstream of the SCR (first plot) and NOx (second plot) and NH3 slip (third plot) downstream of the catalyst for five consecutive WLTC cycles. Left axis: Instantaneous evolution (mg/s). Right axis: cumulative evolution (g) until reaching the threshold limit (24 g). Upper plots: Evolution of one AWS starting at 0s (red dashed line). Bottom plots: Zoom in highlighted interval and evolution of four AWS starting every 300s.

In the bottom figures, which represent a zoom of the highlighted areas, it is possible to visualize that the methodology uses several windows in parallel, starting every 300 seconds. The image presents only four consecutive continuous windows, in order to facilitate the visualization. However, a new window starts every 300 seconds continuously.

Figure 6.9 shows an example for two consecutive WLTCs with $\mathrm{NO}_{\mathrm{x,us}}^{\mathrm{thr}} = 24$ g. Note that despite the first two windows starting with 300 s difference, they both finish around second 1700 s due to the increase in NOx emissions as the driving cycle evolves.

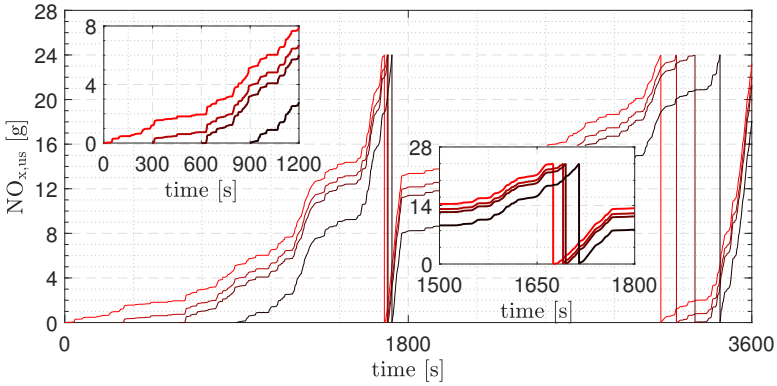

Figure 6.9: Different starting points for the accumulation window of NOx upstream of the SCR catalyst.

Each accumulated value of NOx and NH3 slip can be represented in a NOx-NH3 two-dimensional plane, as shown in the Figure 6.10.

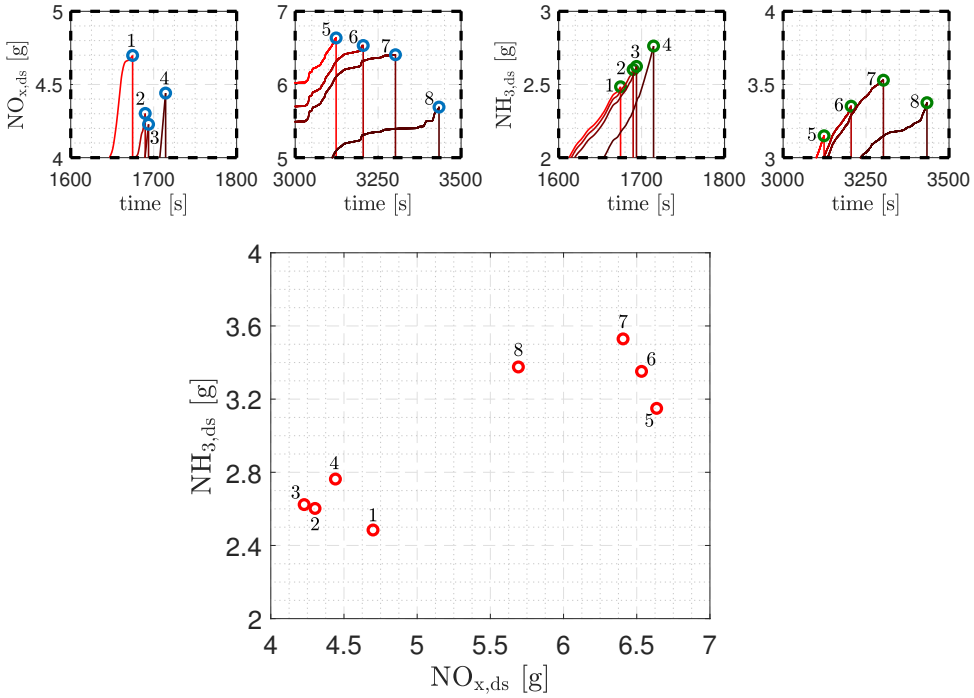

Figure 6.10: Upper plots: Zoom of the highlighted area of NOx and NH3 evolution of Figure 6.8. Bottom plot: Distribution of the first eight accumulated slip values of NOx and NH3.

The previous process is performed for 3 different levels of ammonia injection failure, 25 (I.F. = 0.25), 50 (I.F. = 0.50) and 75 (I.F. = 0.75) percent of the nominal injection, and the nominal injection (I.F. = 1.00). In this way, it is possible to create a distribution of the NOx and NH3 accumulated emissions in the considered windows for every injection failure.

The same steps are performed for different values of $NO_{x,us}^{thr}$, in order to calibrate the value that allows the separation between the distributions for the different injection faults. Figure 6.11 lower plot shows the locations in the two-dimensional plane of the results obtained with different NOx upstream thresholds. Upper plots show the fit to a normal distribution of the results. Note that if the threshold value $NO_{x,us}^{thr}$ is changed, the points will be moved in the NOx-NH3 plane, consequently changing the clusters position. A larger window allows a greater amount of information stored for later diagnosis, on the other hand, a more time-consuming diagnosis, and the need for a system with greater information storage capacity. On the other hand, as the proposed

methodology evaluates the ATS state according to the stored information, a small threshold value might not be enough to differentiate a system with normal operation from one operating with some anomaly. This means that $NO_{x,us}^{thr}$ must be chosen to properly separate the points with the level of failure to be detected.

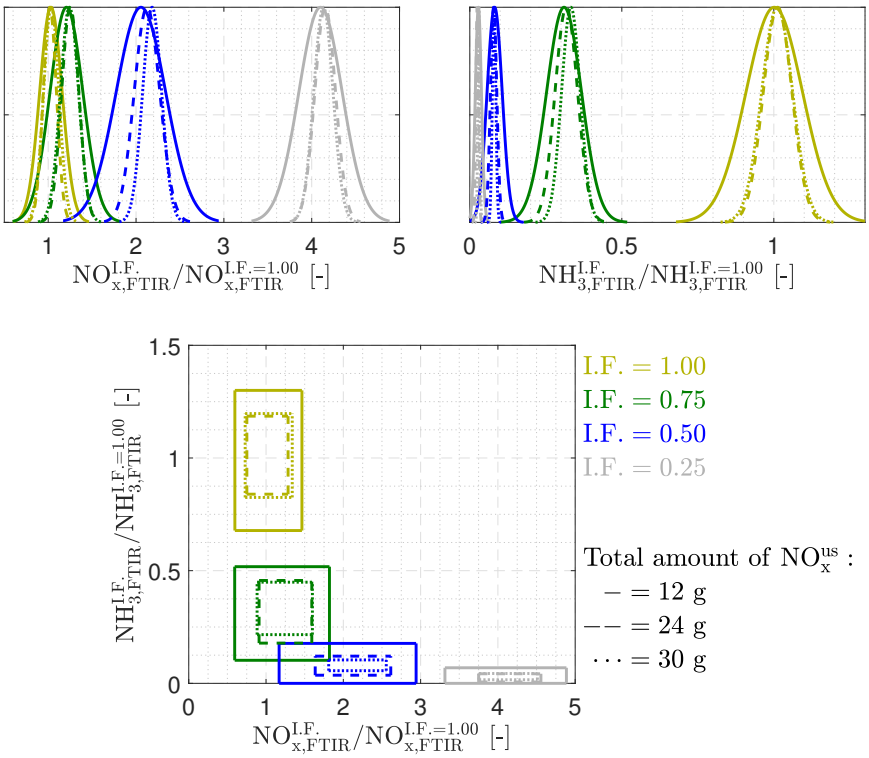

Figure 6.11: Normal distribution of NOx and NH3 slip for different levels of ammonia injection failure and different accumulation windows size (12, 24 and 30 g – upper plots) using the FTIR emissions signal

With the distribution, it was possible to verify that, in terms of NH3, errors higher than 50% of the nominal injection are indistinguishable (grey and blue distributions). With higher injection faults than 50%, the amount of ammonia available is so low that all the injected ammonia reacts with the NOx entering the catalyst, being the NH3 slip very small. Regarding NOx, it is not possible to differentiate the nominal injection from errors lower than 25% (yellow and green distributions). Even for this level of error the catalyst operates with high efficiency rates.

The proposed methodology was also compared when it uses a fixed time

window to reset the accumulation window, instead of SCR NOx upstream, as proposed by Mora et al. [9], the distribution results can be seen in Figure 6.12.

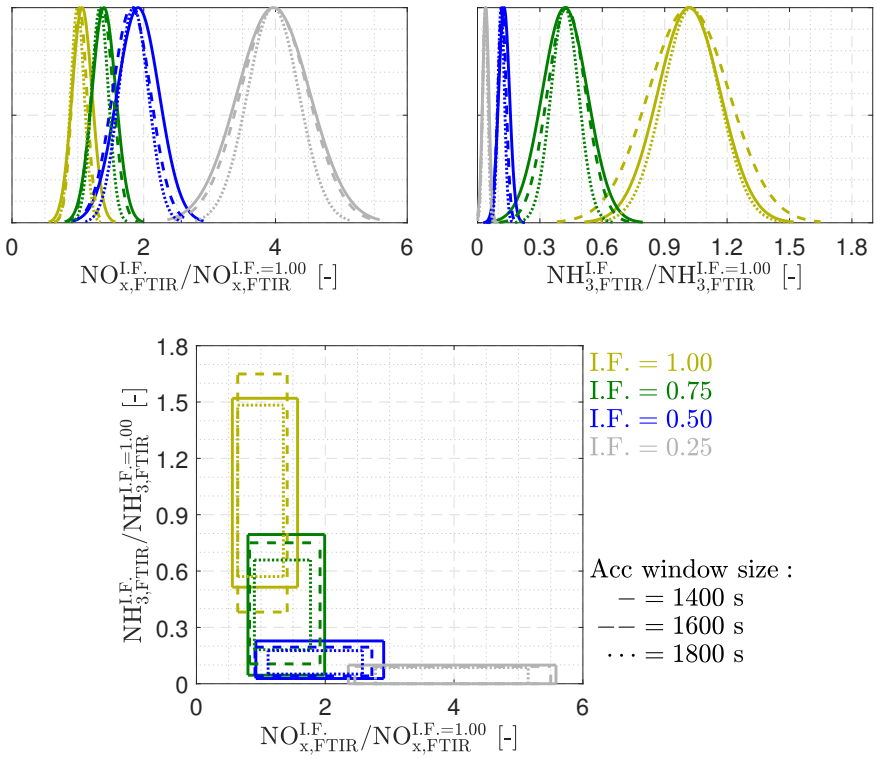

Figure 6.12: Normal distribution of NOx and NH3 slip for different levels of ammonia injection failure and different accumulation windows size (1400, 1600 and 1800 s - upper plots) using the FTIR emissions signal.

Using a fixed time window, it was not possible to separate the error levels in the ammonia injection failure. The use of a fixed time window has several drawbacks, as also commented by Wang et al. [10], mainly because depending on where the time window starts, there will be a big difference in the accumulated values of NOx and NH3 downstream of the catalyst, this difference makes the distribution very broad, since the use of AWS fixed does not create any linkage of pollutants to a physical parameter. The comparison of duration and number of windows between fixed and variable AWS as can be seen in Figure 6.13.

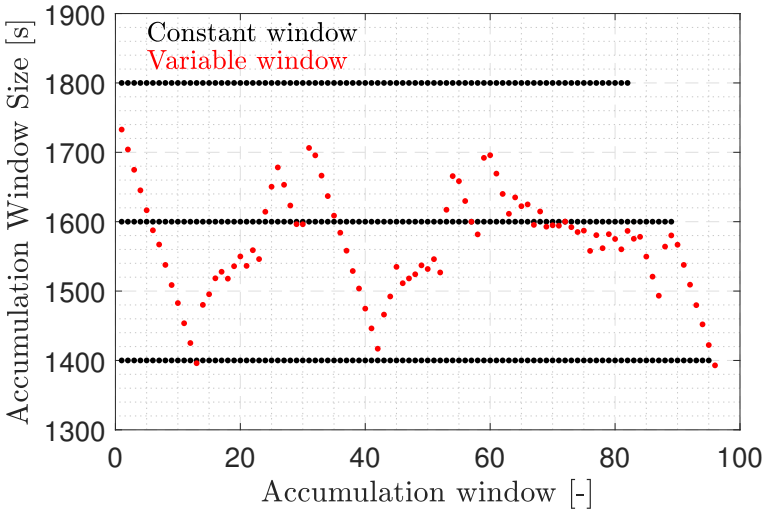

Figure 6.13: Comparison of duration and number of windows for fixed and variable accumulation window size. Dark dots: fixed AWS. Red dots: variable AWS (proposed approach).

As the cycle evolves, the AWS duration decreases as the cycle goes from the low load zone towards the high/very high load zone and starts to grow when AWS starts the next cycle (the evolution of the cycles is presented in Figure 6.8). This approach allows the use of variable time windows, but constant in NOx at the catalyst inlet, consequently in areas where NOx production is low, there is more time for data collection, allowing enough information to detect the level ammonia injection failure.

6.4.1 Proposed methodology extended to control-oriented models and observer

To allow the use of the proposed methodology in real-time application, the previous analysis was extended to the models. Therefore, the ANN is assumed as the representative model of the estimated emissions of the system operating without failure, while the EKF represent the actual emissions levels. The complete structure of inputs and outputs of the models, EKF and the proposed ammonia injection correction strategy can be seen in the following flowchart.

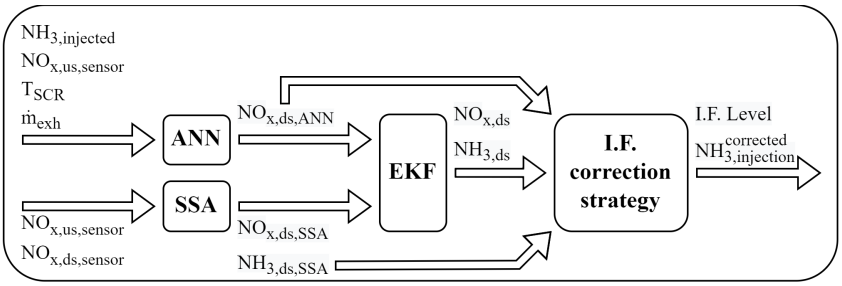

Figure 6.14: Flowchart of inputs and outputs of control-oriented models, EKF and ammonia injection correction strategy.

The ANN can be used as the ATS operating under normal conditions, since it depends on the ammonia injector feedback signal, and its error in estimating emissions increases as injector failure increases. In this sense, the ratio between the observed and modelled emissions is an estimation of the ratio between the emissions with a given injection fault (I.F. < 1) and without fault (I.F. $= 1$).

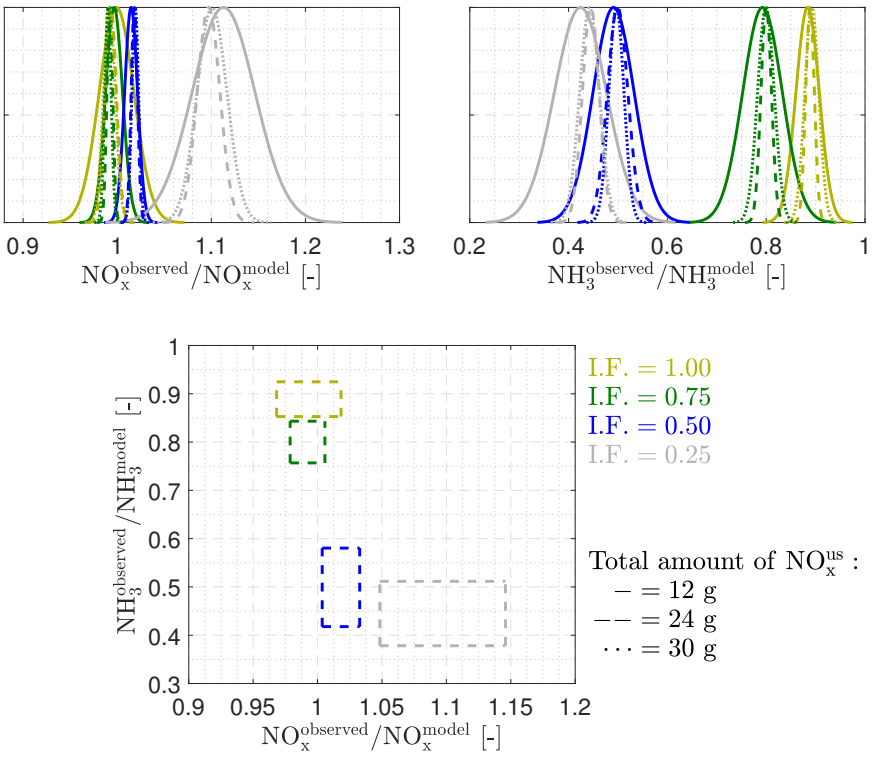

Figure 6.15: Normal distribution of NOx and NH3 slip for different levels of ammonia injection failure and different accumulation windows size (12, 24 and 30 g – upper plots) using the model/observer ratio emissions signal.

Note that, in this case (Figure 6.15), the distribution is not directly the normalized value itself, but rather the relation between the observer and the model's behaviour. With this distribution, it is possible to verify that, as the ammonia injection failure increases, less ammonia is injected, consequently lower NOx conversion, thus, the NOx value estimated by the ANN will be lower than that estimated by the observer, with the ratio tending to values greater than 1. The opposite happens for NH3, as lower levels of injection lead to lower levels of slip.

It is worth mentioning that the accuracy of the diagnosis will depend on the correct calibration of the upstream NOx SCR threshold (eq.6.3) and on the accuracy of the models themselves to estimate NOx and NH3 emissions, being these estimates impacted by the intrinsic error of the computational models, but also after a long period of time by the catalyst ageing.

6.5 Results and discussion

6.5.1 Real-time strategy application for constant failure in ammonia injection

Aiming to assess the capacity of the proposed strategy to track the level of the ammonia injection failure, the model was tested in 20 WLTC cycles in sequence, with different failure levels. In Figure 6.16, the upper part, the dark dashed line is the current level of the ammonia injection failure, and the red circles, the model estimation for the failure level at the end of the AWS.

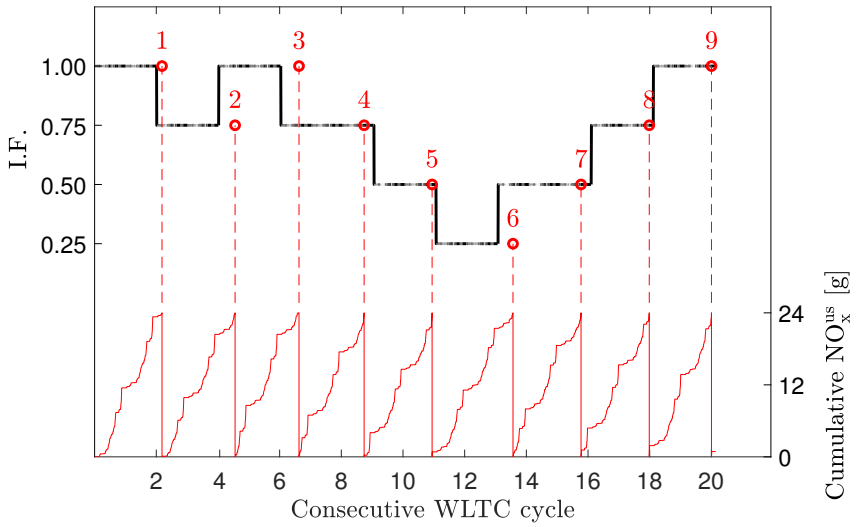

Figure 6.16: Actual level of the ammonia injection failure and estimate at the end of the accumulation window for 20 consecutive WLTC cycles.

As can be seen in Figure 6.16, at the end of each accumulation window, the model was able to estimate the level of error that the system was subjected to during the previous period. In the current case, to accumulate 24 g of NOx before the SCR catalyst, more than one complete WLTC cycle is needed, for this reason, the estimated failure level (red circles) represents the current failure level to which the system is mostly subjected during the accumulation window.

In Figure 6.17, it is possible to verify where each estimated point was placed in the two-dimensional plane.

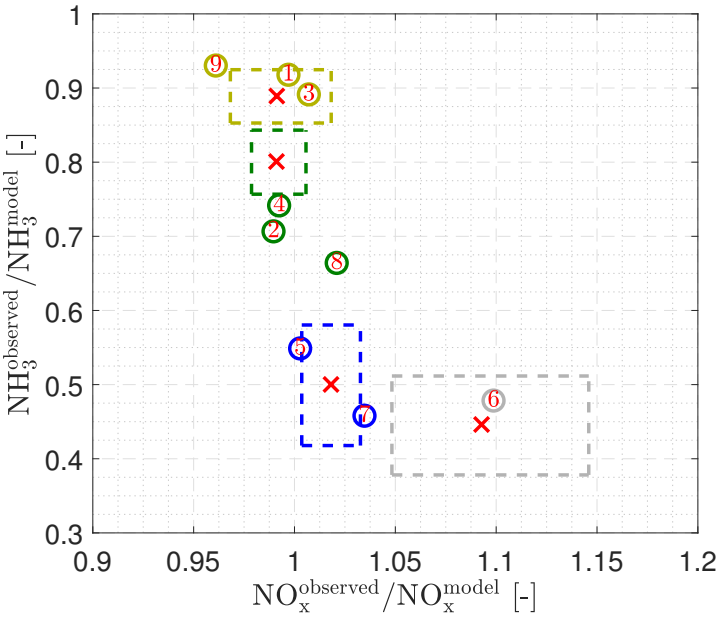

Figure 6.17: Estimated results of the ammonia injection failure level in the normal distribution graph of NOx and NH3 slip in a 24 g accumulation window.

As can be seen, not all the points were within the range of distributions but classifying the points as their closest clusters (eq.6.7) provides accurate results (red x).

$$\text{I.F.} = \text{argmin}_j \sqrt{\left(\frac{NO_x^{obs}}{NO_x^{model}} - C_j^{NO_x}\right)^2 + \left(\frac{NH_3^{obs}}{NH_3^{model}} - C_j^{NH_3}\right)^2}, \qquad (6.7)$$

where, j = $[0.25, 0.50, 0.75, 1.00]$ and C it is the centroid of each distribution.

6.5.2 Real-time strategy application for ammonia injection system degradation

The correction application in the degradation of the ammonia injection system was carried out in two steps: first, a merged cycle was performed, where no correction was made in the ammonia injection, this test was performed to validate the capacity of the proposed methodology in detecting the degradation of the ammonia injection system. In the second step, the same cycle was

carried out, and the correction was applied to the ammonia injection from the error level detected. It consists of increasing the demand of ammonia to compensate the injection error. This test was performed to assess the methodology's capacity to correct the injection failure.

In Figure 6.18, it is possible to see the ratio between the applied ammonia injection and the reference injection without failure for both cases: without correction (grey) and with the proposed correction (black). As the cycle evolves, injector degradation makes the injector factor decrease, while corrections lead to an increase in the injector factor after the fault diagnosis. The markers refer to the points at the end of the accumulation window, being the circles and the triangles, without and with correction of the ammonia injection, respectively.

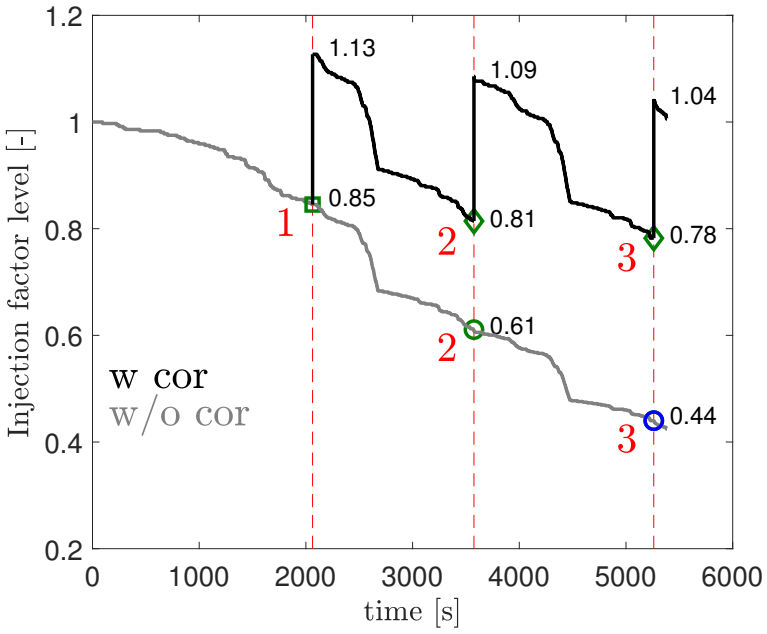

Figure 6.18: Injection factor level during a merged cycle and degradation of the ammonia injection system, with (dark line) and without (grey line) ammonia injection correction.

At the end of each accumulation window, the proposed strategy was able to detect and correct the level of ammonia injection, at the same time reducing the impact of system degradation. Of course, the correction is not able to keep the I.F. = 1 since, it requires some time (where degradation is evolving) for diagnosis, and both the model and observer have some error.

Since the strategy is aimed to correct the ammonia injection, failure levels

greater than 50% of the nominal injection (I.F. = 0.50) are not expected. Therefore, the NOx distribution is unnecessary, as it only distinguishes I.F. = 0.25 from I.F. = 0.50, as shown in Figure 6.15.

Figure 6.19 shows where each estimated point was placed at the end of each accumulation window in the NH3 distribution. As can be seen, for ammonia injection without correction, point 3 (the end of the complete cycle) has an error level of 50% of the nominal injection (I.F. = 0.50), while with the correction the error level remains 25% (I.F. = 0.75). Thus, the proposed methodology is able to reduce the degradation rate of the ammonia injection system.

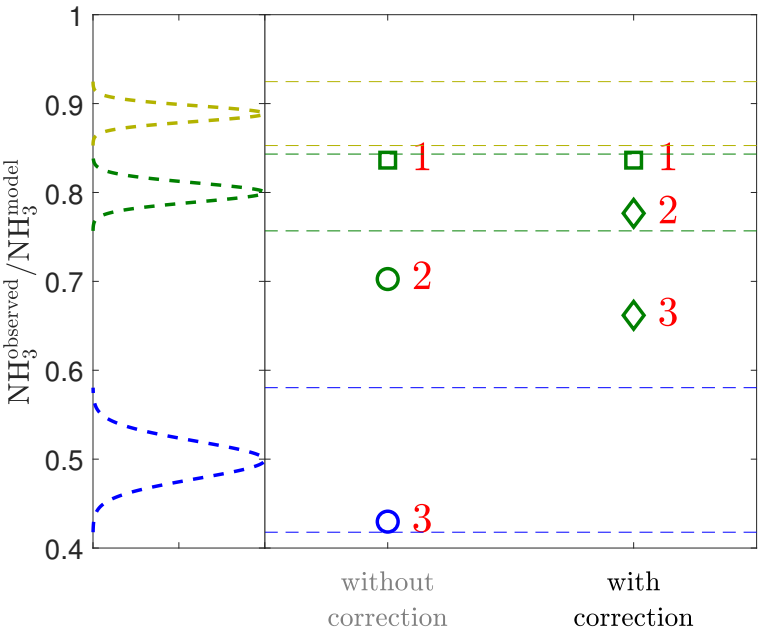

Figure 6.19: Estimated results of the level of failure in ammonia injection in terms of NH3 slip.

As results, Figure 6.20 to Figure 6.22 show the impact on NOx and NH3 emissions and injected ammonia. Dark lines and grey lines refer to the signals with and without correction in the ammonia injection signal, respectively, both performed in cycles with constant degradation of the injection system. While red lines represent the cycle caried out without degradation of the ammonia injection system.

Figure 6.20 shows the NOx slip emissions, as can be seen, when the ammonia injection is corrected it tends to similar levels as when there is no

injection failure, being slightly higher (5.35%). However, when compared to degradation of the ammonia injection system without correction, NOx emissions rise by 23.33%.

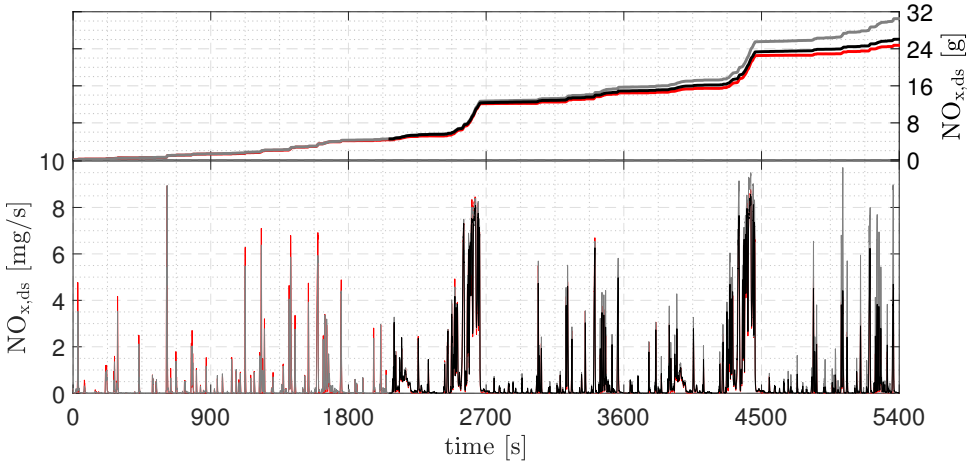

Figure 6.20: NOx slip with (dark line) and without (grey line) ammonia injection correction and NOx slip without ammonia injection failure (red line) during a merged cycle.

It is possible to verify that up to approximately 2700 s the NOx conversion level remains similar for all cases, even in the case of the injection system degradation without correction is about 70%, this is in line with the previous discussion (Figure 6.7), for injection failure levels around 75% the SCR catalyst is still capable of converting NOx with high efficiency, since the NOx conversion occurs by the amount of ammonia previously stored [11]. A higher difference starts to be appreciated around 3500 s, when the failure level is approximately 62%.

In terms of NH3 slip, as can be seen in Figure 6.21, there is a reduction in NH3 emissions for both cases, being 18.67% and 46.41% for tests with and without correction in the ammonia injection, respectively. This behaviour was already expected, since with the reduction of the amount of ammonia injected during the cycle, the catalyst load also decreases, consequently there is smaller slip. Note that this reduction in NH3 emissions is undesirable, as this behaviour leads to an increase in NOx, and appropriate strategies exist to reduce both contaminants simultaneously.

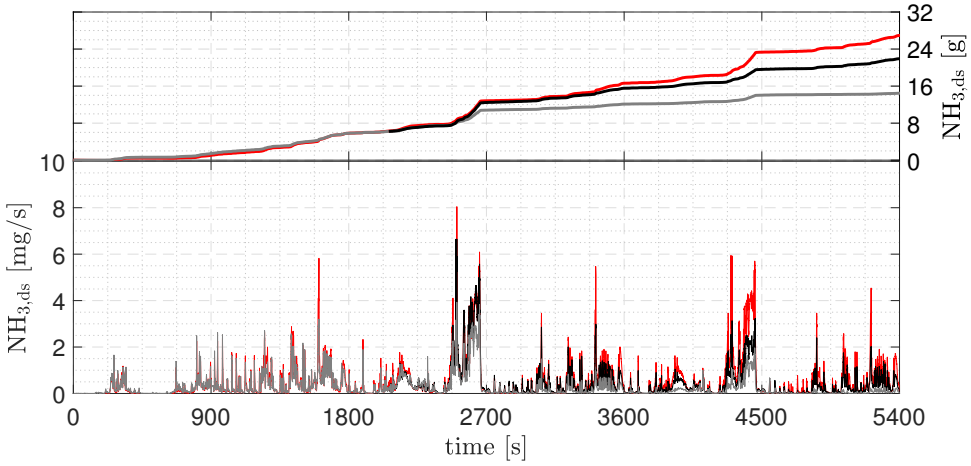

Figure 6.21: NH3 slip with (dark line) and without (grey line) ammonia injection correction and NH3 slip without ammonia injection failure (red line) during a merged cycle.

Regarding the total amount of ammonia injected during the cycle (Figure 6.22), the correction of ammonia injection reaches a similar level to the standard injection strategy, being slightly smaller (5.65%), and as expected, the level of ammonia injected when there is a degradation of the injection system without correction is considerably lower (27.83%).

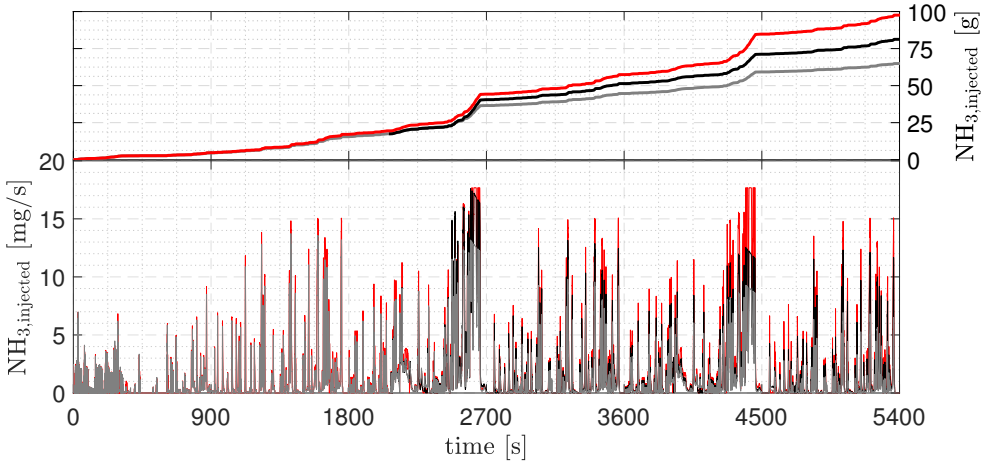

Figure 6.22: Ammonia injection with (dark line) and without (grey line) correction and ammonia injection without failure (red line) during a merged cycle.

As conclusion, the proposed model was able to detect and correct ammonia injection in all failure situations. Both in cases with constant failure in standard driving cycles, as well as in a degradation of the injection system in a merged cycle. Therefore, the proposed methodology through the use of a variable time window linked to a constant NOx threshold at the SCR input, can be applied to the most diverse cycles and engine operating conditions.

6.6 Emissions assessment under ammonia injection failure and catalyst ageing

An effective strategy to improve the emissions reduction is to increase the amount of ammonia injected, keeping the ammonia load inside the SCR catalyst high throughout the operation and adding an ASC to avoid ammonia slip, as well as, increasing the overall ATS NOx conversion efficiency [12], since the ASC also has the capacity to store ammonia and oxidize NOx [13]. The ammonia injection strategy with an SCR+ASC catalyst has two main points.

- The SCR catalyst keeps the ammonia coverage ratio (i.e., the ratio of the amount of ammonia stored in the catalyst to the maximum storage capacity [14]) as high as possible without exceeding a maximum ammonia slip threshold, this limit being higher for an SCR+ASC system than for one with only SCR.
- To avoid excessive ammonia slip in the atmosphere, the control of the ammonia load of the ASC catalyst becomes the main one, since the SCR catalyst works with a high ammonia load, or saturated [15].

However, this ATS composition has the same drawbacks presented in section 6.2, reduced NOx abatement capacity and increased NH3 slip due to ammonia injection failure and catalyst ageing. The importance of the correct detection of ammonia injection failure, as well as the ageing state of the catalyst can be seen in Figure 6.22. The markers represent the average emissions values measured by the FTIR during several WLTC cycles (diamond for aged ASC and circle to new one), the error bar refers to the minimum and maximum values of the performed cycles, while the red dashed lines represent the standard EURO VI-D limit for NOx emissions (0.08 g/km in a WLTC cycle) as well as the NH3 limit for heavy duty engines ($\sum_{i=1}^{n} \frac{NH_{3,i}^{slip}}{i} < 10$ ppm).

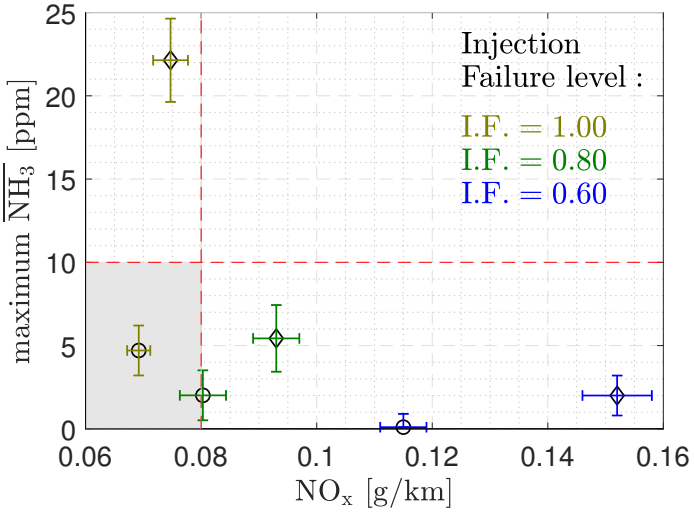

Figure 6.23: NOx and NH3 slip emissions over several WTLC cycles with different levels of ammonia injection failure (yellow – I.F.=1.00; green – I.F.=0.80; blue – I.F.=0.60) and catalyst ageing state (diamond – aged catalyst; circle – new catalyst). The markers represent the average values of the performed cycles, while the error bar the minimum and maximum values. The grey area refers to the allowed emissions levels according to EURO VI-D (NOx for light duty and NH3 for heavy duty engines.

As can be seen in Figure 6.23, the new catalyst operating without ammonia injection failure can achieve the current standards, with I.F.=0.80 the ATS operates at the NOx limit boundary. However, for I.F.=0.60 or operating with an aged ASC catalyst the limits are exceeded. The correct detection may allow the control system to correct the ammonia injection rate or warn about the need for catalyst replacement and/or update the ammonia injection emissions control strategy.

In this part of the work, three set of tests were carried out. Firstly, several cycles as, engine full map, steady-state condition, WLTC and 2RTS were performed with the new ASC catalyst and the standard ammonia injection to develop the ANN model. Followed by the performance of five WLTC cycles for each ASC catalyst (new, partial aged and aged) and three different ammonia injection strategies, these tests were performed to develop both strategies, detection of the catalyst ageing and ammonia failure injection. Finally, a merged cycle between WTLC and 2RTS was used to validate the proposed methodology. Regarding the amount of ammonia injected, tests were carried out with two constant levels of failure (I.F.=[0.80; 0.60]) and with the standard

injection (I.F.=1.00), as well as the 2RTS cycle with continuous reduction of the injection level.

6.7 Proposed methodology extended to the ASC catalyst and simultaneous diagnosis of ammonia injection failure and catalyst ageing

Applying the same methodology used in section 6.3, but considering the NOx and NH3 downstream of the ASC catalyst instead of the SCR, as well as extending the methodology to a new and an aged catalyst and both operating with and without ammonia injection failure. After updating the threshold value ($NO_{x,us}^{thr}$) it is possible to group the results into different clusters not only in terms of ammonia injection failure, but also by catalyst ageing as shown in Figure 6.24.

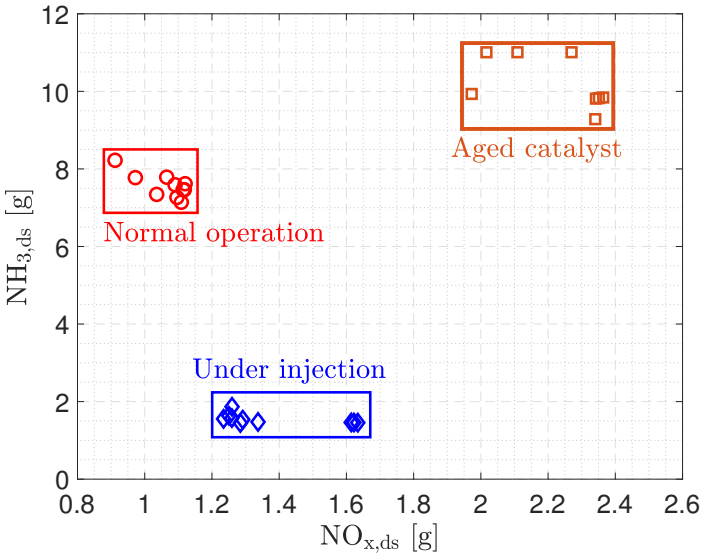

Figure 6.24: Distribution of accumulated slip value of NOx and NH3 under three ATS operating conditions, with $NO_{x,us}^{thr}$=32 g. Red cluster: normal operation. Dark orange cluster: aged catalyst. Blue cluster: under ammonia injection.

The approach was extended to models, as presented in subsection 6.4.1. Therefore, the ANN is assumed as the representative model of the estimated

emissions of the system operating without failure and unaged, while the EKF represent the actual emissions levels.

Note that in this case the ANN remains the representation of the ATS operating under normal conditions, as it depends on the feedback signal from the ammonia injector, and its error in the emission estimation increases with increasing injector failure, as well as with catalyst ageing.

In this sense, as can be seen in Figure 6.25, it is possible to create a ratio between the current value of emissions (NOx and NH3) and the corresponding levels if the ATS is operating properly according to the ANN model. Thus, creating probability zones in the two-dimensional NOx-NH3 plane to differentiate the operating states of the ATS. The impact of injection failure and catalyst ageing, with the metrics proposed follow almost orthogonal directions (Figure 6.24), then promoting the failure isolation. Assuming a linear impact of injection fault and ageing on NOx and NH3 slip, Figure 6.25 allows to identify the failure by means of the ratio between observed and modelled emissions. In this sense, the colormap in Figure 6.25 represents the degradation of the ammonia injection system, while the contour lines the catalyst ageing.

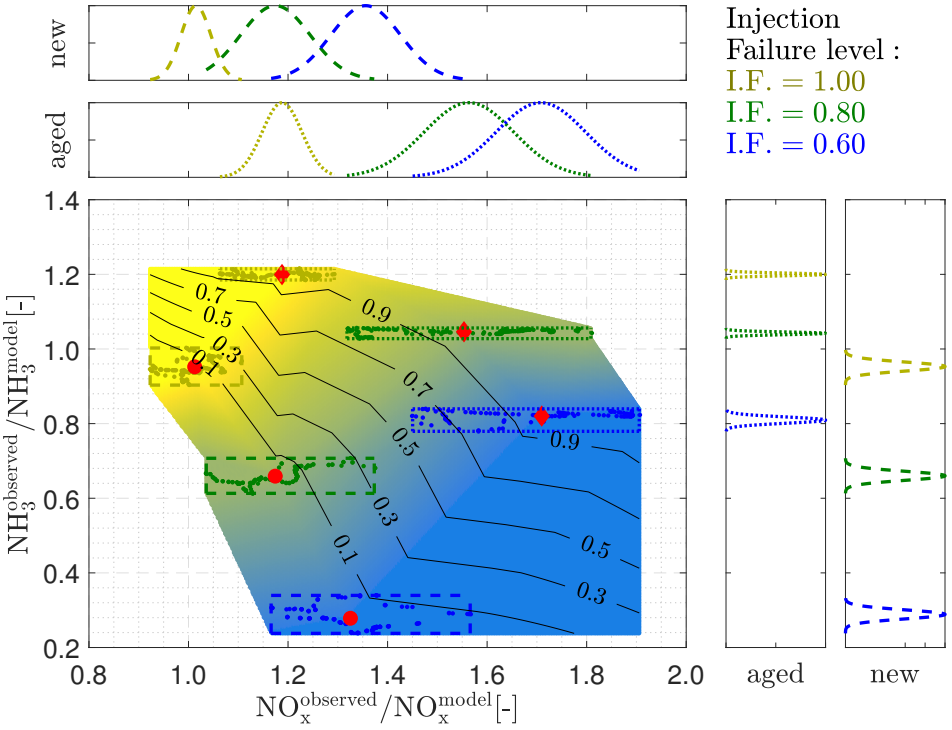

Figure 6.25: Distribution of NOx and NH3 slip for different levels of ammonia injection failure (colourmap) and catalyst ageing (contour lines). Yellow represents the ATS operating under normal ammonia injection conditions (I.F.=1.00), green low or partial injection failure (I.F.=0.80) and blue high or aggressive failure (I.F.=0.60). The dashed line is related to the new catalyst (contour line equal 0), while the dotted line to the aged one (contour line equal 1). Points within the distribution area refer to the values found at the end of each AWS, and the centroid of these points is represented by red markers (diamond – aged catalyst; circle – new catalyst).

As the ammonia injection failure increases, less ammonia is injected, consequently lower NOx conversion, thus, the NOx value estimated by the ANN will be lower than that estimated by the observer, with the ratio tending to values greater than 1. The opposite happens for NH3, as lower levels of injection lead to lower levels of slip. In the case of the catalyst ageing, both pollutants are moved upwards, since ageing leads to lower NOx conversion rates and ammonia storage capacity as well.

Note that the differentiation of the ammonia injection failure level can be done only by observing the distribution in terms of NH3 (y axis), however it

is necessary to combine it with the NOx distribution (x axis) to detect the level of catalyst ageing. Also, note that according to the contour lines and distribution area, the proposed strategy has a maximum ability to differentiate ageing levels of 30%.

6.7.1 Real-time diagnosis for constant ammonia injection failure

To accesses the capacity of the proposed methodology in detect the ammonia injection failure level and differentiate the catalyst ageing state, the strategy was applied over several consecutive WLTC cycles. Figure 6.26 shows the current ageing level of the catalyst (upper plot) and the ammonia injection failure level (Bottom plot: dotted line - aged catalyst, dashed line – new catalyst), and the estimated by the model at the end of the AWS, for cycles performed with an aged (red diamond) and new (red circle) ASC catalyst.

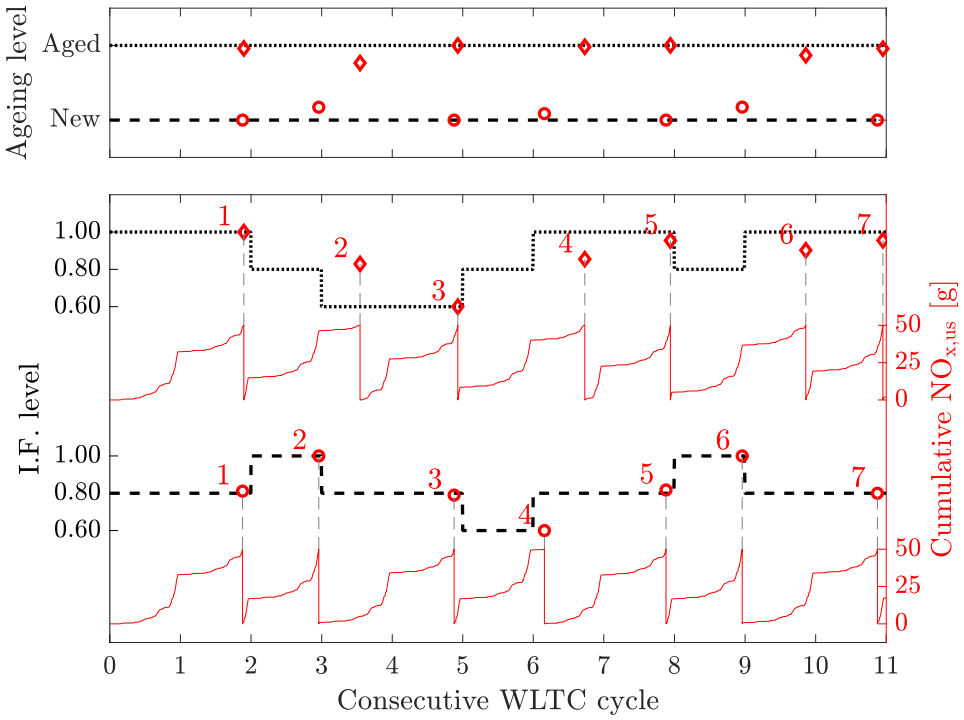

Figure 6.26: Upper plot: Current ageing state of the ASC catalyst and estimated at the end of AWS (markers: diamond – aged; circle – new) over several consecutive WLTC cycles. Bottom plot: Current ammonia injection failure level and estimated at the end of AWS, for an aged (dotted line) and new (dashed line) ASC catalyst. Right axis: NOx accumulated upstream of the SCR catalyst.

As can be seen in Figure 6.26, at the end of each AWS the model was capable of detecting the current failure level with high accuracy, as well as the catalyst ageing state. Note that AWS is linked to NOx accumulated at the SCR catalyst inlet and not to cycle duration, so in some cases the model is subjected to two different levels of failure during the same AWS. It is important to point out, the methodology evaluates the failure level to which the system is subjected throughout the AWS, this means that the failure level estimated by the model will be according to the average failure during AWS and not the current level when the AWS ends.

Figure 6.27 shows where each point was placed on the two-dimensional plane. In the case of the aged catalyst, points 2, 4 and 6 are not within the fault detection zones. Looking at point 4 as an example, during approximately

41% of AWS the model was subjected to a I.F.=1.00, moving the point out of the low-failure zone (I.F.=0.80) towards the none-failure zone (I.F.=1.00). This behaviour elucidates the sensitivity of the model to detect transient failure conditions.

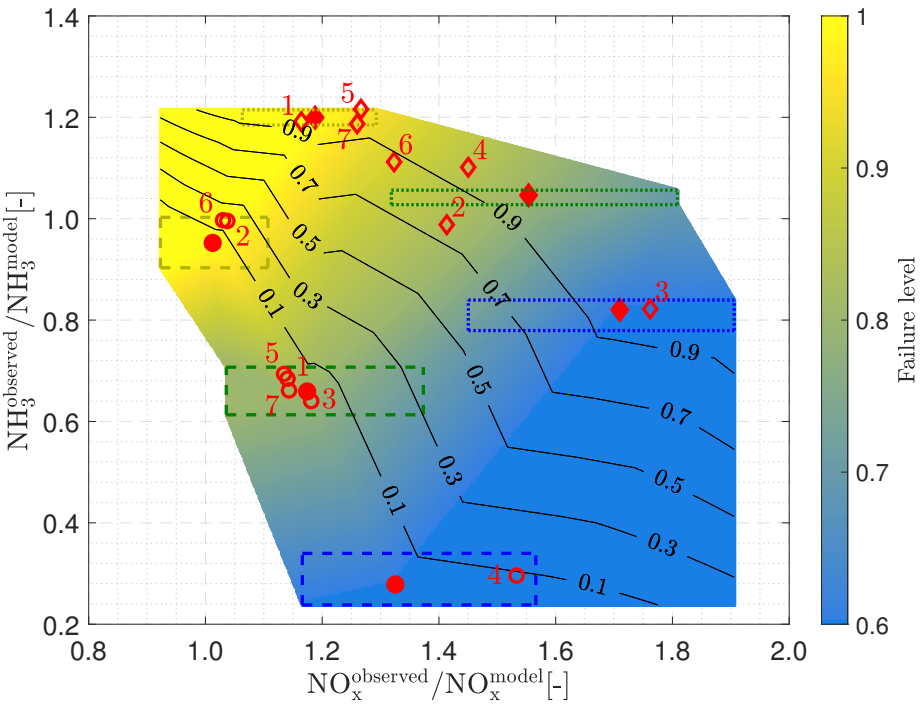

Figure 6.27: Results estimated by the model for different levels of constant ammonia injection failure and catalyst ageing in the two-dimensional plane (markers: diamond – aged catalyst; circle – new catalyst).

Table 6.2 presents the current values of ammonia injection failure and catalyst ageing state, as well as the model estimate at the end of AWS. Note that at the current failure level, the value presented is the weighted average of the failure to which the system was subjected during AWS.

Table 6.2: Comparison between the current value and estimated by the model at the end of the AWS in terms of ammonia injection failure level and ageing state of the catalyst. The values represent the points shown in Figure 6.26.

	I.F.			Ageing level		
AWS	Current	Estimated	Error	Current	Estimated	Error
1 ♦	1.00	1.00	0.0%		96.0%	4.0%
2 ♦	0.75	0.83	-8.4%		76.5%	23.5%
3 ♦	0.60	0.60	0.0%		100.0%	0.0%
4 ♦	0.87	0.86	1.3%	aged = 1	98.2%	1.8%
5 ♦	1.00	0.96	4.0%		100.0%	0.0%
6 ♦	0.90	0.90	-0.4%		86.9%	13.1%
7 ♦	1.00	0.96	4.0%		95.7%	4.3%
1 ●	0.80	0.81	-1.0%		0.0%	0.0%
2 ●	0.98	1.00	-2.1%		17.2%	-17.2%
3 ●	0.80	0.79	1.0%		0.0%	0.0%
4 ●	0.64	0.60	4.4%	new = 0	8.6%	-8.6%
5 ●	0.80	0.82	-2.0%		0.0%	0.0%
6 ●	0.98	1.00	-2.2%		17.4%	-17.4%
7 ●	0.80	0.80	0.4%		0.0%	0.0%

6.7.2 Real-time diagnosis for ammonia injection degradation

To validate the proposed approach, the model was tested with the aged catalyst in a merged cycle with continuous degradation of the ammonia injection system. Figure 6.28 shows the performance of two cycles with different degradation rates. In the bottom plot, the upper line represents a cycle carried out with slower degradation, while the lower line shows a cycle performed with a more aggressive degradation.

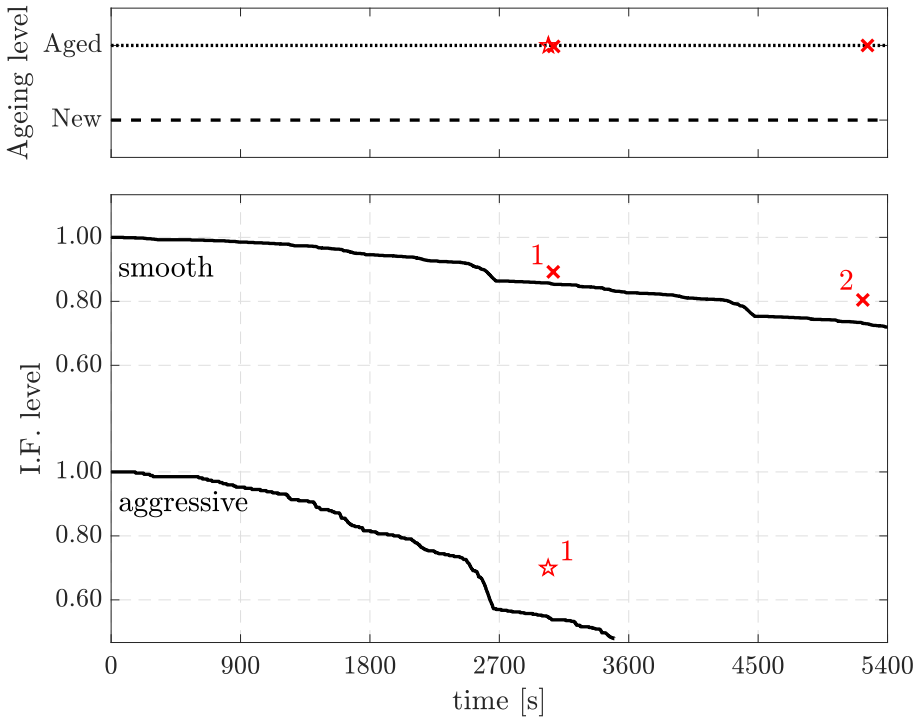

Figure 6.28: Upper plot: Current ageing state of the ASC catalyst and estimated at the end of AWS over two merged cycles with continuous degradation of the ammonia injection system (x for smooth degradation cycle and pentagram for aggressive). Bottom plot: Current level of ammonia injection failure (continuous line) and the level estimated by the model at the end of AWS (markers).

As can be seen in Figure 6.28, the model is able to accurately estimate the level of catalyst ageing, however, it presents an apparent delay in detecting the injection failure. The main reason is because the degradation is continuous and considerably fast, subjecting the model to a large failure interval for the same AWS. As mentioned before, the model estimates the level of failure based on all the information acquired during the AWS, consequently, the greater the degradation gradient, the greater the error in the estimate.

Note that in any case, the tests shown in Figure 6.28 are subject to a degradation rate much higher than what can be presumably found in real driving operation, when it takes several years to degrade the injector, as comment by Kupper et al. [16] information uncertainty (such as wrong feedback information) is increased over a mid to long time horizon, therefore,

the real degradation behaviour of the ammonia injection system would be less abrupt than the smooth degradation applied to the merged cycle. Thus, avoiding the delayed detection of the failure level by the model.

Figure 6.29 shows where each estimated point was placed in the two-dimensional plane, and Table 6.3 the current values and those estimated by the model in relation to injection failure and catalyst ageing state.

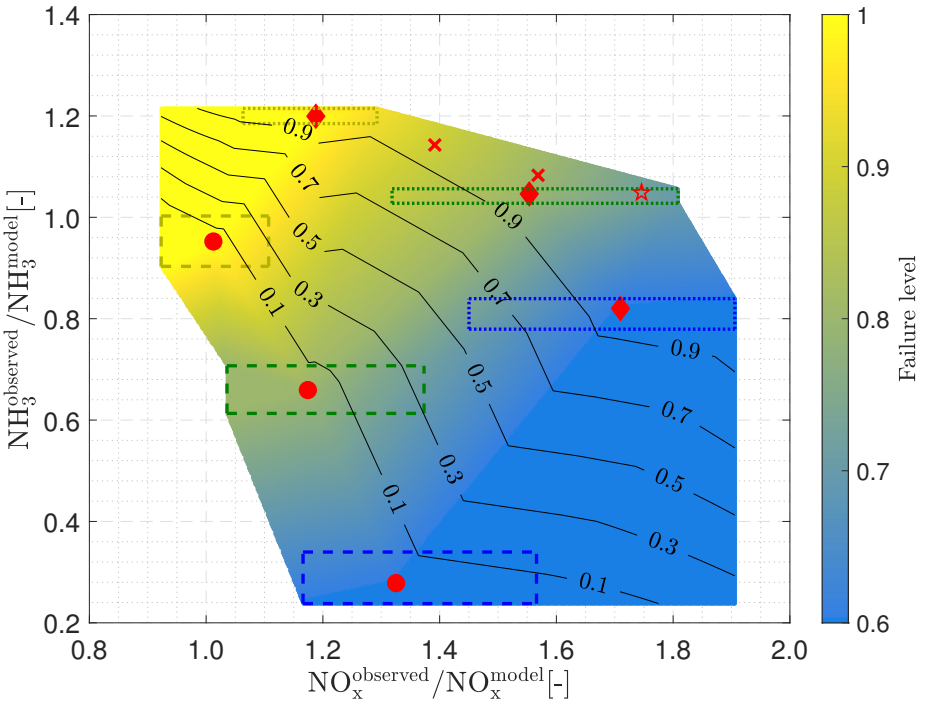

Figure 6.29: Results estimated by the model on the two-dimensional failure plane of two mixed cycles performed on an aged catalyst with continuous degradation of the ammonia injection system (diamond - centroids of the aged catalyst clusters; circle – centroids of the new catalyst clusters; x - smooth degradation cycle; pentagram - aggressive degradation cycle).

Table 6.3: Comparison between the current value and estimated by the model at the end of the AWS in terms of ammonia injection failure level and ageing state of the catalyst. The values represent the points shown in Figure 6.28.

I.F.				Ageing level		
AWS	Current	Estimated	Error	Current	Estimated	Error
1 x	0.86	0.89	-3.0%	aged = 1	98.7%	1.3%
2 x	0.75	0.80	-5.0%		100.0%	0.0%
1 ★	0.56	0.73	-17.0%	aged = 1	100.0%	0.0%

6.7.3 Unknown ageing state diagnosis

In order to assess the catalyst ageing diagnosis capabilities of the proposed method, several WLTC cycles with different levels of ammonia injection failure (I.F.=[1.00; 0.80; 0.60]) operating with an intermediate ageing state catalyst were performed. In Figure 6.30, the square markers represent the average failure level estimated by the models, and the error bar the minimum and maximum values obtained.

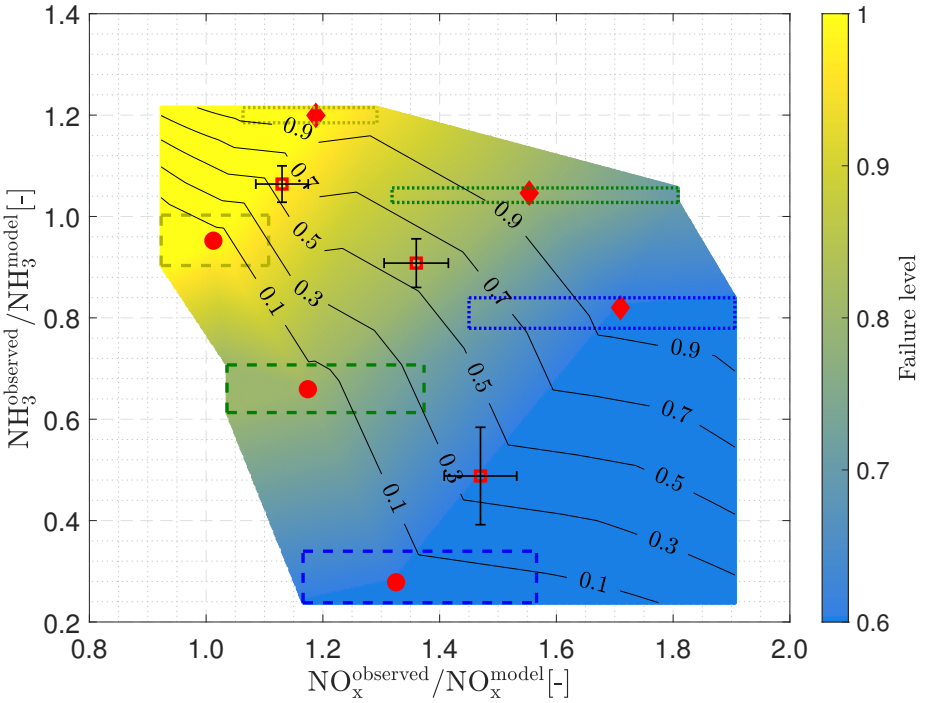

Figure 6.30: Estimated model results for different levels of ammonia injection failure in WLTC cycles operating with a catalyst of unknown ageing level. The square markers represent the average values of the performed cycles, while the error bar the minimum and maximum values. The diamonds represent the centroids of the aged catalyst clusters and the circles the centroids of the new catalyst clusters.

As can be seen, the average catalyst ageing values estimated by the model for the cases I.F.=1.00 and 0.80 are very similar, 57.5% and 58.3%, respectively. However, even though the estimated average value for I.F.=0.60 is 38.0%, the test sets have the same level of ageing when considering the maximum and minimum values obtained. Regarding the estimated injection failure level, the model was very accurate, with values of 0.98, 0.82 and 0.60 for I.F. equal to 1.00, 0.80 and 0.60, respectively.

As results, the proposed model was able to detect at the same time the failure of ammonia injection and the ageing of the catalyst, both in the WLTC cycles with constant failure and in the merged cycle with degradation of the injection system. As well as detect the injection failure and ATS state in a catalyst with unknown ageing level.

References

[1] Lu Bingxu, Jin Qijie, Chu Lin, Pan Youchun, Tao Xingjun, Yang Lei and Shen Yuesong. "Ammonia storage/release characteristics of CeSnWBaOx/TiO2 catalyst in solving the problem of ammonia slip". *Process Safety and Environmental Protection*, Vol. 138, pp. 67–75, jun 2020. (cited in p. 110)

[2] Xu Guangyan, Shan Wenpo, Yu Yunbo, Shan Yulong, Wu Xiaodong, Wu Ye, Zhang Shaojun, He Liqiang, Shuai Shijin, Pang Hailong, Jiang Xuefeng, Zhang Heng, Guo Lei, Wang Shufen, Xiao Feng-Shou, Meng Xiangju, Wu Feng, Yao Dongwei, Ding Yan, Yin Hang and He Hong. "Advances in emission control of diesel vehicles in China". *Journal of Environmental Sciences*, dec 2021. (cited in p. 111)

[3] Cheng Ying, He Liqiang, He Weinan, Zhao Pei, Wang Pinxi, Zhao Jin, Zhang Kesong and Zhang Shaojun. "Evaluating on-board sensing-based nitrogen oxides (NOX) emissions from a heavy-duty diesel truck in China". *Atmospheric Environment*, Vol. 216, nov 2019. (cited in p. 111)

[4] Hu Jie, Zeng Jiawei and Wei Li. "Failure diagnosis and tolerant control method for hydrothermally aged SCR system by utilizing EKF observer and MRAC controller". *Energy*, Vol. 156, pp. 103–121, aug 2018. (cited in pp. 26 and 111)

[5] Dhillon Pritpal S., Harold Michael P., Wang Di, Kumar Ashok and Joshi Saurabh Y. "Enhanced transport in washcoated monoliths: Application to selective lean NOx reduction and ammonia oxidation". *Chemical Engineering Journal*, Vol. 377 n^o August, dec 2019. (cited in pp. 26, 84, and 111)

[6] Börnhorst M. and Deutschmann O. "Advances and challenges of ammonia delivery by urea-water sprays in SCR systems". *Progress in Energy and Combustion Science*, Vol. 87 n^o August, nov 2021. (cited in p. 111)

[7] Donkers M.C.F., Schijndel J Van, Heemels W.P.M.H. and Willems F.P.T. "Optimal control for integrated emission management in diesel engines". *Control Engineering Practice*, Vol. 61, pp. 206–216, apr 2017. (cited in p. 119)

[8] Rajesh Chundru Venkata, Parker Gordon G. and Johnson John H. "Development of a Kalman filter estimator for simulation and controlof NO x and PM in a SCR catalyston a DPF". *International Journal of Engine Research*, Vol. 22 n^o 8, pp. 2407–2421, aug 2021. (cited in pp. 97 and 119)

[9] Mora J., Willems F., Seykens X. and Guardiola C. "An OBD strategy to estimate SCR ageing and detect urea injection faults". *IFAC-PapersOnLine*, Vol. 51 n^o 31, pp. 369–376, 2018. (cited in pp. 26, 119, and 125)

[10] Wang Yue-Yun, Sun Yu, Chang Chen-Fang and Hu Yiran. "Model-Based Fault Detection and Fault-Tolerant Control of SCR Urea Injection Systems". *IEEE Transactions on Vehicular Technology*, Vol. 65 n^o 6, pp. 4645–4654, jun 2016. (cited in pp. 27 and 125)

[11] Pla Benjamin, Bares Pau, Sanchis Enrique and Aronis André. "Ammonia injection optimization for selective catalytic reduction aftertreatment systems". *International Journal of Engine Research*, Vol. 22 n^o 7, pp. 2169–2179, jul 2021. (cited in pp. 20, 30, and 133)

[12] Guan Bin, Zhan Reggie, Lin He and Huang Zhen. "Review of state of the art technologies of selective catalytic reduction of NOx from diesel engine exhaust". *Applied Thermal Engineering*, Vol. 66 n^o 1-2, pp. 395–414, may 2014. (cited in pp. 10, 70, 95, and 135)

[13] Zhang Yunhua, Lou Diming, Tan Piqiang, Hu Zhiyuan and Fang Liang. "Effect of SCR downsizing and ammonia slip catalyst coating on the emissions from a heavy-duty diesel engine". *Energy Reports*, Vol. 8, pp. 749–757, nov 2022. (cited in pp. 10 and 135)

[14] Yang Shichun, Feng Song, Sun Kangfeng, Wang Shuai and Cao Yaoguang. "Square-root unscented Kalman filter for ammonia coverage ratio and input ammonia estimations in diesel-engine urea-SCR system". *ISA Transactions*, Vol. 96, pp. 299–308, jan 2020. (cited in pp. 84 and 135)

[15] Shiyu Liu, Boyuan Wang, Zexian Guo, Buyu Wang, Zhaohuan Zhang, Xiao Ma, Chen-Teng Chang, Peng Wang, Xin He, Xingyu Sun and Shijin Shuai. "Experimental investigation of urea injection strategy for close-coupled SCR aftertreatment system to meet ultra-low NO emission regulation". *Applied Thermal Engineering*, Vol. 205, mar 2022. (cited in p. 135)

[16] Kupper Frank, Mentink Paul, Avramis Nikos, Meima Niels, Lazovik Elena, Wilkins Steven and Willems Frank. "Towards Self-Learning Energy Management for Optimal PHEV Operation Around Zero Emission Zones". In *SAE Technical Papers*, number 2022, pp. 1–13, mar 2022. (cited in p. 144)

Chapter 7

Optimisation of dynamic systems

The important thing in science is not so much to obtain new facts as to discover new ways of thinking about them.

— William Lawrence Bragg

Contents

7.1 Introduction

There are several ways to improve emission abatement. Usually through system diagnosis, ensuring that the developed strategies work properly or

applying some kind of technique that enhances the system's performance. As described in Chapter 2, one way to improve the performance of the ATS is via the control system, which in turn has two main addressing paths:

- On-line optimisation: aims to control the system in real-time applications. In this type of approach the decisions made by the control system are updated as the data comes in, making the applied strategy able to adapt as the system evolves; however the time constraint is a major drawback, since complex and accurate models require higher computational cost [1, 2].
- Off-line optimisation: aims to achieve the highest system performance, usually used to design a control strategy or as a benchmark approach. In off-line optimisation only static dataset is available; therefore different inputs can lead the system to mistaken decisions. The great advantage is the possibility of using complex systems with high accuracy since the time cost is of less relevance [3, 4].

In the current thesis both approaches have been implemented. Firstly a benchmark off-line optimisation approach that uses anticipated knowledge of the driving cycle to achieve maximum system capability to abate NOx with minimum NH3 consumption. Secondly, real-time optimisation through MPC technique aiming at maximum NOx reduction with NH3 slip downstream of ASC catalyst below a pre-set threshold.

The identification of the control variables is a fundamental point in the optimisation of dynamic systems. Looking at zeolite-based catalysts, their behaviour is governed by the ammonia coverage ratio (ACR), which in turn is basically determined by the dynamics of the exhaust gases, the catalyst temperature and the amount of ammonia injected. As the NOx reduction efficiency and the NH3 slip are directly linked to the ACR level inside the catalyst, a suitable optimisation approach is to use the ammonia injection strategy to improve the control of the ACR aiming to reduce pollutant emission as well as the ammonia consumption by the system.

As described, the control approach employed has a significant impact on how well a particular design performs, as the SCR is a complex dynamic system interacting with other systems and phenomena in the ICE. Moreover, it may be found that the control strategy or even calibration with good performance for a given SCR may provide negative outcomes with a different design. In this sense, it is useful to have a fair basis for comparison of the design and controls of the SCR. Advances in computation capabilities made optimal control theory attractive to optimise a complex dynamic system. The Optimal Control theory was introduced by Lev Pontryagin et al. and Richard

Bellman, and a more detailed explanation of the subject can be found in their work [5–7]. Optimal Control theory is a model-based control approach, where different mathematical methods are used to calculate the controls that should be applied to a system in order to minimise a predefined cost index. Therefore, it is a suitable tool to provide a fair basis for comparison since it will lead to the best possible performance of any SCR assessed.

7.2 Optimal control problem

Briefly, an OCP is a mathematical approach that consists in finding the trajectories of the control variables of a dynamic system such that the operational cost is minimized [8, 9]. The cost is the value that defines the magnitude to be optimised, which can be in terms of energy, economy, time, among others. Therefore, the trajectory is optimal when the cost is minimal. The cost function (J) can be defined as a function of the trajectory of the system states (x) and control variables (u) that minimises the cost function over the control horizon (0 to τ).

$$\mathrm{J} = \min_{\mathrm{u}} \int_0^{\tau} \mathrm{L}(\mathrm{x}, \mathrm{u})\mathrm{dt} + \mathrm{V}(\mathrm{x}(\tau)), \tag{7.1}$$

where L is the Lagrangian function and represents the operational cost at each time step. and $\mathrm{V}(\mathrm{x}(\tau))$ is an additional cost if a defined end state is not reached, this penalisation may or may not be included. Regarding the system states they are governed by ordinary differential equations (ODEs):

$$\dot{\mathrm{x}} = \mathrm{f}(\mathrm{x},\mathrm{u}), \tag{7.2}$$

Usually the systems are subject to boundary conditions and constraints, such as:

$$\text{Initial state} : \mathrm{x}(0) = \mathrm{x}_0, \tag{7.3}$$

$$\text{Boundaries constraints} : [\mathrm{x}\ \mathrm{u}]_{\min} \leqslant [\mathrm{x}\ \mathrm{u}] \leqslant [\mathrm{x}\ \mathrm{u}]_{\max}, \tag{7.4}$$

$$\text{Path constraints} : \mathrm{c}(\mathrm{x}, \mathrm{u}) \leqslant 0, \tag{7.5}$$

$$\text{Integral constraints} : \int_0^{\tau} \mathrm{q}(\mathrm{x}, \mathrm{u})\mathrm{dt} \leqslant 0, \tag{7.6}$$

The set of eq.7.1 to 7.6 define an Optimal Control Problem (OCP).

7.3 Mathematical methods for dynamic optimisation

OCP is fundamentally a time domain solving problem. A straightforward approach is to solve it analytically. Although it can be possible in some cases, OCPs usually contemplate complex models with several restrictions, which are not feasible for an analytical approach. However, they can be approached numerically, taking advantage of the high calculation capacity of computers in detriment of discretizing the time variables.

7.3.1 Dynamic programming

Dynamic Programming (DP) is a numerical method that has as a fundamental idea to divide the complete problem into sub-problems simpler to be solved [10]. According to the principle of optimality described by Bellman [11], the set of optimal sub-problems is a global optimum; therefore, the DP theory seeks to find at each time interval the best trajectory of the control variable (u) that minimises the cost function, and that in the end will lead to the best global trajectory. The DP solution is according to the following equation.

$$\min_{\mathrm{u}}\{\int_{\mathrm{t_i}}^{\mathrm{t_{i+1}}} \mathrm{L(x,u,t)dt} + \mathcal{J}(\mathrm{x},\mathrm{t_{i+1}})\}, \tag{7.7}$$

where $\mathcal{J}$ refers to the *cost-to-go*, i.e., the accumulated cost when executing the optimal controller. In this way, DP pursues the cheapest trajectory from each interval by recursively solving the optimal one-step cost ($\mathrm{L(x,u,t)dt}$) plus *cost-to-go* ($\mathcal{J}(\mathrm{x},\mathrm{t_{i+1}})$) from each step to the goal.

An important point in solving DP is the need for discretization of the system states and variables. The discretization of the system constraints the trajectories to a finite set. Consequently, the constraints can lead the solution of the problem outside the discretised grid. In this case, the constraints must be within an acceptance bound or the grid density must be increased. Ultimately, it is a trade-off between solving accuracy and computational cost [12].

The previous discussion leads to the main drawback in the DP optimisation, the so-called *curse of dimensionality* coined by Richard Bellman in 1957 [11], it refers to the increase in the total number of elements that must be allocated in memory (n) for a generic DP problem with the increase in the number of system states (N_{x}), control variables (N_{u}) and discretization of the prediction horizon (n_{t}), which can be calculated from eq.7.8.

$$n = (n_{\mathrm{t}}N_{\mathrm{u}} + 1)n_{\mathrm{x}}^{N_{\mathrm{x}}}, \tag{7.8}$$

where, n_x is the number of elements in which each state is discretised. Note that the number of elements to be allocated grows linearly with the number of controllers but as a power with the number of states. Moreover, in terms of computational cost it is better to increase the discretization of the states than to increase their number. Furthermore, the current processing capacity of desktop computers presents a limit to the number of model states, control variables and their discretization. Thus, these drawbacks must be taken into consideration during the development of dynamic system models.

7.3.2 Direct methods

Direct Method (DM) is part of the mathematical approaches to solve an OCP. It basically consists in transcribing a dynamic problem into a huge static problem, by discretizing the control variables into a finite succession of values approachable as a non-linear programming (NLP) problem. One of the advantages of using DM is that there are commercial and freeware NLP solvers that make use of advanced and efficient state-of-the-art algorithms to find an optimal solution [13, 14]. This approach allows dealing with large scale problems featuring multiple states and controllers with reduced computational effort, as this approach is not affected by the *curse of dimensionality*.

Among the different methods to transcribe a continuous OCP into a finite NLP, Euler's collocation method is used since it is a first-order numerical method and thus only two terms are needed to approximate an ordinary differential equation then contributing to the sparsity of the problem matrix. As a main disadvantage this method does not guarantee convergence to the global optimum, since the minimum achieved by the solver depends on the initial seed, and in some cases, it may converge to the local minimum. Anyway, a global optimum is considerably difficult to guarantee, even more for highly non-linear systems.

As a global overview, the DM approach is used when it is desired to optimise a complex and heavy system, while DP is usually preferred for a complex discrete system with low number of states and controllers. A summary of the characteristics of both methods can be found in Table 7.1.

Table 7.1: Comparison of the main characteristics of each OCP method.

	DP	DM
Computationally cheap		●
Complex problems	●	●
Large # of x,u		●
Discrete systems	●	
State constraints	●	●
Global optimum	●	
Derivative-free	●	
Discretising-free		●

7.4 Off-line Optimisation

Regarding the computational model, although it is necessary to keep it simple, the complexity of the model must be able to reproduce the behaviour of the ATS in dynamic applications. In this way, to apply the off-line optimisation of the SCR catalyst it was used the zero-dimensional model presented in Chapter 5.2.

The problem is addressed by aiming to find the optimal ammonia injection profile that minimises its consumption in a given driving cycle with NOx emission constraints. In particular, the problem can be mathematically formulated as:

$$\min\{\int_0^\tau \dot{m}_{NH_{3,injected}}(u,x,w)dt\}, \tag{7.9}$$

where u is the control variable, x is the vector of state variables (states of the SCR model described in Chapter 5.2, eq.5.8-5.12), and w is the vector of disturbance variables (mass flow, temperature, and concentrations at the SCR inlet).

$$u = [NH_{3,injected}] \tag{7.10a}$$
$$x = [NO_{ds}, NO_{2,ds}, NH_{3,ds}, \theta_{NH_3}] \tag{7.10b}$$
$$w = [\dot{m}_{exh}, T_{SCR}, NO_{us}, NO_{2,us}] \tag{7.10c}$$

The limitations in the SCR and injection system can be included in the optimisation problem as constraints in the states and controls respectively.

$$0 \leqslant [\mathrm{NH_{3,injected}}] \leqslant 525 \text{ kg/h}, \tag{7.11a}$$
$$0 \leqslant [\mathrm{NO_{ds}}, \mathrm{NO_{2,ds}}] \leqslant 1850 \text{ ppm}, \tag{7.11b}$$
$$0 \leqslant [\mathrm{NH_{3,ds}}] \leqslant 1100 \text{ ppm}, \tag{7.11c}$$
$$0 \leqslant [\theta_{\mathrm{NH_3}}] \leqslant 1, \tag{7.11d}$$

The NOx emission limit can be included in the OCP formulation as an integral constraint

$$\int_0^{\tau} \dot{\mathrm{m}}_{\mathrm{NO_{x,ds}}}(\mathrm{u,x,w})\mathrm{dt} \leqslant \bar{\mathrm{m}}_{\mathrm{NO_{x,ds}}}, \tag{7.12}$$

where $\bar{\mathrm{m}}_{\mathrm{NO_{x,ds}}}$ is the NOx emission limit.

Regarding the optimisation algorithm employed, the OCP described previously has four states ($\mathrm{NO_{ds}}, \mathrm{NO_{2,ds}}, \mathrm{NH_{3,ds}}, \theta_{\mathrm{NH_3}}$) and a single control action ($\mathrm{NH_{3,injected}}$). The model complexity and the relatively high number of states (4) suggest the use of a DM implementation instead of other alternatives such as DP or Pontryagin's minimum principle.

Figure 7.1 shows the Jacobian matrix of the addressed OCP, where it can be observed that despite being considerably large (201829 x 252284), only few elements are non-zero, in particular 0.0021% of the matrix elements.

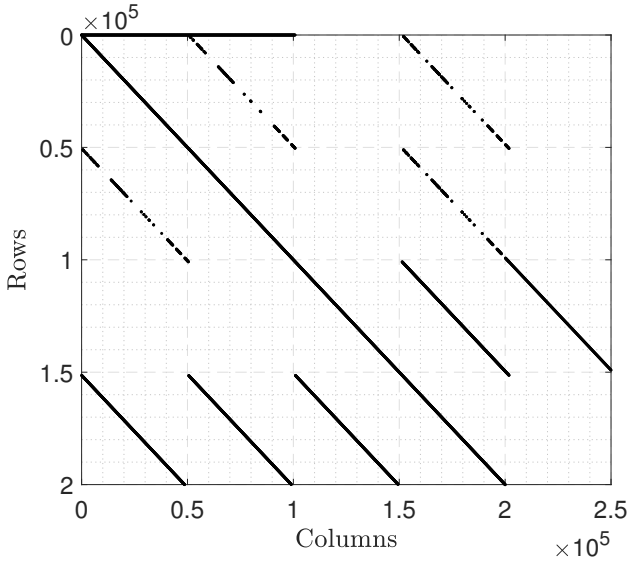

Figure 7.1: Jacobian matrix of the transcribed NLP. Black dots are non-zero elements.

Further details on the DM algorithm employed can be found in Reig Bernad [15]. Regarding the NLP solver, in this work, IPOPT [16] an open-source solver has been used.

7.4.1 Optimisation results

With the optimisation tool working properly, a WLTC cycle with different NOx downstream limits was optimised. Figure 7.2 shows the pareto front obtained from the model optimisation and the dark star (point "A") represents the experimental results with standard calibration, where the x-axis indicates the amount of NOx downstream and the y-axis indicates the total amount of ammonia injected during the cycle.

One can identify two cases of particular interest: strategy "B" that minimises the ammonia consumption to keep the NOx emissions in the same level compared to the standard strategy (Iso NOx) and strategy "C" that is aimed to minimise the NOx emissions with the same ammonia consumption compared to the standard strategy (Iso NH3). In the simulated results, for Iso NH3, the NOx downstream is reduced by 14.1%, and for Iso NOx a 33.5% ammonia consumption was saved.

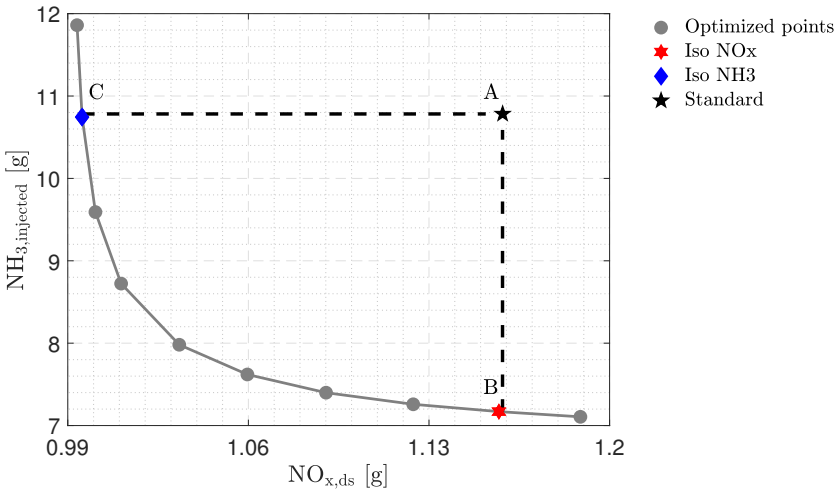

Figure 7.2: Comparison between the optimisation model and standard calibration for the total amount of NOx downstream and NH3 injected in a WLTC cycle.

The experimental validation of the previously described optimisation is done by imposing the ammonia injection profile in the test bench during a

WLTC. This procedure is performed by blocking the signal coming from the ECU and bypassing the optimised signal.

Figure 7.3 shows the comparison of the experimental results obtained with the standard strategy and the Iso NH3 optimised strategy. Two main differences between the standard and the optimised strategy can be observed. On one hand, the standard strategy provides a smoother evolution in the injection, while the optimised strategy shows frequent jumps between relatively no injection and injecting relatively high amounts of ammonia. On the other hand, one can observe that, in order to minimise the NOx emissions with a given amount of ammonia injected, it is more efficient to increase the ammonia injection at the beginning of the cycle to keep the SCR with a high load, and therefore high NOx efficiency, during the complete cycle. The increase in ammonia consumption during the first phases of the cycle can be compensated for at the end of the cycle since the SCR dynamics will prevent the ammonia injected in this last phase of the cycle to have a substantial impact on the NOx emissions in the cycle. This policy, jumping from high to low levels in the actuation and focusing the actuation in the first phases of the cycle, is in line with the general solution of dynamic system optimisation that usually leads to maximum power at the early phases of the problem and coasting in the last phases. Some examples of similar policies applied to other powertrain optimisation problems can be found in Guardiola et al. [17], María Desantes et al. [18], and Zhu et al. [19].

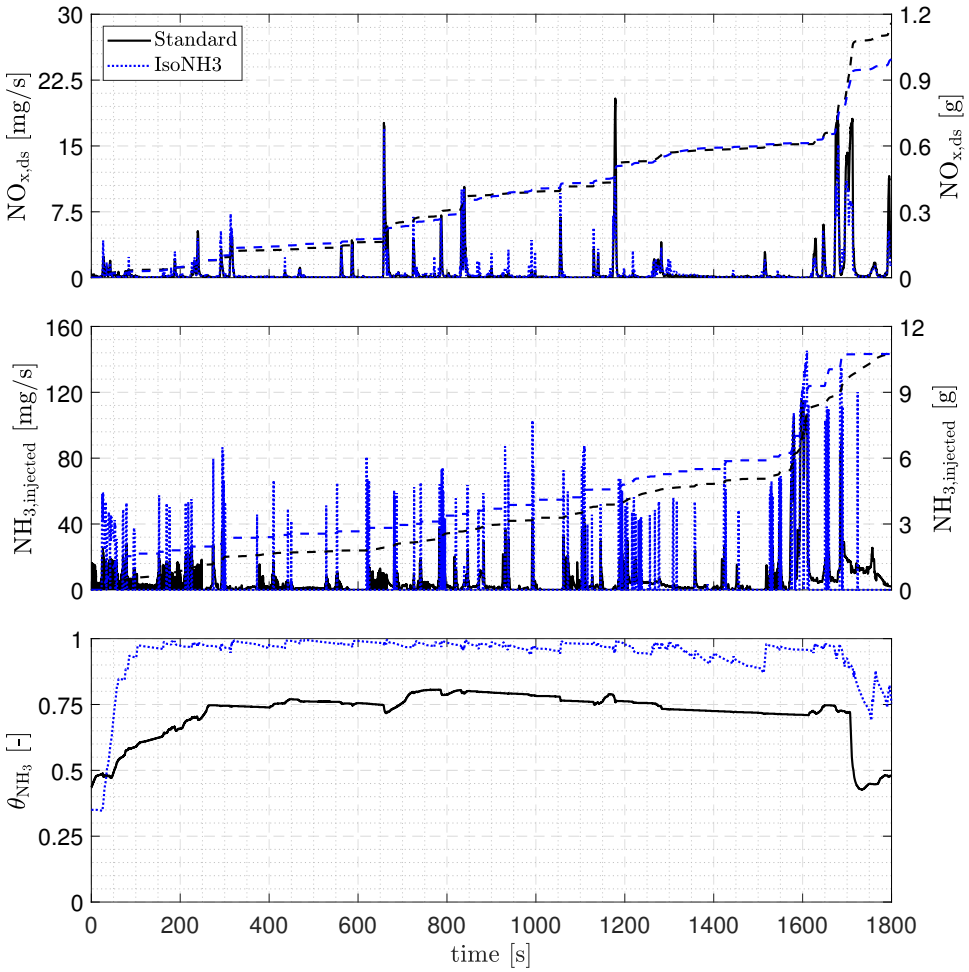

Figure 7.3: Comparison between the experimental results obtained with the standard calibration and the Iso NH3 optimal strategy for NOx emissions (upper plot), NH3 injected (medium plot), and SCR ammonia loading (θ_{NH_3}) in the WLTC. Continuous lines represent the instantaneous value of the standard calibration, dotted lines represent the instantaneous value of Iso NH3, and dashed lines represent the cumulative value (right axis).

Results also point out that NOx can barely be further reduced from the Iso NH3 results since the ammonia load of the SCR is kept nearly at maximum levels during the complete cycle. This conclusion can also be observed in Figure 7.2 where NOx approaches asymptotically 0.99 g at the expense of noticeable increases in ammonia injection.

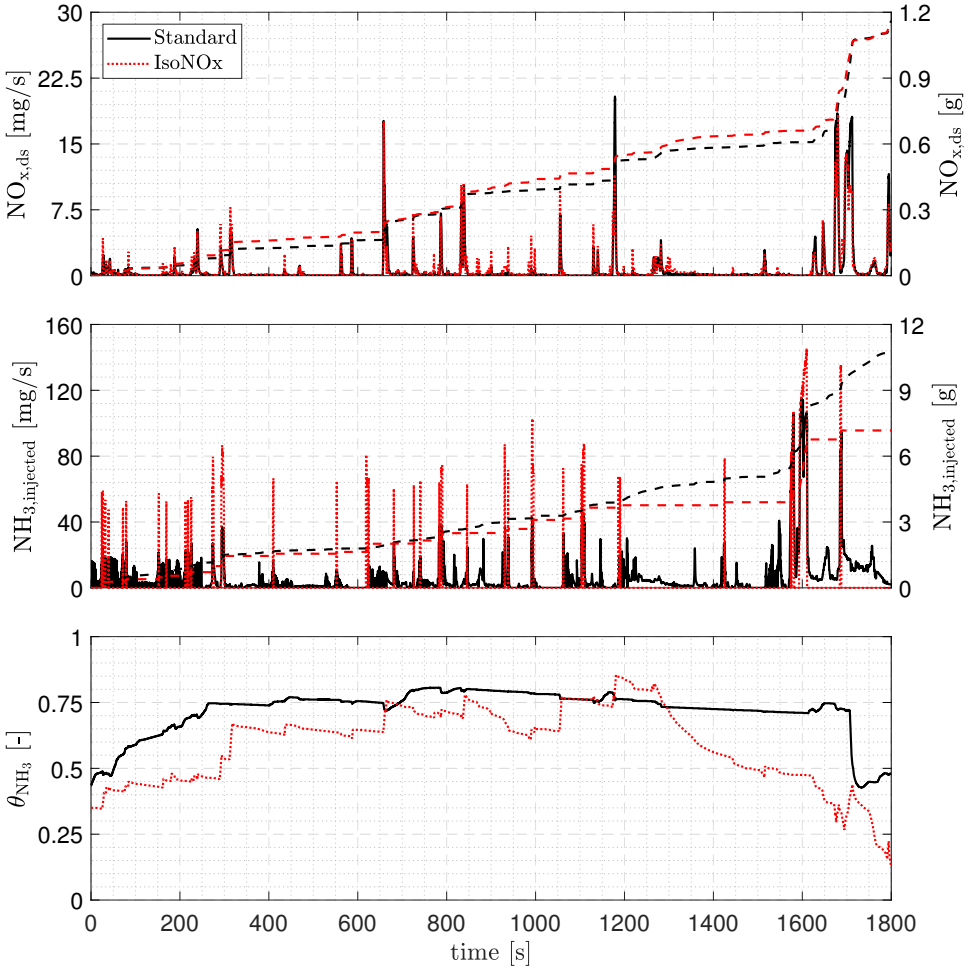

Figure 7.4: Comparison between the experimental results obtained with the standard calibration and the Iso NOx optimal strategy for NOx emissions (upper plot), NH3 injected (medium plot), and SCR ammonia loading (θ_{NH_3}) in the WLTC. Continuous lines represent the instantaneous value of the standard calibration, dotted lines represent the instantaneous value of Iso NOx, and dashed lines represent the cumulative value (right axis).

Analogously, Figure 7.4 shows the comparison of the experimental results obtained with the standard SCR control and the NOx optimised strategy. Results show how the efficiency of the ammonia injection can be improved to keep the same NOx emissions compared to the standard strategy with a substantial saving in ammonia consumption. Again, the results point out that a switching strategy between high and low ammonia injections is more

efficient than introducing ammonia in a smoother way. However, in this case, the required efficiency in the SCR is not as high as that in the case of Iso NH3 strategy, so the NH3 storage level is kept at medium values.

The experimental ammonia consumption and NOx emissions of the different tests carried out are shown together with the modelling results shown in Figure 7.5. The model and experimental results show a high correlation, thus validating the OCP approach as a method to optimise the ammonia injection in a predefined driving cycle.

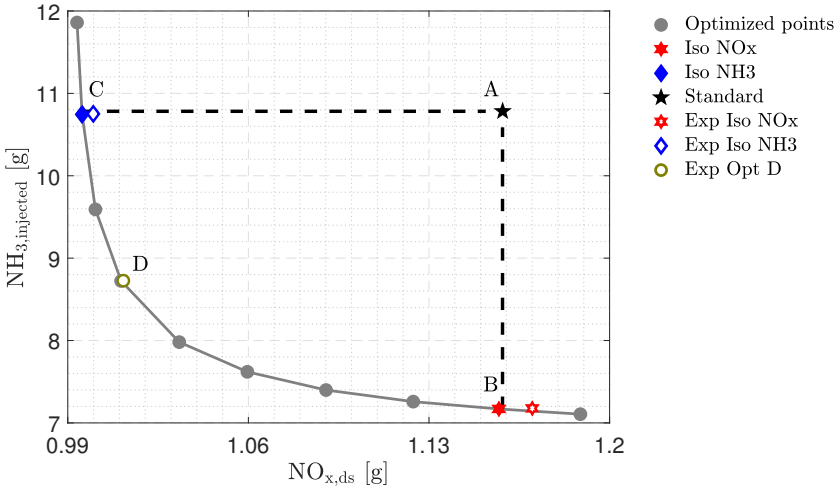

Figure 7.5: Comparison between the optimisation model and experimental results for the total amount of NOx downstream and NH3 injected in a WLTC cycle.

As shown in Figure 7.5, an experimental test was carried out at another point in the optimisation strategy (Opt D). This test aimed to verify the model in a condition of simultaneous optimisation, where the improvement is in terms of ammonia consumption and NOx emissions. Also at this point, the similarity of the simulated and experimental results was very high.

Table 7.2 shows the results of the amount of ammonia injected and NOx downstream with the standard and optimised (simulated and experimental) ammonia injection strategies. With the experimental results, for Iso NOx ammonia consumption was saved 33.5%, for Iso NH3 NOx downstream was reduced 13.7%, and for the condition of simultaneous optimisation (Opt D), a reduction of 19.1% in ammonia consumption and that of 12.7% in NOx emissions were observed.

Table 7.2: Comparison between the proposed strategies (simulated and experimental) and the standard one.

Strategy	NH3 [g]		NOx [g]			
			Simulated		Experimental	
Standard	10.783		1.159		1.159	
Iso NH3	10.751	[0.3%]	0.996	[14.1%]	1.000	[13.7%]
Iso NOx	7.169	[33.5%]	1.157	[0.2%]	1.170	[-0.9%]
Opt D	8.726	[19.1%]	1.011	[12.8%]	1.012	[12.7%]

The obtained results place the standard control strategy of the SCR in the plane of ammonia consumption and NOx emissions of the vehicle allowing its evaluation. Eventually, the previous procedure can be done with a different SCR design and the comparison of the obtained pareto fronts will rank them according to its potential performance. In addition, the analysis of the optimised strategies gives an insight into the design of real-time control strategies; in the case at hand, it is more efficient to use more aggressive ammonia injection strategies, with frequent changes in the ammonia injection level between low and high values than using a smooth ammonia evaluation. In the same line, the comparison of ammonia load in the SCR of Iso NOx and Iso NH3 strategies allows a correlation between the average ammonia load and the final NOx emissions to be observed. Accordingly, a model-based control strategy aimed at maintaining the ammonia loading of the SCR seems a feasible approach for real-time SCR control with near-optimal results.

Finally, it should be noted that the OCP approach allowed to include other constraints in the problem such as NH3 slip, maximum or minimum SCR temperatures, or, in general, any variable that can be obtained from the model states, disturbances, and actuators.

In conclusion, it was proved that the OCP is a valuable tool for the SCR design (including its control strategy), since the obtention of the Pareto front made it possible to compare different design alternatives.

7.5 On-line optimisation

On-line optimisation is always challenging task. On one hand, if the representative model of the system is accurate, on-line optimisation allows to improve its performance in the most diverse operating situations, on the other hand there is always a trade-off between accuracy and the required model simplicity for on-line implementation. Following this idea, a Model

Predictive Control (MPC) approach was followed to provide an on-line control implementation for the SCR-ASC control in dynamic conditions. While most of the literature uses a linear model to be able to reach real-time implementation, in this work the non-linear zero-dimensional model with reduced states presented in Chapter 5.2 has been directly embedded in the MPC. The optimisation has been solved at any prediction horizon with DP showing a good compromise between accuracy with a limited number of states (3) and controls (1) feasible for real-time application.

7.5.1 MPC methodology for SCR+ASC system

A widely used control strategy is the MPC, which in short, calculates the best trajectory of the control variable, that optimises the behaviour of the model output, aiming to minimise a cost function within a time-window (prediction horizon) and respecting some boundaries. The structure of the MPC can be summarised in the following points:

- Prediction horizon: is how far into the future is desired that the model estimates, a short horizon can lead to an inefficiency of the optimisation process, while a long horizon can have a very high computational cost.
- Receding horizon control: although the optimal control trajectory is completely described within the horizon window, the effective control input to the model is only the first sample of the optimised signal, while the rest of the trajectory is discarded. This is a key aspect of MPC since estimations in the prediction horizon are always subject to uncertainty.
- Current status update: at each time step current information must be sent to the model to update the model states, which can be either measured or estimated signals. Then the optimisation in the next prediction horizon will be done and the first action will be applied according to the receding horizon. In this sense, the current status update is the way to introduce feedback in the control strategy.
- Cost function: to make the best control decision, a criterion that reflects the objective is required, this being related to a cost function (J). This function is based on the difference between the model outputs and the actual values, where the optimal control action (u) is the trajectory that minimises the cost function within the optimisation window.

The problem is addressed aiming to find the optimal ammonia injection profile that minimises NOx emissions downstream of the ASC catalyst, as

well as the amount of ammonia injected. In particular, the problem can be incorporated to the OCP framework as:

$$\mathrm{J} = \min\{\mathrm{a} \int_0^{\tau} \frac{\dot{\mathrm{m}}_{\mathrm{NO_{x,ds}}}}{\max(\mathrm{NO_{x,ds}})}(\mathrm{u},\mathrm{x},\mathrm{w})\mathrm{dt} + (1-\mathrm{a}) \int_0^{\tau} \frac{\dot{\mathrm{m}}_{\mathrm{NH_{3,injected}}}}{\max(\mathrm{NH_{3,injected}})}(\mathrm{u},\mathrm{x},\mathrm{w})\mathrm{dt}, \quad (7.13)$$

where, τ is the size of the prediction horizon, the "max" in the denominator of the integrals are used to equalize the order of magnitude of both parameters, while the constant "a" determines the weight of the parameter that should have most relevance. The model has three states (x): NOx ($\mathrm{NO_{x,ds}}$) and NH3 ($\mathrm{NH_{3,ds}}$) concentration downstream of the ASC catalyst and ammonia load inside the SCR+ACS catalyst ($\theta_{\mathrm{NH_3}}$); one control variable (u): ammonia injection inside the SCR catalyst ($\mathrm{NH_{3,injected}}$); and three disturbances (w): exhaust gas mass flow rate ($\dot{\mathrm{m}}_{\mathrm{exh}}$); SCR catalyst temperature ($\mathrm{T_{SCR}}$) and NOx upstream of the SCR catalyst ($\mathrm{NO_{x,us}}$).

To avoid inconsistencies the model states and the control variable were bounded.

$$0 \leqslant [\mathrm{NH_{3,injected}}] \leqslant 525 \text{ kg/h}, \quad (7.14a)$$
$$0 \leqslant [\mathrm{NO_{x,ds}}] \leqslant 1850 \text{ ppm}, \quad (7.14b)$$
$$0 \leqslant [\mathrm{NH_{3,ds}}] \leqslant 1100 \text{ ppm}, \quad (7.14c)$$
$$0 \leqslant [\theta_{\mathrm{NH_3}}] \leqslant 1, \quad (7.14d)$$

Regarding disturbances, there are usually three ways to approach it in the prediction horizon:

- Known value: in this case, the real value is used during the whole prediction horizon. Note that this approach does not allow real-time control, since the complete evolution of disturbances must be loaded beforehand at each prediction horizon [20].
- Stochastic model: In this methodology, stochastic processes are used to estimate the disturbances evolution over the prediction horizon, such as the Markov chain, which uses a stochastic model to describe a series of potential events in which the probability of each event depends only on the state of the previous one [21].

- Constant value: In this approach, a constant value equal to the current disturbance value is considered throughout the prediction horizon. In this work, such an approach was implemented [22].

To allow the model to run in real-time the grid of states were set as $N_{NO_{x,ds}}$=15, $N_{NH_{3,ds}}$=10 and $N_{\theta_{NH_3}}$=10, and for control variable $N_{NH_{3,injected}}$=11. In the case of the prediction horizon different sizes were tested.

Note that this grid density is relatively low, which would not allow optimal control of the system. However, the states $NH_{3,ds}$ and θ_{NH_3} have a slow evolution, making it possible to update the grid position as the cycle evolves, that is, even if the grid density remains constant its position varies within the state boundary. Even in the case of $NO_{x,ds}$, which have high dynamics, it is not feasible for concentrations to vary from maximum to minimum value in one time step, thus allowing the use of this approach for the model states grid discretization, an example of the grid evolution can be seen in Figure 7.6.

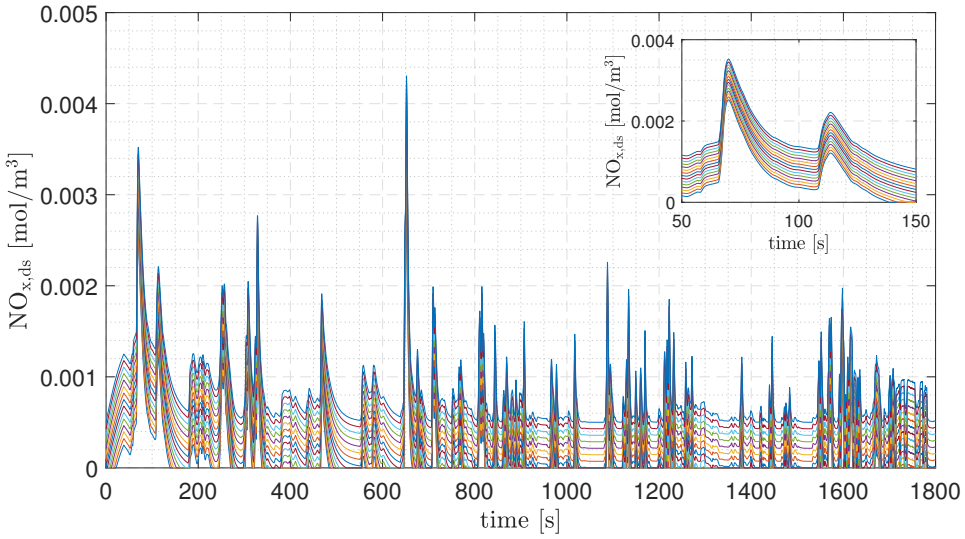

Figure 7.6: Evolution of the grid position of the NOx downstream model state.

It is important to highlight that Figure 7.6 shows the final evolution of the grid; however, at each time step the grid is constant during the prediction horizon and is distributed around the current state level at the beginning of the prediction horizon.

Figure 7.7 presents an example of the evolution of the grid and the prediction horizon in three consecutive time steps. In the first graph it is

possible to see the past evolution of the state (dark line) and of the grid (grey lines), as well as the grid evolution during the prediction horizon in time k (red lines). Note that the grid distribution occurs uniformly around the current state level (black circle), and at each time interval the grid is updated from the new state, as represented in the second and third graphs. This approach enables the grid distribution to cover the following state level without the need to populate the entire state spectrum.

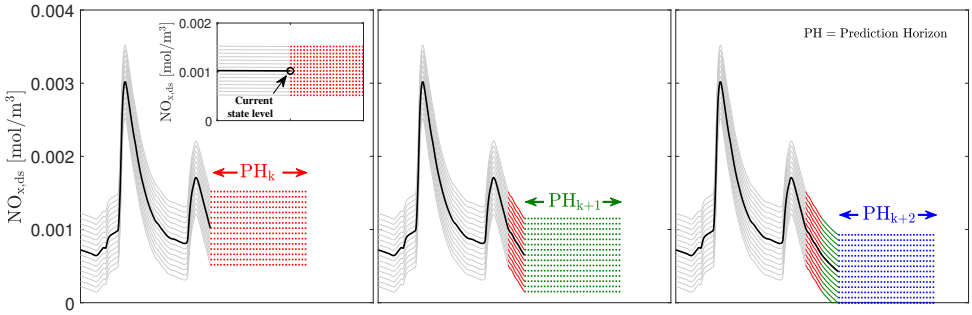

Figure 7.7: Evolution and discretization of the prediction horizon state grid in three consecutive time steps.

Once the model and the control strategy are defined it is possible to implement it. The schematic diagram of the MPC structure is illustrated in Figure 7.8.

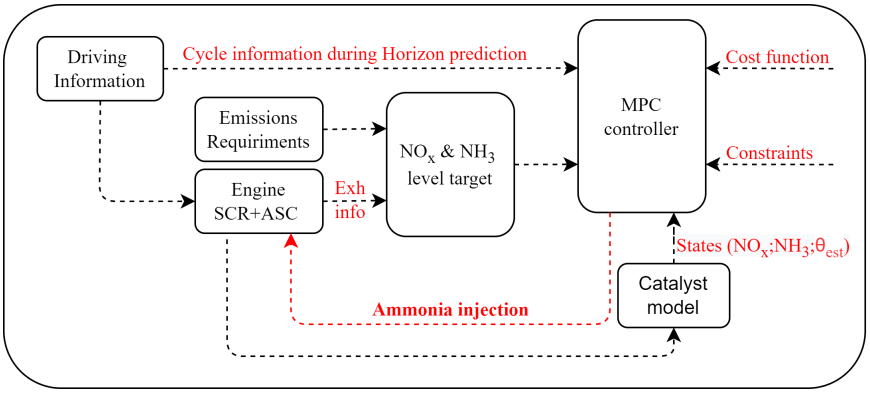

Figure 7.8: Schematic diagram of the MPC structure.

As can be seen, the MPC controller provides the amount of ammonia that must be injected in order to achieve the target limits. The ammonia dosage is calculated considering the cycle information during the prediction horizon, as

well as the evolution of the model states, where at each step the values of the variables that feed the model are updated.

The MPC algorithm consists in applying the *cost-to-go* equation for a state (x) and control (u) at time (t), represented by the following equation.

$$J(x, u) = L(x, u, t)\Delta t + \mathcal{J}_{k+1}(\hat{x}) + I(x, u, t), \tag{7.15}$$

where Δt is the division of the prediction horizon (τ) into equidistant points and $\hat{x}$ is the resultant state when applied the above control to the system, and being calculated as:

$$\hat{x} = x + f(x, u, t)\Delta t, \tag{7.16}$$

Note that the state $\hat{x}$ may not correspond to the grid value, in which case it can be interpolated. Regarding the term I, it represents the penalty to the system when the constraints are violated, in this case a near-infinite value is assumed.

Continuing, the same procedure is repeated for the entire control grid (u) and the minimum *cost-to-go* is chosen:

$$\mathcal{J}(x) = \min_{u}\{J(x, u)\}, \tag{7.17}$$

Note that this approach is solved by brute-force search. Thus, the cost function (J) is evaluated at each time step and for the entire grid of states and controls.

The entire process outlined in eq.7.15-7.17 is reproduced in a sequential backward manner until t_0 is reached. Then, choosing $\mathcal{J}_0(x_0)$ satisfies the initial value constraints (eq.7.3) and the corresponding control variable $u_0(x_0)$ produces the optimal OCP control trajectory.

7.5.2 Optimisation results

The proposed strategy was evaluated in two stages, first the MPC model was tested using the information acquired on the test bench. In this way it was possible to adjust the model parameters and assess the level of improvement compared to the standard strategy. The second step was the application of the strategy directly on the test bench, for this purpose the MPC model was developed in the Simulink platform based on dSpace Real-Time Interface (RTI), allowing to update the input information as the cycle evolves, while the model delivers the amount of ammonia that must be injected into the system, the upper layer of the model can be seen in Figure 7.9.

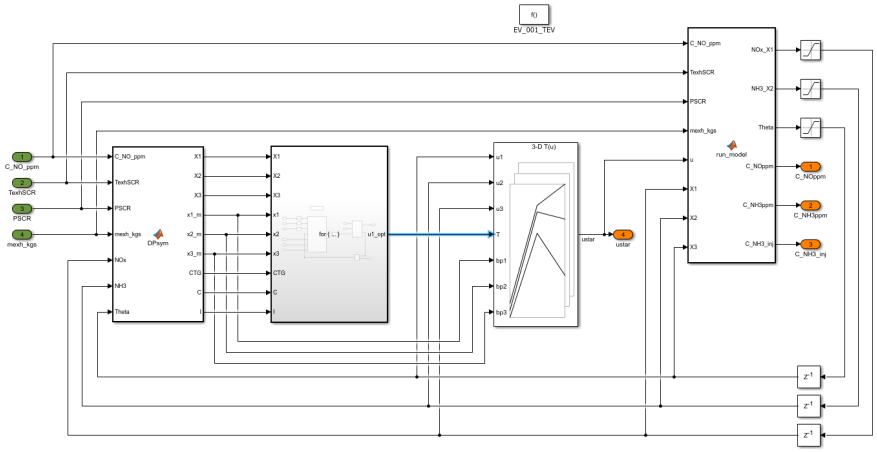

Figure 7.9: Upper layer of the MPC model on the Simulink platform.

The comparison between the proposed methodology (coloured markers) and the standard strategy (dark square) can be visualised in Figure 7.10, where the x-axis represents the total amount of NOx slip downstream of the ASC catalyst and the y-axis the total amount of ammonia injected during the cycle. The model was simulated with different prediction horizons, varying the parameter ”a” of eq.7.13 and with a NH3 slip constraint of 10 ppm. Thereby it was possible to obtain different Pareto fronts of the relationship between the total amount of NOx slip and ammonia injected during the cycle (coloured dots), it can also be visualized the experimental results referring to two points performed with the same conditions, but with different prediction horizons (coloured x).

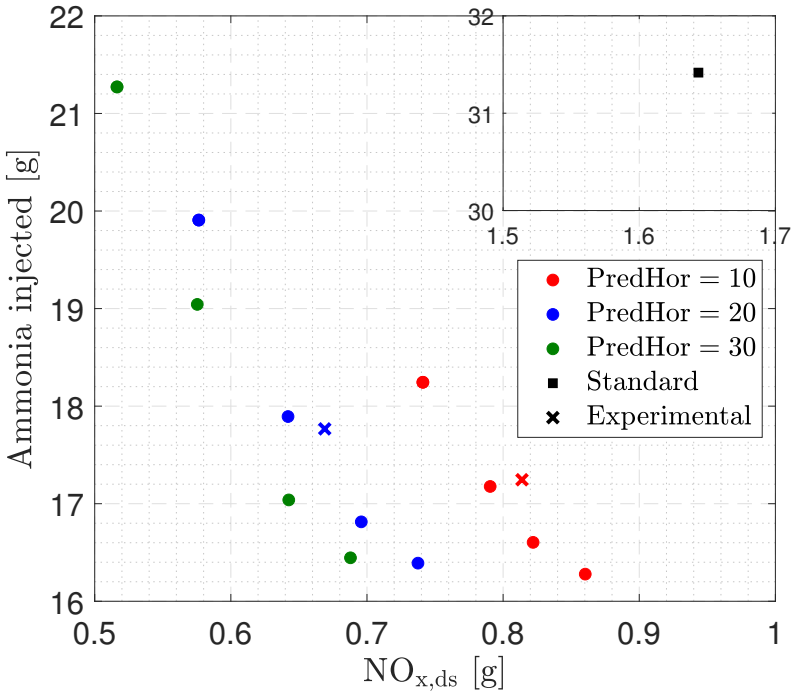

Figure 7.10: Total amount of NOx slip downstream of the ASC catalyst (x-axis) and injected ammonia during the cycle (y-axis). Coloured dots: simulated results; Coloured x: experimental results; Dark square: standard strategy. Red, blue, and green markers represent the prediction horizon of 10, 20 and 30 seconds, respectively.

As it can be seen in Figure 7.10, with a larger prediction horizon it is possible to move the Pareto front towards lower values of NOx emissions for the same amount of ammonia injected, this enhancement is related to the fact that the further into the future the model can visualize, better will be the controller's decisions, at the expense of a higher computational cost. It can also be seen that the results obtained experimentally are very close to the simulated ones, 3.0% and 4.2% for the prediction horizons of 10 and 20 s, respectively. Note that there is a considerable large gap between the results of the standard and the optimised strategy, however it is worth mentioning that the standard strategy is focused on reducing NOx emissions downstream of the SCR catalyst and with a rather loose NH3 slip constraint, as well as it does not consider the use of the ASC catalyst in the ATS. The evolution of NOx slip and ammonia injection of the standard strategy and the experimental

MPC are presented in Figure 7.11.

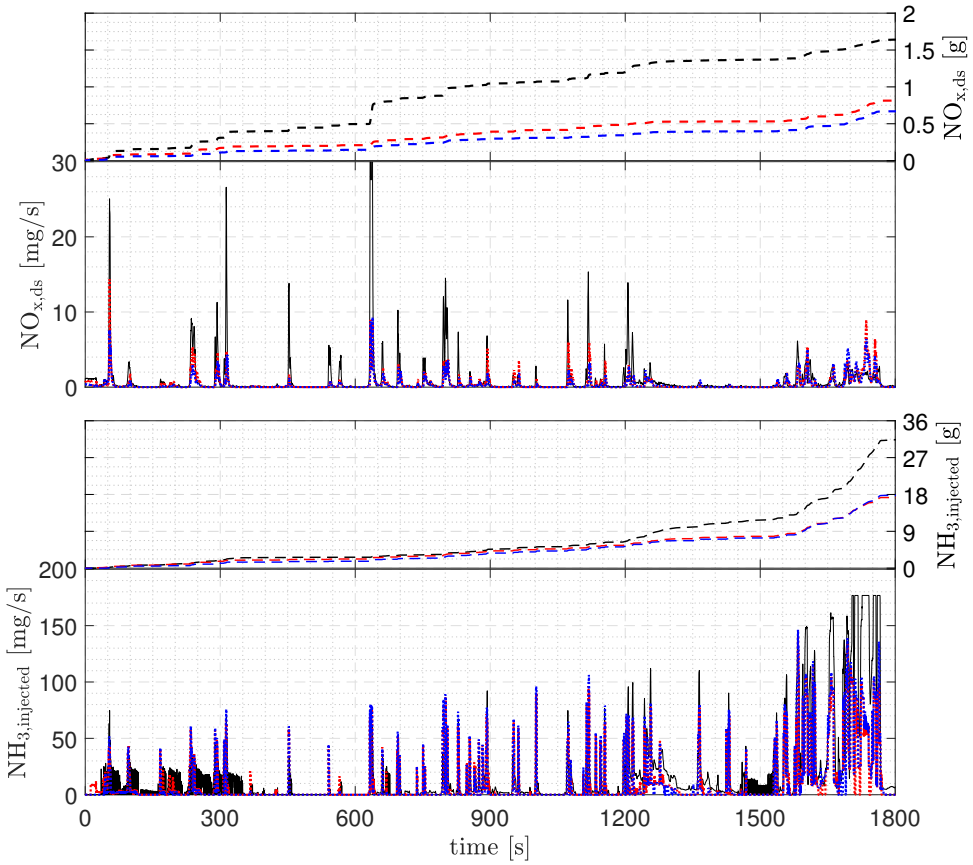

Figure 7.11: Evolution of NOx emissions downstream of ASC catalyst (upper plot) and ammonia injection (bottom plot). Dark continuous line represents the instantaneous values of the standard strategy, while the dotted lines represent the results using the MPC controller. The accumulated values are presented at the top of each plot with the dashed line. Red and blue lines representing prediction horizons of 10 and 20 seconds, respectively.

As can be seen in figure 7.12, the evolution behaviour of NOx emissions are similar in both approaches, the main difference is in the level of the emissions peak. As an example, in the second 54 the standard strategy presents a slip of 25.1 mg/s, while for the MPC a slip of 14.4 and 7.6 mg/s for prediction horizon 10 and 20 s, respectively. The same phenomenon is observed throughout the cycle, leading to a considerable difference in the final accumulated value. Regarding the ammonia injection profile, the MPC performs similarly to

the off-line optimisation (see Figure 7.3 and Figure 7.4), switching between relatively high injections and no injections. The evolution of NH3 slip is presented in Figure 7.12.

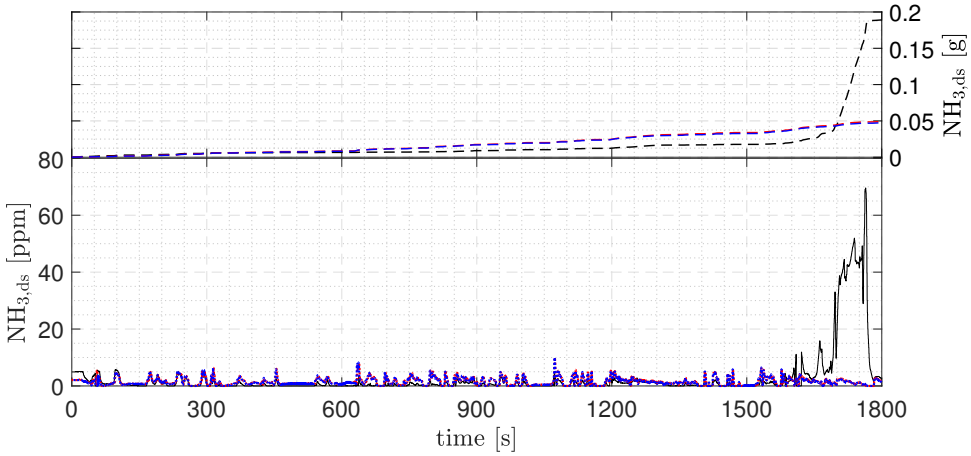

Figure 7.12: Evolution of NH3 slip downstream of ASC catalyst. Dark continuous line represents the instantaneous values of the standard strategy, while the dotted lines represent the results using the MPC controller. The cumulative values are presented at the upper part with the dashed line. Red and blue lines representing prediction horizons of 10 and 20 seconds, respectively.

In both cases the NH3 slip is quite low since the ASC catalyst has a high ammonia storage capacity. In the standard strategy only in the final part of the cycles it is possible to appreciate some significant slip. Concerning the MPC it is possible to see that the controller was able to respect the NH3 slip constraint of less than 10 ppm.

References

[1] Keogh Eamonn and Mueen Abdullah. *Curse of Dimensionality*, pp. 314–315. Springer US, Boston, MA, 2017. (cited in pp. 70 and 152)

[2] Maksimov Vyacheslav. "Analysis of Differential Inclusions: Feedback Control Method". In *Springer Optimization and Its Applications*, volume 39, pp. 259–275. 2010. (cited in p. 152)

[3] Vrabie Draguna and Lewis Frank. "Online Adaptive Optimal Control Based on Reinforcement Learning". In *Springer Optimization and Its Applications*, volume 39, pp. 309–323. 2010. (cited in p. 152)

[4] Pesch H J. *Offline and Online Computation of Optimal Trajectories in the Aerospace Field*, pp. 165–220. Springer US, Boston, MA, 1994. (cited in p. 152)

[5] Bellman Richard. "The theory of dynamic programming". *Bulletin of the American Mathematical Society*, Vol. 60 n^o 6, pp. 503–515, 1954. (cited in p. 153)

[6] Gamkrelidze R. V. "Discovery of the maximum principle". *Journal of Dynamical and Control Systems*, Vol. 5 n^o 4, pp. 437–451, 1999. (cited in p. 153)

[7] Blum E. K., Pontryagin, Boltyanskii, Gamkrelidze and Mishchenko. "The Mathematical Theory of Optimal Processes.". *The American Mathematical Monthly*, Vol. 70 n^o 10, pp. 1114, dec 1963. (cited in p. 153)

[8] Bryson Arthur E. *Applied Optimal Control*. Routledge, New York, NY, 1st edition, 1975. (cited in p. 153)

[9] Buldaev Alexander S. "Perturbation Methods in Optimal Control Problems". In *Springer Optimization and Its Applications*, volume 39, pp. 325–373. 2010. (cited in p. 153)

[10] Cornuéjols Gérard, Peña Javier and Tütüncü Reha. *Dynamic Programming: Theory and Algorithms*, pp. 212–224. Cambridge University Press, 2 edition, 2018. (cited in p. 154)

[11] Bellman Richard. *Dynamic Programming*. Princeton University Press, Princeton, NJ, 1957. (cited in p. 154)

[12] Goetschalckx Robby, Sanner Scott and Driessens Kurt. "Reinforcement Learning with the Use of Costly Features". In Girgin Sertan, Loth Manuel, Munos Rémi, Preux Philippe and Ryabko Daniil, editors, *Recent Advances in Reinforcement Learning*, pp. 124–135, Berlin, Heidelberg, 2008. Springer Berlin Heidelberg. (cited in p. 154)

[13] Fagundez Fabio D., Facó João Lauro D. and Xavier Adilson E. "A Nonlinear Optimal Control Approach to Process Scheduling". In *Springer Optimization and Its Applications*, volume 39, pp. 409–421. 2010. (cited in p. 155)

[14] Böhme Thomas J and Frank Benjamin. *Direct Methods for Optimal Control*, pp. 233–273. Springer International Publishing, Cham, 2017. (cited in p. 155)

[15] Bernad A Reig. *Optimal Control for Automotive Powertrain Applications*. PhD Thesis, Universitat Politècnica de València, 2017. (cited in pp. 62 and 158)

[16] Wächter Andreas and Biegler Lorenz T. "On the implementation of an interior-point filter line-search algorithm for large-scale nonlinear programming". *Mathematical Programming*, Vol. 106 n^o 1, pp. 25–57, mar 2006. (cited in p. 158)

[17] Guardiola Carlos, Pla Benjamín, García Antonio and Boronat Vicente. "Optimal heat release shaping in a reactivity controlled compression ignition (RCCI) engine". *Control Theory and Technology*, Vol. 15 n^o 2, pp. 117–128, may 2017. (cited in p. 159)

[18] María Desantes José, Guardiola Carlos, Pla Benjamín and Real Marcelo. "Oxygen catalyst depletion strategy based on TWC control-oriented modelling". *IFAC-PapersOnLine*, Vol. 51 n^o 31, pp. 355–361, 2018. (cited in p. 159)

[19] Zhu Jiamin, Ngo Caroline and Sciarretta Antonio. "Real-Time Optimal Eco-Driving for Hybrid-Electric Vehicles". *IFAC-PapersOnLine*, Vol. 52 n^o 5, pp. 562–567, 2019. (cited in p. 159)

[20] Seborg Dale E, Mellichamp Duncan A and Edgar Thomas F. *Process Dynamics and Control*. Wylie Series in Chemical Engineering. John Wiley & Sons, third edition, 2011. (cited in p. 165)

[21] Zhou Yang, Ravey Alexandre and Péra Marie-Cécile. "A survey on driving prediction techniques for predictive energy management of plug-in hybrid electric vehicles". *Journal of Power Sources*, Vol. 412 n^o October 2018, pp. 480–495, feb 2019. (cited in p. 165)

[22] Sawma J., Khatounian F., Monmasson E., Ghosn R. and Idkhajine L. "The effect of prediction horizons in MPC for first order linear systems". In *2018 IEEE International Conference on Industrial Technology (ICIT)*, volume 2018-Febru, pp. 316–321. IEEE, feb 2018. (cited in p. 166)

Part IV

Conclusions and future work

Chapter 8

Conclusions and future work

If we knew what it was we were doing, it would not be called research, would it?

— Albert Einstein

Contents

8.1 Main contributions

This thesis focused on the study of control and diagnosis of deNOx after-treatment systems, particularly SCR and ASC catalysts. Thus, present dissertation proposed different control-oriented models embedded in an extended Kalman filter observer to accurately estimate the NOx and NH3 emissions downstream of both SCR and ASC catalyst. This design was used to detect and correct possible failures in the ammonia injection system and also estimate the ageing state of the ASC catalyst. On the control side, zero-dimensional physical models were used to evaluate the maximum efficiency capacity of the after-treatment system, as well as implement a real-time NOx and NH3 emission control strategy.

The main conclusions and specific contributions obtained in the development of the doctoral thesis are detailed below.

8.1.1 Control-oriented models

Two types of control-oriented models were addressed in the course of the thesis: physical models and data-driven models. Each approach was employed for a different type of application, the data-driven models were used for diagnostics of the after-treatment system, while the physical models for control strategy.

8.1.1.1 Data-driven models

In the case of the data-driven approach, three different models have been proposed:

- Sensor signal analysis: This model uses the information from sensors placed upstream and downstream of the catalyst to estimate the NOx conversion efficiency of the after-treatment system. The major advantage of this approach is that it does not require any feedback signal other than the NOx sensors to estimate NH3 slip with very high accuracy (similar levels of physical models). As a main disadvantage the model has poor capabilities to estimate NOx emissions, since this approach is not able to adjust to the high dynamics of the NOx emissions.

- Artificial neural network: ANN are parallel processing algorithms whose inherent property is the ability to learn non-linear relationships, such as engine emissions. Since the dynamics of NOx at the catalyst output are basically controlled by the input dynamics, the signals from the NOx sensor upstream of the SCR catalyst and the ammonia injection rate

are used to accurately estimate the NOx emissions downstream of the after-treatment system. As a drawback, ANN is susceptible to failures due to incorrect feedback information; thus, this approach is not able to identify ammonia injection failures or deviations due to catalyst ageing.

- Cross sensitivity model: The proposed model aims to predict the cross-sensitivity of the NOx sensor to ammonia by estimating the sensor cell temperature or through the correlation of the NH3 concentration in the exhaust gas. Both approaches proved to be a better option than the one usually used by the industry, constant value [1]. However, the model based on the sensor cell temperature showed the greatest improvement in all tests and with two different NOx sensors.

8.1.1.2 Zero-dimensional physical models

The state-of-the-art of the zero-dimensional control-oriented models were able to represent with a substantial degree of accuracy the catalyst behaviour with low computational burden, estimating NOx and NH3 emissions with very high precision in different duty cycles, thus enabling its integration with control strategies. During the thesis two zero-dimensional models were developed:

- Four-state model: This approach was used for off-line optimisation, considering as model states, NO, NO2, NH3 and ammonia load of the catalyst.

- Three-state model: This approach was used for on-line optimisation, considering as model states, NO, NH3 and ammonia load of the catalyst. The removal of NO2 as a state was possible, since this approach is used for a SCR+ASC model, in which the NO2 concentration downstream of both catalysts is extremely low.

8.1.1.3 Extended Kalman filter

The data fusion technique was implemented to take advantage of the best of each model (ANN and SSA), mainly in situations of ammonia injector failure and catalyst ageing. In the case of failure, the feedback information received by the ECU is wrong leading to an incorrect ammonia injection rate. Regarding catalyst ageing, the adsorption capacity and NOx conversion efficiency are reduced, promoting a deviation of the current catalyst state from the one used to calibrate the model.

The highlight of EKF was in its ability to adapt to different drawbacks, and to achieve accuracy levels of NOx and NH3 emissions estimation similar

to the physical zero-dimensional model.

8.1.2 After-treatment system monitoring and diagnostics

The complexity of today's after-treatment systems requires robust monitoring and diagnostic strategies to ensure the proper operation of such systems and compliance with current regulations. Due to this scenario, a strategy was proposed to detect possible failures in two usual situations, ammonia injection failure and catalyst ageing.

8.1.2.1 Ammonia injection failure

Ammonia injection failure can be generated by the blocking of the urea injection nozzles due to the progressive deposition of urea over time, leading to a reduction in the amount of injected ammonia demanded and, consequently, to low levels of NOx conversion.

The approach combines the control-oriented models, ANN and SSA with the extended Kalman filter, to accurately predict NOx and NH3 emissions. The emissions estimated by the EKF observer are compared within a time-window with those expected if the ATS were working properly, and then through a two-dimensional NOx-NH3 statistical model it is possible to determine the level of ammonia injection failure and correct it to standard operating levels. The main advantage of this approach is the use of a variable time-window linked to a physical parameter, engine-out NOx emissions. This concept allows the proposed strategy to be used in several cycles and engine operating conditions, since the time-window duration is conditioned to the engine operating condition and not to the cycle.

8.1.2.2 Catalyst ageing state

Regarding catalyst ageing, this phenomenon develops in a passive manner after the catalyst is subjected to a long period of operation at high temperature. To address this issue, the methodology proposed to detect ammonia injection failure was applied and extended to assess the ageing of the ASC catalyst.

This approach is possible since the impact of injection failure and catalyst ageing follow almost orthogonal directions (Figure 6.24), thus promoting the possibility of fault isolation. Thereby, assuming a linear impact of the injection failure and ageing on the NOx and NH3 slip, it was possible to separately identify the failures by means of the ratio between the observed and modelled emissions.

8.1.3 Optimisation of dynamic systems

As described by Vignesh et al. [2], one way to improve the performance of the after-treatment systems is to address optimization strategies. Thus, in the present thesis, two different applications of optimal control were proposed to optimise the after treatment system.

8.1.3.1 Off-line optimisation

The off-line optimisation aimed to achieve the highest performance of the system, in the case at hand it was used as a benchmark approach. The methodology uses the anticipated knowledge of the driving cycle to optimise the ammonia injection strategy in the SCR catalyst. With this approach it was possible to create a trade-off between the total amount of NOx downstream of the catalyst and ammonia injection in the cycle.

As a result, the proposed strategy is able to reduce ammonia consumption in 33.5% keeping the same NOx emissions, or conversely, NOx can be reduced in 13.7% without increasing ammonia injection. It is also possible to simultaneously improve ammonia consumption and NOx emissions.

8.1.3.2 On-line optimisation

The on-line optimization aimed to control the system in real-time application, using the incoming information to make the control decision. In the proposed methodology the zero-dimensional model with reduced states was embedded within an MPC approach, in which the model uses the ammonia injection rate to minimise NOx emissions downstream of the ASC catalyst, with a constraint on NH3 slip.

As a result, it was possible to create different trade-offs between NOx emissions and ammonia consumption in the cycle, depending on the size of the prediction horizon; however, in all cases the improvement compared to the standard ECU strategy was extremely high.

8.2 Future work

This thesis was intended to demonstrate the potential for improvement of the current state-of-the-art of deNOx after-treatment systems, more specifically in the area of control and diagnostics. However, in the course of the thesis several other topics emerged, although interesting, they were not possible to be covered in the development of this work. In this way, it is expected the

continuity of this research work addressing such topics, where it is possible to highlight two of them.

8.2.1 Stochastic models embedded in the on-line optimisation approach

As discussed in Chapter 7.5.1, one way to approach the disturbance evolution over the prediction horizon is through a stochastic model. In this way, instead of having a constant signal, a probabilistic model is used to estimate the evolution of the disturbances during the entire horizon. This approach may allow further improvement, since the closer to a real evolution, the better the control variable decision.

8.2.2 Integration of after-treatment system models into a hybrid vehicle design

Another interesting research point is to integrate the after-treatment system control-oriented models into the hybrid vehicle power-split strategy. Thus, including the catalyst temperature as an additional system state would allow addressing problems such as cold-start and catalyst low-temperature operation, drawbacks commonly faced in hybrid systems.

References

[1] Frobert Arnaud, Raux Stephane, Creff Yann and Jeudy Eric. "About Cross-Sensitivities of NOx Sensors in SCR Operation". In *SAE Technical Papers*, volume 2, apr 2013. (cited in pp. 28, 29, 30, 31, 77, 78, 79, and 179)

[2] Vignesh R. and Ashok B. "Critical interpretative review on current outlook and prospects of selective catalytic reduction system for De-NOx strategy in compression ignition engine". *Fuel*, Vol. 276 n^o March, sep 2020. (cited in pp. 17, 21, 25, 83, and 181)

Bibliografy

Alphabetic Index of Authors

Afzal Adeel, Cioffi Nicola, Sabbatini Luigia and Torsi Luisa. "NOx sensors based on semiconducting metal oxide nanostructures: Progress and perspectives". *Sensors and Actuators B: Chemical*, Vol. 171-172 n^o 2012, pp. 25–42, aug 2012. (cited in p. 78)

Ajanovic Amela and Haas Reinhard. "The impact of energy policies in scenarios on GHG emission reduction in passenger car mobility in the EU-15". *Renewable and Sustainable Energy Reviews*, Vol. 68, pp. 1088–1096, feb 2017. (cited in p. 4)

Aliramezani Masoud, Koch Charles Robert, Secanell Marc, Hayes Robert E. and Patrick Ron. "An electrochemical model of an amperometric NOx sensor". *Sensors and Actuators B: Chemical*, Vol. 290, pp. 302–311, jul 2019. (cited in p. 28)

Andress David, Nguyen T. Dean and Das Sujit. "Reducing GHG emissions in the United States' transportation sector". *Energy for Sustainable Development*, Vol. 15 n^o 2, pp. 117–136, jun 2011. (cited in p. 4)

Arioli Magdala Satt, D'Agosto Márcio de Almeida, Amaral Fernando Gonçalves and Cybis Helena Beatriz Bettella. "The evolution of city-scale GHG emissions inventory methods: A systematic review". *Environmental Impact Assessment Review*, Vol. 80 n^o November 2019, jan 2020. (cited in p. 4)

Arsie Ivan, Cricchio Andrea, De Cesare Matteo, Lazzarini Francesco, Pianese Cesare and Sorrentino Marco. "Neural network models for virtual sensing of NO x emissions in automotive diesel engines with least square-based adaptation". *Control Engineering Practice*, Vol. 61, pp. 11–20, apr 2017. (cited in p. 91)

Asghar Usama, Rafiq Sikander, Anwar Adeel, Iqbal Tanveer, Ahmed Ashfaq, Jamil Farrukh, Khurram M. Shahzad, Akbar Majid Majeed, Farooq Abid, Shah Noor S. and Park Young-Kwon. "Review on the progress in emission control technologies for the abatement of CO2, SOx and NOx from fuel combustion". *Journal of Environmental Chemical Engineering*, Vol. 9 n^o 5, oct 2021. (cited in p. 8)

Ayodhya Archit Srinivasacharya and Narayanappa Kumar Gottekere. "An overview of after-treatment systems for diesel engines". *Environmental Science and Pollution Research*, Vol. 25 n^o 35, pp. 35034–35047, dec 2018. (cited in p. 9)

Bartley Gordon J., Chadwell Christopher J., Kostek Theodore M. and Zhan Reggie. "SCR Deactivation Kinetics for Model-Based Control and Accelerated Aging Applications". In *SAE Technical Papers*, apr 2012. (cited in p. 26)

Beatrice Carlo, Rispoli Natale, Di Blasio Gabriele, Konstandopoulos Athanasios G., Papaioannou Eleni and Imren Abdurrahman. "Impact of Emerging Engine and After-Treatment Technologies for Improved Fuel Efficiency and Emission Reduction for the Future Rail Diesel Engines". *Emission Control Science and Technology*, Vol. 2 n^o 2, pp. 99–112, apr 2016. (cited in p. 9)

Bellman Richard. "The theory of dynamic programming". *Bulletin of the American Mathematical Society*, Vol. 60 n^o 6, pp. 503–515, 1954. (cited in p. 153)

Bellman Richard. *Dynamic Programming*. Princeton University Press, Princeton, NJ, 1957. (cited in p. 154)

Bernad A Reig. *Optimal Control for Automotive Powertrain Applications*. PhD Thesis, Universitat Politècnica de València, 2017. (cited in pp. 62 and 158)

Bian Mengyao, Liu Kaijie, Han Xinyu, Fang Yangfei, Liu Qiuwen, Zhang Yibo and Yang Xiangguang. "Novel manganese-based assembled nanocatalyst with "nitrous oxide filter" for efficient NH3-SCR in wide low-temperature window: Optimization, design and mechanism". *Fuel*, Vol. 331, jan 2023. (cited in p. 21)

Blum E. K., Pontryagin, Boltyanskii, Gamkrelidze and Mishchenko. "The Mathematical Theory of Optimal Processes.". *The American Mathematical Monthly*, Vol. 70 n^o 10, pp. 1114, dec 1963. (cited in p. 153)

Böhme Thomas J and Frank Benjamin. *Direct Methods for Optimal Control*, pp. 233–273. Springer International Publishing, Cham, 2017. (cited in p. 155)

Bonfils Anthony. *Experimental closed-loop control of SCR aftertreatment systems using NOx sensors cross-sensitive to NH3*. Theses, Ecole Nationale Supérieure des Mines de Paris, 2013. (cited in p. 29)

Börnhorst M. and Deutschmann O. "Advances and challenges of ammonia delivery by urea-water sprays in SCR systems". *Progress in Energy and Combustion Science*, Vol. 87 n^o August, nov 2021. (cited in p. 111)

Bowen Melanie, Freidank Jan, Wannow Stefanie and Cavallone Mauro. "Effect of Perceived Crisis Response on Consumers' Behavioral Intentions During a Company Scandal – An Intercultural Perspective". *Journal of International Management*, Vol. 24 n^o 3, pp. 222–237, sep 2018. (cited in p. 7)

Brand Christian. "Beyond 'Dieselgate': Implications of unaccounted and future air pollutant emissions and energy use for cars in the United Kingdom". *Energy Policy*, Vol. 97, pp. 1–12, oct 2016. (cited in p. 7)

Brookshear D. William, Pihl Josh A., Toops Todd J., West Brian and Prikhodko Vitaly. "The selective catalytic reduction of NO over Ag/Al2O3 with isobutanol as the reductant". *Catalysis Today*, Vol. 267, pp. 65–75, jun 2016. (cited in p. 22)

Bryson Arthur E. *Applied Optimal Control*. Routledge, New York, NY, 1st edition, 1975. (cited in p. 153)

Buldaev Alexander S. "Perturbation Methods in Optimal Control Problems". In *Springer Optimization and Its Applications*, volume 39, pp. 325–373. 2010. (cited in p. 153)

Canova Marcello, Midlam-Mohler Shawn, Pisu Pierluigi and Soliman Ahmed. "Model-based fault detection and isolation for a diesel lean trap aftertreatment system". *Control Engineering Practice*, Vol. 18 n^o 11, pp. 1307–1317, nov 2010. (cited in p. 23)

Charabi Y., Al Nasiri N., Al Awadhi T., Choudri B.S. and Al Bimani A. "GHG emissions from the transport sector in Oman: Trends and potential decarbonization pathways". *Energy Strategy Reviews*, Vol. 32, nov 2020. (cited in p. 4)

Chen Guisheng, Di Lei, Shen Yinggang, Zhang Wei and Mao Bin. "Strategies for emissions control in heavy-duty diesel engines to achieve low-emissions combustion with a high efficiency". *Proceedings of the Institution of Mechanical Engineers, Part D: Journal of Automobile Engineering*, Vol. 230 n^o 5, pp. 593–608, apr 2016. (cited in p. 62)

Cheng Ying, He Liqiang, He Weinan, Zhao Pei, Wang Pinxi, Zhao Jin, Zhang Kesong and Zhang Shaojun. "Evaluating on-board sensing-based nitrogen oxides (NOX) emissions from a heavy-duty diesel truck in China". *Atmospheric Environment*, Vol. 216, nov 2019. (cited in p. 111)

Chenoweth James A., Albertson Timothy E. and Greer Matthew R. "Carbon Monoxide Poisoning". *Critical Care Clinics*, Vol. 37 n^o 3, pp. 657–672, jul 2021. (cited in p. 8)

Chundru Venkata Rajesh, Parker Gordon G. and Johnson John H. "The Effect of NO 2 /NO x Ratio on the Performance of a SCR Downstream of a SCR Catalyst on a DPF". *SAE International Journal of Fuels and Lubricants*, Vol. 12 n^o 2, jun 2019. (cited in pp. 25 and 83)

Colombo Massimo, Nova Isabella and Tronconi Enrico. "A comparative study of the NH3-SCR reactions over a Cu-zeolite and a Fe-zeolite catalyst". *Catalysis Today*, Vol. 151 n^o 3-4, pp. 223–230, jun 2010. (cited in p. 65)

Colombo Massimo, Nova Isabella, Tronconi Enrico, Schmeißer Volker, Bandl-Konrad Brigitte and Zimmermann Lisa. "NO/NO2/N2O–NH3 SCR reactions over a commercial Fe-zeolite catalyst for diesel exhaust aftertreatment: Intrinsic kinetics and monolith converter modelling". *Applied Catalysis B: Environmental*, Vol. 111-112 n^o 2, pp. 106–118, jan 2012. (cited in p. 64)

Colombo Massimo, Nova Isabella, Tronconi Enrico, Schmeißer Volker, Bandl-Konrad Brigitte and Zimmermann Lisa. "Experimental and modeling study of a dual-layer (SCR+PGM) NH3 slip monolith catalyst (ASC) for automotive SCR aftertreatment systems. Part 1. Kinetics for the PGM component and analysis of SCR/PGM interactions". *Applied Catalysis B: Environmental*, Vol. 142-143, pp. 861–876, oct 2013. (cited in p. 24)

Cornuéjols Gérard, Peña Javier and Tütüncü Reha. *Dynamic Programming: Theory and Algorithms*, pp. 212–224. Cambridge University Press, 2 edition, 2018. (cited in p. 154)

D'Aniello Federica, Arsie Ivan, Pianese Cesare and Stola Federico. "Development of an Integrated Control Strategy for engine and SCR system basedon effective EGR rate". *IFAC-PapersOnLine*, Vol. 53 n^o 2, pp. 14034–14039, 2020. (cited in p. 23)

Dhillon Pritpal S., Harold Michael P., Wang Di, Kumar Ashok and Joshi Saurabh Y. "Enhanced transport in washcoated monoliths: Application to selective lean NOx reduction and ammonia oxidation". *Chemical Engineering Journal*, Vol. 377 n^o August, dec 2019. (cited in pp. 26, 84, and 111)

Donkers M.C.F., Schijndel J Van, Heemels W.P.M.H. and Willems F.P.T. "Optimal control for integrated emission management in diesel engines". *Control Engineering Practice*, Vol. 61, pp. 206–216, apr 2017. (cited in p. 119)

Ebrahimi Mojtaba, Najafi Mohammad and Jazayeri Seyed Ali. "Multi-input–multi-output optimization of reactivity-controlled compression-ignition combustion in a heavy-duty diesel engine running on natural gas/diesel fuel". *International Journal of Engine Research*, Vol. 21 n^o 3, pp. 470–483, mar 2020. (cited in p. 84)

Environmental Protection Agency. "Inventory of U.S. Greenhouse Gas Emissions and Sinks: 1990-2020". Technical report, 2022. (cited in p. 6)

Fagundez Fabio D., Facó João Lauro D. and Xavier Adilson E. "A Nonlinear Optimal Control Approach to Process Scheduling". In *Springer Optimization and Its Applications*, volume 39, pp. 409–421. 2010. (cited in p. 155)

Feng Renhua, Hu Xiulin, Li Guanghua, Sun Zhengwei and Deng Banglin. "A comparative investigation between particle oxidation catalyst (POC) and diesel particulate filter (DPF) coupling aftertreatment system on emission reduction of a non-road diesel engine". *Ecotoxicology and Environmental Safety*, Vol. 238 n^o April, jun 2022. (cited in pp. 26 and 83)

Filip Florin-Gheorghe and Leiviskä Kauko. *Large-Scale Complex Systems*, pp. 619–638. Springer Berlin Heidelberg, Berlin, Heidelberg, 2009. (cited in p. 62)

Frobert Arnaud, Raux Stephane, Creff Yann and Jeudy Eric. "About Cross-Sensitivities of NOx Sensors in SCR Operation". In *SAE Technical Papers*, volume 2, apr 2013. (cited in pp. 28, 29, 30, 31, 77, 78, 79, and 179)

Gamkrelidze R. V. "Discovery of the maximum principle". *Journal of Dynamical and Control Systems*, Vol. 5 n^o 4, pp. 437–451, 1999. (cited in p. 153)

Goetschalckx Robby, Sanner Scott and Driessens Kurt. "Reinforcement Learning with the Use of Costly Features". In Girgin Sertan, Loth Manuel, Munos Rémi, Preux Philippe and Ryabko Daniil, editors, *Recent Advances in Reinforcement Learning*, pp. 124–135, Berlin, Heidelberg, 2008. Springer Berlin Heidelberg. (cited in p. 154)

Gu Hyerim, Chun Kwang Min and Song Soonho. "The effects of hydrogen on the efficiency of NO x reduction via hydrocarbon-selective catalytic reduction (HC-SCR) at low temperature using various reductants". *International Journal of Hydrogen Energy*, Vol. 40 n^o 30, pp. 9602–9610, aug 2015. (cited in p. 22)

Guan Bin, Zhan Reggie, Lin He and Huang Zhen. "Review of state of the art technologies of selective catalytic reduction of NOx from diesel engine exhaust". *Applied Thermal Engineering*, Vol. 66 n^o 1-2, pp. 395–414, may 2014. (cited in pp. 10, 70, 95, and 135)

Guardiola Carlos, Pla Benjamín, García Antonio and Boronat Vicente. "Optimal heat release shaping in a reactivity controlled compression ignition (RCCI) engine". *Control Theory and Technology*, Vol. 15 n^o 2, pp. 117–128, may 2017. (cited in p. 159)

Haagen-Smit A J. "The Control of Air Pollution". *Scientific American*, Vol. 210 n^o 1, pp. 24–31, 1964. (cited in p. 6)

Han Lupeng, Cai Sixiang, Gao Min, Hasegawa Jun-ya, Wang Penglu, Zhang Jianping, Shi Liyi and Zhang Dengsong. "Selective Catalytic Reduction of NO x with NH 3 by Using Novel Catalysts: State of the Art and Future Prospects". *Chemical Reviews*, Vol. 119 n^o 19, pp. 10916–10976, oct 2019. (cited in p. 10)

Henle Jeremy J., Zahrt Andrew F., Rose Brennan T., Darrow William T., Wang Yang and Denmark Scott E. "Development of a Computer-Guided Workflow for Catalyst Optimization. Descriptor Validation, Subset Selection, and Training Set Analysis". *Journal of the American Chemical Society*, Vol. 142 n^o 26, pp. 11578–11592, jul 2020. (cited in p. 63)

Heywood John B. *Internal Combustion Engine Fundamentals*. McGraw-Hill Education, Cambridge, Massachusetts, second edition, 2018. (cited in pp. 3, 8, and 20)

Hjelkrem Odd André, Arnesen Petter, Aarseth Bø Torstein and Sondell Rebecka Snefuglli. "Estimation of tank-to-wheel efficiency functions based on type approval data". *Applied Energy*, Vol. 276 n^o February, oct 2020. (cited in p. 7)

Hooftman Nils, Messagie Maarten, Van Mierlo Joeri and Coosemans Thierry. "A review of the European passenger car regulations – Real driving emissions vs local air quality". *Renewable and Sustainable Energy Reviews*, Vol. 86 n^o January, pp. 1–21, apr 2018. (cited in p. 7)

Hsieh Ming-Feng and Wang Junmin. "Development and experimental studies of a control-oriented SCR model for a two-catalyst urea-SCR system". *Control Engineering Practice*, Vol. 19 n^o 4, pp. 409–422, apr 2011. (cited in p. 31)

Hu Jie, Liao Jianxiong, Hu Youyao, Lei Jun, Zhang Ming, Zhong Jing, Yan Fuwu and Cai Zhizhou. "Experimental investigation on emission characteristics of non-road diesel engine equipped with integrated DOC + CDPF + SCR aftertreatment". *Fuel*, Vol. 305 n^o August 2021, dec 2021. (cited in p. 19)

Hu Jie, Zeng Jiawei and Wei Li. "Failure diagnosis and tolerant control method for hydrothermally aged SCR system by utilizing EKF observer and MRAC controller". *Energy*, Vol. 156, pp. 103–121, aug 2018. (cited in pp. 26 and 111)

Inagaki Hiroshi, Oshima Takafumi, Miyata Shigeru and Kondo Noriaki. "NOx Meter Utilizing ZrO2 Pumping Cell". volume 1998, feb 1998. (cited in pp. 28 and 30)

International Energy Agency (IEA). *Net Zero by 2050: A Roadmap for the Global Energy Sector*. OECD, 2021. (cited in pp. 5 and 6)

International Energy Agency (IEA). "Energy Statistics Data Browser", 2022. (cited in pp. 5 and 6)

Jiang Kai, Zhang Hui and Lin Jing. "NH3 Coverage Ratio Estimation of Diesel-Engine SCR Systems by a Dual Time-Scale Extended Kalman Filter". *IEEE Transactions on Vehicular Technology*, Vol. 67 n^o 4, pp. 3625–3629, apr 2018. (cited in p. 84)

Jiang Yu, Yang Jiacheng, Tan Yi, Yoon Seungju, Chang Hung-Li, Collins John, Maldonado Hector, Carlock Mark, Clark Nigel, McKain David, Cocker David, Karavalakis Georgios, Johnson Kent C. and Durbin Thomas D. "Evaluation of emissions benefits of OBD-based repairs for potential application in a heavy-duty vehicle Inspection and Maintenance program". *Atmospheric Environment*, Vol. 247 n^o December 2020, feb 2021. (cited in p. 27)

Kato Nobuhide, Kokune Nobuyuki, Lemire Bertrand and Walde Tim. "Long Term Stable NOx Sensor with Integrated In-Connector Control Electronics". In *SAE Technical Papers*, number 724, mar 1999. (cited in p. 28)

Keogh Eamonn and Mueen Abdullah. *Curse of Dimensionality*, pp. 314–315. Springer US, Boston, MA, 2017. (cited in pp. 70 and 152)

Khair Magdi K. "A Review of Diesel Particulate Filter Technologies". In *SAE Technical Papers*, number 724, jun 2003. (cited in p. 10)

Kim Hyung Jun, Jo Seongin, Kwon Sangil, Lee Jong-Tae and Park Suhan. "NOX emission analysis according to after-treatment devices (SCR, LNT + SCR, SDPF), and control strategies in Euro-6 light-duty diesel vehicles". *Fuel*, Vol. 310, feb 2022. (cited in p. 27)

Kunimoto Akira, Hasei Masaharu, Yan Yongtie, Gao Yunzhi, Ono Takashi and Nakanouchi Yukio. "New Total-NOx Sensor Based on Mixed Potential for Automobiles". In *SAE Technical Papers*, number 724, mar 1999. (cited in p. 28)

Kupper Frank, Mentink Paul, Avramis Nikos, Meima Niels, Lazovik Elena, Wilkins Steven and Willems Frank. "Towards Self-Learning Energy Management for Optimal PHEV Operation Around Zero Emission Zones". In *SAE Technical Papers*, number 2022, pp. 1–13, mar 2022. (cited in p. 144)

Leach Felix, Kalghatgi Gautam, Stone Richard and Miles Paul. "The scope for improving the efficiency and environmental impact of internal combustion engines". *Transportation Engineering*, Vol. 1 n^o April, jun 2020. (cited in p. 3)

Lee Ingun, Jung Byounghyo, Park Jinsu, Lee Chunbum, Hwang Jeongsug and Park C.O. "Mixed potential NH3 sensor with LaCoO3 reference electrode". *Sensors and Actuators B: Chemical*, Vol. 176, pp. 966–970, jan 2013. (cited in p. 33)

Lu Bingxu, Jin Qijie, Chu Lin, Pan Youchun, Tao Xingjun, Yang Lei and Shen Yuesong. "Ammonia storage/release characteristics of CeSnWBaOx/TiO2 catalyst in solving the problem of ammonia slip". *Process Safety and Environmental Protection*, Vol. 138, pp. 67–75, jun 2020. (cited in p. 110)

Maass J., Eppler A., Scholz J., Gentgen H., Grumbrecht F. and Marohn R. "Influences of AdBlue® spray targeting and mixing devices on the UWS distribution upstream of the SCR catalyst". In *Fuel Systems for IC Engines*, number 1, pp. 21–41. Elsevier, 2012. (cited in p. 22)

Majewski W Addy. "Selective catalytic reduction". *Ecopoint Inc. Revision*, 2005. (cited in p. 21)

Maksimov Vyacheslav. "Analysis of Differential Inclusions: Feedback Control Method". In *Springer Optimization and Its Applications*, volume 39, pp. 259–275. 2010. (cited in p. 152)

María Desantes José, Guardiola Carlos, Pla Benjamín and Real Marcelo. "Oxygen catalyst depletion strategy based on TWC control-oriented modelling". *IFAC-PapersOnLine*, Vol. 51 n^o 31, pp. 355–361, 2018. (cited in p. 159)

Masson-Delmotte V., Zhai P., Pirani A., Connors S.L., Péan C., Berger S., Caud N., Chen Y., Goldfarb L., Gomis M.I., Huang M., Leitzell K., Lonnoy E., Matthews J.B.R., Maycock T.K., Waterfield T., Yelekçi O., Yu R. and Zhou B. "Climate Change 2021: The Physical Science Basis". Technical report, Cambridge University Press, Cambridge, England, 2022. (cited in p. 5)

Matula R A. *Mechanism of Hydrocarbon Formation in Combustion Processes*, pp. 77–151. Springer US, Boston, MA, 1973. (cited in p. 8)

McKinley Thomas L. and Alleyne Andrew G. "Adaptive Model Predictive Control of an SCR Catalytic Converter System for Automotive Applications". *IEEE Transactions on Control Systems Technology*, Vol. 20 n^o 6, pp. 1533–1547, nov 2012. (cited in p. 23)

Miao Yong, Chen Lea-Der, He Yongsheng and Kuo Tang-wei. "Study of SCR cold-start by energy method". *Chemical Engineering Journal*, Vol. 155 n^o 1-2, pp. 260–265, dec 2009. (cited in p. 22)

Mohammadpour Javad, Franchek Matthew and Grigoriadis Karolos. "A survey on diagnostics methods for automotive engines". In *Proceedings of the 2011 American Control Conference*, pp. 985–990. IEEE, jun 2011. (cited in p. 27)

Mora J., Willems F., Seykens X. and Guardiola C. "An OBD strategy to estimate SCR ageing and detect urea injection faults". *IFAC-PapersOnLine*, Vol. 51 n^o 31, pp. 369–376, 2018. (cited in pp. 26, 119, and 125)

Mora Pérez Javier. *Control-oriented modelling and diagnostics of diesel after-treatment catalysts*. PhD Thesis, Universitat Politècnica de València, Valencia (Spain), dec 2018. (cited in p. 84)

Müller Volker, Pieta Holger, Schaub Joschka, Ehrly Markus and Körfer Thomas. "On-Board Monitoring to meet upcoming EU-7 emission standards – Squaring the circle between effectiveness and robust realization". *Transportation Engineering*, Vol. 10 n^o March, dec 2022. (cited in p. 27)

Nahavandi M. "Selective Catalytic Reduction (SCR) Of No By Ammonia Over V2o5/Tio2 Catalyst In A Catalytic Filter Medium And Honeycomb Reactor: A Kinetic Modeling Study". *Brazilian Journal of Chemical Engineering*, Vol. 32 n^o 4, pp. 875–893, dec 2015. (cited in p. 63)

NAKATSUJI T, YAMAGUCHI T, SATO N and OHNO H. "A selective NOx reduction on Rh-based catalysts in lean conditions using CO as a main reductant". *Applied Catalysis B: Environmental*, Vol. 85 n^o 1-2, pp. 61–70, dec 2008. (cited in p. 22)

Ni Peiyong, Wang Xiangli and Li Hu. "A review on regulations, current status, effects and reduction strategies of emissions for marine diesel engines". *Fuel*, Vol. 279 n^o May, nov 2020. (cited in p. 7)

Nova Isabella, Lietti Luca, Tronconi Enrico and Forzatti Pio. "Transient response method applied to the kinetic analysis of the DeNOx–SCR reaction". *Chemical Engineering Science*, Vol. 56 n^o 4, pp. 1229–1237, feb 2001. (cited in pp. 62 and 64)

of science Web. "Web of Science Core Collection". (cited in p. 18)

Ofoli Abdul R. "Experimental Demonstration of Ammonia Storage and Slip Modeling With Control for an SCR Aftertreatment System". *IEEE Transactions on Industry Applications*, Vol. 50 n^o 4, pp. 2342–2348, jul 2014. (cited in p. 23)

Olabi A.G., Maizak David and Wilberforce Tabbi. "Review of the regulations and techniques to eliminate toxic emissions from diesel engine cars". *Science of The Total Environment*, Vol. 748, dec 2020. (cited in p. 83)

Ono Takashi, Yan Yongtie, Hasei Masaharu, Sato Masayuki, Kunimoto Akira, Tanaka Akio and Saito Toshitaka. "Total-NOx Sensor Based on Mixed-Potential for Detecting of Low NOx Concentrations". In *SAE Technical Papers*, number 724, apr 2005. (cited in p. 28)

Palash S.M., Masjuki H.H., Kalam M.A., Masum B.M., Sanjid A. and Abedin M.J. "State of the art of NOx mitigation technologies and their effect on the performance and emission characteristics of biodiesel-fueled Compression Ignition engines". *Energy Conversion and Management*, Vol. 76, pp. 400–420, dec 2013. (cited in p. 8)

Payri Raul, Bracho Gabriela, Gimeno Jaime and Moreno Armando. "Investigation of the urea-water solution atomization process in engine exhaust-like conditions". *Experimental Thermal and Fluid Science*, Vol. 108 n^o March, pp. 75–84, nov 2019. (cited in p. 22)

Pesch H J. *Offline and Online Computation of Optimal Trajectories in the Aerospace Field*, pp. 165–220. Springer US, Boston, MA, 1994. (cited in p. 152)

Peyton Jones James C. and Geveci Mert. "Smart Sensing and Decomposition of NO x and NH 3 Components from Production NO x Sensor Signals". *SAE International Journal of Engines*, Vol. 4 n^o 1, apr 2011. (cited in p. 29)

Pezzini A., Canova M., Onori S., Rizzoni G. and Soliman A. "A Methodology for Fault Diagnosis of Diesel NOx Aftertreatment Systems". *IFAC Proceedings Volumes*, Vol. 42 n^o 8, pp. 911–916, 2009. (cited in p. 24)

Pla Benjamin, Bares Pau, Sanchis Enrique and Aronis André. "Ammonia injection optimization for selective catalytic reduction aftertreatment systems". *International Journal of Engine Research*, Vol. 22 n^o 7, pp. 2169–2179, jul 2021. (cited in pp. 20, 30, and 133)

Pla Benjamín, Bares Pau, Sanchis Enrique José and Nakaema Aronis André. "Ammonia injection failure diagnostic and correction in engine after-treatment system by NOx and NH3 emissions observation". *Fuel*, Vol. 322 n^o March, aug 2022. (cited in pp. 21 and 62)

Pla Benjamin, Piqueras Pedro, Bares Pau and Aronis André. "Simultaneous NOx and NH3 slip prediction in a SCR catalyst under real driving conditions including potential urea injection failures". *International Journal of Engine Research*, Vol. 23 n^o 7, pp. 1213–1225, jul 2022. (cited in p. 21)

Posada Francisco. "On-board diagnostics for heavy-duty vehicles : Considerations for Mexico". *International Council on Clean Transportation*, n^o February, 2014. (cited in p. 28)

Posada Francisco and Bandivadekar Anup. "Global overview of on-board diagnostic (OBD) systems for heavy-duty vehicles". *The International Council on Clean Transportation*, n^o January, 2015. (cited in p. 28)

Posada Francisco and German John. "Review of Ldv Obd Requirements Under the European , Korean and Californian Emission Programs". Technical Report March, 2016. (cited in p. 10)

Praveena V and Martin M Leenus Jesu. "A review on various after treatment techniques to reduce NOx emissions in a CI engine". *Journal of the Energy Institute*, Vol. 91 n^o 5, pp. 704–720, oct 2018. (cited in p. 19)

Pukelsheim Friedrich. "The Three Sigma Rule". *The American Statistician*, Vol. 48 n^o 2, pp. 88–91, may 1994. (cited in p. 69)

Rajesh Chundru Venkata, Parker Gordon G. and Johnson John H. "Development of a Kalman filter estimator for simulation and controlof NO x and PM in a SCR catalyston a DPF". *International Journal of Engine Research*, Vol. 22 n^o 8, pp. 2407–2421, aug 2021. (cited in pp. 97 and 119)

Raza Hassan, Woo Sanghee and Kim Hongsuk. "Investigation of an ammonium carbamate–based SCR system for NOx reduction in diesel engines under transient conditions". *Energy*, Vol. 251, jul 2022. (cited in p. 20)

Reşitoğlu İbrahim Aslan, Altinişik Kemal and Keskin Ali. "The pollutant emissions from diesel-engine vehicles and exhaust aftertreatment systems". *Clean Technologies and Environmental Policy*, Vol. 17 n^o 1, pp. 15–27, jan 2015. (cited in p. 9)

Rheaume Jonathan Michael. *Solid State Electrochemical Sensors for Nitrogen Oxide (NOx) Detection in Lean Exhaust Gases*. PhD Thesis, University of California, Berkeley, 2010. (cited in p. 74)

Riegel Johann. "Exhaust gas sensors for automotive emission control". *Solid State Ionics*, Vol. 152-153, pp. 783–800, dec 2002. (cited in p. 28)

Ritchie Hannah, Roser Max and Rosado Pablo. "CO2 and GHG emissions", 2020. (cited in p. 5)

Rizzoni Giorgio, Kim Yong-wha and Soliman Ahmed. "Estimation Problems in Engine Control and Diagnosis". *IFAC Proceedings Volumes*, Vol. 33 n^o 11, pp. 125–131, jun 2000. (cited in p. 27)

Rocha Cachim Pedro, Gomes João and Ventura Rodrigo. "Autonomous orbit determination for satellite formations using relative sensing: Observability analysis and optimization". *Acta Astronautica*, Vol. 200 n^o August, pp. 301–315, nov 2022. (cited in p. 98)

Romiti Filippo, del Pozo Juan, Paioti Paulo H S, Gonsales Stella A, Li Xinghan, Hartrampf Felix W W and Hoveyda Amir H. "Different Strategies for Designing Dual-Catalytic Enantioselective Processes: From Fully Cooperative to Non-cooperative Systems". *Journal of the American Chemical Society*, Vol. 141 n^o 45, pp. 17952–17961, nov 2019. (cited in p. 62)

Rosa William. *A New Era in Global Health*. Springer Publishing Company, New York, NY, jun 2017. (cited in p. 4)

Russell April and Epling William S. "Diesel Oxidation Catalysts". *Catalysis Reviews*, Vol. 53 n^o 4, pp. 337–423, oct 2011. (cited in p. 9)

Salam Satishchandra, Choudhary Tushar, Pugazhendhi Arivalagan, Verma Tikendra Nath and Sharma Abhishek. "A review on recent progress in computational and empirical studies of compression ignition internal combustion engine". *Fuel*, Vol. 279 n^o May, nov 2020. (cited in p. 62)

Sasaki Hisashi, Scholl David, Parsons Mike, Inagaki Hiroshi, Shiotani Koji, Visser Jaco, Zawacki Garry, Kawai TakeshiI, Teramoto Satoshi and Kubinski David. "Development of an Al2O3/ZrO2-Composite High-Accuracy NOx Sensor". apr 2010. (cited in p. 28)

Sawma J., Khatounian F., Monmasson E., Ghosn R. and Idkhajine L. "The effect of prediction horizons in MPC for first order linear systems". In *2018 IEEE International Conference on Industrial Technology (ICIT)*, volume 2018-Febru, pp. 316–321. IEEE, feb 2018. (cited in p. 166)

Scheuer A., Hauptmann W., Drochner A., Gieshoff J., Vogel H. and Votsmeier M. "Dual layer automotive ammonia oxidation catalysts: Experiments and computer simulation". *Applied Catalysis B: Environmental*, Vol. 111-112, pp. 445–455, 2012. (cited in pp. 24 and 25)

Scheuer A., Votsmeier M., Schuler A., Gieshoff J., Drochner A. and Vogel H. "NH3-slip catalysts: Experiments versus mechanistic modelling". *Topics in Catalysis*, Vol. 52 n^o 13-20, pp. 1847–1851, 2009. (cited in p. 24)

Seborg Dale E, Mellichamp Duncan A and Edgar Thomas F. *Process Dynamics and Control*. Wylie Series in Chemical Engineering. John Wiley & Sons, third edition, 2011. (cited in p. 165)

Selleri Tommaso, Nova Isabella and Tronconi Enrico. "An efficient reduced model of NH3-SCR converters for mobile aftertreatment systems". *Chemical Engineering Journal*, Vol. 377, dec 2019. (cited in p. 19)

Seo Choong-kil, Kim Hwanam, Choi Byungchul, Lim Myung Taeck, Lee Chun-Hwan and Lee Chun-beom. "De-NOx characteristics of a combined system of LNT and SCR catalysts according to hydrothermal aging and sulfur poisoning". *Catalysis Today*, Vol. 164 n^o 1, pp. 507–514, apr 2011. (cited in p. 21)

Shibata Gen, Shibayama Naoki, Araki Keita, Kobashi Yoshimitsu, Ogawa Hideyuki, Nakasaka Yuta and Shimizu Ken-ichi. "Steady-state kinetic modeling of NH3-SCR by monolithic Cu-CHA catalysts". *Catalysis Today*, n^o June, jun 2022. (cited in p. 19)

Shin Youngjin, Jung Yongjin, Cho Chong Pyo, Pyo Young Dug, Jang Jinyoung, Kim Gangchul and Kim Tae Min. "NOx abatement and N2O formation over urea-SCR systems with zeolite supported Fe and Cu catalysts in a nonroad diesel engine". *Chemical Engineering Journal*, Vol. 381, feb 2020. (cited in p. 65)

Shiyu Liu, Boyuan Wang, Zexian Guo, Buyu Wang, Zhaohuan Zhang, Xiao Ma, Chen-Teng Chang, Peng Wang, Xin He, Xingyu Sun and Shijin Shuai. "Experimental investigation of urea injection strategy for close-coupled SCR aftertreatment system to meet ultra-low NO emission regulation". *Applied Thermal Engineering*, Vol. 205, mar 2022. (cited in p. 135)

Shost Mark, Noetzel John, Wu Ming-cheng, Sugiarto Tanto, Bordewyk Todd, Fulks Gary and Fisher Galen B. "Monitoring, Feedback and Control of

Urea SCR Dosing Systems for NOx Reduction: Utilizing an Embedded Model and Ammonia Sensing". In *SAE International*, number 724, apr 2008. (cited in p. 63)

Sinha A.K. and Loparo K.A. "A computational model for complex systems analysis: Causality estimation". *Physica D: Nonlinear Phenomena*, Vol. 423, sep 2021. (cited in p. 62)

Sinigaglia Tiago, Eduardo Santos Martins Mario and Cezar Mairesse Siluk Julio. "Technological evolution of internal combustion engine vehicle: A patent data analysis". *Applied Energy*, Vol. 306, jan 2022. (cited in p. 3)

Skaf Zakwan, Aliyev Timur, Shead Leo and Steffen Thomas. "The State of the Art in Selective Catalytic Reduction Control". In *SAE Technical Papers*. SAE International, apr 2014. (cited in p. 84)

Soleimani Morteza, Campean Felician and Neagu Daniel. "Integration of Hidden Markov Modelling and Bayesian Network for fault detection and prediction of complex engineered systems". *Reliability Engineering & System Safety*, Vol. 215 n^o May, nov 2021. (cited in p. 24)

Sreekanth K.J. "Review on integrated strategies for energy policy planning and evaluation of GHG mitigation alternatives". *Renewable and Sustainable Energy Reviews*, Vol. 64, pp. 837–850, oct 2016. (cited in p. 5)

Tan Pi-qiang, Zhang Shu-chen, Wang Shi-yan, Hu Zhi-yuan and Lou Di-Ming. "Simulation on catalytic performance of fresh and aged SCR catalysts for diesel engines". *Journal of the Energy Institute*, Vol. 93 n^o 6, pp. 2280–2292, dec 2020. (cited in pp. 25 and 83)

Tan Piqiang, Li Xiaoyu, Wang Shiyan, Hu Zhiyuan and Lou Diming. "Selective catalytic reduction failure of low NH3-NO ratio". *Chinese Journal of Chemical Engineering*, Vol. 32, pp. 231–240, apr 2021. (cited in p. 26)

Tang Wei, Cai Yixi and Wang Jun. "Experimental studies on the diesel engine urea-SCR system using a double NOx sensor system". *Environmental Engineering Research*, Vol. 20 n^o 4, pp. 397–402, dec 2015. (cited in p. 31)

Upadhyay Devesh and Van Nieuwstadt Michiel. "Modeling of a Urea SCR Catalyst With Automotive Applications". In *Dynamic Systems and Control*, pp. 707–713. ASMEDC, jan 2002. (cited in p. 63)

van Dooren Stijn, Amstutz Alois and Onder Christopher H. "A causal supervisory control strategy for optimal control of a heavy-duty Diesel engine with SCR aftertreatment". *Control Engineering Practice*, Vol. 119 n^o November 2021, feb 2022. (cited in p. 23)

Velmurugan Dhinesh Vilwanathan. *Supervisory control of complex propulsion subsystems*. PhD Thesis, Chalmers University of Technology, 2022. (cited in pp. 8 and 9)

Vestreng V., Ntziachristos L., Semb A., Reis S., Isaksen I. S. A. and Tarrasón L. "Evolution of NOx emissions in Europe with focus on road transport control measures". *Atmospheric Chemistry and Physics*, Vol. 9 n^o 4, pp. 1503–1520, feb 2009. (cited in p. 6)

Vignesh R. and Ashok B. "Critical interpretative review on current outlook and prospects of selective catalytic reduction system for De-NOx strategy in compression ignition engine". *Fuel*, Vol. 276 n^o March, sep 2020. (cited in pp. 17, 21, 25, 83, and 181)

Vrabie Draguna and Lewis Frank. "Online Adaptive Optimal Control Based on Reinforcement Learning". In *Springer Optimization and Its Applications*, volume 39, pp. 309–323. 2010. (cited in p. 152)

Wächter Andreas and Biegler Lorenz T. "On the implementation of an interior-point filter line-search algorithm for large-scale nonlinear programming". *Mathematical Programming*, Vol. 106 n^o 1, pp. 25–57, mar 2006. (cited in p. 158)

Wang Da Yu, Yao Sheng, Shost Mark, Yoo Joon Ho, Cabush David, Racine David, Cloudt Robert and Willems Frank. "Ammonia sensor for closed-loop SCR control". *SAE Technical Papers*, Vol. 1 n^o 1, 2008. (cited in p. 33)

Wang De-yuan, Cao Jian-hong, Tan Pi-qiang, Wang Zhi-xin, Li Wen-long, Liu Zuo-wei and Wang Jun. "Full course evolution characteristics of DPF active regeneration under different inlet HC concentrations". *Fuel*, Vol. 310, feb 2022. (cited in pp. 25 and 83)

Wang Guoyang, Awad Omar I., Liu Shiyu, Shuai Shijin and Wang Zhiming. "NOx emissions prediction based on mutual information and back propagation neural network using correlation quantitative analysis". *Energy*, Vol. 198, may 2020. (cited in p. 86)

Wang Guoyang, Qi Jinzhu, Liu Shiyu, Li Yanfei, Shuai Shijin and Wang Zhiming. "Zonal control for selective catalytic reduction system using a model-based multi-objective genetic algorithm". *International Journal of Engine Research*, Vol. 22 n^o 3, pp. 911–920, mar 2021. (cited in pp. 20 and 30)

Wang Ying, Liu Hong and Lee Chia-Fon F. "Particulate matter emission characteristics of diesel engines with biodiesel or biodiesel blending: A review". *Renewable and Sustainable Energy Reviews*, Vol. 64, pp. 569–581, oct 2016. (cited in p. 8)

Wang Yue-Yun, Sun Yu, Chang Chen-Fang and Hu Yiran. "Model-Based Fault Detection and Fault-Tolerant Control of SCR Urea Injection Systems". *IEEE Transactions on Vehicular Technology*, Vol. 65 n^o 6, pp. 4645–4654, jun 2016. (cited in pp. 27 and 125)

Willems Frank and Cloudt Robert. "Experimental Demonstration of a New Model-Based SCR Control Strategy for Cleaner Heavy-Duty Diesel Engines". *IEEE Transactions on Control Systems Technology*, Vol. 19 n^o 5, pp. 1305–1313, sep 2011. (cited in p. 23)

Willems Frank, Cloudt Robert, van den Eijnden Edwin, van Genderen Marcel, Verbeek Ruud, de Jager Bram, Boomsma Wiebe and van den Heuvel Ignace. "Is Closed-Loop SCR Control Required to Meet Future Emission Targets?". In *SAE Technical Papers*, volume 2007, apr 2007. (cited in pp. 34 and 95)

Wu Binyang, Deng Longfei, Liu Yize, Sun Dezeng and Su Wanhua. "Urea injection control strategy in urea-selective catalytic reduction for heavy-duty diesel engine under transient process". *International Journal of Engine Research*, Vol. 22 n^o 2, pp. 516–527, feb 2021. (cited in pp. 63 and 84)

Xi Yuanzhou, Ottinger Nathan A. and Liu Z. Gerald. "New insights into sulfur poisoning on a vanadia SCR catalyst under simulated diesel engine operating conditions". *Applied Catalysis B: Environmental*, Vol. 160-161 n^o 1, pp. 1–9, nov 2014. (cited in p. 21)

Xi Yuanzhou, Su Changsheng, Ottinger Nathan A. and Liu Z. Gerald. "Effects of hydrothermal aging on the sulfur poisoning of a Cu-SSZ-13 SCR catalyst". *Applied Catalysis B: Environmental*, Vol. 284 n^o November 2020, may 2021. (cited in p. 21)

Xin Qianfan. "The analytical design process and diesel engine system design". In *Diesel Engine System Design*, pp. 3–112. Elsevier, 2013. (cited in p. 7)

Xu Guangyan, Shan Wenpo, Yu Yunbo, Shan Yulong, Wu Xiaodong, Wu Ye, Zhang Shaojun, He Liqiang, Shuai Shijin, Pang Hailong, Jiang Xuefeng, Zhang Heng, Guo Lei, Wang Shufen, Xiao Feng-Shou, Meng Xiangju, Wu Feng, Yao Dongwei, Ding Yan, Yin Hang and He Hong. "Advances in emission control of diesel vehicles in China". *Journal of Environmental Sciences*, dec 2021. (cited in p. 111)

Xu Junqiang, Zou Xianlin, Chen Guorong, Zhang Yanrong, Zhang Qiang and Guo Fang. "Tailored activity of Ce–Ni bimetallic modified V2O5/TiO2 catalyst for NH3-SCR with promising wide temperature window". *Vacuum*, Vol. 191 n^o 66, sep 2021. (cited in p. 21)

Xue Lina, Xiong Ka, Chen Haijun, Cho Kyeongjae and Wang Weichao. "Investigation of the hydrothermal aging of an Mn-based mullite SmMn 2 O 5 catalyst of NO oxidation". *RSC Adv.*, Vol. 7 n^o 77, pp. 49091–49096, 2017. (cited in pp. 21 and 26)

Yadav Deepak, Singh Pratichi and Prasad Ram. "MnCo2O4 spinel catalysts synthesized by nanocasting method followed by different calcination routes for low-temperature reduction of NOx using various reductants". *International Journal of Hydrogen Energy*, Vol. 43 n^o 10, pp. 5346–5357, mar 2018. (cited in p. 22)

YAN Dong-jie, GUO Tong, YU Ya and CHEN Zhao-hui. "Lead poisoning and regeneration of Mn-Ce/TiO2 catalysts for NH3-SCR of NO at low temperature". *Journal of Fuel Chemistry and Technology*, Vol. 49 n^o 1, pp. 113–120, jan 2021. (cited in p. 22)

Yang Shichun, Feng Song, Sun Kangfeng, Wang Shuai and Cao Yaoguang. "Square-root unscented Kalman filter for ammonia coverage ratio and input ammonia estimations in diesel-engine urea-SCR system". *ISA Transactions*, Vol. 96, pp. 299–308, jan 2020. (cited in pp. 84 and 135)

Yuan Xinmei, Gao Ying and Wang Xiulei. "A novel NH 3 slip control for diesel engine selective catalytic reduction aftertreatment system". *International Journal of Engine Research*, Vol. 17 n^o 2, pp. 169–178, feb 2016. (cited in p. 20)

Yuan Xueliang, Zhang Mofan, Wang Qingsong, Wang Yutao and Zuo Jian. "Evolution analysis of environmental standards: Effectiveness on air pollutant emissions reduction". *Journal of Cleaner Production*, Vol. 149, pp. 511–520, apr 2017. (cited in p. 4)

Zeng Yiqing, Wu Zihua, Guo Lina, Wang Yanan, Zhang Shule and Zhong Qin. "Insight into the effect of carrier on N2O formation over MnO2/MOx (M = Al, Si and Ti) catalysts for selective catalytic reduction (SCR) of NOx with NH3". *Molecular Catalysis*, Vol. 488 n^o March, jun 2020. (cited in p. 20)

Zhang Hui and Wang Junmin. "Improved NO and NO2 Concentration Estimation for a Diesel-Engine-Aftertreatment System". *IEEE/ASME Transactions on Mechatronics*, Vol. 23 n^o 1, pp. 190–199, feb 2018. (cited in p. 63)

Zhang S. M., Tian F., Ren G. F. and Yang L. "SCR control strategy based on ANNs and Fuzzy PID in a heavy-duty diesel engine". *International Journal of Automotive Technology*, Vol. 13 n^o 5, pp. 693–699, aug 2012. (cited in p. 23)

Zhang Shaojun, Zhao Pei, He Liqiang, Yang Yanyan, Liu Baoxian, He Weinan, Cheng Ying, Liu Ying, Liu Shijie, Hu Qingyao, Huang Cheng and Wu Ye. "On-board monitoring (OBM) for heavy-duty vehicle emissions in China: Regulations, early-stage evaluation and policy recommendations". *Science of The Total Environment*, Vol. 731, aug 2020. (cited in p. 27)

Zhang Yunhua, Lou Diming, Tan Piqiang, Hu Zhiyuan and Fang Liang. "Effect of SCR downsizing and ammonia slip catalyst coating on the emissions from a heavy-duty diesel engine". *Energy Reports*, Vol. 8, pp. 749–757, nov 2022. (cited in pp. 10 and 135)

Zhou Yang, Ravey Alexandre and Péra Marie-Cécile. "A survey on driving prediction techniques for predictive energy management of plug-in hybrid electric vehicles". *Journal of Power Sources*, Vol. 412 n^o October 2018, pp. 480–495, feb 2019. (cited in p. 165)

Zhu Jiamin, Ngo Caroline and Sciarretta Antonio. "Real-Time Optimal Eco-Driving for Hybrid-Electric Vehicles". *IFAC-PapersOnLine*, Vol. 52 n^o 5, pp. 562–567, 2019. (cited in p. 159)

Zhu Minghui, Lai Jun-Kun and Wachs Israel E. "Formation of N2O greenhouse gas during SCR of NO with NH3 by supported vanadium oxide catalysts". *Applied Catalysis B: Environmental*, Vol. 224 n^o November 2017, pp. 836–840, may 2018. (cited in p. 20)